Abstract

Adipose tissue engineering holds promise for the development of therapeutic strategies for subcutaneous adipose tissue regeneration to treat defects resulting from congenital birth defects, invasive surgical procedures and traumatic injuries. Decellularized adipose tissue (DAT) scaffolds represent a potential off-the-shelf tissue substitute for volume augmentation. Seeding the DAT with adipose-derived stromal cells (ASCs) has been shown to enhance adipose tissue regeneration in immunocompetent animals *in vivo*. Although promising, this strategy is limited by low cell attachment on the DAT. As such, this thesis focused on the development of bioreactor strategies to enhance the capacity of human ASCs to stimulate angiogenesis and adipogenesis within the DAT.

Culturing human ASCs on the DAT scaffolds within a perfusion bioreactor under hypoxia (2% O_2) promoted ASC expansion, and altered cell phenotype, upregulating the expression of hypoxia inducible factor 1-alpha (HIF-1α), inducible nitric oxide synthase (iNOS) and tumour necrosis factor-alpha (TNF-α) in the ASCs in the peripheral regions of the DAT. Further, bioreactor culture modulated the expression of pro-angiogenic and immunomodulatory paracrine factors, suggesting that the capacity of the ASCs to stimulate regeneration may have been altered by shear stress stimulation. *In vivo* testing in athymic nude mice demonstrated that angiogenesis and adipogenesis within the DAT were markedly enhanced when the ASCs were cultured for 14 days within the perfusion bioreactor under 2% O_2 prior to implantation as compared to bioreactor culture under 20% O_2, as well as static-cultured, freshly-seeded and unseeded controls. Analysis of host cell infiltration indicated that there was increased $CD31^+$ endothelial cell recruitment and potentially adipogenic progenitor cell recruitment into the DAT implants, as well as a shift towards a more pro-regenerative macrophage response, in the 2% O_2 bioreactor group relative to static cultured controls.

Building from this work, a novel scalable rocking bioreactor platform was explored as an expansion and preconditioning system for ASCs. Preliminary studies indicated that culturing ASCs on DAT coatings within the rocking bioreactor enhanced the expression of the pro-angiogenic and immunomodulatory markers CD146 and iNOS. Collectively, this work

supports that dynamic culture systems can be applied to enhance the pro-regenerative potential of ASC-seeded DAT bioscaffolds.

Keywords

Adipose tissue engineering; Adipose-derived stromal cells; Perfusion bioreactors; Decellularized adipose tissue; Angiogenesis; Immunomodulation;

Summary for Lay Audience

The adipose (fat) tissue layer underneath the skin has limited ability for self-healing. Damage or loss of these tissues resulting from conditions including trauma, cancer, burns, or congenital birth defects can cause functional impairment and affect self-image, potentially causing anxiety and post-traumatic stress disorder (PTSD). Current therapeutic strategies have numerous limitations and there is a clear need for new approaches that promote the stable regeneration of adipose tissue for volume augmentation applications in plastic and reconstructive surgery.

To address this challenge, human adipose tissue discarded as surgical waste was processed to extract cellular components that would cause an immune response and produce protein-based decellularized adipose tissue (DAT) scaffolds. In combination with adipose-derived stromal cells (ASCs), a population of regenerative cells found in fat, the DAT was previously shown to promote the regeneration of fat tissues in pre-clinical models. Building from this work, the current thesis primarily focused on investigating whether culturing the ASCs on the DAT within a custom perfusion bioreactor system could enhance their capacity to stimulate blood vessel formation and adipose tissue regeneration. Using this perfusion bioreactor system, conditions were identified that promoted human ASC proliferation and infiltration on the DAT. Further, in-depth biological characterization indicated that human ASC function was altered by culturing within the bioreactor under low oxygen tension. More specifically, these cells were shown to produce higher levels of a range of proteins that could stimulate tissue regeneration. Testing in a pre-clinical mouse model demonstrated that culturing the ASCs on the DAT scaffolds for 14 days using the established perfusion bioreactor strategy was effective at promoting adipose tissue regeneration within the DAT. Characterization studies suggested that these effects were mediated by enhancing the infiltration of cells from the host tissues that contributed to the formation of new blood vessels and fat cells, as well as by promoting a more pro-regenerative host immune response.

Although promising, it may be challenging to scale up the perfusion bioreactor for clinical applications in humans where a large number of cells are needed, particularly in cases where a large volume of fat tissue regeneration is required. As such, the development of a more scalable rocking bioreactor was explored as an alternative to the perfusion bioreactor. Initial

results showed that this system could also promote the expression of proteins that have been identified as positive markers of the regenerative capacity of ASCs. Overall, the work in this thesis represents an advancement towards a clinically translatable strategy to support the stable and predictable regeneration of the fat tissue layer below the skin.

Co-Authorship Statement

Chapter 1

I wrote this chapter, which was reviewed and edited by Dr. Lauren Flynn.

Chapter 2

A version of this chapter has been published as a pre-print on BioRxiv (Tim Tian Y Han, Lauren E Flynn. Perfusion bioreactor culture of adipose-derived stromal cells on decellularized adipose tissue scaffolds enhances *in vivo* regeneration. 2020.04.10.036194) ahead of submission to a field-specific journal. I performed the experiments, data analysis and preparation of figures. Dr. Lauren Flynn contributed to the study direction, experimental design and provided critical feedback. The manuscript was written in collaboration with Dr. Lauren Flynn.

Chapter 3

The work presented in this chapter forms the basis for a manuscript that is in preparation for submission. I performed the experiments, data analysis and preparation of figures and tables. Dr. Lauren Flynn contributed to the study direction, experimental design and provided critical feedback. Dr. John Walker provided input on the PCR Array data analysis and contributed to the design of the multi-colour flow cytometry study. Dr. Aaron Grant provided clinical input and adipose tissue samples required for the studies. Dr. Gregory Dekaban contributed to the study design for the flow cytometry analyses and *in vivo* characterization of the macrophage response. The manuscript was written in collaboration with Dr. Lauren Flynn.

Chapter 4

I performed the experiments, data analysis and preparation of figures and tables. Dr. Lauren Flynn contributed to the study direction, experimental design and provided critical feedback. Ms. Cherry Liang provided technical assistance with the immunocytochemistry study. I drafted the chapter, which was reviewed and edited by Dr. Lauren Flynn.

Chapter 5

I wrote this chapter, which was reviewed and edited by Dr. Lauren Flynn.

Acknowledgments

First and foremost, I would like to express my most sincere gratitude to my supervisor Dr. Lauren Flynn. Over the past 7 years working with Dr. Flynn, she has always inspired me to be the best that I can be. Looking back, she always knew when to let me fall, and was always there to lift me up. Through all of this, she has taught me so many valuable lessons that I will continue to learn for the rest of my days.

I also want to extend my gratitude towards my advisory committee members, Dr. Cheryle Seguin, Dr. Martin Sandig and Dr. Alison Allan. Thank you so much for always being patient, available and critical with your feedback.

I would also like to thank the generous support and assistance from Dr. Kristen Chadwick, Dr. Eric Arts and the staff at the Animal Care Veterinary Services.

A big thank you to all the past and present brilliant minds at the Flynn lab. Thank you all for your help and support every step of the way. I sincerely appreciate Laura Juignet, Anna Kornmuller, Kevin Robb for generously offer their time. Special thanks to Cody Brown for the countless number of times he has bailed me out of trouble, Pascal Morissette Martin for being an awesome brother-in-arm that helps me associate adversities with smiley emojis, Chris LeClerc for the hour-long conversations and Courtney Brooks for being a hilarious ‘Badass’.

I am incredibly grateful for the selfless support of everyone at the Western Kendo Club and St. Lawrence Presbyterian Church.

Finally, to my parents with love - thank you for all your sacrifices. No word here can describe how much your support means to me.

Table of Contents

List of Tables

List of Figures

List of Appendices

List of Abbreviations

Ang-1	Angiopoietin 1
ASC	Adipose-derived stromal cells
bFGF	Basic fibroblast growth factor
BMP-2	Bone morphogenic protein 2
BSA	Bovine serum albumin
CEBP-α	CCAAT/enhancer binding protein alpha
CXCL-2	Chemokine C-X-C motif ligand 2
CXCL-5	C-X-C motif chemokine 5
CXCL-6	C-X-C motif chemokine 6
CXCL-10	C-X-C motif chemokine 10
DAT	Decellularized adipose tissue
DDM	Decellularized dermal matrix
DPM	Decellularized placental matrix
DPPIV	Dipeptidylpeptidase IV
ECM	Extracellular matrix
EGF	Epidermal growth factor
EGFR	Epidermal growth factor receptor
ERK1/2	Extracellular signal-regulated kinase 1/2
ESC	Embryonic stem cell

FAK	Focal adhesion kinase
FISH	Fluorescence *in situ* hybridization
FSC-A	Forward scatter area
G-CSF	Granulocyte colony-stimulating factor
GAG	Glycosaminoglycan
GFP	Green fluorescence protein
GPDH	Glycerol-3-phosphate dehydrogenase
H&E	Hematoxylin & eosin
HA	Hyaluronic acid
HGF	Hepatocyte growth factor
HIF-1α	Hypoxia inducible factor 1 alpha
hMito	Human mitochondria
HS	Heparan sulfate
HUVEC	Human umbilical vein endothelial cell
iNOS	Inducible nitric oxide synthase
iPSC	Induced pluripotent stem cells
IGF-1	Insulin-like growth factor 1
IGFR	Insulin-like growth factor receptor
IFN-γ	Interferon gamma
IL-1β	Interleukin 1 beta

IL-4	Interleukin 4
IL-4R	Interleukin 4 receptor
IL-6	Interleukin 6
IL-8	Interleukin 8
IL-10	Interleukin 10
IL-11	Interleukin 11
IL-12	Interleukin 12
JNK	c-Jun N-terminal kinase
LPS	Lipopolysaccharides
MAPK	Mitogen-activated protein kinase
MCP-1	Monocyte chemoattractant protein 1
MCS	Methacrylated chondroitin sulfate
MMP-2	Matrix metalloproteinase 2
MMP-9	Matrix metalloproteinase 9
MMP-13	Matrix metalloproteinase 13
MMP-14	Matrix metalloproteinase-14
MSC	Mesenchymal stromal cell
NO	Nitric oxide
P1	Passage 1
P3	Passage 3

PBS	Phosphate buffered saline
PDGF-B	Platelet-derived growth factor B
PDGFR-β	Platelet-derived growth factor receptor beta
PEG	Polyethylene glycol
PET	Polyethylene-terephthalate
PGA	Polyglycolic acid
PGE-2	Prostaglandin E2
PLA	Poly-lactic acid
PLGA	Poly(lactic-co-glycolic) acid
PPAR-γ	Peroxisome proliferator-activated receptor gamma
Pref-1	Preadipocyte factor-1
PTSD	Post-traumatic stress disorder
RUNX-2	Runt-related transcription factor 2
SCA-1	Stem cell antigen 1
SCID	Severe combined immunodeficient
SDF-1α	Stromal cell-derived factor 1 alpha
SLRP	Small leucine-rich proteoglycans
SVF	Stromal vascular fraction
TCPS	Tissue culture polystyrene
TGF-β1	Transforming growth factor beta 1

TIMP-1	Tissue inhibitor of metalloproteinase 1
TNF-α	Tumour necrosis factor alpha
VEGFA	Vascular endothelial growth factor A
VEGFR-1	Vascular endothelial growth factor receptor 1

Chapter 1

1 Literature review

1.1 Overview of the integumentary system

The integumentary system, comprised of the skin and its appendage structures, along with the subcutaneous adipose tissue layer, is one of the largest organ systems in the body (Figure 1.1)[1]. The skin consists of two distinct layers, termed the epidermis and dermis. The epidermis is composed of a thin layer of keratinized squamous epithelium, which is largely made up of keratinocytes, but also contains melanocytes, Langerhans cells and Merkel cells[2]. The epidermis is avascular and dependent on the dermal layer for oxygenation and nutrients[2]. The epidermal layer is organized into several sub-layers, from the deep stratum basale, also referred to as the stratum germinativum, to the apical stratum corneum.

The dermal layer is located between the epidermis and the subcutaneous tissues. The dermis is enriched in lymphatic vessels, blood vessels, and nerve endings necessary for the physiological function of the skin[3]. Further, the dermis also contains hair follicles, as well as apocrine, sebaceous and eccrine glands[4]. In addition, the dermal layer contains a high density of collagen and elastin, which are essential for maintaining the structural integrity and elasticity of the skin. Notably, collagen accounts for approximately 70% of the dry mass of the skin[2].

The hypodermis, also known as subcutaneous tissue, is a part of the integumentary system that is located below the dermis[4]. The subcutaneous tissue layer is predominantly composed of adipose tissue that can be anatomically divided into two layers: the superficial adipose tissue layer and the deep adipose tissue layer[5]. While the superficial layer can be variable in depth depending on the fat depot, it averages around 1 cm in thickness[6]. In addition to being rich in adipocytes, this layer contains a dense network of blood and lymphatic vessels. Adipose tissue in this layer is organized into lobules that are separated by connective tissue[6]. The deep adipose tissue layer is separated from its superficial counterpart by a thin layer of highly fibrous fascia, known as the *fascia*

superficialis[5]. While the superficial fat layer is relatively resistant to hypertrophic and hyperplastic expansion in adult humans, the deep fat layer accounts for the majority of overall adipose tissue growth in instances of increased fat accumulation[6]. Additionally, fat tissue in this layer is also more sensitive to glucose, which could explain its susceptibility for expansion compared to the superficial adipose tissue depots[6]. Functionally, the subcutaneous adipose tissue layer is an important endocrine organ, and has been shown to regulate metabolism[7–10]. Additionally, subcutaneous adipose tissue is involved in thermoregulation, and also provides structural support to the dermis and epidermis[4].

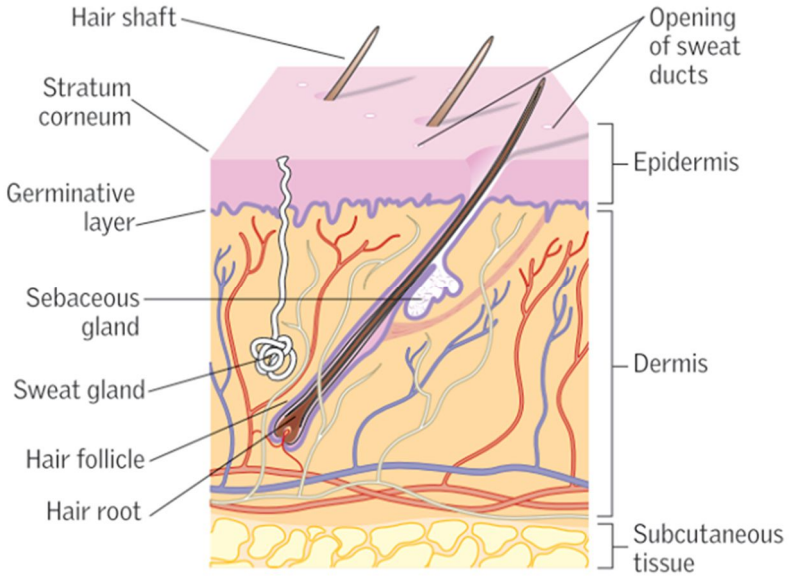

Figure 1.1 Overview of the structure of the integumentary system showing the anatomy of the epidermis, dermis and hypodermis (subcutaneous tissue). Image re-printed with permission from publisher[1].

1.2 Clinical need for soft tissue augmentation strategies

Subcutaneous adipose tissue damage or loss are prevalent issues that can be caused by trauma, birth defects, aging and surgical procedures, such as oncologic resection surgeries[11]. It was estimated that over 5.8 million reconstructive procedures were performed in the U.S. in 2018 alone to address these issues, including more than 480,000 scar, burn or laceration repairs, 101,000 breast reconstructions, and 4.4 million tumour

removals[12]. Existing clinical interventions and therapeutic strategies generally aim to augment the volume of the damaged or missing tissues.

The current gold standard to correct large-volume defects is the transfer of vascularized flaps of skin, fat and muscle from a distant depot on the patient's body[12]. For example, deep inferior epigastric perforator flaps are common procedures where subcutaneous tissues and a small portion of the muscle tissue from the abdominal region of the patient are directly grafted to augment the breast[13]. However, these types of surgical interventions are associated with serious complications including tissue necrosis, weakening of the abdominal wall, and abdominal hernia[14–16].

Common clinical interventions for medium-volume defects (50 – 150 cc) include autologous fat grafting, where subcutaneous adipose tissue from a distal fat depot is extracted, processed and injected into the target site[17,18]. This strategy requires a high degree of surgical precision, and the grafted tissue may be quickly resorbed following implantation due to a lack of supporting vascularization[19]. In addition, poorly vascularized fat grafts can lead to complications such as the formation of oil cysts and calcification[13].

For small-volume augmentations, such as the treatment of wrinkles, dermal fillers are the primary treatment strategies. These dermal fillers are typically composed of injectable hyaluronic acid (HA) formulations[20–22]. However, the augmentation effects of these fillers are transient, typically lasting 3-6 months[19]. Inappropriate techniques can lead to swelling, pain, infections and tissue necrosis[19]. Additionally, these materials do not support the natural regeneration of host adipose tissue[23].

While existing clinical interventions can address soft tissue damage or loss to varying degrees, these treatment strategies are associated with risks and complications as outlined above. In addition, these strategies have not demonstrated the capacity to support tissue regeneration, which often leads to transient and/or unpredictable augmentation[22]. The lack of intervention strategies to address soft tissue damage that are effective in the long-term can lead to anxiety and depression[24]. For patients with injuries caused by trauma or cancer, an inability to address these issues can also precipitate post-traumatic stress

disorder (PTSD)[25]. As such, there is a critical need for alternative clinical treatment strategies that can provide long-term augmentation and support the stable and predictable regeneration of damaged or deficient subcutaneous adipose tissue.

1.3 Adipose tissue engineering

Adipose tissue engineering has generated promising advances toward strategies that can promote subcutaneous adipose regeneration. A common approach involves a combination of pro-regenerative cell populations and biocompatible scaffolds[26–28]. The scaffolds can provide immediate volume augmentation and serve as a delivery vehicle for the regenerative cell populations. In addition, depending on the properties of the biomaterials, they can also provide the necessary biomechanical and biochemical support to promote host-derived regenerative processes[29–31]. Existing biomaterials that have been investigated for adipose tissue engineering applications can be categorized as either synthetic polymers, such as poly(lactic-co-glycolic) acid (PLGA), polyglycolic acid (PGA) and polyethylene glycol (PEG)[32–34], or naturally-derived biomaterials, which include extracellular matrix (ECM) components such as collagen, HA, or decellularized ECM bioscaffolds[35–37]. Key studies involving a variety of scaffolds will be described in more detail in Section 1.6.

Pro-regenerative cell populations are often delivered within the bioscaffolds to help stimulate regeneration. To date, the majority of studies have incorporated either mature adipocytes[38] or adult mesenchymal stromal cell (MSC) populations[39–41]. The specifics of these cell populations will be discussed in detail in the next section.

1.4 Cell sources for adipose tissue engineering

To develop a therapeutic strategy for adipose tissue regeneration, potential cell sources should be readily available and accessible, and ideally provide a high density of pro-regenerative cells to support clinical translation in humans[42]. A range of cell sources such as adipocytes, embryonic stem cells (ESCs), induced pluripotent stem cells (iPSCs) and MSC populations, such as bone marrow-derived MSCs and adipose-derived stromal cells (ASCs) have been examined for this application[43–46]. This section will discuss the

specifics of these cell populations and how they can contribute to the processes involved in adipose tissue regeneration, with a particular focus on MSCs as the most predominant cell source studied to date.

Among cell types investigated for adipose tissue regeneration, mature adipocytes have been used to provide immediate tissue augmentation to the target site, similar to autologous fat grafting[47]. While studies have demonstrated that this cell population could be promising, it is unclear if adipocytes can survive long-term and maintain volume over time. A recent study by Eto *et al.* demonstrated that human adipocytes that were delivered *in vivo* into mice did not survive under hypoxia[48]. In particular, the lack of vascularization near the newly grafted tissue led to the loss of ~80% of the delivered adipocytes within 3 days[48]. Additionally, mature adipocytes can be fragile to handle, which could add further challenges for clinical translation[49,50]. In light of these findings, studies have largely shifted away from delivering mature adipocytes.

In addition to mature adipocytes, ESCs, a population of pluripotent cells derived from the inner cell mass of blastocysts[51], have also been studied as a potential cell source for adipose tissue engineering[52]. This cell population has the capacity to differentiate into mature cells derived from the endoderm[53,54], mesoderm[55,56] and ectoderm[57,58] layers, which makes them promising for a wide range of therapeutic applications. However, grafting ESCs into patients had led to the formation of teratomas[59]. This, in addition to their embryonic sourcing, raises ethical concerns associated with their use[60]. Similarly, iPSCs generated from reprogrammed adult somatic cells have also been considered for the regeneration of adipose tissue[61]. However, the process involved in reprogramming has the potential to be tumorigenic and delivery of these cells into patients can also lead to teratoma formation[61]. Overall, while ESCs and iPSCs have demonstrated promise for adipose tissue regeneration, their associated safety and ethical concerns represent barriers to clinical translation that currently limit their investigation for this application.

1.4.1 Mesenchymal stromal cells

MSCs are a heterogenous cell population that was first identified within the bone marrow[62]. Since then, MSCs have also been isolated from numerous other sources

including adipose tissue[63], synovial fluid[64], umbilical cords[65] and peripheral blood[66]. To address their diverse sourcing and heterogenous nature, MSCs were broadly defined as a cell population that is adherent to tissue culture plastic, expresses the cell surface markers CD73, CD90 and CD105, and lacks expression of CD14, CD31 and CD45[67]. Additionally, MSCs also have the capacity to undergo adipogenic, chondrogenic and osteogenic differentiation when cultured *in vitro* under inductive conditions[67].

1.4.2 Adipose-derived stromal cells

The stromal vascular fraction (SVF) of adipose tissue contains fibroblasts, committed adipogenic progenitors, endothelial cells, hematopoietic cell populations and a small subpopulation of MSC-like cells called ASCs [68]. The SVF can be isolated from adipose tissue through enzymatic digestion with collagenase, followed by centrifugal separation and filtration techniques[69]. The ASCs are broadly classified as the population within the SVF that adheres to tissue culture polystyrene (TCPS)[69]. It is estimated that between 5 x 10^5 to 2 x 10^6 nucleated cells can be isolated per gram of fat, and ASCs account for 20% of this population[70,71]. As such, ASCs are considerably more abundant than MSCs within the bone marrow, which are estimated to represent only 0.04% of the nucleated cell population[71]. Additionally, ASCs can be isolated from surgically discarded fat, which is a highly abundant and readily available source material, making them a particularly promising source of regenerative cells for adipose tissue engineering strategies.

In addition to being plastic-adherent, ASCs are also defined by the expression of selected cell surface markers and their potential to undergo tri-lineage differentiation into adipocytes, chondrocytes and osteoblasts when induced in culture[72]. Immunophenotypically, ASCs are characterized by their positive expression of CD29, CD44, CD73, CD90 and CD105 and their lack of expression of CD31 and CD45. Additionally, ASCs may also have variable expression of CD26, CD34 and CD146[70]. A comprehensive list of ASC surface markers and their associated functions is shown in Table 1.1.

Table 1.1 Key positive, negative and variable ASC surface markers.

Positive Surface Markers		
Surface Marker	**Protein**	**Function(s)**
CD29	Integrin β1	Component of cell surface integrins, which can mediate cell adhesion and a diverse range of functions including tissue regeneration and immunoregulation[73]
CD44	Homing cell adhesion molecule	Cell surface glycoprotein, receptor for hyaluronic acid[74,75]
CD73	Ecto-5'-nucleotidase	Catalyzes the production of ECM adenosine, modulates transforming growth factor beta 1 (TGF-β1) expression[76]
CD90	Thymocyte differentiation antigen 1	Maintenance of progenitor-like phenotype[77]
CD105	Endoglin	Surface glycoprotein, component of the TGF-β1 receptor complex[78]
Negative Surface Markers		
Surface Marker	**Protein**	**Function(s)**
CD31	Platelet endothelial cell adhesion molecule 1	Endothelial cell marker. Attenuates VEGFA-mediated angiogenesis[79]
CD45	Protein tyrosine phosphatase receptor type C	Hematopoietic marker. Membrane glycoprotein involved in cell activation and differentiation[80]
Variable Surface Markers		
Surface Marker	**Protein**	**Function(s)**
CD26	Dipeptidyl peptidase 4	Modulates macrophage recruitment by degrading key cytokines and paracrine factors[81,82] Associated with a pro-fibrotic phenotype in dermal fibroblast populations[83]
CD34	Transmembrane glycoprotein	Associated with maintenance of clonogenicity[84] and pro-angiogenic functionality[85].
CD146	melanoma cell adhesion molecule	Expressed in vascular endothelial cells, smooth muscle cells and pericytes. Cell surface receptor for laminin, mediates blood vessel maturation[86,87]

As mentioned, in addition to their characteristic cell surface marker expression profile, ASCs also have the capacity to differentiate into adipocytes, chondrocytes and osteoblasts in culture using differentiation media formulations incorporating lineage-specific supplements and factors[88]. For example, human ASCs can be induced to undergo

adipogenic differentiation in culture by administering adipo-inductive hormones and glucocorticoids, such as hydrocortisone, dexamethasone and insulin[89]. The sequential addition of these factors can lead to growth arrest, and activation of the transcription factors CCAAT/enhancer binding protein alpha (CEBP-α) and peroxisome proliferator-activated receptor gamma (PPAR-γ)[90,91]. Activation of these two master regulators of adipogenesis causes upregulation of a range of genes that are associated with intracellular lipid accumulation and adipogenic differentiation[92]. Similarly, ASCs can be induced to undergo chondrogenic differentiation by administering cytokines and growth factors such as transforming growth factor-beta (TGF-β1) and bone morphogenetic protein-2 (BMP-2), to cells cultured in 3-D aggregates[89]. These culture conditions induce the ASCs to undergo cellular condensation and commit towards chondrogenic differentiation[93]. ASCs can also be induced to undergo osteogenic differentiation using a combination of dexamethasone, ascorbic acid and β-glycerophosphate[94]. These factors activate the transcriptional factor, Runt-related transcription factor 2 (RUNX-2), which commits ASCs towards the osteogenic lineage[94].

ASC isolation protocols were initially developed using lipoaspirated fat from rats[95]. Since then, the isolation protocols have been adapted for numerous tissue sources including human adipose tissue[96]. Advances in this field have led to an increasingly diverse range of isolation methodologies[69]. One recent study compared several common isolation protocols, including methods with collagenase digestion, trypsin digestion, red blood cell lysis buffer solution-based isolation and a centrifugation-based protocol for lipoaspirated human fat tissue[97]. This study demonstrated that while ASC yield was higher with the collagenase digestion method, there was no difference in cell viability and key cell surface marker expression between the protocols[97]. Recently, a study by Priya *et al.* showed that outgrowth cultures from extracted adipose tissue could yield ASCs with similar cell surface marker expression patterns and tri-lineage differentiation potential as compared to cells extracted through traditional enzymatic isolation methods[98]. Additionally, magnetic bead purification methods have also been developed, where cells with negative markers of ASCs, such as CD31 and CD45, were removed from the SVF using antibodies conjugated to magnetic beads[99,100]. While this was effective at obtaining a more homogenous starting cell population, it did not significantly impact the expression

of positive ASC cell surface markers or the capacity of the cells for tri-lineage differentiation.

1.5 Mechanisms of ASC-mediated tissue regeneration

While past studies have attempted to harness the differentiation potential of ASCs for adipose tissue engineering, recent work has suggested that transplanted ASCs primarily stimulate regeneration by remodeling the cellular microenvironment and secreting paracrine factors that promote host-derived angiogenesis, macrophage recruitment and adipogenesis[101–103].

ASCs are highly metabolically active and secrete a range of ECM components, growth factors and cytokines[104–106]. A recent study comparing the results from 5 independent studies on the ASC secretome showed 68 proteins that were expressed in common[107]. Interestingly, ASCs were shown to secrete a range of ECM-associated proteins, most notably, collagen I, II, III, IV, V, VI, XII, fibronectin, laminin, heparan sulfate (HS), matrix metalloproteinase 2 (MMP-2) and tissue inhibitor of metalloproteinases-1 (TIMP-1)[105], which suggests an active role in both the degradation and deposition of ECM components. Their capacity for ECM remodeling is supported by a previous *in vitro* study that demonstrated that ASCs seeded in a fibrin-based matrix could degrade the hydrogel via matrix metalloproteinase 14 (MMP-14) activity and deposit collagen type IV, which led to an increased invasion and tubule formation by seeded human umbilical vein endothelial cells (HUVECs)[108]. In addition to supporting angiogenesis, ASCs can also participate in remodeling the ECM to establish a more pro-adipogenic microenvironment. Previously, ASCs were found to degrade a collagen-based matrix *in vitro* and deposit collagen type IV[109]. In particular, the deposition of collagen VI has been shown to play an important role in adipogenesis[110]. Collectively, ECM remodeling is a mechanism for ASCs to mediate both angiogenesis and adipogenesis to support adipose tissue regeneration.

ASCs are well recognized for their capacity to support regeneration through the secretion of paracrine factors and cytokines that mediate angiogenesis and modulate the immune response[101,107,111]. Previous studies have shown that ASCs can be stimulated to produce

pro-angiogenic factors such as basic fibroblast growth factor (bFGF), hepatocyte growth factor (HGF), TGF-β1, and vascular endothelial growth factor (VEGFA)[112–115]. For example, a previous study showed that HGF can increase the diameter of endothelial tubules *in vitro*, whereas VEGFA resulted in an increased branching of tubules[115], suggesting that these two pro-angiogenic factors that can be secreted by ASCs can play distinct and complementary roles during neovascularization. Additional details of the functions of key angiogenic factors secreted by ASCs are outlined in Table 1.2.

Table 1.2 Key pro-angiogenic factors secreted by human ASCs and their functions

Pro-angiogenic Factors	Function(s)
Basic fibroblast growth factor (bFGF)	Promotes endothelial cell survival, proliferation, migration and differentiation[112] Binds and activates fibroblast growth factor receptor 1 on endothelial cells, and activates MAPK to promote angiogenesis[116]
Granulocyte colony stimulating factor (G-CSF)	Stimulates the proliferation, survival and recruitment of innate immune cells[113] Chemoattractant for endothelial progenitor cells; promotes the differentiation of endothelial cells[117]
Hepatocyte growth factor (HGF)	Promotes endothelial cell survival, proliferation and mobilization[114] Creates an autocrine loop that drives angiogenesis[118] Works synergistically with VEGFA to increase vessel diameter[115]
Vascular endothelial growth factor A (VEGFA)	Potent driver of vessel sprouting and neovascularization[115]
Platelet-derived growth factor (PDGF-B)	Promotes endothelial cell proliferation[119] Chemoattractant for pericytes and promotes blood vessel stabilization[120,121]
Angiopoietin 1 (Ang-1)	Promotes endothelial cell survival, proliferation and motility[122] Supports blood vessel maturation and stabilization[122]

In addition to angiogenesis, ASCs can promote tissue regeneration by mediating both pro-inflammatory and anti-inflammatory immune responses[123,124]. ASCs can be induced towards a pro-inflammatory phenotype by treatment with lipopolysaccharide (LPS)[125,126]. Upon induction, ASCs can produce an array of pro-inflammatory cytokines, including tumor necrosis factor alpha (TNF-α)[127]. At the molecular level, TNF-α can not only lead to an increased expression of pro-inflammatory cytokines by effector cells, such as monocytes, it can also act in an autocrine loop on ASCs, which leads to the increased expression of additional pro-inflammatory mediators, such as interleukin 6 (IL-6), interleukin 8 (IL-8), monocyte chemoattractant protein-1 (MCP-1) and interferon gamma (IFN-γ)[128,129]. Interestingly, TNF-α also plays an important role in angiogenesis[130,131]. An *in vitro* study by Yuan *et al.* demonstrated that TNF-α can increase the expression of VEGFA and promote tube formation in human omental tissue microvascular endothelial cells[127].

While the transient exposure of MSCs to these factors could be pro-angiogenic, chronic exposure to TNF-α and the pro-inflammatory mediator interferon gamma (IFN-γ) have been shown to impair the proliferation and differentiation capacity of MSCs *in vitro* and in athymic nude mice *in vivo*[129]. IFN-γ can also increase the expression of inducible nitric oxide synthase (iNOS) and the production of nitric oxide (NO)[132]. In an inflamed microenvironment, NO can mediate tissue regeneration and inhibit fibrotic pathways[133]. Moreover, interferon gamma (IFN-γ), along with prostaglandin E2 (PGE-2) can also promote the expression of the anti-inflammatory cytokine interleukin-10 (IL-10), which subsequently downregulates the expression of pro-inflammatory cytokines in ASCs as well as immune cell populations[134,135]. Additionally, IL-10 can promote the polarization of macrophages towards a more pro-regenerative phenotype[136]. A detailed discussion of the roles of IL-10 and pro-regenerative macrophage populations in tissue regeneration is provided in Section 1.9.2. A list of key immunomodulatory cytokines secreted by ASCs is summarized in Table 1.3.

Table 1.3 Key pro- and anti-inflammatory cytokines expressed by ASCs.

Cytokines	Function(s)
Tumor necrosis factor-alpha (TNF-α)	Binds to surface receptors on monocytes, T cells, endothelial cells and fibroblasts, activates IKK/NFκB signaling cascade[137] to modulate cell survival[138] and mobilization[139] Promotes the release of pro-inflammatory mediators[140], such as IL-6[141] and IFN-γ[142]
Interleukin-6 (IL-6)	Binds to surface receptors on monocytes and endothelial cells, leading to survival, proliferation and differentiation of monocytes[143,144]
Interleukin-10 (IL-10)	Expression in ASCs induced by IFN-γ and PGE-2[145] Downregulates the expression of pro-inflammatory factors (e.g. TNF-α)[146] Promotes the polarization of monocytes towards a pro-regenerative phenotype and inhibits the maturation of dendritic and pro-inflammatory macrophages[147]
Interferon gamma (IFN-γ)	Activates pro-inflammatory immune cells such as T cells, natural killer cells[148] Upregulates iNOS expression in ASCs[132]
Nitric oxide (NO)	Inhibits fibrotic pathways by inhibiting the TGF-β1 signaling pathway[133] Inhibits T-cell activation by inhibiting STAT5 and the expression of pro-inflammatory cytokines[149]

1.6 Biomaterials for adipose tissue engineering

Both synthetic and naturally-derived biomaterials have been explored for adipose tissue engineering. Scaffolds that are fabricated from synthetic materials can offer advantages in terms of their tunability, as they typically have more highly adjustable mechanical and chemical properties[150]. Biodegradable polymers such as poly-lactic acid (PLA) and PGA have been investigated for adipose tissue engineering[44,151–153]. For example, PLA-based scaffolds, when seeded with human ASCs and implanted into the muscularis layer of the

subcutaneous tissue of nude rats, promoted adipose tissue formation after 4 weeks[44]. Furthermore, this study demonstrated that seeding the PLA scaffold with the ASCs promoted the degradation of the polymer and supported adipogenesis *in vivo*[44]. Similarly, Weiser *et al.* investigated the adipogenic and angiogenic potential of PGA-based scaffolds[151]. When these scaffolds were seeded with 3T3-L1 preadipocytes exposed to adipogenic induction media and implanted subcutaneously into athymic nude mice, blood vessels and adipose tissue were observed within the scaffolds at 12 weeks[151].

PLGA, a co-polymer of PLA and PGA, has also been investigated for adipose tissue engineering, and has been shown to support adipogenesis in animal models with moderate success[154–157]. For example, Patrick *et al.* demonstrated that PLGA, when seeded with rat ASCs, can support the formation of adipocytes at 2 weeks following implantation in an immunocompetent rat model[158]. Similarly, when PLGA spheres were seeded with rabbit bone marrow-derived MSCs that were transfected to express green fluorescence protein (GFP), exposed to a short-period of adipogenic induction, and implanted in nude mice for 2 weeks, GFP^+ cells with lipid accumulation were observed in the implanted scaffold[159]. Moreover, a study by Cho *et al.* showed that PLGA scaffolds seeded with human ASCs and loaded with bFGF can also support adipose tissue formation in nude mice at 6 weeks[157].

Overall, while biodegradable synthetic materials have shown promise in supporting adipose tissue formation in rodent models, these effects are largely transient, and the scaffolds are unable to maintain long-term volumetric augmentation following degradation of the polymer[44]. Further, while providing a supporting structure, synthetic polymers typically lack the innate bioactivity of naturally-derived biomaterials, which have greater potential to have intrinsic pro-angiogenic and/or pro-adipogenic properties that may be favorable for adipose tissue regeneration[160–162].

1.6.1 Naturally-derived biomaterials

In addition to synthetic polymers, naturally-derived biomaterials have also been investigated for adipose tissue engineering. Broadly, these biomaterials can be categorized based on their compositional complexity. For example, purified structural

components of the ECM, such as HA and collagen, have been fabricated into bioscaffolds for adipose tissue engineering[163–165]. In addition, more highly complex biomaterials derived from decellularized tissues have also been explored, which contain a diverse range of ECM components[166–170].

HA is a naturally-derived biomaterial found within the ECM of connective, epithelial and neural tissues[171]. HA is a non-sulfated glycosaminoglycan (GAG) that plays an important role in tissue hydration, nutrient diffusion and proteoglycan organization[172–174]. HA has been studied for adipose tissue regeneration because its mechanical properties can mimic native soft tissues, and it has the potential to be fabricated into an injectable material[163]. In addition, studies have shown that HA scaffolds can support the attachment, proliferation and adipogenic differentiation of seeded ASCs in culture[175]. The adipose tissue regenerative effects of HA have also been examined in animal models. Borzacchiello *et al.* designed HA-based scaffolds that maintained mechanical and viscoelastic properties similar to that of adipose tissue when implanted into rats for up to 12 weeks[164]. When seeded with human ASCs and implanted into athymic nude mice for 3, 5 and 8 weeks, HA-based scaffolds demonstrated increased cell infiltration and blood vessel formation compared to unseeded control scaffolds, as well as hydrogels without HA[176]. Moreover, ASC-seeded HA-based scaffolds were shown to support blood vessel and adipose tissue formation when delivered into the subcutaneous tissue of pigs for 6 weeks, although the implants were highly degraded at this timepoint[36]. Collectively, these studies demonstrated that HA-based scaffolds have the potential to support adipose tissue regeneration, but have been unable to maintain long-term volume augmentation when tested in animal models due to rapid scaffold degradation.

HA-based composite materials have also been explored with the goal of improving handleability, as well as enhancing the stability and tuning the mechanical properties of the scaffolds[177–181]. For example, composite HA-g-poly(N-isopropylacrylamide) scaffolds have been developed, which can function as thermo-responsive injectable biomaterials[177]. Furthermore, these composite hydrogels could be crosslinked *in situ,* supported cell infiltration and were stable when delivered subcutaneously in athymic nude mice over 5 days[177]. In another study, HA was incorporated with gelatin to form naturally-derived

composite hydrogels[165]. This study showed that porcine ASCs encapsulated in the HA-gelatin composites could survive and undergo adipogenic differentiation *in vitro,* as well as promote adipose tissue remodeling *in vivo* when implanted in athymic nude mice and pigs for 8 weeks[165].

In addition to GAGs such as HA, collagen has also been used to fabricate bioscaffolds for adipose tissue engineering[160–162,182–185]. Collagen is a highly abundant and essential structural component of the ECM that is highly conserved between species[186–188]. Culture studies have confirmed that collagen-based scaffolds can support the attachment of MSCs[126] and ASCs[138]. Further, previous animal studies have demonstrated that collagen scaffolds have the potential to both augment volume and act as a carrier for growth factors and/or regenerative cell populations[183,184,189]. For example, increased blood vessel formation and adipose tissue remodeling were observed at 6 weeks in collagen-based microspheres loaded with bFGF that were implanted into C57BL/6 mice compared to control scaffolds without bFGF[190]. This observation was further supported by a study by Hiraoka *et al*., who demonstrated that composite collagen and gelatin bioscaffolds that were loaded with bFGF could support angiogenesis and adipogenesis when delivered into the inguinal tissues in Wistar rats at 6 weeks[191]. In addition, a study by von Heimberg *et al.* demonstrated that seeding human ASCs on collagen sponge bioscaffolds better supported angiogenesis than unseeded controls when implanted subcutaneously in athymic nude mice for 12 weeks[162]. Collectively, these studies indicate that collagen-based bioscaffolds alone may not adequately support adipose tissue regeneration, and often require additional cellular components or growth factors to enhance their pro-regenerative capacity.

Collagen scaffolds can also be combined with other naturally-derived or synthetic materials to form composite scaffolds that may have enhanced properties for adipose tissue engineering[182,185,189,192,193]. For example, composite chitosan/collagen scaffolds seeded with rat ASCs were found to better support adipogenesis and angiogenesis as compared to unseeded control scaffolds when implanted in Lewis rats as early as 14 days[184]. In another study, collagen scaffolds combined with alginate microspheres seeded with both adipogenic-induced human ASCs and HUVECs were shown to better support

adipogenesis and angiogenesis than acellular controls when implanted into athymic nude mice at 12 weeks[185]. Additionally, this study also demonstrated that composite collagen scaffolds with human ASCs and HUVEC showed greater volume retention than the acellular controls at 12 weeks[185]. As another example, Zhang *et al.* demonstrated that composite chitosan-collagen scaffolds incorporating PEG/PLGA microspheres loaded with VEGFA and seeded with human ASCs showed enhanced adipose tissue remodeling, as well as infiltration of $CD31^+$ endothelial cells and $CD163^+$ pro-regenerative macrophages when compared to control scaffolds without PEG/PLGA microspheres or human ASCs[193].

Collectively, prior studies have demonstrated that naturally-derived bioscaffolds such as HA and collagen can act as supportive cell and/or growth factor delivery platforms for adipose tissue engineering. However, these materials often degrade rapidly and are unable to provide long term volumetric augmentation required to be clinically translatable.

1.6.2 Extracellular matrix-derived bioscaffolds

The ECM is the non-cellular structural and functional network of proteins, proteoglycans, and glycoproteins that surrounds cells within tissues[31,194,195]. Together, these components provide biochemical, structural and biomechanical cues that regulate cell behaviour[31,194,195]. ECM proteins such as collagen, laminin and fibronectin not only provide important structural support for cells, but they also contain binding sites for cell surface receptors such as integrins, which can guide cell attachment and function[31,196–198].

Collagen is the most abundant structural protein in the ECM. To date, 29 types of collagen have been identified, with collagen I, II, III, IV and V being the most abundant within human tissues[31]. A characteristic feature of collagens is their triple helical structure comprised of three alpha chains[186]. However, there can be interruptions within the helical structures that enable interactions with other matrix proteins[31]. Many types of collagens can form fibrils, such as I, II, III, V, IX, XIV, XVII[186] . Collagen IV is a network-type collagen that forms the structural meshwork of the basement membrane, which is present in high abundance around adipocytes[199]. Collagens contain multiple

receptor-binding sites that facilitate cell attachment. For example, a well-studied specialized collagen binding site is the GFOGER motif that binds with α1β1 and α2β1 integrins with high affinity[186,200] and also bind to integrins with a β_2 component, such as $\alpha_m\beta_2$ and $\alpha_x\beta_2$ integrins[201].

In addition to collagen, fibronectin is also highly abundant in the adipose tissue ECM[199]. This cell-adhesive glycoprotein associates with collagen and can also form fibrillar structures. While fibronectin can exist in a soluble form in plasma, it is insoluble in the ECM[202,203]. Functionally, fibronectin can bind with integrin receptors on the cell surface and mediate cell adhesion. For example, one of the most well studied adhesion motifs is the tripeptide Arg-Gly-Asp (RGD) sequence, which enables cell adhesion through integrins such as α4β1[31], αvβ3 and α5β1[204]. In addition, fibronectin can also bind to heparan sulfate, which acts as a reservoir for growth factors in the ECM[205,206]. In adipose tissue, fibronectin is associated with the pro-inflammatory cytokine, TNF-α, and the cell surface receptor preadipocyte factor-1 (Pref-1), which play important roles in mediating angiogenesis and adipogenesis, respectively[207,208].

Laminin is another important structural and bioactive component of the adipose tissue ECM. Laminins are a family of heterotrimeric glycoproteins that are composed of an α-, β- and γ- chain and are a key component within all basement membranes[209]. Functionally, laminin binds to cell surface integrins, as well as glycoproteins, dystroglycan and syndecan within the ECM[209,210]. The interaction of laminin with these extracellular components is crucial for cell adhesion, morphogenesis and differentiation, as well as tissue integrity[211–213].

Functioning in concert with the structural proteins within the ECM, proteoglycans can influence the cellular response via biochemical cues[214,215]. Additionally, with their high capacity to hold water, proteoglycans can also be important in maintaining the structural integrity and mechanical properties of the ECM. Proteoglycans are composed of a core protein and one or more GAG chains[210]. GAGs are linear polysaccharides that are negatively charged, which enables them to sequester growth factors, cytokines and chemokines[214,216]. As such, GAGs often serve as a reservoir for growth factors. One such

GAG that is present in adipose tissue is HA[217]. As discussed in the previous section, HA has been used as an injectable dermal filler due to its high abundance and compatibility with adipose tissue. In addition to contributing to the structural integrity of the adipose tissue ECM, HA has also been implicated in adipose tissue metabolism, as recent studies have shown that it can mediate insulin sensitivity[218,219] and lipid biogenesis[220].

The combination of structural proteins and proteoglycans can guide cell behavior via biomechanical and biochemical cues[211]. Cells can also remodel the ECM by degrading existing components and depositing new matrices. The degradation of the existing ECM is achieved via the secretion of extracellular proteases[221]. To date, over 569 matrix-associated proteases have been identified[221]. These proteins can be classified based on their roles and properties in protein hydrolysis and can be categorized as MMPs, serine proteases, cysteine proteases, aspartic acid proteases and threonine proteases[222].

By far the most well characterized ECM proteases are the MMPs, which are secreted by the cells as inactive pro-enzymes, and can be converted into an active form by pro-protein convertases[194,223,224]. Once activated, MMPs can degrade structural proteins in the ECM. Moreover, the enzymatic activities of MMPs can be regulated by glycoproteins such as TIMPs[210]. In addition, studies have shown that ECM-bound growth factors and cytokines liberated through matrix degradation can act on cell surface receptors, such as epidermal growth factor receptor (EGFR) and insulin-like growth factor receptor (IGFR) to downregulate the production of MMPs[57].

Recognizing the innate capacity of the ECM to direct cell function, there has been growing interest in the development of ECM-derived bioscaffolds for a broad range of applications in tissue engineering[37,166,169,226–232]. One of the earliest forms of ECM-derived biomaterials is Matrigel®, which is comprised of purified basement membrane components secreted by Engelbreth-Holm-Swarm mouse sarcoma cells[233]. While the precise composition of Matrigel® is not fully defined, it contains structural proteins, such as collagen IV and laminin, as well as heparan sulfate[233]. In previous studies, Matrigel® was shown to support angiogenesis and adipogenesis when injected with bFGF in athymic nude mice for 6 weeks[190]. Furthermore, seeding the bFGF-loaded Matrigel® with

human ASCs was shown to further promote host-derived angiogenesis and adipogenesis in the same animal model for up to 9 weeks[234]. While Matrigel® has shown promise in promoting tissue regeneration, its tumour cell origin represents a significant barrier to clinical translation[235].

Tissue decellularization is another approach that has been applied to generate a broad range of tissue-specific ECM-derived bioscaffolds[195,236,237]. In general, the goal of decellularization is to remove antigenic cellular components, including cellular proteins, lipids and nucleic acids, while preserving the structure and composition of the native ECM as much as possible[228,236]. Decellularization is typically accomplished by subjecting tissues to a combination of mechanical, chemical and biological treatment steps that lyse cells and extract cellular debris[236]. Mechanical and physical treatments are applied to breakdown cellular structures and expose the intracellular antigens[236]. These methods are often supplemented with chemical treatments, such as acid, base and/or detergent extractions, to degrade and extract cellular components[236]. Furthermore, biological treatments in the form of enzymes such as trypsin can further facilitate cell disruption, and the addition of DNase and RNase can cleave residual nucleic acids[236]. It is inevitable that the decellularization processes will alter the native ECM composition to some extent, as well as causing some structural changes. However, the degree of disruption is highly dependent on the nature of the tissues being processed and the protocols used for decellularization. To date, several types of decellularized ECM scaffolds have been investigated for applications in adipose tissue regeneration, as discussed below.

Decellularized placental matrix (DPM) has been studied for adipose tissue engineering[26,238,239]. The placenta is rich in ECM and is composed of structural proteins including collagen I, III, IV, V, VI and laminin, many of which are present in adipose tissue[238]. In addition, it is a reservoir for growth factors and has a rich vascular network that may provide structural cues that are conducive for angiogenesis[240]. The DPM was demonstrated to support the attachment and adipogenic differentiation of human ASCs[239]. In a subsequent study, the DPM was combined with crosslinkable HA hydrogels as a possible strategy to enhance volume augmentation and modulate the cellular response to promote adipose tissue regeneration[239]. Subsequently, ASCs were seeded in the DPM-HA

composite scaffolds or DPM alone and implanted subcutaneously in athymic nude mice for up to 8 weeks[26]. Results from this study showed that both types of scaffolds macroscopically retained their volume and were able to promote blood vessel formation and adipose tissue remodeling within the implants, with mouse-to-mouse variability observed in the response[26].

In addition to DPM, decellularized dermal matrix (DDM) has also been explored for adipose tissue engineering[241–243]. Decellularized dermal tissue has been used clinically in plastic surgery because of its low immunogenicity and robust mechanical properties[242]. In a previous study, human ASCs were found to attach, survive, proliferate and remodel DDM *in vitro*[241]. Subsequently, when the ASC-seeded DDM was implanted *in vivo* in nude mice, angiogenesis was observed in the bioscaffolds as early as 2 weeks[243].

Collectively, ECM-derived bioscaffolds such as Matrigel®, DPM and DDM have shown promise in supporting angiogenesis and to a certain degree, adipogenesis[238,243,244]. However, it is possible that the regenerative effects could be further enhanced by applying a tissue-specific approach to designing ECM-derived bioscaffolds. For example, adipose ECM-derived bioscaffolds can be fabricated to possess biomechanical properties that closely mimic the native tissues, which could be favourable for adipose tissue regeneration[245–247]. Additionally, the composition of the ECM is also tissue-specific, containing a unique array of bioactive factors that can influence cell behaviour. Together, this provides a strong rationale for exploring a tissue-specific approach to designing ECM-derived bioscaffolds for adipose tissue regeneration.

1.6.3 Adipose tissue-derived bioscaffolds

Adipose tissue is important for maintaining energy homeostasis and also supports many of the endocrine functions of the body[248]. This organ is composed largely of adipocytes, with preadipocytes, endothelial cells, fibroblasts, immune cells and ASCs also found within the SVF[70]. The mature adipocytes are encased in a meshwork of collagen type IV[187]. Previous studies have demonstrated that the adipose tissue ECM plays a crucial role in regulating the metabolic function of this organ[199,249–252]. For example, Khan *et al.* demonstrated that an imbalance in collagen type IV and collagen type VI in the ECM of

adipose tissue in collagen type VI knockout mice leads to uninhibited hypertrophic expansion of adipocytes and decreased sensitivity to insulin[109]. These findings support that the composition of adipose tissue-derived bioscaffolds could be important for promoting adipose tissue regeneration and function.

In the past, the Flynn lab group and others have made significant advances in developing decellularized adipose tissue (DAT) as a bioscaffold to support adipose tissue regeneration[169,227,253–255]. In the Flynn lab, DAT scaffolds are fabricated from surgically discarded human fat by first lysing cells through repeated freeze-thaw cycles. Cell-cell interactions are then disrupted via enzymatic digestion with trypsin, and the lipids are extracted through repeated rinsing in isopropanol[253]. Finally, residual lipids and nucleic acids are digested with a combination of lipase, DNase and RNase[253]. Notably, this decellularization process is entirely detergent-free, which avoids potential cytotoxicity concerns associated with residual detergents in the matrix[199,249–252]. Moreover, a detergent-free process may also be favorable for preserving GAGs and sequestered growth factors in the adipose tissue ECM[253]. DAT bioscaffolds processed using these methods have been shown to retain similar structural ECM components and architecture as the native adipose tissue ECM, including collagen IV, fibronectin, and laminin[253]. Using high-throughput mass spectrometry techniques, over 1000 proteins were detected in the DAT, including a diverse array of glycoproteins, proteoglycans, ECM-affiliated proteins and secreted factors[256]. Additionally, the DAT bioscaffolds were also shown to have similar viscoelastic properties as native adipose tissue[246,247], which may be favorable for promoting adipogenic differentiation[245].

Previously, culturing human ASCs on DAT scaffolds has been shown to upregulate genes associated with adipogenesis, including the master regulators PPAR-γ and CEBP-α, enhance activity of glycerol-3-phosphate dehydrogenase (GPDH), an enzyme associated with lipid biosynthesis relative to TCPS controls, and induce low levels of intracellular lipid accumulation, under proliferation conditions that would normally suppress adipogenesis[227,253–255]. More recently, unseeded DAT scaffolds were demonstrated to support adipose tissue and blood vessel formation in Wistar rats at 8 weeks[227]. These findings suggest that the DAT exhibits pro-adipogenic properties and may provide an

inductive microenvironment for adipose tissue regeneration. In addition, when allogeneic rat ASCs were seeded on the DAT bioscaffolds prior to subcutaneous implantation in the Wistar rat model, significant increases in angiogenesis and adipogenesis were observed at both 8 and 12 weeks[169]. In addition, the allogeneic ASCs were shown to promote a more pro-regenerative macrophage response, which may have contributed to the enhanced adipose tissue regeneration observed[169]. Together, these studies provide a strong case for applying the DAT as a tissue-specific bioscaffold for adipose tissue regeneration.

The DAT can also be fabricated into other forms of bioscaffolds, such as microcarriers, gels and composite hydrogels, which have also shown similar pro-adipogenic effects on human ASCs in culture as the intact DAT scaffolds[254,255]. Microcarriers can be produced by first digesting the DAT with enzymes to create an ECM suspension, which can be electrosprayed into liquid nitrogen to form microcarriers[257]. Previous *in vitro* studies have shown that human ASCs expanded on these DAT microcarriers showed enhanced adipogenic capacity relative to ASCs expanded on TCPS, with elevated adipogenic gene expression and intracellular lipid accumulation after 2 weeks in culture in adipogenic differentiation medium[257].

In addition to microcarriers, adipose tissue can also be decellularized and fabricated into injectable gels[258,259]. Previous work by Wang *et al.* demonstrated that the solubilized human adipose tissue matrix stimulated host cell infiltration when injected subcutaneously in Fischer rats for 30 days[181]. Additionally, when this scaffold was seeded with human ASCs and injected into nude rats, blood vessel formation and adipose tissue remodeling were observed in the scaffolds as early as 2 weeks and continued to be present at 8 weeks[258]. In a similar study, adipose tissue matrix hydrogels fabricated from lipoaspirates that were seeded with human ASCs and injected subcutaneously in nude mice showed an increase in macrophage infiltration as early as 1 week and an increase in blood vessel and adipose tissue formation at 4 weeks when compared to unseeded hydrogels[259].

DAT can also be fabricated into composite hydrogels for adipose tissue engineering applications[255]. For example, previous work from the Flynn lab investigated DAT

particles encapsulated with human ASCs within methacrylated chondroitin sulfate (MCS) hydrogels[255]. Adipogenic differentiation *in vitro* was enhanced in the hydrogel composites at 7 and 14 days relative to ASCs encapsulated in the MCS alone[260]. In addition, when similar composite hydrogels were delivered subcutaneously into Wistar rats, blood vessel formation and adipose tissue remodeling were observed within the implanted hydrogels at 12 weeks[255].

Collectively, these studies demonstrate that DAT scaffolds hold promise as pro-adipogenic scaffolds for adipose tissue engineering, and that *in vivo* regeneration can be enhanced by combining them with ASCs.

1.7 Cell preconditioning strategies

ASCs have shown promise for a broad range of cell therapy applications and there has been emerging interest in the development of *in vitro* preconditioning strategies to enhance their pro-regenerative functionality prior to *in vivo* delivery[261–267]. More specifically, preconditioning strategies can involve culturing the cells within a controlled environment that provides specific biochemical and/or biomechanical cues that can help guide the cells to respond in a desired manner[261]. For example, preconditioning strategies may involve treatment with specific factors to promote lineage-specific differentiation towards the goal of replacing cell populations within damaged tissues[268]. Alternatively, ASCs can also be preconditioned to enhance their expression of paracrine factors and cytokines that can promote angiogenesis and modulate the immune response, to indirectly support tissue regeneration[269]. Given that there is a growing body of evidence to support that this is the primary mechanism for ASC-mediated regeneration, this section will focus on preconditioning approaches that harness bioactive factors, oxygen tension and/or mechanical stimulation to enhance the pro-regenerative paracrine functionality of ASCs.

1.7.1 Application of bioactive factors to precondition ASCs

Treatment with bioactive factors can be a powerful approach to stimulate MSC populations including ASCs to express higher levels of various pro-regenerative growth factors and cytokines[261,262,268]. For example, MSCs that were cultured in medium supplemented with TGF-β1 for 24 h produced higher levels of VEGFA compared to

controls and increased vessel formation when delivered into isolated rat cardiac tissue *ex vivo*[262]. In another culture study, the pro-inflammatory cytokine TNF-α was used to precondition ASCs for 3 days, which resulted in increased cell migration, proliferation and expression of BMP-2[268]. A study by Baer *et al.* compared the paracrine effects of preconditioning mouse ASCs in either TNF-α or epidermal growth factor (EGF) for 48 h and demonstrated that each upregulated the secretion of different paracrine factors and cytokines[261]. Preconditioning mouse ASCs with TNF-α upregulated the expression of IL-10 and interleukin 11 (IL-11), whereas EGF preconditioning upregulated the expression of HGF and bFGF[261]. While these approaches have shown promise, these bioactive factors can be costly, which could limit the scalability of these strategies for clinical applications.

1.7.2 Effects of hypoxic preconditioning on ASCs

Oxygen tension can also regulate the paracrine response of pro-regenerative cell populations[111,262,265,270,271]. Cells that are grown in culture under atmospheric conditions are generally exposed to a hyperoxic environment, as the oxygen tension in most tissues in the human body is significantly lower than 21%[272]. Within adipose tissue, the normal oxygen tension typically ranges between 7 – 9%, with an oxygen tension less than 5% considered to be hypoxic[273,274].

At the molecular level, the intracellular protein hypoxia inducible factor 1-alpha (HIF-1α) is degraded following the hydroxylation of oxygen-dependent prolyl hydroxylase under physiological normoxic states[275–277] (Figure 1.2). Under hypoxia, this degradation pathway is inhibited, leading to the stabilization of HIF-1α and the activation of the Akt and P38 mitogen-activated protein kinase (MAPK) pathways that drive cell proliferation and paracrine factor secretion[278,279].

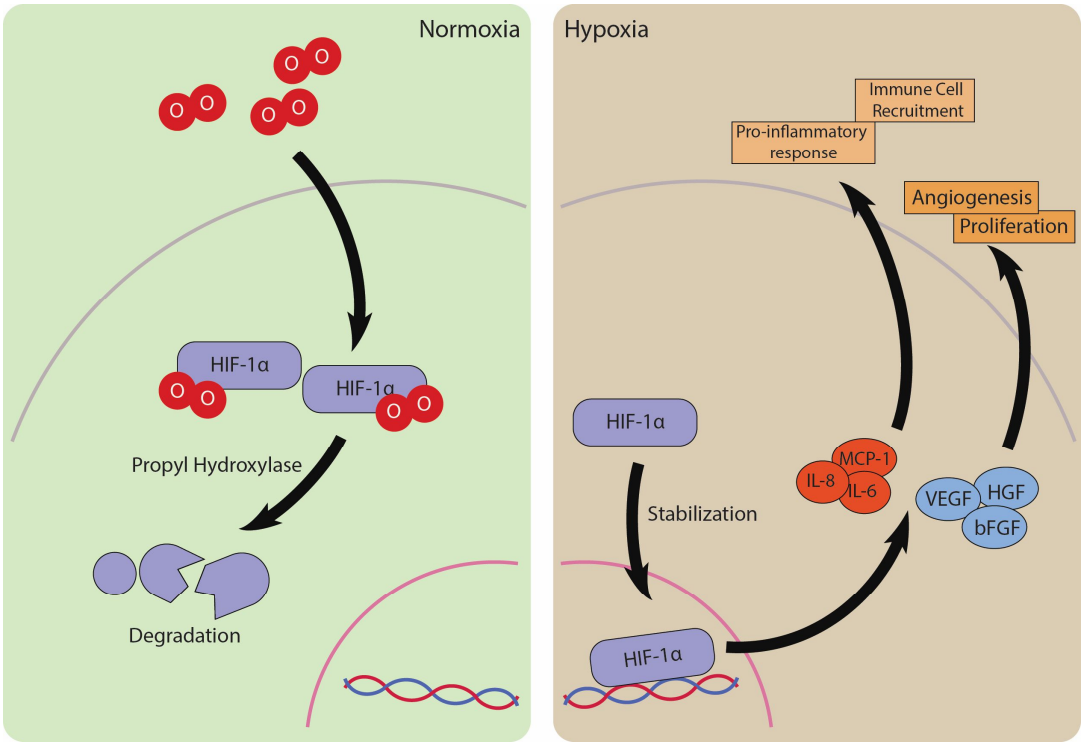

Figure 1.2 Normoxic oxygen tension leads to the degradation of HIF-1α, whereas hypoxia leads to the stabilization and nuclear translocation of this transcription factor, leading to the expression of pro-angiogenic factors and immunomodulatory cytokines.

In MSCs, hypoxia (1-3% O_2) has been shown to increase cell proliferation[263]. More specifically, a previous study demonstrated that when mouse bone marrow-derived MSCs were cultured at 3% O_2, they entered the exponential expansion phase earlier than controls cultured under 21% O_2[280]. Similarly, when human ASCs were cultured at 2% O_2, the cells exhibited greater gene expression of the stem cell markers *REX14*, *SOX2*, *OCT4*, *NANOG*, and were more proliferative, with the effects mediated through HIF-1α activation[281]. Moreover, the modulation of cell proliferation through HIF-1α-dependent mechanisms was further supported by a study by Kakudo *et al.*, who demonstrated that HIF-1α expression led to increased bFGF expression in human ASCs, which accelerated cell proliferation[282].

In addition to proliferation, HIF-1α activation can also enhance the secretion of pro-angiogenic factors in cultured MSC populations[263,283]. For example, a study by Chen *et al.* showed that culturing human bone marrow-derived MSCs at 2% O_2 increased VEGFA

secretion through a HIF-1α dependent mechanism[283]. Additionally, when human placenta-derived MSCs were preconditioned under 2% O_2 for 3 days, the conditioned media from these cell cultures was found to contain elevated levels of TGF-β1, insulin-like growth factor 1 (IGF-1), HGF, VEGFA and bFGF[269]. This study also demonstrated when these preconditioned cells were delivered into cutaneous wounds in Goto-Kakizaki rats, the rate of wound closure was enhanced, with a 90% decrease in wound area as compared to only 40% in the control group at 15 days[269]. In addition, studies have shown that culturing rat bone marrow-derived MSCs at 5% O_2 increased the expression of HGF, bFGF and PDGF-B through a HIF-1α mediated mechanism also involving the activation of Akt[284,285].

In addition to pro-angiogenic growth factors, hypoxia can also upregulate immunomodulatory cytokine expression in MSC populations including ASCs[261]. Previous studies have shown that when human bone marrow-derived MSCs were cultured in 2% O_2 for 3 days, the cells expressed higher levels of the pro-angiogenic factors VEGFA and bFGF as well as the pro-inflammatory cytokines IL-6 and IL-8[283]. Furthermore, studies have also shown that culturing fetal human astrocytes under 2% O_2 can increase the expression of pro-inflammatory cytokines such as IL-8 and MCP-1 through a HIF-1α-mediated mechanism[286].

The increased secretion of pro-angiogenic factors and immunomodulatory cytokines as a result of hypoxic preconditioning has been harnessed to promote adipose tissue regeneration[265,287]. For example, a study by Hsiao *et al.* showed that the conditioned media from human ASCs cultured under 0.1% O_2 for 3 days had a greater effect on stimulating angiogenesis at 2 weeks following subcutaneous delivery in C57BL/6 mice relative to control media prepared with ASCs cultured under 21% O_2[111]. In another study, rat ASCs that were cultured under 0.5% O_2 for 2 days were found to be better than control cells cultured under 21% O_2 at supporting the vascularization of fat flap grafts in Lewis rats over 7 days[288].

1.7.3 ASC response to mechanical stimulation

Mechanical stimulation, including shearing forces from fluid flow, can provide important biomechanical cues that guide the secretory behaviour of ASCs[289–291]. These cues can activate mechanosignalling pathways through tensegrity, integrin-mediated mechanotransduction and membrane fluidity[292]. Tensegrity-mediated mechanosensing takes place when a mechanical force applied on the cell leads to changes in the cytoskeleton, which transmits the signal to the nucleus[293]. Integrin-mediated signaling generally involves the activation of the extracellular domains of integrins, which triggers the phosphorylation and activation of focal adhesion kinase (FAK)-mediated intracellular pathways[294]. Membrane fluidity is a mechanosensing mechanism by which shearing forces can induce a change in membrane viscosity, which also leads to the activation of mechanotransduction pathways[294].

Mechanical stimulation often results in the activation of the MAPK and c-Jun N-terminal kinase (JNK) pathways[295,296], which can trigger a range of cellular responses including migration, differentiation and paracrine factor secretion[138,297,298]. A study from Yuan *et al.* showed that inhibiting JNK and p38 inhibited the migration of human bone marrow-derived MSCs that is typically induced by fluid flow[296]. In the context of biomaterials, the application of shearing forces was shown to enhance the mobilization of human ASCs on acellular blood vessel grafts[299]. More specifically, when the human ASCs were seeded and perfused through the lumen of the vessel graft, migration was enhanced and the cells aligned in the direction of the fluid flow[299].

The application of shearing forces can also promote paracrine factor secretion in MSC populations. A previous study demonstrated that when human bone marrow-derived MSCs were cultured under fluid flow at 2 Pa, increased VEGFA expression was observed relative to static culture controls[290]. Additionally, studies have shown that shearing forces can stimulate the production of NO, which can act in an autocrine loop to increase the expression of VEGFA[289]. A recent study by Becquart *et al.* further supported this observation and showed that the NO production during shearing stress was mediated through the extracellular signal-regulated kinase 1/2 (ERK1/2) intracellular signaling

pathway[291]. Collectively, these studies support that shearing forces can be applied to precondition ASCs to enhance their expression of pro-angiogenic factors.

1.8 3-D bioreactor systems for tissue engineering

Bioreactors are systems that allow for the close monitoring and control of biological processes. Parameters that can be regulated within these systems include pH, temperature, pressure and oxygenation, which generates a highly controlled environment for cell growth[300]. A range of bioreactors have been explored for both MSC expansion and tissue engineering applications including spinner flask systems, rotating wall bioreactors, and perfusion bioreactor systems.

1.8.1 Spinner flask systems

Spinner flask systems allow for the culturing of cell-seeded bioscaffolds in suspension or fixed within a holding device, with stirring of the culture media controlled through an impellor (Figure 1.3A)[300]. Spinner flask bioreactors can increase the efficiency and uniformity of cell seeding on scaffolds, which may be favorable for tissue regeneration[301–303]. For example, previous studies have shown that the seeding efficiency of chondrocytes on PGA scaffolds was 70% greater when a spinner flask system was used as compared to static culturing[304]. Spinner flasks have also been successfully applied for human bone marrow-derived MSC expansion on 3-D polymer microcarriers, while maintaining their immunophenotype and capacity for tri-lineage differentiation potential[305]. Additionally, previous work from the Flynn lab also showed that spinner flask bioreactor systems could be used to culture and expand human ASCs on DAT microcarriers, while maintaining their potential for adipogenic differentiation *in vitro*[254]. More recently, the spinner flask system were also demonstrated to better support ASC expansion on the DAT than commercially available Cultispher-S microcarriers following 28 days of culture[257]. Together, spinner flask bioreactors have been shown to be an effective 3-D culture system for MSC expansion. However, studies to date have not yet explored whether spinner flasks could also be applied as preconditioning systems to increase the pro-regenerative functionality of cultured cell populations. One potential

limitation is that the stirring motion in spinner flask bioreactor systems can result in heterogenous shear stresses being applied, which may lead to variable cell properties[306].

1.8.2 Rotating wall bioreactor systems

Rotating wall bioreactor systems can also be used to expand regenerative cell populations. Within rotating wall vessels, the culture media, cells and scaffolds are placed in between two concentric cylinders (Figure 1.3B)[300]. The vessel is then placed horizontally, and the cells and scaffolds are maintained in a constant state of suspension by the competing forces of gravity and the stirring caused by the rotation of the outer cylindrical wall[307]. The rotation of the outer wall can generate a low amount of shear forces, which can modulate cell functions including proliferation and differentiation[308]. For example, one previous study showed that epithelial cells cultured on synthetic ECM-coated beads in a rotating wall vessel proliferated well and formed multi-layer cell aggregates[307]. Furthermore, cells cultured on these synthetic beads could be digested and dynamically cultured under a bead-free environment within the rotating wall vessel[307]. Rotating wall bioreactors have also been used to expand MSCs[309]. Nishi *et al.* showed that rabbit bone marrow-derived MSCs seeded on a porous PLA bead scaffold cultured within a rotating wall bioreactor proliferated and showed evidence of being primed for osteogenic differentiation[309]. Moreover, a study by Chen *et al.* showed that human bone marrow-derived MSCs cultured in a rotating wall vessel bioreactor expanded significantly faster than statically cultured controls after 16 days *in vitro*[306]. Additionally, a study by Ben-David *et al.* demonstrated that human bone marrow-derived MSCs could be cultured on gelatin microspheres within a rotating wall bioreactor, and when implanted subcutaneously in athymic nude mice could support *in vivo* osteogenesis at 8 weeks[88]. Overall, while rotating wall vessel bioreactors are a promising expansion platform for pro-regenerative cell populations, to date these systems have been primarily applied for bone tissue engineering applications.

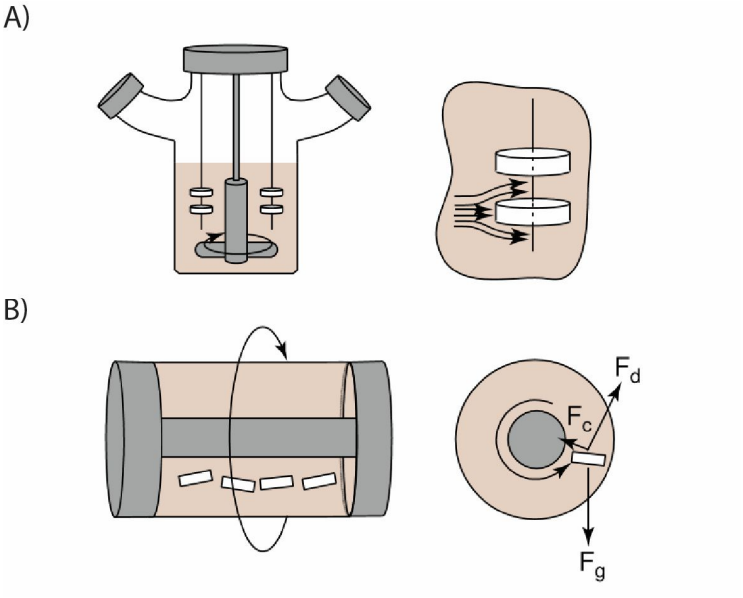

Figure 1.3 Schematic of A) spinner flask and B) rotating wall vessel bioreactor systems. Image re-printed with permission from publisher[300].

1.8.3 Perfusion bioreactor systems

Perfusion bioreactors are systems that circulate media via pumps through porous scaffolds housed within customized chambers, with the goal of enhancing nutrient delivery and waste removal throughout the 3-D constructs[300]. Relative to static cultures, perfusion bioreactors can offer greater control over the media conditions and oxygen tension experienced by cells within scaffolds[300,310]. Perfusion of the media also applies shear stress, which can modulate cell function[311–313].

Perfusion bioreactor systems have been investigated for a range of applications in tissue engineering to support the proliferation of pro-regenerative cell populations within scaffolds[310,312,314–317]. While media perfusion can potentially enhance proliferation, the fluid flow rate must be carefully refined to prevent newly secreted factors and ECM components from being rapidly removed[310]. In previous studies, perfusion bioreactors have been shown to maintain a constant oxygen tension within the perfused regions of scaffolds, and increase the uniformity of attached cells[318]. Another study using a two-stage perfusion bioreactor optimized for nutrient delivery and waste removal showed that human ESCs seeded on polyethylene-terephthalate (PET) scaffolds and cultured in this system maintained their stem cell phenotype and also expanded significantly faster than

cells grown in spinner flask systems[314]. Moreover, a recent study by Papadimitropoulos *et al.* showed that human bone marrow-derived MSCs seeded on ceramic-based bioscaffolds in an oscillating perfusion bioreactor system attached and proliferated under perfusion, while maintaining their immunophenotype and trilineage differentiation capacity[312]. Further, the cells that were cultured in the perfusion bioreactor were demonstrated to express more immunomodulatory cytokines including IL-8, C-X-C motif chemokine 5 (CXCL-5) and C-X-C motif chemokine 6 (CXCL-6) than 2-D and static culture controls[312].

Perfusion bioreactor systems have also been explored as a strategy to enhance the differentiation of MSC populations[313,319–323]. More specifically, the shearing forces applied to cells within these systems can potentially be harnessed to help direct MSCs towards the osteogenic lineage[319,323–325]. A previous study demonstrated that when PLGA scaffolds seeded with MSCs were perfused in an oscillating bioreactor for 21 days, the cells exhibited greater mRNA expression of key osteogenic genes relative to static culture controls[326]. This observation was supported by the work of Alvarez-Barreto *et al.*, who showed intracellular calcium accumulation in rat bone marrow-derived MSCs that were seeded on an RGD-conjugated PLA scaffold and perfused in a bioreactor at a rate of 1 mL/min for 8 days[313]. Interestingly, a study conducted with a hollow-fibre bioreactor showed that when ASCs were perfused within this system, they could be induced to differentiate towards the adipogenic lineage over 3 weeks of culture[327].

1.9 *In vivo* adipose tissue regeneration

Adipose tissue regeneration within engineered bioscaffolds *in vivo* is a multistep process that involves the interaction of diverse cell populations. One of the first key stages is an angiogenic response that results in the development of a vascular network to support seeded and infiltrating cell populations[328]. These newly-established vessels can facilitate the recruitment of immune cells and other pro-regenerative cell populations that contribute to scaffold remodeling and tissue regeneration[329]. The next sections will discuss current understanding of angiogenesis, macrophages and adipogenesis in the context of adipose tissue regeneration.

1.9.1 Angiogenesis in soft tissue regeneration

Angiogenesis is a key step in achieving soft tissue regeneration. The development of a vascular network is required for the delivery of oxygen and nutrients, and enables the recruitment of pro-regenerative host cell populations[328,330]. When tissue-engineered implants remain poorly vascularized, it can lead to the death of delivered cell populations and tissue necrosis, impeding regeneration[48].

Broadly, sprouting angiogenesis is a multistep process that includes vessel sprouting, lumen formation and finally anastomosis[331]. More specifically, vessel sprouting involves outgrowth of endothelial cells from the existing vasculature in response to biochemical cues within the local microenvironment[332–334]. Subsequently, lumen formation and extension takes place, where endothelial cells proliferate and migrate as the length of the newly-formed vessels increases[335]. These new extensions also form lumens that resemble endothelial tubes. Finally, anastomosis leads to the fusion of existing sprouts, and allows vascularization and blood flow to be fully established in these newly-built blood vessels[331].

Vessel sprouting typically begins with existing blood vessels within the target site. Endothelial cells from these existing vessels send out extensions known as filopodia[336], which are crucial in sensing and responding to biochemical cues within the microenvironment[332]. The filopodia on these leading endothelial cells, termed tip cells, can respond and extend to the presence of pro-angiogenic growth factors, such as bFGF and VEGFA[332,337], and can be repelled by angiogenic inhibitory proteins, such as semaphorin[338]. The combination of these biochemical attractants and repellents guides the direction of the sprouting. Endothelial cell proliferation occurs, with stalk cells trailing the endothelial tip cell, resulting in extension of the sprouts and ultimately lumen formation[339].

As endothelial sprouts continue to extend, the stalk cells will begin the process of forming a unicellular lumen[339]. These unicellular lumens will eventually become a multicellular vessel, as the sprouts continue to extend in length. Although the precise mechanisms of lumen formation have not been clearly delineated, it is possible that

lumen formation can be achieved through an intracellular hollowing process, where endothelial cells generate a hollow vacuole, and eventually fuse with the hollow vacuoles in neighbouring endothelial cells to form an extended hollow lumen[340].

Anastomosis is a multistep process where connections are built between the developing vessels resulting in the formation of functional vasculature[331]. During anastomosis, the filopodia from neighbouring tip cells interact to establish a stable connection via cell junctions[331]. Once connected, these tip cells deposit basement membrane to support and guide lumen connection[341].

During soft tissue regeneration, newly-formed capillaries will continue to expand in length and diameter. Stabilization is required for the long-term viability of these newly-formed and growing vessels[333]. Endothelial tube stabilization is achieved, primarily, by pericytes. Pericytes are recruited to endothelial tubes by pro-angiogenic factors, such as angiopoietin 1 (Ang-1), VEGFA and PDGF-BB[342–345]. Among these factors, PDGF-BB can lead to an increased expression of stromal cell-derived factor 1 (SDF-1) from endothelial cells, which is a potent chemoattractant for pericytes[344]. Studies have shown that when platelet-derived growth factor receptor beta (PDGFR-β) that is specific for PDGF-BB is inhibited, vessel growth and stabilization are stalled[346]. Moreover, when both vascular endothelial growth factor receptor 1 (VEGFR-1) and PDGFR-β are inhibited, the ability of pericytes to stabilize vessels is also blocked[347]. Collectively, this supports the importance of VEGFA and PDGF-BB signaling in initiating and supporting vessel stabilization. Once the connection between endothelial cells and pericytes is established, remodeling of the basement membrane occurs through the action of secreted MMPs and TIMPs to support the stabilized vessel[348,349].

ASCs can play a critical role in mediating angiogenesis by secreting key paracrine factors. As previously discussed in Section 1.4.2, ASCs can secrete HGF, VEGFA and bFGF under hypoxia[269,284,285], which can guide vessel sprouting and promote endothelial tube extension. SDF-1 with Ang-1 and PDGF-B secreted from ASCs leads to the recruitment of pericytes to stabilize the extending endothelial tubes[269,284,285] (Figure 1.4).

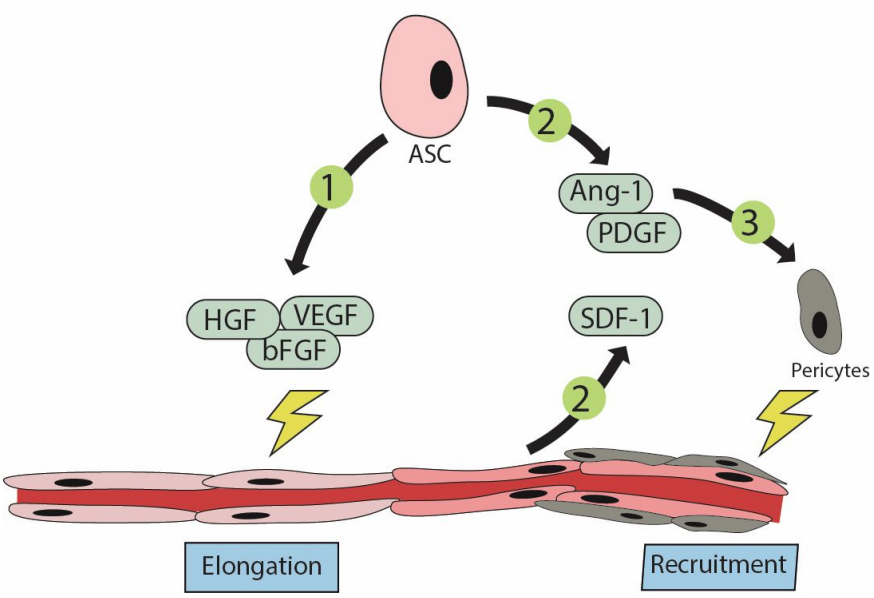

Figure 1.4 Schematic showing the role of paracrine factors secreted by ASCs in mediating endothelial tube elongation and the recruitment of supporting pericytes to stabilize blood vessels. (1) ASCs initiate vessel sprouting by first secreting paracrine factors such as VEGFA, HGF and bFGF, which drive endothelial cell proliferation and tube elongation. (2) Endothelial cells can secrete SDF-1, in combination with PDGF and Ang-1 from ASCs, to recruit pericytes to stabilize the newly formed endothelial tube.

1.9.2 Role of macrophages in mediating soft tissue regeneration

Although early work considered macrophages as a phagocytic cell population that was a barrier to regeneration, recent studies have shown that this diverse cell population plays essential roles in mediating soft tissue repair and regeneration[350]. In particular, macrophages can modulate regenerative responses through the secretion of cytokines, angiogenic growth factors and MMPs[351]. The macrophage secretion profile is highly dependent on the stage of the inflammatory/regenerative response[352].

Macrophages are highly plastic cells that historically have been classified as having the capacity to be polarized towards either a pro-inflammatory M_1-subtype or a pro-regenerative M_2-subtype[351]. However, recent evidence supports that there are a wide range of macrophage subpopulations that exist on a spectrum between these two extremes, and can often exhibit characteristics of both the M_1-subtype and M_2-subtype[353,354]. To better categorize the diversity of macrophages involved in tissue regeneration, a new classification system has been proposed, which is based on the factor

that activates the macrophages[355]. For example, M(IFN-γ) denotes pro-inflammatory macrophages that are activated by IFN-γ. This macrophage population can also be identified by the co-stimulatory molecule CD80[356,357]. M(IL-4) denotes pro-regenerative macrophages activated by interleukin 4 (IL-4), and finally M(IL-10) denotes pro-regenerative macrophages that are activated by IL-10[355]. The M(IL-10) macrophage population can be identified by the hemoglobin scavenger receptor CD163[358].

Monocytes and tissue-resident macrophages that are initially recruited to the target tissue site are typically polarized towards a more pro-inflammatory macrophage phenotype[359]. These populations are crucial in initiating tissue repair and regeneration[359]. For example, previous studies suggest that depleting monocytes and dendritic cells immediately following renal injury delays tissue regeneration[360]. These infiltrating monocytes are activated by IFN-γ, which can be secreted by ASCs[128,129] and innate immune cells, such as natural killer cells[361], to polarize toward a M(IFN-γ) phenotype[355,362] (Figure 1.5). These pro-inflammatory macrophages can subsequently release cytokines such as TNF-α, interleukin 1 beta (IL-1β), IL-6 and interleukin-12 (IL-12), which promotes the recruitment of further immune cells, such as neutrophils and eosinophils[363]. Moreover, these cytokines can act in an autocrine fashion to polarize more infiltrating monocytes toward a pro-inflammatory phenotype[364]. A previous study in a hindlimb injury model in rabbits suggested these pro-inflammatory macrophages are important in stimulating vascularization, as the infiltrating macrophages were shown to express TNF-α and bFGF, suggesting they were both pro-inflammatory and pro-angiogenic[365].

Pro-inflammatory M(IFN-γ) macrophages can promote an increase in M(IL-4) macrophages, as IL-6 secreted by M(IFN-γ) macrophages can upregulate the expression of interleukin 4 receptor (IL-4R)[366]. These M(IL-4) macrophages can often exhibit both pro-inflammatory and pro-regenerative characteristics and can mediate pro-regenerative processes (Figure 1.5). More specifically, this macrophage subpopulation was shown to secrete VEGFA and PDGF-B to support angiogenesis[351]. Further, these cells also secrete TGF-β1, which can act on fibroblasts to stimulate matrix deposition[367]. In addition, these M(IL-4) macrophages are also capable of remodeling the matrix through the secretion of

MMP-2, matrix metalloproteinase 9 (MMP-9) and matrix metalloproteinase 13 (MMP-13)[368].

Following the initial inflammatory response, macrophages can be polarized toward a more pro-regenerative phenotype through the secretion of IL-10 by Th2 and Treg cells[359]. Moreover, M(IL-10) macrophages can further secrete IL-10, which generates an autocrine loop that further promotes a more anti-inflammatory response (Figure 1.5). Overall, the increased expression of IL-10 contributes to the resolution of tissue inflammation and establishes a microenvironment that is more conducive for tissue repair and regeneration[369].

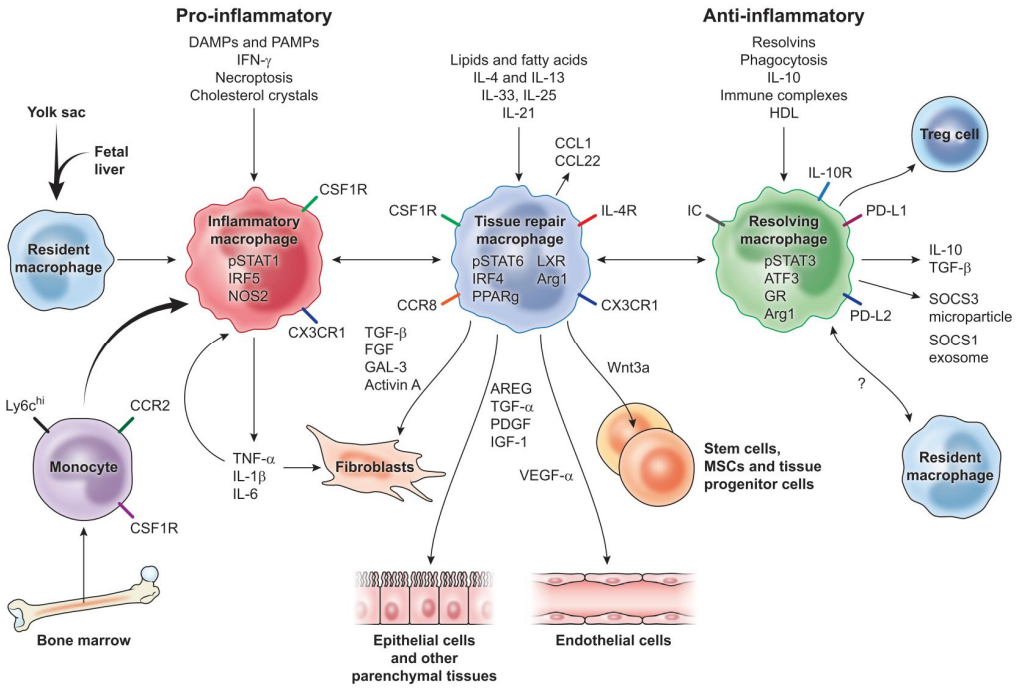

Figure 1.5. Schematic highlighting the roles of pro-inflammatory and pro-regenerative macrophages in mediating tissue regeneration. Inflammatory mediators, such as IFN-γ, present at the target site polarize infiltrating monocytes and tissue resident macrophages towards a pro-inflammatory phenotype. These pro-inflammatory macrophages secrete additional chemokines and cytokines to further increase the accumulation of pro-inflammatory cells. The increase in pro-inflammatory mediators promotes an increase in pro-regenerative macrophage populations that can secrete growth factors and cytokines to increase angiogenesis and ECM remodeling. Once the early inflammatory response subsides, IL-10 secreted from T cells mediates an anti-inflammatory response from the macrophages. Image re-printed with permission from the publisher[362].

1.9.3 Adipogenesis in soft tissue regeneration

Adipose tissue formation and expansion under physiological states can be achieved through hyperplasia and hypertrophy[370–372]. Hyperplastic expansion involves increasing the number of adipocytes in response to a need to store lipid, whereas hypertrophic expansion refers to an increase in the size of existing adipocytes[373]. It is important to note that both mechanisms of adipose tissue expansion require existing adipocytes. In the context of adipose tissue engineering, fat tissue formation is often required in target sites without existing adipocytes. As such, different mechanisms of adipogenesis are involved during adipose tissue remodeling and regeneration within engineered scaffolds, at least during the early stages of the process.

As previously discussed, while delivering mature adipocytes and adipogenic-induced ASCs have been investigated as a way to provide immediate adipocytes to the target tissue, it is unclear if these exogenous cells are maintained or form stable adipocytes over the long-term[190,234,244]. Alternatively, *de novo* adipose tissue formation in the context of adipose tissue engineering has been speculated to be initiated by the recruitment of host-derived cells. One interesting study by Stillaert *et al*. delivered human fat grafts that were embedded in Matrigel® into the groin of severe combined immunodeficient (SCID) mice[234]. At 6 weeks post implantation, host-derived adipose tissue formation was observed, whereas limited adipogenesis was observed in control implants without the human fat graft. Moreover, host-derived blood vessels were observed in the SVF of the implanted fat[234]. These observations support that cell populations in the SVF are pro-angiogenic, and may be responsible for the recruitment of host cells that formed the adipocytes. Interestingly, a study by Rodeheffer *et al.* showed that a $CD29^{+}CD34^{+}$ cell population present in the SVF that were also stem cell antigen 1 $(Sca\text{-}1)^{+}$ and $CD24^{+}$ possesses the capacity to support adipogenesis *in vivo*, and therefore, could be an adipocyte precursor population[374]. Additionally, Shook *et al.* demonstrated that this adipocyte precursor population are also $CD26^{+}$, and can be recruited to wounded dermal tissue to facilitate tissue repair[375]. Given its proximity to dermal tissue, it is plausible that this adipocyte precursor population could also play a role in subcutaneous adipose tissue regeneration.

Finally, there is some evidence that macrophages could also be a potential source of adipocytes during tissue regeneration. Previous *in vitro* studies showed that when macrophages were co-cultured with human adipocytes and ASCs, the macrophages accumulated intracellular lipid droplets[102]. This study provided initial evidence that macrophages could be directly involved in *de novo* adipogenesis. More recently, work from the Flynn lab group showed that infiltrating $CD163^+$ host macrophages expressed the adipogenic markers perilipin and adiponectin in ASC-seeded DAT implants in an immunocompetent rat model[169]. While these studies provide evidence for a possible direct role of macrophages in adipose tissue formation, additional studies are required to more fully understand the involvement of these cell populations in adipose tissue regeneration.

1.10 Project overview

DAT is a promising adipo-inductive biomaterial for applications in adipose tissue engineering that can support regenerative processes such as angiogenesis and adipogenesis[227]. Further, previous studies indicate that combining DAT scaffolds with allogeneic ASCs can augment adipose tissue regeneration in an immunocompetent Wistar rat model by enhancing angiogenesis, adipogenesis, and modulating the host macrophage response[169,255].

While the delivery of ASCs on DAT bioscaffolds has shown potential for stimulating tissue regeneration, limitations of previous work include the static seeding and culture methods employed that result in a heterogenous distribution of ASCs predominantly on the surface of the scaffolds. Perfusion bioreactor systems represent a promising approach to promote cell expansion and infiltration on 3-D scaffolds. In the second chapter of this doctoral thesis, a perfusion bioreactor strategy for culturing human ASCs on DAT scaffolds was developed. Using this system, the effects of both shear stress stimulation and hypoxic preconditioning were explored both *in vitro* and *in vivo*, with the goal of enhancing angiogenesis and adipose tissue regeneration within the DAT. In the third chapter, the effects of dynamic culturing of the human ASCs on the DAT scaffolds under hypoxic conditions (2% O_2) within the perfusion bioreactor system were assessed through comparison to static culture controls. In particular, these studies focused on

exploring the impact of shear stress stimulation induced by bioreactor culture on the ASC phenotype and paracrine function through *in vitro* culture studies. Further, *in vivo* characterization was performed to probe whether dynamic culture of the ASCs on the DAT altered host cell recruitment into the implants, with a focus on angiogenesis and the host macrophage response. Finally, in the fourth chapter, the development of an alternative and more scalable rocking bioreactor platform was explored as a possible strategy to precondition the ASCs to enhance their pro-regenerative paracrine functionality. More specifically, the effects of dynamic culture on the rocking platform in combination with DAT coatings on human ASC phenotype and pro-regenerative marker expression were assessed as a first step to assess the potential of this new approach.

1.11 Hypothesis and specific aims

The underlying hypothesis for this work is that dynamic culture of human ASCs on DAT-based biomaterials can enhance their capacity to stimulate regeneration by altering their paracrine factor expression profile, which will contribute to enhanced host-derived angiogenesis and adipogenesis within DAT implants.

To test this hypothesis, three specific aims have been formulated:

1. To apply dynamic culture of human ASCs on DAT bioscaffolds within a 3-D perfusion bioreactor system to enhance ASC expansion *in vitro* and angiogenesis and adipogenesis within DAT implants *in vivo*.

2. To characterize how dynamic culture of human ASCs on the DAT bioscaffolds within the perfusion bioreactor system enhances the capacity of the ASCs to stimulate soft tissue regeneration via paracrine-mediated mechanisms.

3. To develop a novel rocking bioreactor platform to dynamically culture ASCs on DAT-based coatings to promote a more pro-regenerative ASC phenotype.

Chapter 2

2 Perfusion bioreactor culture of adipose-derived stromal cells on decellularized adipose tissue scaffolds enhances *in vivo* regeneration

2.1 Abstract

Adipose tissue engineering holds promise to address the unmet need in plastic and reconstructive surgery for strategies that promote the stable and predictable regeneration of adipose tissue for volume augmentation applications. Previous studies have demonstrated that decellularized adipose tissue (DAT) scaffolds can provide a pro-adipogenic microenvironment, and that seeding with adipose-derived stromal cells (ASCs) can enhance *in vivo* angiogenesis and adipogenesis within DAT implants. Recognizing that bioreactor systems can promote cell expansion and infiltration on tissue-engineered scaffolds, this study evaluated the effects of culturing human ASCs on DAT scaffolds within a perfusion bioreactor. Using this system, the impact of both shear stress stimulation and hypoxic preconditioning were explored *in vitro* and *in vivo*. Initial studies compared the effects of 14 days of culture within the perfusion bioreactor under 2% O_2 or ~20% O_2 on human ASC expansion and hypoxia inducible factor 1 alpha (HIF-1α) expression *in vitro* relative to static cultured controls. The findings indicated that culturing within the bioreactor under 2% O_2 significantly increased ASC proliferation on the DAT, with a higher cell density observed in the scaffold periphery. HIF-1α expression was significantly higher when the scaffolds were cultured under 2% O_2. Subsequent characterization in a subcutaneous implant model in athymic nude mice revealed that *in vivo* angiogenesis and adipogenesis were markedly enhanced when the ASCs were cultured on the DAT within the perfusion bioreactor under 2% O_2 for 14 days prior to implantation relative to the other culture conditions, as well as additional freshly-seeded and unseeded DAT control groups. Overall, culture within the perfusion bioreactor system under hypoxia represents a promising approach for preconditioning ASCs on DAT scaffolds to enhance their capacity to stimulate blood vessel formation and infiltration, as well as host-derived adipose tissue regeneration.

2.2 Introduction

The subcutaneous adipose tissue layer plays important structural and functional roles within the integumentary system[1]. Due to the limited capacity of adipose tissue for self-repair, damage or loss resulting from trauma, burns, tumour resections, disease or aging can alter the normal body contours and result in scarring, deformities and loss of function[376]. While reconstruction can have a major positive impact on self-image and quality of life, there are numerous limitations to the existing clinical interventions that rely on tissue transfer from other sites on the body or on current implants used for volume augmentation[18,377].

Adipose tissue engineering represents a promising approach to address the unmet clinical need in plastic and reconstructive surgery for strategies that can promote the stable regeneration of healthy host-derived soft tissues[27,378]. Towards this goal, our lab has pioneered the development of off-the-shelf bioscaffolds derived from human decellularized adipose tissue (DAT), demonstrating that they provide a pro-adipogenic microenvironment both *in vitro* and *in vivo*[227,253]. DAT contains a diverse array of extracellular matrix (ECM) components, including a variety of matricellular proteins, small leucine-rich proteoglycans (SLRPs), growth factors and chemokines[256] that may have bioactive effects on seeded and infiltrating host cell populations. Moreover, the DAT has similar biomechanical properties to native human fat[246,247], which may be favorable for both implant integration and adipogenic differentiation[245,253].

Previously, seeding the DAT with allogeneic adipose-derived stromal cells (ASCs) enhanced angiogenesis and adipogenesis within the implants in an immunocompetent Wistar rat model[169]. More specifically, our study suggested that the ASCs indirectly contributed to host-derived adipose tissue regeneration through paracrine mechanisms, rather than through long-term engraftment and differentiation. It is well-established that ASCs secrete a variety of pro-regenerative growth factors and cytokines that can promote the recruitment of host progenitor cells, stimulate angiogenesis, and modulate the response of infiltrating immune cell populations, to help coordinate tissue regeneration[106,146,379].

A key limitation to the previous approach was that the static seeding and culture methods employed resulted in low cellular infiltration and a heterogeneous distribution of the ASCs within the dense ECM of the DAT, which may have limited their long-term survival and functionality following *in vivo* implantation. As such, the primary goal of this study was to explore the potential of dynamic culture as a strategy to enhance human ASC expansion, infiltration and pro-regenerative function on the DAT bioscaffolds. In particular, perfusion bioreactors represent a promising approach for promoting cell growth on 3-D bioscaffolds by enhancing nutrient delivery and waste removal[380,381]. Further, the shear forces applied by these systems can modulate cell phenotype and function[290,291,296,382], which may alter their capacity to stimulate regeneration.

In the current experimental design, human ASCs were pre-seeded on the DAT under dynamic conditions on an orbital shaker and then transferred into a custom-designed perfusion bioreactor system and cultured for 14 days. As oxygen tension has been shown to modulate ASC survival[287], proliferation[282], differentiation[271,281], and pro-angiogenic factor production[106,111,283] through the regulation of hypoxia inducible factor-1 alpha (HIF-1α)[282,284,285], the effects of culturing the cells under both normoxic (~20% O_2) and hypoxic (2% O_2) conditions were explored. The selection of 2% O_2 was based on studies showing enhanced ASC expansion *in vitro* at this level[271,383]. Initial studies focused on characterizing human ASC distribution, proliferation, and HIF-1α expression *in vitro* relative to control scaffold groups cultured under static conditions. Subsequently, *in vivo* testing was performed to probe the effects of dynamic culture within the perfusion bioreactor on human ASC retention, angiogenesis and adipogenesis within a subcutaneous implant model in athymic nude (*nu/nu*) mice relative to static cultured, freshly-seeded and unseeded DAT scaffold controls.

2.3 Methods

2.3.1 Materials

Unless otherwise stated, all chemicals and reagents were purchased from Sigma Aldrich Canada Ltd. (Oakville, Canada), and all antibodies were purchased from Abcam (Cambridge, USA).

2.3.2 Adipose tissue processing

Subcutaneous adipose tissue was collected with informed consent from elective breast reduction or abdominoplasty surgeries at the University Hospital and St. Joseph's Hospital in London, Canada. All studies were approved by the Human Research Ethics Board at Western University (HREB# 105426). The tissues were transported on ice in sterile phosphate buffered saline (PBS) with 2% bovine serum albumin (BSA) and processed within 2 h of collection for ASC isolation[238] or DAT scaffold fabrication[253] using published protocols. Processed DAT was pooled from multiple tissue donors for all subsequent experiments.

ASCs were cultured in proliferation medium comprised of DMEM:Ham's F12 supplemented with 10% fetal bovine serum (FBS) (Wisent, St. Bruno, Canada) and 100 U/mL penicillin/0.1 mg/mL streptomycin (1% pen-strep) (ThermoFisher, Waltham, USA) at 37°C with 5% CO_2 and ~20% O_2. Freshly isolated cells were passaged at 80% confluence, and passage 3 (P3) cells were used in all studies.

Following decellularization, the DAT was lyophilized and cut into scaffolds with a mass of 8 ± 1 mg. In preparation for seeding, the DAT scaffolds were rehydrated in deionized water for 24 h and then decontaminated by repeated rinsing in 70% ethanol. Next, the scaffolds were rinsed in sterile PBS and incubated in proliferation medium for 24 h.

2.3.3 Scaffold seeding and bioreactor setup

To seed the scaffolds, 1 x 10^6 P3 human ASCs were combined with individual DAT scaffolds in 3 mL of proliferation medium within 15 mL vented cap conical tubes (CellTreat Scientific Products, Pepperell, USA). The tubes were transferred into an

incubator and agitated on an orbital shaker at a 15° incline and 100 RPM for 24 h (37°C, 5% CO_2). Following seeding, the scaffolds were transferred into culture inserts that could be positioned within the individual sample chambers of the customized perfusion bioreactor system (Tissue Growth Technologies, Instron) (Appendix Figure A.1). The cell-seeded scaffolds were cultured under a flow rate of 0.5 mL/min for 14 days in proliferation medium under either normoxic (~20% O_2: 5% CO2/95% air) or hypoxic (5% CO_2/93% N_2/2% O_2) conditions, controlled through the use of a tri-gas incubator (ThermoFisher Forma Series II 3130), at 37°C. Static control scaffolds were included by culturing within the inserts under static conditions within vented cap conical tubes.

2.3.4 Assessment of ASC density and distribution

After 14 days of culture, scaffold samples were collected (n=4 replicate scaffolds/trial, N=3 trials with different ASC donors) for analysis of total cell density using the Quant-iT® PicoGreen® dsDNA Assay Kit (ThermoFisher, Waltham, USA). For all trials, control groups were included of freshly-seeded (collected after the 24 h dynamic seeding phase) and unseeded DAT scaffolds. The scaffolds were finely minced with surgical scissors and digested in 1 mL of 4 mg/mL collagenase (Worthington Type I) in Kreb's Ringer Buffer supplemented with 1% BSA, 2 mM glucose, and 25 mM HEPES under agitation at 100 RPM on an orbital shaker for 1 h at 37°C. The digested scaffolds were then centrifuged for 10 min at 1200 xg at room temperature, resuspended in Tris-EDTA buffer (10 mM Tris base, 1 mM EDTA, pH 8), and briefly sonicated using an ultrasonic dismembrator (ThermoFisher Model 100). The samples were then centrifuged at 5000 xg for 10 min at room temperature to remove debris, and the supernatant was analyzed using the PicoGreen® Assay kit according to the manufacturer's instructions using a CLARIOstar® microplate reader (BMG Labtech, Guelph, Canada). All plates included a standard curve generated with known numbers of ASCs to estimate the total number of ASCs per scaffold.

To corroborate the PicoGreen® data, the density of ASCs on the scaffolds was also assessed after 14 days of culture through quantification of DAPI staining (n=3, N=3). Scaffold samples were fixed in 4% paraformaldehyde for 24 h at 4°C before being embedded in paraffin and cut into 7 µm sections. Three non-adjacent cross-sections

100 µm apart were stained with DAPI, mounted and imaged with an EVOS® FL Cell Imaging System (ThermoFisher) under the 20X objective. $DAPI^+$ cells from 10 randomly selected non-adjacent fields from each scaffold cross-section were quantified using ImageJ software.

Hematoxylin & eosin (H&E) staining was also performed on scaffold cross-sections following standard procedures to assess the cell distribution within the DAT scaffolds after 14 days of culture. The samples were visualized using an EVOS® XL Cell Imaging System (ThermoFisher).

2.3.5 Immunohistochemical analysis of Ki-67 and HIF-1α expression

Immunohistochemical staining was performed on additional scaffold sections (3 non-adjacent sections at least 100 µm apart/scaffold; n=3, N=4) to examine the expression of Ki-67 as a proliferation marker and HIF-1α to probe potential changes under hypoxia. Heat-mediated antigen retrieval was performed in target antigen retrieval solution (pH=6.0) (Agilent, Santa Clara, USA) for 25 min. The slides were allowed to cool for 25 min and then washed in PBS and blocked in PBS-T (0.1% Tween-20) supplemented with 10% goat serum for 1 h at room temperature. Sections were then incubated with rabbit anti-Ki-67 antibody (1:100 dilution) or mouse anti-HIF-1α antibody (Novus Biologicals, Oakville, Canada; 1:100 dilution) overnight at 4°C. Alexa Fluor® 594 conjugated goat anti-rabbit (1:100 dilution) or Alexa Fluor® 680 conjugated goat anti-mouse (1:100 dilution) secondary antibody was subsequently applied for 1 h at room temperature and the samples were mounted in Fluoroshield Mounting Medium with DAPI (Abcam, Cambridge, USA). Mouse skin tissues and hypoxically cultured human ASCs were used as positive controls for Ki-67 and HIF-1α, respectively, and no primary antibody controls were included in all trials. Stained sections were visualized with the EVOS® FL Cell Imaging System, and 10 randomly selected non-adjacent fields of view from both the peripheral (< 200 µm from the scaffold edge) and central (>200 µm from the scaffold edge) regions of the scaffolds were imaged under the 20X objective. The number of $Ki\text{-}67^+DAPI^+$ cells and $HIF\text{-}1\alpha^+DAPI^+$ within each region were quantified using ImageJ Software.

2.3.6 Subcutaneous implantation surgeries

Following the *in vitro* testing, studies were performed to assess the effects of bioreactor culture on the capacity of the human ASCs to stimulate *in vivo* angiogenesis and adipogenesis within the DAT scaffolds. More specifically, these studies compared 6 scaffold groups including the ASC-seeded scaffolds that had been cultured for 14 days within the perfusion bioreactor or under static conditions at both 20% and 2% O_2 (i.e. (i) 20% O_2 static, (ii) 20% O_2 dynamic, (iii) 2% O_2 static, (iv) 2% O_2 dynamic) to (v) freshly-seeded (after the 24 h seeding phase) and (vi) unseeded DAT scaffold controls. For each scaffold group, duplicate samples were implanted for each trial and a total of 3 trials were performed using ASCs isolated from 3 different donors. All studies followed the Canadian Council on Animal Care (CCAC) guidelines and the protocols were approved by the Animal Care Committee at Western University (Protocol # 2015-049).

The scaffolds were implanted subcutaneously in female Nu-*Foxn1*^{nu} mice (Charles River Laboratories, Sherbrooke, Canada) that were 10-13 weeks of age for 4 and 8 weeks. A total of 36 mice were used for this study (N=6 mice per scaffold group at each timepoint). The mice were anaesthetized with isoflurane and given pre-operative analgesics via subcutaneous injections of meloxicam (2 mg/kg loading dose; 1 mg/kg follow up dose at 24 h) and bupivacaine (2 mg/kg). Two small incisions (~7 mm) were made on the dorsa of each mouse below each scapula, and pockets were created using blunt-ended forceps. One scaffold was then carefully positioned within each pocket and the incisions were closed with surgical staples. At each timepoint, the mice were euthanized by CO_2 overdose and the scaffolds were excised within their surrounding tissues. The samples were fixed in 4% paraformaldehyde overnight at 4°C, prior to paraffin embedding and sectioning (7 μm thick) in preparation for histological and immunohistochemical analyses. For all staining analyses, 3 cross-sections per implant (N=6 per time point) were analyzed that were a minimum of 100 μm apart.

2.3.7 Masson's trichrome staining

Masson's trichrome staining was performed using standard procedures to assess implant integration and remodeling, as well as the density of erythrocyte-containing blood vessels

within the scaffolds. The entire scaffold cross-section in each sample was imaged using the EVOS® XL Cell Imaging System at 20X magnification and combined into a single cross-sectional image using Adobe® Photoshop® CS6 Software. Within each complete cross-section, the number of erythrocyte-containing blood vessels was quantified within the DAT implant to determine the overall blood vessel density. Further, the distance to the closest scaffold edge and diameter were measured for each vessel using ImageJ Software. Vessel infiltration within 500 µm of the scaffold surface was analyzed using frequency distribution graphs with a bin size of 25 µm.

2.3.8 Immunohistochemical analysis of perilipin expression

At both timepoints, immunohistochemical staining was performed to assess perilipin expression as a marker of adipocyte formation within the DAT implants. The sections were prepared as described in section 2.3.5 and incubated overnight in rabbit anti-perilipin A antibody (1:200 dilution) at 4°C, followed by a goat anti-rabbit HRP-conjugated secondary antibody (1:500 dilution) for 1 h at room temperature. The samples were then processed with a DAB peroxidase (HRP) substrate kit (Vector Labs, Burlington, Canada), followed by counterstaining with hematoxylin and mounting with Permount® Mounting Medium (ThermoFisher, Waltham, USA). Mouse adipose tissues were used as a positive control, and no primary antibody controls were included in all trials. The entire scaffold region was imaged at 10X magnification and stitched into a single cross-sectional image as previously described. Positive pixel counting was performed to analyze the relative perilipin expression levels between the implant groups, with the values normalized to the total scaffold area within each cross-section measured using ImageJ Software.

2.3.9 Immunohistochemical analysis of human ASC engraftment and differentiation

To detect the human ASCs within the DAT implants, cross-sections were stained for human-specific Ku80[384] using a rabbit anti-Ku80 antibody (Cedarlane, Burlington, Canada; 1:100 dilution) followed by Alexa Fluor® 594 conjugated goat anti-rabbit (1:200 dilution) secondary antibody using methods described in section 2.3.5. Tissue positive

and no primary antibody controls were included in all trials. The stained cross-sections were imaged using the EVOS® FL Cell Imaging System. Quantification of $Ku80^{+}DAPI^{+}$ cells was performed on 10 randomly selected non-overlapping fields of view taken at 20X magnification using ImageJ analysis software.

To probe whether the human ASCs were differentiating into adipocytes within the DAT implant region, co-staining was performed using rabbit anti-perilipin A antibody as an adipocyte marker in combination with a mouse anti-human mitochondria (hMito) antibody conjugated with Cy3 (EMD Millipore, Burlington, USA; 1:100 dilution). hMito was used as an alternative to Ku80 based on the availability of antibodies compatible for co-staining. The samples were incubated overnight at 4°C and then incubated for 1 h at room temperature with a goat anti-rabbit secondary antibody conjugated with Alexa Fluor® 680 (1:100 dilution). The stained sections were visualized with the EVOS® FL Cell Imaging System and imaged under 20X magnification.

2.3.10 Statistical analysis

All numerical values are represented as the mean ± standard deviation. Statistical analyses were performed using GraphPad Prism® version 6 by one way or two-way ANOVA and followed by a Tukey's post-hoc test. Differences were considered statistically significant at $p<0.05$.

2.4 Results

2.4.1 Dynamic culturing in the bioreactor under hypoxic conditions for 14 days enhanced ASC density on the DAT bioscaffolds

To quantitatively assess cell density on the DAT, the scaffolds were digested and analyzed with the PicoGreen® dsDNA Assay. Freshly-seeded scaffolds had an average of $1.49 \pm 0.19 \times 10^5$ cells per scaffold following the 24 h seeding period. After 14 days of culture, the total cell density was significantly higher in the 2% O_2 dynamic group as compared to the freshly-seeded scaffolds and the 20% O_2 static and 2% O_2 static groups (Figure 2.1A). DAPI staining showed similar patterns in terms of the ASC density on the DAT scaffolds, corroborating the PicoGreen® results (Figure 2.1B).

To complement the quantitative findings, H&E staining was performed to assess the ASC distribution within the DAT scaffolds following the 14-day culture period. The ASCs were predominantly localized to the surface of the DAT scaffolds in the samples that were cultured under static conditions at both 20% and 2% O_2 (Figure 2.1C). A higher density of ASCs was observed in the scaffolds cultured for 14 days within the bioreactor, with a dense cell layer observed along the surface of the scaffolds. Consistent with the PicoGreen® results, the 2% O_2 dynamic group appeared to have a qualitatively higher density of cells, with greater infiltration into the central scaffold regions.

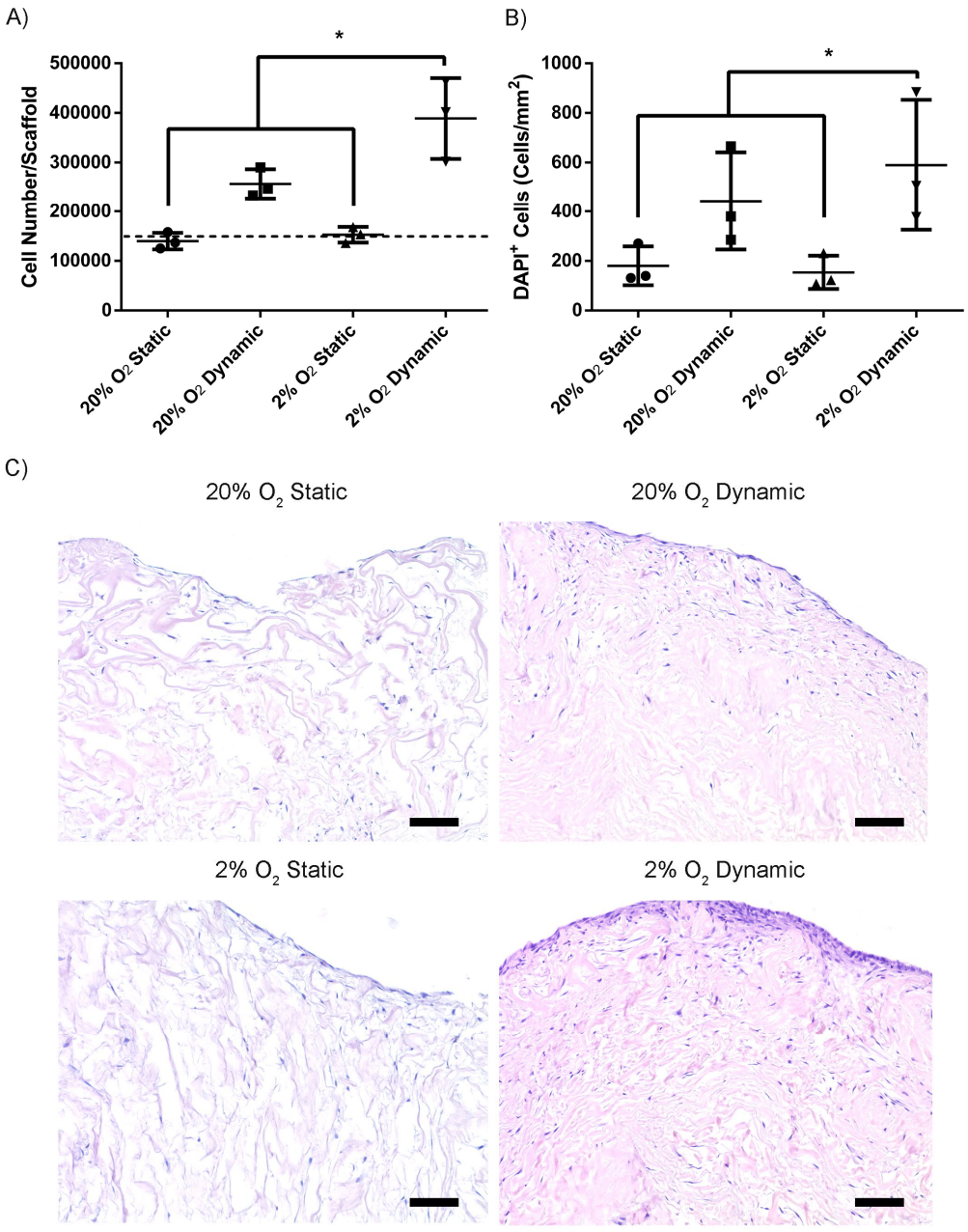

Figure 2.1 ASC density was enhanced on the DAT scaffolds following 14 days of culture within the perfusion bioreactor under 2% O_2. A) Average number of ASCs/scaffold based on total dsDNA content following 14 days of culture. Dashed line represents the average cell density in the freshly-seeded group. Error bars represent standard deviation (n=4 replicate scaffolds, N=3 trials with different ASC donors). B) The average number of ASCs per mm^2 of the DAT bioscaffold as measured by DAPI quantification following 14 days of culture. Error bars represent standard deviation (n=3 cross-sections/scaffold, N=3 trials with different ASC donors). * = 2% O_2 dynamic is significantly different than 20% O_2 static and 2% O_2 static group ($p<0.05$). C) Representative H&E staining showing the distribution of ASCs on the DAT scaffolds following 14 days of culture. Scale bars represent 100 µm.

2.4.2 Dynamic culturing in the bioreactor under hypoxic conditions for 14 days enhanced Ki-67 expression in the scaffold periphery

Immunostaining identified a low density of Ki-67$^+$DAPI$^+$ cells distributed throughout the scaffolds at 14 days. Qualitatively, there appeared to be more Ki-67$^+$DAPI$^+$ cells in the 2% O_2 dynamic group, with a higher density in the scaffold periphery (Figure 2.2A). Representative images of the central scaffold regions are shown in Appendix Figure A.2. These observations were confirmed by quantification of the number of Ki-67$^+$DAPI$^+$ cells within the peripheral (< 200 μm from edge) and central (> 200 μm from edge) regions of the scaffolds, which revealed that there was a significantly higher density of Ki-67$^+$DAPI$^+$ cells in the periphery in the 2% O_2 dynamic group as compared to both the peripheral and central regions of all other culture conditions. Additionally, a greater density of Ki-67$^+$DAPI$^+$ cells was measured in the central region of 2% O_2 dynamic group as compared to the central region of 2% O_2 static group (Figure 2.2B).

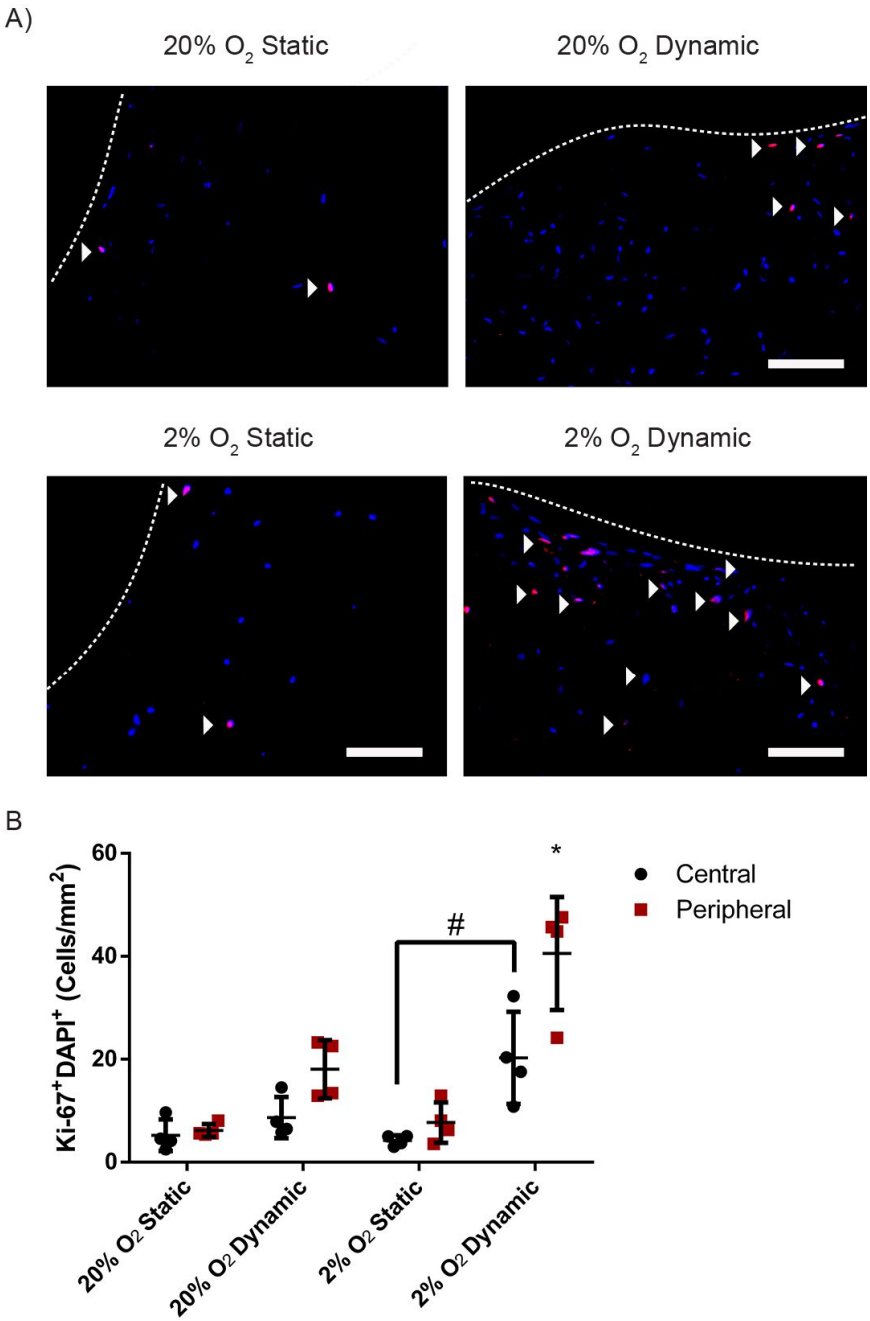

Figure 2.2 Ki-67 expression at 14 days was enhanced in the ASCs dynamically cultured on the DAT scaffolds within the perfusion bioreactor under 2% O_2. A) Representative images showing Ki-67$^+$ cells (red) counterstained with DAPI (blue) in the peripheral regions of the scaffolds after 14 days of culture. White arrowheads denote positively labelled cells and dashed lines represents the edge of the bioscaffolds. Scale bars represent 100 µm. B) The average number of Ki-67$^+$DAPI$^+$ cells in the peripheral and central regions of the scaffolds at 14 days. Error bars represent standard deviation (n=3 cross-sections/scaffold, N=4 trials with different ASC donors). * = significant difference between 2% O_2 dynamic group and all other groups, # = significant difference between the central region of 2% O_2 dynamic and 2% O_2 static groups ($p<0.05$).

2.4.3 Culturing under hypoxia increased the number of HIF-1α$^+$ cells within the scaffolds at 14 days

Immunohistochemical staining revealed that there were very few HIF-1α$^+$DAPI$^+$ cells in both the peripheral (< 200 μm from edge) and central (> 200 μm from edge) regions of the scaffolds cultured either dynamically or statically for 14 days under 20% O_2 (Figure 2.3A). In contrast, HIF-1α expression was observed in the majority of the cells in the 2% O_2 static and dynamic groups. Representative images of the central scaffold regions are shown in Appendix Figure A.3. Quantification of the staining indicated that the density of HIF-α$^+$DAPI$^+$ cells was significantly higher in the 2% O_2 dynamic group as compared to all other groups within both the peripheral and central scaffold regions (Figure 2.3B). In addition, the density of HIF-1α$^+$ DAPI$^+$ cells was also significantly greater in the 2% O_2 static group as compared to the 20% O_2 static and dynamic groups within both the peripheral and central scaffold regions (Figure 2.3B).

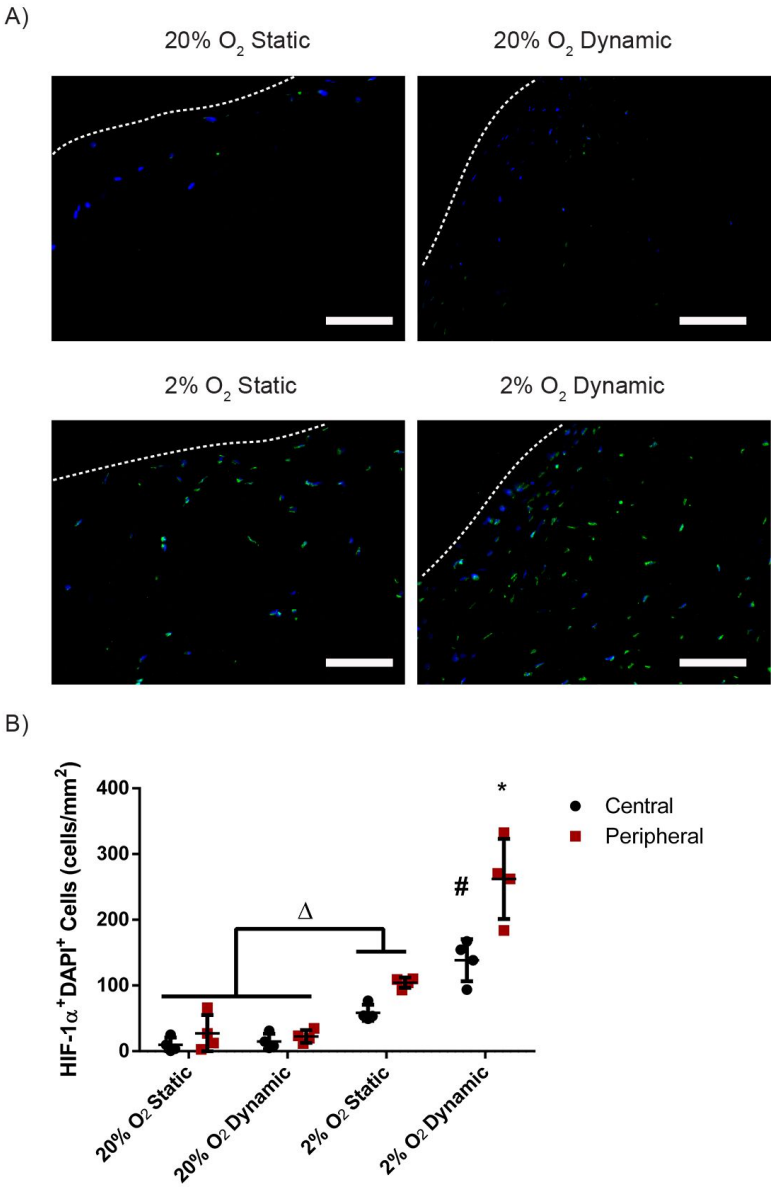

Figure 2.3 HIF-1α expression was enhanced at 14 days in the ASCs cultured on the DAT scaffolds under 2% O_2. A) Representative immunostaining showing HIF-1α^+ ASCs (green) counterstained with DAPI (blue) in the peripheral (< 200 µm from the edge) regions of the scaffolds following 14 days of culture. Scale bars represent 100 µm. Dashed lines represent the border of the bioscaffolds. B) The average number of HIF-1α^+DAPI$^+$ cells in the peripheral and central regions of the scaffolds at 14 days. Error bars represent standard deviation (n=3 cross-sections/scaffold, N=4 trials with different ASC donors). * = significant difference between the peripheral region of the 2% O_2 dynamic group and both the central and peripheral regions of all other groups , # = significant difference between the central region of the 2% O_2 dynamic group and the central region of all other conditions, Δ = significant difference between the 2% O_2 static group as compared to the 20% O_2 static and 20% O_2 dynamic groups in both regions ($p<0.05$).

2.4.4 DAT scaffolds cultured within the bioreactor for 14 days under hypoxic conditions showed enhanced blood vessel formation at 4 and 8 weeks following subcutaneous implantation

In vivo studies were subsequently performed using a subcutaneous implantation model in *nu/nu* mice to compare angiogenesis and adipogenesis in the scaffolds that had been cultured for 14 days within the bioreactor or statically (20% O_2 static, 20% O_2 dynamic, 2% O_2 static, 2% O_2 dynamic) to freshly-seeded and unseeded controls. Masson's trichrome staining at 4 and 8 weeks revealed that the scaffolds were well integrated into the host tissues and showed evidence of implant remodeling (Figure 2.4A). Small blood vessels and adipocytes were observed in the peripheral regions of the DAT implants starting at 4 weeks. At 8 weeks, more vessels were observed in the 2% O_2 dynamic group as compared to all other conditions, along with a greater number of adipocytes extending into the more central scaffold regions (Figure 2.4A).

Quantification of the number of erythrocyte-containing blood vessels in the scaffolds revealed that there was a significantly higher vessel density in the 2% O_2 dynamic group as compared to all other conditions at 8 weeks (Figure 2.4B), with a significant difference between the two timepoints for this group. The diameter of the erythrocyte-containing blood vessels was also measured, with results indicating that there were no significant differences in the average diameter between the groups at both 4 and 8 weeks, with an average diameter in the range of ~25 - 35 μm (Appendix Figure A.4A).

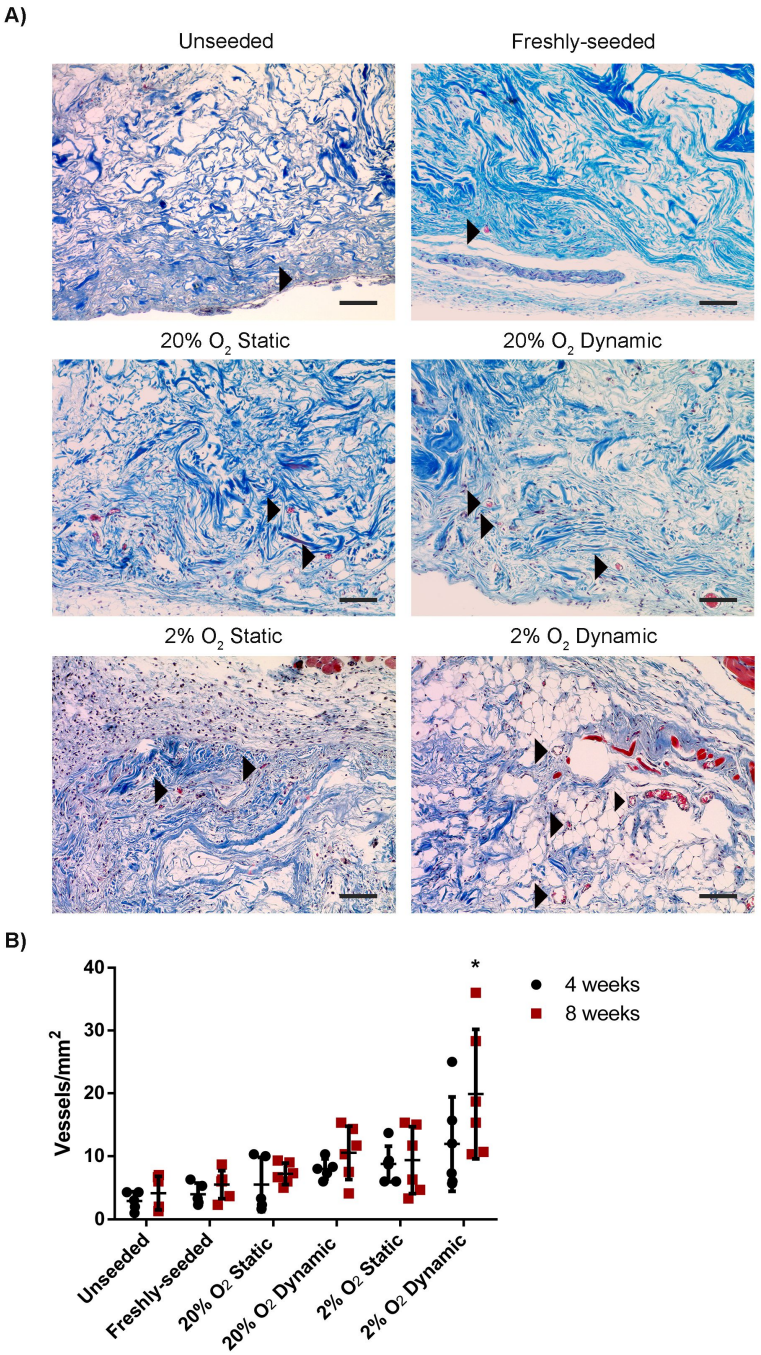

Figure 2.4 The density of erythrocyte-containing blood vessels was enhanced at 4 and 8 weeks in the DAT scaffolds that were cultured in the bioreactor under 2% O_2 for 14 days prior to subcutaneous implantation in *nu/nu* mice. A) Representative Masson's trichrome staining of the DAT implants at 8 weeks, with black arrowheads highlighting erythrocyte-containing blood vessels within the scaffolds. Scale bars represent 100 µm. B) Density of erythrocyte-containing blood vessels within the scaffolds at 4 and 8 weeks. Error bars represent standard deviation (n=3 cross-sections/implant, N=6 implants/group). * = 2% O_2 dynamic group at 8 weeks is significantly different compared to all other groups at 8 weeks ($p<0.05$).

Blood vessel infiltration was also probed by measuring the shortest distance from each vessel to the scaffold periphery. No significant difference in the average distance of blood vessel infiltration was measured between the groups at 4 weeks, with the average values ranging from ~70 - 125 μm and a high degree of variability observed (Appendix Figure A.4B). At 8 weeks, the average distance of vessel infiltration was significantly higher in the 2% O_2 dynamic group (198.8 ± 32.1 μm) as compared to all other groups with the exception of the 20% O_2 static (100.7 ± 38.3 μm) and 20% O_2 dynamic (125.1 ± 46.6 μm) groups.

Vessel infiltration within 500 μm of the scaffold surface was further analyzed by frequency distribution plots with pooled counts of the total number of vessels within 25 μm intervals for each of the scaffold groups (Figure 2.5). Based on this analysis, an increase in the number of vessels within the first 100 μm of the scaffolds was observed in the 2% O_2 dynamic and static groups at 4 weeks, suggesting that hypoxic culture promoted vessel formation in the scaffold periphery. At 8 weeks, a shift towards greater infiltration (i.e. rightwards) was observed for both the 2% O_2 dynamic and 20% O_2 dynamic groups, suggesting that dynamic culture enhanced the number of vessels infiltrating into the 100 – 200 μm depth range, with a higher number of vessels in the 2% O_2 dynamic group in this range, as well as farther into the scaffolds. Interestingly, the distributions for the freshly-seeded and unseeded groups were similar at both timepoints, indicating that the ASCs had little impact on vessel formation within the DAT under the conditions in this study. While the distribution for the 20% O_2 static group was similar to these groups at 4 weeks, an increase in the number of vessels within the first 50 μm was observed in this group at 8 weeks, suggesting that there was some benefit of culturing the ASCs on the scaffolds prior to implantation in terms of vessel formation within the most peripheral regions of the DAT scaffolds (Figure 2.5).

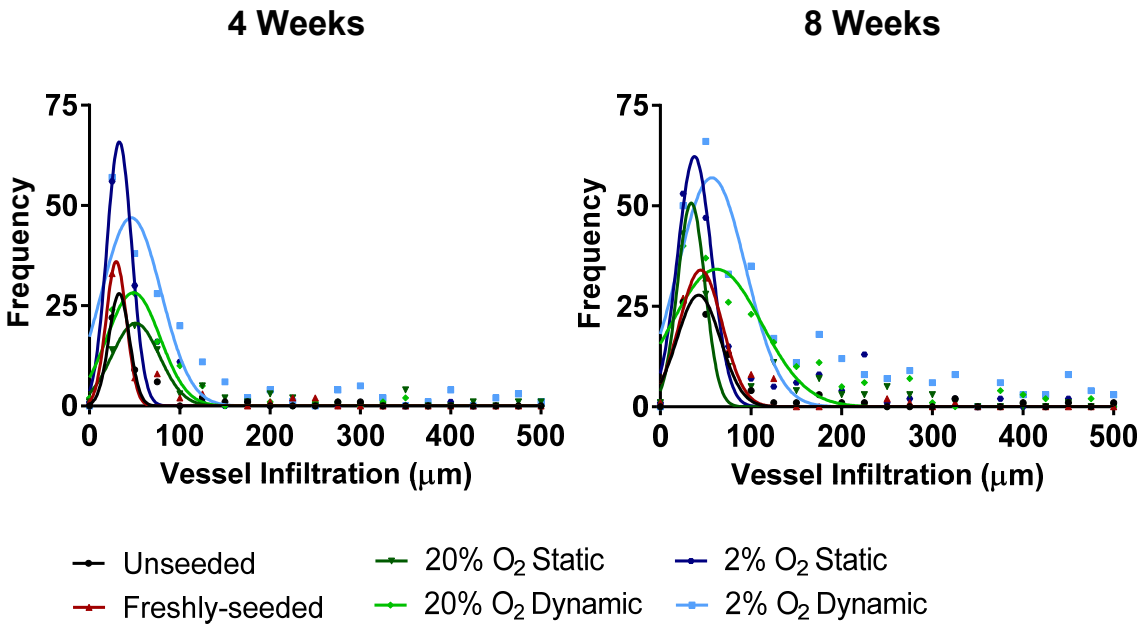

Figure 2.5 Frequency distribution plots showing the total number of erythrocyte-containing blood vessels at increasing depths from the scaffold periphery within the DAT implants. Coloured lines represent non-linear Gaussian fits of the data sets. Pooled data is shown representing the combined counts from 3 cross-sections at varying depths from 6 implants per condition at both 4 and 8 weeks.

2.4.5 DAT scaffolds cultured within the bioreactor for 14 days under hypoxic conditions showed enhanced adipose tissue remodeling at 8 weeks following subcutaneous implantation

Immunohistochemical staining for perilipin was performed to identify adipocytes containing intracellular lipid as a measure of adipose tissue formation within the implanted scaffolds at 4 (Appendix Figure A.5) and 8 weeks (Figure 2.6A). At 4 weeks, a small number of adipocytes were observed within the peripheral regions of the scaffolds in all of the groups. At 8 weeks, there were qualitatively more adipocytes in the scaffolds that incorporated ASCs as compared to the earlier timepoint, with more perilipin^{+} cells observed in the 2% O_2 dynamic group as compared to all other conditions.

Semi-quantitative image analysis confirmed that the relative levels of perilipin expression within the implant region were similar between the groups at 4 weeks (Figure 2.6B). In contrast, at 8 weeks, the 2% O_2 dynamic group showed significantly greater perilipin

expression levels as compared to all other groups at both 4 and 8 weeks, with a significant increase observed within this group from 4 to 8 weeks. Collectively, these findings are indicative of enhanced remodeling of the DAT implant into adipose tissue in the 2% O_2 dynamic condition. (Figure 2.6B).

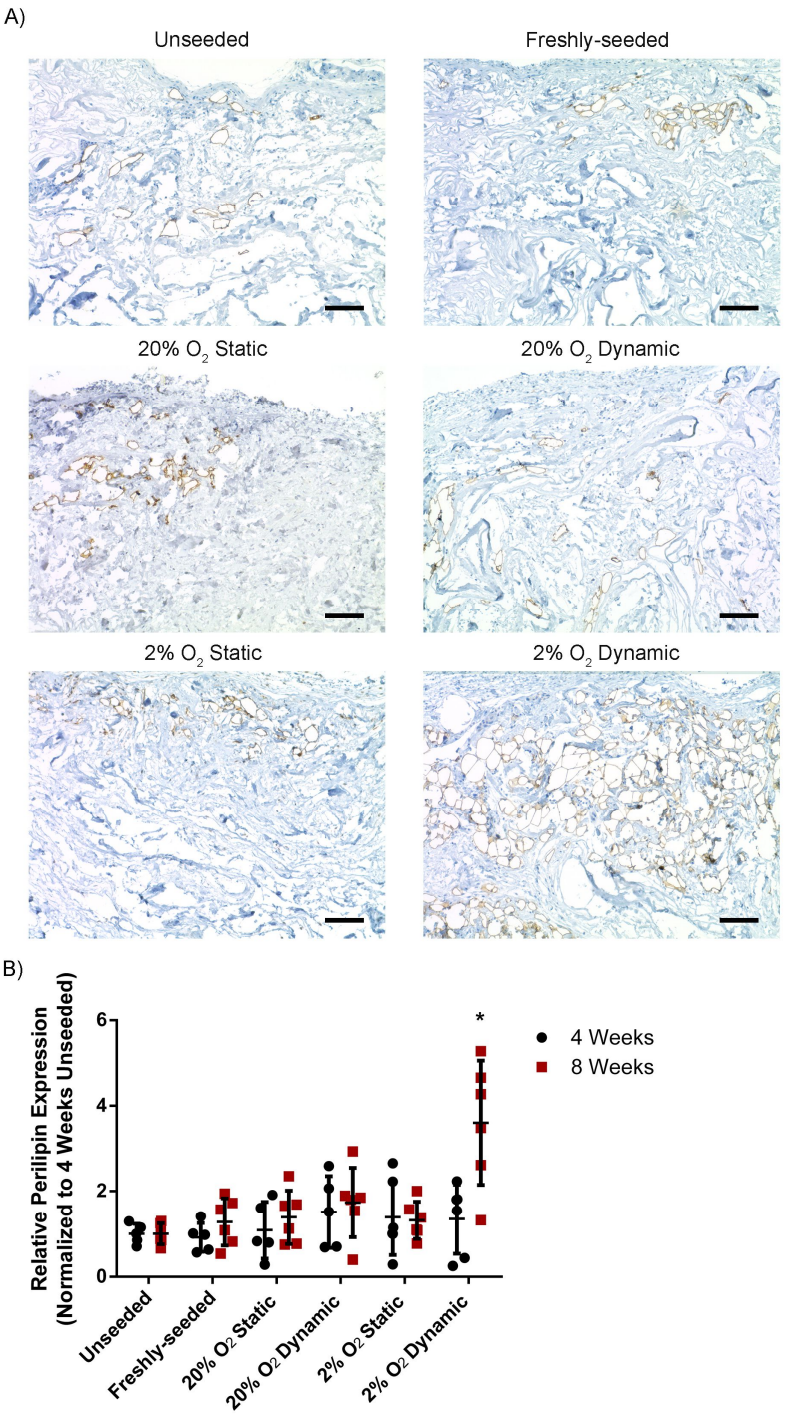

Figure 2.6 Remodeling of the DAT into adipose tissue was enhanced in the 2% O_2 dynamic group at 8 weeks following subcutaneous implantation in the nu/nu mouse model. A) Representative immunostaining showing regions of perilipin$^+$ adipocytes (brown) within the implanted scaffolds at 8 weeks. Scale bars represent 100 µm. B) The expression of perilipin relative to the unseeded group at 4 weeks. Error bars represent standard deviation (n=3 cross-sections/implant, N=6 implants/group). * = significant difference between the 2% O_2 dynamic group at 8 weeks and all other groups at both 4 and 8 weeks, as well as the 2% O_2 dynamic group at 4 weeks ($p<0.05$).

2.4.6 Human ASCs were detected in the DAT implants at similar levels at both 4 and 8 weeks

Immunohistochemical staining was performed for human-specific Ku80 to identify human ASCs within the DAT implants at both 4 (Appendix Figure A.6) and 8 weeks (Figure 2.7A). $Ku80^{+}$ cells were visualized throughout the seeded scaffolds at both timepoints. Quantification of the number of $Ku80^{+}DAPI^{+}$ cells within the scaffold regions revealed that there were no significant differences in the density of human ASCs detected between the seeded implant groups at both 4 and 8 weeks (Figure 2.7B).

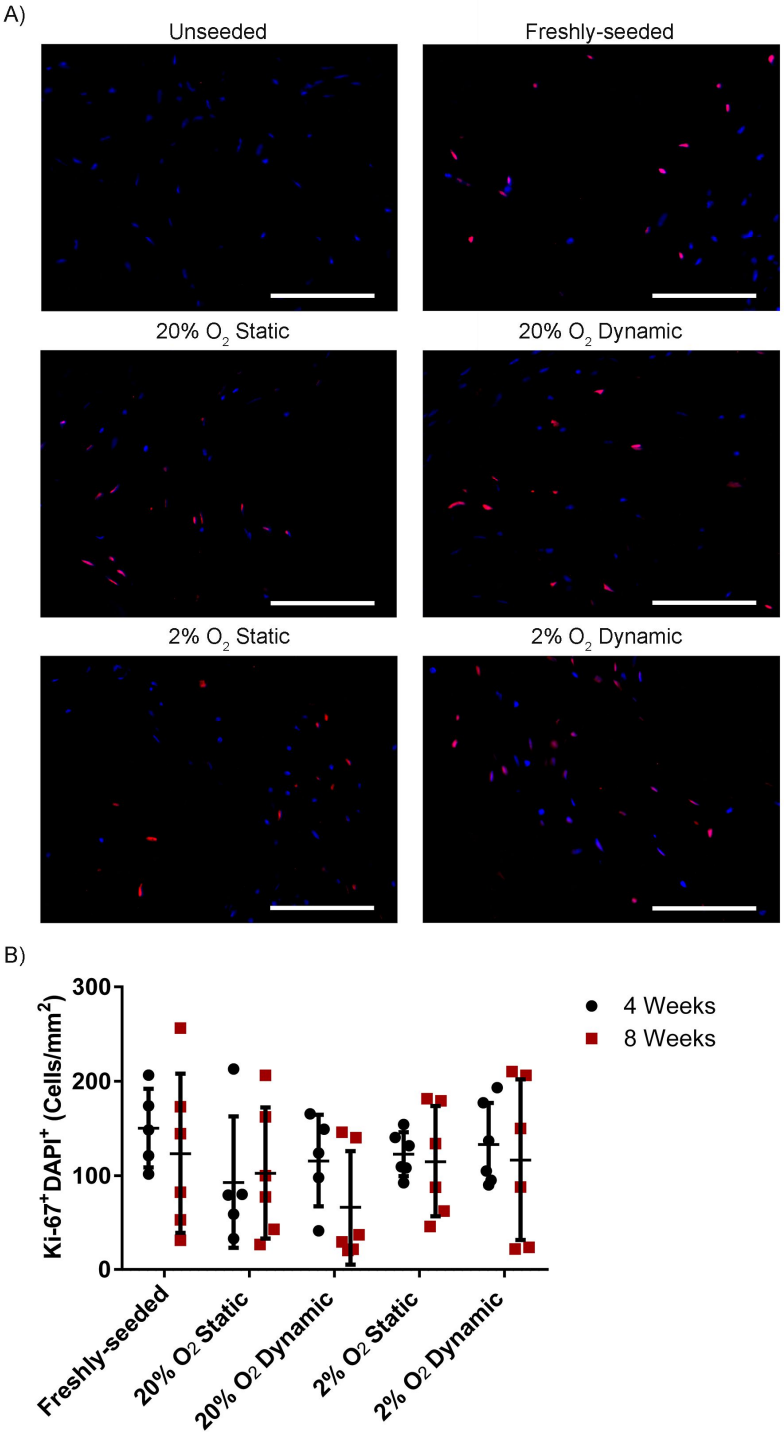

Figure 2.7 Ku80$^+$ cell density was similar between all seeded groups at both 4 and 8 weeks post-implantation. A) Representative immunostaining showing Ku80 labelled cells (red) counterstained with DAPI (blue). Scale bars represent 100 µm. B) Bar graph showing the density of Ku80$^+$DAPI$^+$ ASCs in the implants at 4 and 8 weeks. Data was compiled from 6 implants per group (N=6), with 3 cross-sections per scaffold taken from varying depths and 10 random fields analyzed per cross-section. Error bars represent standard deviation.

2.4.7 No evidence of human ASC differentiation into adipocytes *in vivo*

Co-staining with a human anti-mitochondrial (hMito) antibody in combination with perilipin was performed to probe human ASC differentiation into adipocytes within the DAT implants. No perilipin^{+}hMito^{+} cells were identified, indicating that the newly-forming adipocytes within the DAT implants were predominantly host-derived (Figure 2.8).

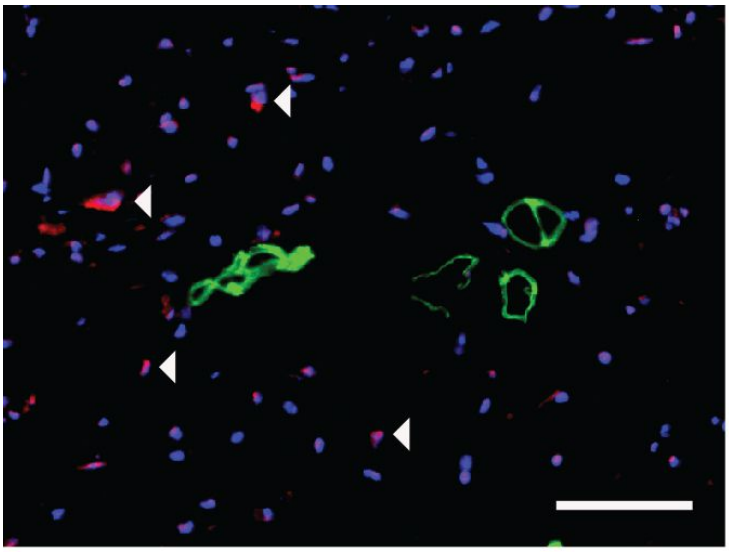

Figure 2.8 Staining patterns suggest that the human ASCs did not differentiate into adipocytes within the DAT implants over 8 weeks. Representative image showing distinct hMito^{+} (red) and perilipin^{+} (green) cell populations with DAPI (blue) counterstaining. White arrowheads indicate human ASCs in close proximity to perilipin^{+} cells. Scale bars represent 50 μm.

2.5 Discussion

New strategies that can promote the regeneration of healthy host-derived adipose tissue and enable stable and predictable volume augmentation would be of great value for a broad range of applications in plastic and reconstructive surgery. With the long-term goal of advancing towards clinical translation, the Flynn lab has been developing a broad range of off-the-shelf bioscaffolds derived from the ECM of human adipose tissue[227,229,253,255,385]. Previous *in vivo* study exploring DAT scaffolds in a subcutaneous implant model in immunocompetent rats indicated that seeding the DAT with allogeneic rat ASCs significantly enhanced blood vessel formation and remodeling of the DAT into

host-derived adipose tissue[169]. In that study, the DAT scaffolds were seeded with the ASCs within tissue culture inserts and then cultured statically for 72 h to promote cell attachment. However, these static seeding and culture methods result in a heterogeneous and sparse distribution of ASCs on the relatively dense intact DAT scaffolds, with limited cell infiltration into the central scaffold regions. Therefore, a higher density and more even distribution of cells throughout the scaffold may be favorable for enhancing the rate and extent of adipose tissue regeneration within the DAT. Further, in the current study, human ASCs were used as a more clinically relevant cell population.

Dynamic culture methods can enhance cell proliferation and infiltration into 3-D porous scaffolds by promoting the exchange of nutrients and waste, as well as by providing mechanical stimulation that can modulate cell function[300,386,387]. Stirred culture systems, such as spinner flasks, have been most extensively explored for the expansion of mesenchymal stromal cell (MSC) populations including ASCs, incorporating a range of microcarrier types to support cell attachment and growth[257,301,388–392]**.** Using an alternative design, Papadimitropoulos *et al.* investigated the use of a ceramic scaffold-based perfusion bioreactor for human bone marrow-derived MSC expansion[312], and Kim and Ma applied a perfusion bioreactor system for the expansion of human MSCs from bone marrow on polyethylene terephthalate (PET) scaffolds[319]. In general, the overall goal in these strategies was to harness the benefits of dynamic culture within a 3-D system to better preserve MSC function in terms of their capacity to proliferate and differentiate towards the adipogenic, osteogenic and/or chondrogenic lineages, as compared to the progressive functional decline that is observed when the cells are expanded on 2-D tissue culture polystyrene under static conditions[257,393]**.** The cells expanded within these systems can typically be released, such as through enzymatic digestion, and subsequently incorporated within a range of delivery platforms depending on the application of interest[303,394].

In the current study, an integrated approach was applied using a custom 3-D perfusion bioreactor to expand the human ASCs on the same DAT scaffold on which they would be delivered. While similar perfusion bioreactor strategies have been explored for bone tissue engineering applications using biomaterials with properties that mimic bone[303,394],

to the best of our knowledge this is the first study to investigate the use of a scaffold-based perfusion bioreactor for adipose tissue regeneration. Culturing within the perfusion bioreactor system was shown to enhance the cell density within the peripheral regions of the DAT scaffolds, with a more marked effect in the samples that were cultured under 2% O_2. These findings supporting the benefits of perfusion culture are similar to a previous study using a double chamber perfusion bioreactor that demonstrated that media perfusion enhanced bone marrow-derived MSC homogeneity within decellularized porcine tracheal scaffolds[395]. Additionally, a study by Sailon *et al.* showed that that the density of MC3T3-E1 murine pre-osteoblastic cells was enhanced on porous polyurethane scaffolds when cultured within a perfusion bioreactor system as compared to static controls, with the cells typically localized in the more porous regions of the scaffolds[316]. The enhanced cell density within the peripheral regions of the DAT suggests that there may have been limited media perfusion into the central regions of the scaffolds over time, which is a potential limitation. Regardless, the *in vivo* findings clearly support that culturing the ASCs on the DAT within the perfusion bioreactor under 2% O_2 significantly augmented angiogenesis and adipogenesis within the implants, supporting the benefits of the approach.

Based on the PicoGreen® and Ki-67 staining results, culturing under dynamic conditions within the bioreactor stimulated ASC proliferation on the DAT. Interestingly, there was no benefit of culturing the scaffolds under static conditions for 14 days in terms of the total cell number per scaffold relative to the freshly-seeded group. In addition to promoting ASC proliferation, bioreactor culture may have enhanced long-term cell survival[387,396], contributing to the higher cell density observed. Further, the media used in this study contains both mitotic factors as well as potent chemotactic factors[397,398] that may have promoted cell migration from the scaffold interior to the more highly perfused periphery.

The ASCs cultured both statically and dynamically under 2% O_2 were also shown to express HIF-1α, consistent with hypoxia in adipose tissue being < 5% O_2[273,274]. HIF-1α activation is associated with MSC proliferation[279,399], which may have contributed to the enhanced Ki-67 expression in the hypoxic dynamic group. A previous study by Choi *et*

al. demonstrated that culturing human ASCs under 2% O_2 increased proliferation relative to culture under ~21% O_2 through HIF-1α-mediated mechanisms[281]. In a more recent study, human ASCs were found to be more proliferative when cultured under 1% O_2 as compared to 2% O_2 for 7 days[282]. Moreover, the increased proliferation was shown to be mediated through the HIF-1α-dependent upregulation of bFGF[282]. In addition to stimulating proliferation, HIF-1α is an important transcription factor that regulates the expression of a range of angiogenic growth factors[400]. As such, it is possible that culturing under 2% O_2 may have modulated the paracrine factor secretion profile of the ASCs within the DAT, which would be interesting to explore in future work.

Following *in vitro* characterization, *in vivo* testing was performed to assess the effects of bioreactor culture on the capacity of the ASCs to promote angiogenesis and adipogenesis within the DAT. Athymic nude mice, which have been used in a number of adipose tissue engineering studies[159,165,176,189,259,401–403], were applied to enable the investigation of human ASCs. Angiogenesis was probed by quantifying the number of erythrocyte-containing blood vessels within the implants, indicative of functional vasculature. Previously in the rat model, seeding the DAT with allogeneic rat ASCs resulted in an increase in the number and diameter of erythrocyte-containing blood vessels within the implants starting at 8 weeks[169]. In the current study, the vessel density was significantly higher in the 2% O_2 dynamic group at 8 weeks as compared to all other conditions. Since the ASC density at 14 days was significantly higher in this group, it is possible that enhanced cell delivery may have contributed to increased angiogenesis. A study by Al-Khaldi *et al.* demonstrated there was a dose-dependent increase in *in vivo* blood vessel formation at 28 days when varying densities of mouse MSCs (up to 2 x 10^6 cells/mL) were delivered subcutaneously in Matrigel in C57BL/6 mice[404]. In addition to vessel density, the increased blood vessel infiltration observed in the hypoxic bioreactor group could be an indicator of an enhanced vessel sprouting effect. Previous studies have shown that vascular endothelial growth factor A (VEGFA) and bFGF are key paracrine factors that are crucial in driving vessel sprouting[283], which are secreted by ASCs at enhanced levels under hypoxia[284,285]. Moreover, there is also evidence to support that MSCs subjected to shear stress induced by dynamic culturing systems can show enhanced

VEGFA secretion[290,296]. As discussed, it would be worthwhile to explore the effects of dynamic culture on the DAT on ASC phenotype and paracrine function in future studies.

In addition to enhanced angiogenesis, culturing the ASCs on the DAT within the bioreactor under 2% O_2 for 14 days prior to implantation resulted in a significant increase in the number of perilipin$^+$ adipocytes within the implants at 8 weeks as compared to all other groups, consistent with enhanced remodeling of the DAT into adipose tissue. Adipose tissue regeneration is typically a gradual process that is coupled with angiogenesis, as a rich vascular supply is required to support mature adipocytes[405,406]. In previous rat study, seeding the DAT with allogeneic rat ASCs enhanced adipogenesis within the implants at both 8 and 12 weeks[169]. However, the response at 8 weeks was quite variable, with 20.1 ± 15.3% of the seeded DAT having remodeled into mature fat, as compared to 3.9 ± 5.7% in the unseeded group, based on area analysis of Masson's trichrome stained cross-sections[169]. The lack of difference observed between the other ASC-seeded groups in the current study relative to the unseeded controls may be related to species variability in terms of both the ASC source and animal model employed, as well as to differences in the ASC dose delivered. In addition, it is possible that further differences would be observed between the groups at later timepoints. Regardless, the present findings clearly demonstrate that dynamic culture of human ASCs on the DAT within the perfusion bioreactor under 2% O_2 significantly augmented both angiogenesis and adipogenesis within the implants at 8 weeks, supporting the use of this new strategy for adipose tissue regeneration.

While the density of ASCs was higher on the 2% O_2 dynamic scaffolds at the time of implantation, there were no significant differences between the groups in terms of the number of human ASCs detected within the implants at both 4 and 8 weeks. It is possible that the enhanced vascularization observed in the bioreactor-cultured samples may have contributed to this decline by promoting the recruitment of immune cell populations such as monocytes/macrophages that may recognize the human ASCs as being foreign. In previous rat study, using fluorescence *in situ* hybridization (FISH) to track the allogeneic ASCs sourced from male donors via the Y-chromosome, a progressive reduction in the number of donor cells within the DAT implants was observed over time, with only a

small number of donor ASCs visualized at 8 weeks and no positive cells detected at 12 weeks, indicating that the newly-formed adipose tissues were predominantly host-derived[169]. Similarly, Parisi-Amon *et al.* showed that mouse ASCs delivered subcutaneously in nude mice within a peptide-based hydrogel showed an 80% reduction in exogenous cells after 7 days *in vivo* based on bioluminescence imaging[407]. Additionally, a more recent study using a poly(N-isopropylacrylamide)-polyethylene glycol co-polymer to encapsulate human ASCs demonstrated ~13% retention at 14 days following subcutaneous delivery in athymic nude mice[408]. The persistence of a relatively high density of human ASCs in the current study at 8 weeks in all of the seeded groups suggests that the DAT may provide a supportive platform for their delivery. The functional role of these cells remains unclear, but the staining patterns suggest that there was limited differentiation into adipocytes. It would be interesting to explore how long these cells persist in future studies, as well as probing differences in possible paracrine-mediated effects at later timepoints including host adipogenic progenitor cell recruitment.

2.6 Conclusions

The perfusion bioreactor system represents a novel and promising platform for the dynamic expansion of pro-regenerative cell populations on 3-D bioscaffolds for adipose tissue engineering, and also an advancement towards a clinically viable strategy to support adipose tissue regeneration. The findings in this study demonstrated that the perfusion bioreactor system is effective at increasing the density of ASCs on the DAT, which suggests that it could address the previous limitations of the ASC-seeded DAT bioscaffolds. Increasing the ASC density on the DAT bioscaffolds via culturing within the perfusion bioreactor system under hypoxia subsequently translated into an enhanced capacity to support blood vessel formation and adipose tissue remodeling *in vivo*. Collectively, the body of work in the present study provided support for the use of a perfusion bioreactor system to increase the pro-regenerative potential of the ASC-seeded bioscaffolds. Moving forward, future studies should explore the mechanisms through which the ASC-seeded DAT supports angiogenesis and adipogenesis *in vivo* as the next step towards developing a clinically translatable subcutaneous adipose tissue regeneration strategy.

Chapter 3

3 Dynamic culture of human adipose-derived stromal cells on decellularized adipose tissue scaffolds modulates ASC paracrine factor expression and promotes a robust pro-regenerative host response

3.1 Abstract

Adipose-derived stromal cells (ASCs) have shown great promise as a pro-regenerative cell population that can be combined with decellularized adipose tissue (DAT) scaffolds to promote adipose tissue regeneration. Previous studies have shown that culturing human ASCs on DAT scaffolds within a perfusion bioreactor under 2% O_2 can significantly enhance *in vivo* angiogenesis and adipogenesis within the DAT. The focus of the current study was on exploring how dynamic culture within the bioreactor over 14 days modulated the phenotype and paracrine function of the ASCs on the DAT relative to controls cultured under static conditions. Multi-colour flow cytometry analysis of enzymatically-digested scaffolds indicated that there were no significant differences in the ASC immunophenotype between the groups. Immunohistochemical analyses suggested that shear stress stimulation induced by dynamic culture modulated the ASC response within the peripheral regions of the DAT, promoting the expression of inducible nitric oxide synthase (iNOS) and tumour necrosis factor alpha (TNF-α). Moreover, a greater fraction of the ASCs within this region co-expressed iNOS and arginase-1 (Arg-1), as well as TNF-α and interleukin 10 (IL-10). Gene and protein expression analyses indicated that dynamic culturing modulated the expression of a range of pro-angiogenic and immunomodulatory factors in the ASCs on the DAT, suggesting that their capacity to stimulate regeneration via paracrine mechanisms may be altered. *In vivo* studies comparing the response of the two groups in a subcutaneous implant model in athymic nude mice showed that culturing the ASCs on the DAT within the perfusion bioreactor prior to implantation enhanced the infiltration of $CD31^+$ endothelial cells and $CD26^+$ host cells into the DAT. While no significant difference was observed in total macrophage recruitment between the groups, there was increased infiltration of $CD163^+$ macrophages in the dynamic group at 8 weeks, suggesting there was a shift towards a

more pro-regenerative macrophage response. Overall, this work supports that dynamic culturing of human ASCs on DAT scaffolds in the perfusion bioreactor can alter the ASC phenotype in addition to promoting cell expansion, which may have contributed to the enhanced host-derived adipose tissue regeneration observed in this group.

3.2 Introduction

Tissue engineering strategies represent a promising approach for the long-term augmentation and regeneration of damaged or deficient subcutaneous adipose tissue for applications in plastic and reconstructive surgery. Recent advances in the field have focused on using a combined approach involving cell-seeded scaffolds as a means to provide both immediate volumetric augmentation and promote the stable regeneration of host-derived soft tissues[27,150,409]. In particular, decellularized adipose tissue (DAT) has emerged as a promising pro-adipogenic platform for this application[229,253]. DAT scaffolds can be fabricated from human adipose tissue that is abundantly discarded as surgical waste, and have been shown to retain biochemical and biophysical properties that mimic the native tissue source, which may be favorable for adipose tissue regeneration[246,256].

While applying DAT as an off-the-shelf scaffold is appealing, studies have suggested that the rate and extent of adipose tissue regeneration can be enhanced by seeding the scaffolds with regenerative cells[169,255,258,259,410], which may be critical for larger volume augmentation applications. In particular, previous work from our lab supports that seeding the DAT with allogeneic adipose-derived stromal cells (ASCs) enhanced both angiogenesis and adipogenesis within DAT implants in an immunocompetent rat model[169]. ASCs are a logical cell source for this application given their relative abundance and accessibility[70,71], their high tolerance of ischemic conditions such as those following implantation[411], as well as their enhanced adipogenic potential compared to other mesenchymal stromal cell (MSC) sources[412].

In our previous work[169], the static seeding methods used resulted in a sparse and heterogeneous distribution of ASCs on the DAT scaffolds, which may have restricted their capacity to stimulate regeneration. To address this limitation, we recently

investigated the effects of culturing human ASCs on the DAT within a scaffold-based perfusion bioreactor[413]. Our findings demonstrated that dynamic culture under 2% O_2 promoted human ASC expansion on the DAT. Further, culturing within the bioreactor under 2% O_2 for 14 days prior to implantation significantly augmented blood vessel infiltration and adipose tissue formation within the DAT scaffolds in a subcutaneous implant model in athymic nude (*nu/nu*) mice in comparison to scaffolds that had been cultured within the bioreactor for 14 days under 20% O_2, as well as scaffolds that had been cultured statically, and freshly-seeded or unseeded controls[413].

Although the delivery of a higher density of ASCs likely contributed to the enhanced adipose tissue regeneration observed in the 2% O_2 bioreactor group, the dynamic culture conditions may have also primed the ASCs to have a more pro-regenerative phenotype. A growing body of evidence supports that ASCs delivered within scaffolds primarily stimulate regeneration through transient paracrine-mediated effects, rather than through long-term engraftment and differentiation[101–103]. More specifically, ASCs can secrete a diverse range of growth factors and cytokines that can promote the recruitment and/or modulate the response of host cells, including immune cell populations, endothelial cells and adipogenic progenitors that can contribute to implant remodeling, angiogenesis and adipogenesis[105–107,414]. While the stimulatory effects of hypoxia on pro-angiogenic factor[106,111,263,288] and cytokine secretion[283,286] are well documented, the effects of dynamic culture on MSC paracrine factor expression remain largely unexplored, with most bioreactor studies to date focused on characterizing the effects on proliferation and/or differentiation[305,313,314,316,325].

Recognizing that dynamic culture may enhance the pro-regenerative capacity of the ASCs, the current study investigated how dynamic culture on the DAT scaffolds within the bioreactor modulated human ASC phenotype and paracrine function. To assess the effects of shear stress stimulation, the ASCs were cultured on the DAT scaffolds under 2% O_2 either within the perfusion bioreactor or statically for 14 days. As discussed, our previous studies clearly demonstrated that adipose tissue regeneration was markedly enhanced in the DAT scaffolds in the 2% O_2 dynamic group relative to all other groups, including the 2% O_2 static group, at 8 weeks post-implantation in the *nu/nu* mouse

model[413]. *In vitro* analyses were first performed to assess the effects of dynamic culturing on the DAT on ASC surface marker expression, phenotype and paracrine factor expression. Subsequently, the impact of dynamic culture on the pro-regenerative paracrine functionality of the human ASCs cultured and delivered on the DAT scaffolds was explored by characterizing the effects on host cell recruitment at 1, 4 and 8 weeks post-implantation in the *nu/nu* mouse model.

3.3 Methods

3.3.1 Materials

Unless otherwise stated, all reagents were purchased from Sigma Aldrich Canada Ltd. and used as received (Oakville, Canada).

3.3.2 Human adipose tissue collection and processing

Surgically-discarded subcutaneous adipose tissue was collected with informed consent from female donors undergoing elective lipo-reduction surgeries at the University Hospital or St. Joseph's Hospital in London, Canada. Human Research Ethics Board approval for this study was obtained from Western University (HSREB# 105426). The fresh tissues were transported to the lab in sterile phosphate buffered saline (PBS) supplemented with 2% bovine serum albumin (BSA) on ice. Within 2 h of collection, the adipose tissue was processed for either ASC isolation[238] or decellularization[253] following established protocols. Processed DAT was pooled from multiple tissue donors for all subsequent studies.

The human ASCs were cultured on T75 flasks (Corning, Fisher Scientific, Ottawa, Canada) in proliferation medium (DMEM:Ham F12 (Wisent, St. Bruno, Canada) supplemented with 10% fetal bovine serum (FBS) (Wisent, St. Bruno, Canada) and 100 U/mL penicillin and 0.1 mg/mL streptomycin ((1% pen-strep) (ThermoFisher, Waltham, USA)).

To prepare the DAT scaffolds for cell culture, DAT samples were lyophilized and cut into individual scaffolds having a mass of 8 ± 1 mg. The scaffolds were rehydrated in deionized water, decontaminated through repeated rinsing in 70% ethanol, and finally

washed in sterile PBS. Prior to seeding, the scaffolds were equilibrated in fresh proliferation medium for 24 h.

3.3.3 Scaffold seeding and culture

ASCs were seeded at passage 3 at a density of 1 x 10^6 cells/scaffold by combining the ASCs and individual DAT scaffolds in 3 mL of proliferation medium within a 15 mL vented cap conical tube (CellTreat Scientific Products, Pepperell, USA). The samples were cultured (37°C, 5% CO_2) under agitation at 100 RPM for 24 h on an orbital shaker at a 15° incline. Following seeding, the scaffolds were transferred into custom inserts[413] and cultured in proliferation medium for 14 days either statically in vented-cap conical tubes or dynamically within a customized perfusion bioreactor system (Tissue Growth Technologies, Instron) (Figure 2.1) under a flow rate of 0.5 mL/min. Hypoxic conditions (2% O_2/93% N_2/5% CO_2, 37°C) were maintained for all cultures using a tri-gas incubator (ThermoFisher Forma Series II 3110).

3.3.4 ASC immunophenotype

After 14 days of dynamic or static culture on the DAT, multi-colour flow cytometry was performed using a cell surface marker panel including CD90, CD29, CD26, CD34, CD146, CD31 and CD45. To isolate the ASCs, 6 replicate scaffolds (n=6 pooled) from each condition were pooled, finely minced and digested with Type IV collagenase (4 mg/mL, Gibco) diluted in sterile PBS at 37°C for 60 min. The scaffold digests were filtered through a 40 μm nylon mesh filter and stained with calcein violet-AM (BioLegend) for 25 min. The samples were then centrifuged at 500 xg for 7 min at 4°C and stained with the antibody cocktail summarized in Table 3.1 (prepared in sterile PBS supplemented with 5% FBS) for 30 min at 4°C. All antibodies were purchased from BioLegend. Fluorescence minus one (FMO) controls for calcein violet-AM and all 7 antibodies were included for each cell donor prepared using ASCs cultured on tissue culture polystyrene (TCPS). Single stain controls for all antibodies listed in Table 3.1 were included and performed with UltraComp eBeads (ThermoFisher).

The samples were analyzed with an LSR II Flow Cytometer (BD Biosciences) at the London Regional Flow Cytometry Facility. A total of 1 x 10^5 events were collected per

sample and a total of 3 trials were performed using ASCs from different donors (N=3). Sample analysis and colour compensations were performed with FlowJo Software. Gating was performed by first selecting single cells based on forward and side scatter. Live cells were then selected based on calcein violet-AM staining using the 405 nm laser with a 450/50 filter. Additionally, the $CD31^+$ endothelial cell and $CD45^+$ hematopoietic cell populations were gated out using the 561 nm laser with the 780/60 filter. The $CD31^-$ $CD45^-$ population was then gated for both CD90 and CD29 using the 405 nm and 488 nm lasers and the 610/20 and 530/30 filters, respectively. Finally, CD34 expression within the $CD90^+CD29^+$ ASC population was analyzed with the 561 nm laser with the 610/20 filter, along with CD26 and CD146 expression using the 640 nm laser with the 670/30 and 780/60 filters, respectively.

Table 3.1 Antibody conjugations and dilutions used for the multi-colour flow cytometry study.

Antigen	Conjugation	Dilution	Catalog Number
CD29	Alexa® Fluor 488	1:100	303015
CD90	Brilliant Violet 605	1:400	328128
CD31	PE-Cy7	1:200	303117
CD45	PE-Cy7	1:100	368531
CD26	APC	1:50	302709
CD34	PE-Dazzle 594	1:50	343533
CD146	APC-Fire750	1:50	361027

3.3.5 Immunohistochemical assessment of phenotypic markers in ASCs cultured on DAT scaffolds *in vitro*

Immunohistochemical analysis was performed to assess the expression of inducible nitric oxide synthase (iNOS), a marker associated with the immunomodulatory effects of MSCs[124,133,415], as well as arginase-1 (Arg-1) in the ASCs within the peripheral (< 200 µm from the scaffold edge) or central (> 200 µm from the scaffold edge) regions of the DAT scaffolds cultured either dynamically or statically for 14 days. In addition, triple staining was performed for Arg-1 with the pro-regenerative cytokine IL-10 and the pro-inflammatory cytokine tumour necrosis factor-α (TNFα). Primary and secondary antibodies and dilutions used in these studies are summarized in Table 3.2.

For both analyses, scaffolds (n=3) were fixed in 4% paraformaldehyde for 24 h at 4°C before being embedded in paraffin and sectioned into 7 μm sections. The sections were de-waxed in an ethanol series and heat-mediated antigen retrieval was performed with Tris-EDTA buffer (10 mM tris base, 1 mM EDTA, 0.05% Tween-20, pH 9.0) for 25 min. The sections were cooled for 25 min and then blocked with 5% BSA in PBS-T (0.1% Tween 20) for 1 h at room temperature before being incubated with the primary antibodies for (i) iNOS in combination with Arg-1 or (ii) Arg-1 in combination with TNF-α and IL-10 at 4°C overnight. Next, the sections were washed three times for 5 min with PBS, prior to being incubated with the appropriate secondary antibodies for 1 h at room temperature. Mouse spleen and liver were used as tissue positive controls, and no primary antibody controls were included in all trials.

Stained cross-sections were mounted in Fluoroshield Mounting Medium with DAPI (Abcam, Cambridge, USA) and visualized with an EVOS® FL Cell Imaging System (ThermoFisher). Positively-stained cells from 5 non-overlapping fields of view from both the central and peripheral regions were quantified using ImageJ Software in 3 non-adjacent cross-sections taken at least 100 μm apart from each scaffold. A total of 3 trials were performed with ASCs from different donors (N=3).

Table 3.2 Primary and secondary antibodies and dilutions used for immunostaining in the *in vitro* studies.

Primary antibody	Primary Dilution	Secondary antibody	Secondary Dilution
Arg-1 (Millipore ABS535)	1:100	Goat anti-chicken Alexa® 488 (Abcam 150169)	1:200
iNOS (Abcam AB15323)	1:100	Goat anti-rabbit Alexa® 594 (Abcam 150080)	1:200
TNF-α (Abcam AB6671)	1:200	Goat anti-rabbit Alexa® 594 (Abcam 150080)	1:400
IL-10 (R&D AF519)	1:50	Donkey anti-goat Alexa® 680 (ThermoFisher 1871998)	1:100

3.3.6 Human Angiogenic Growth Factor RT^2 Profiler PCR array

A Human Angiogenic Growth Factor RT^2 PCR Profiler Array was performed to screen for changes in gene expression of 84 different markers associated with angiogenesis between the static and dynamic groups after 14 days of culture. A list of these genes can

be found in Appendix Table A.1. For each trial, four replicate scaffolds seeded with ASCs from the same donor were pooled, and a total of 4 trials were performed using ASCs from different donors (n=4 scaffolds pooled/trial, N=4 trials with different ASC donors). The scaffolds were frozen in liquid nitrogen, crushed with a mortar and pestle, and resuspended in 1 mL of PureZol® (BioRad) and briefly sonicated 3 times in 4 second bursts. mRNA was then isolated with the Aurum® Total RNA Mini kit (BioRad) and the yield and purity were measured using a Nanodrop 1000 spectrophotometer (ThermoFisher). cDNA was immediately synthesized with 400 ng of input RNA using an RT^2 First Strand Kit (Qiagen). The Human Angiogenic Growth Factor RT^2 PCR Profiler Array (Qiagen) was then prepared in accordance with the manufacturer's protocols, with all samples loaded in technical duplicates. Genes without consistent patterns of amplification across the 4 ASC donors were excluded from further analysis. The expression of the remaining genes of interest was normalized to a panel of housekeeping genes (*HGPRT*, *GAPDH*, *B2M*). The $2^{-\Delta Ct}$ values were expressed as a ratio (dynamic/static) for each of the ASC donors, and the results were compared with a multiple t-test, with a False Discovery Rate of 15%.

3.3.7 Human Magnetic Luminex® Assay

A Human Magnetic Luminex® Assay was performed to compare the protein expression levels of TNF-α, IL-10, interleukin-6 (IL-6), hepatocyte growth factor (HGF), chemokine C-X-C motif ligand 2 (CXCL-2) and chemokine C-X-C motif 10 (CXCL-10) between the static and dynamic groups at 14 days, selected based on the PCR array data. For this assay, 3 replicate scaffolds from each group (n=3) were analyzed with cells from a single ASC donor, and a total of 5 trials were performed with different ASC donors (N=5). In preparation for the Luminex® assay, the individual scaffolds were frozen in liquid nitrogen, crushed with a mortar and pestle, and resuspended in a lysis buffer (50 mM Tris-HCl, 100 mM NaCl, 10% glycerol, 1% Triton X-100, pH 7.4). The samples were then briefly sonicated with ultrasonic dismembrator (ThermoFisher Model 100) and centrifuged at 13,000 xg for 10 min at 4°C. The supernatant from each sample was then analyzed with a Human Magnetic Luminex® Assay (R&D Systems), in accordance with the manufacturer's protocols. In brief, the protein samples were diluted 2-fold with the

provided diluent solution (buffer RD6-52) before being loaded into a 96-well plate along with the provided standards. Pre-mixed magnetic beads were then added and incubated for 2 h at room temperature under constant agitation. The diluted biotin-antibody cocktail was then added to each sample and incubated for 1 h at room temperature under constant agitation before the Streptavidin-PE cocktail was added. The 96-well plate was then assayed using a MAGPIX® System (Millipore). Protein concentrations were determined based on comparison to the standard curves and normalized to the dsDNA content measured in each sample using a PicoGreen® dsDNA Assay[413], following the manufacturer's instructions.

3.3.8 Subcutaneous implantation surgeries

In vivo studies were performed to compare the effects of culturing the ASCs on the DAT scaffolds for 14 days either statically or dynamically on the host cell response. All animal studies followed Canadian Council on Animal Care (CCAC) guidelines and the protocols were reviewed and approved by the Western University Animal Care Committee (Protocol #2015-049). Female athymic nude mice (Nu-*Foxn1*^{nu}) (Charles River Laboratories, Sherbrooke, Canada) of 10 – 13 weeks of age were used for this study (N=6 mice per scaffold group/timepoint). Subcutaneous implantation surgeries were performed in accordance with established protocols[413]. At 1, 4 and 8 weeks, the mice were sacrificed by CO_2 overdose and the scaffolds were excised within their surrounding tissues. The samples were fixed in 4% paraformaldehyde at 4°C overnight before being embedded in paraffin and sectioned (7 μm) for immunohistochemical analysis.

3.3.9 Immunohistochemical analysis of host cell recruitment

Immunostaining was performed to assess host cell infiltration into the scaffolds at 1, 4 and 8 weeks. More specifically, CD31 staining was performed to examine host endothelial cell recruitment. In addition, co-staining was performed for CD26, a marker that has been associated with highly proliferative multipotent progenitors that give rise to preadipocytes in murine subcutaneous adipose tissue[416], along with the human cell marker Ku80[384], to distinguish the host-derived CD26^{+} population. Finally, host immune cell recruitment was characterized through triple staining for the pan-leukocyte marker

CD45, the murine macrophage marker F4/80, and the phagocytic macrophage marker CD68. The phenotype of the infiltrating macrophages was also probed by co-staining for CD45 in combination with the pro-regenerative macrophage marker CD163[358]. Primary and secondary antibodies and dilutions used in these studies are summarized in Table 3.3. For each explanted scaffold, 3 non-adjacent cross-sections at least 100 μm apart were analyzed.

Table 3.3 Primary and secondary antibodies and dilutions used for immunostaining in the *in vivo* study.

Primary antibody	Primary Dilution	Secondary antibody	Secondary Dilution
CD31 (Abcam ab28364)	1:100	Goat anti-rabbit Alexa® 594 (Abcam 150080)	1:200
Ku80 (Cell Signaling 2180)	1:200	Goat anti-rabbit Alexa® 594 (Abcam 150080)	1:400
CD26 (R&D AF954)	1:50	Donkey anti-goat Alexa® 680 (ThermoFisher 1871998)	1:100
CD45 (R&D AF114)	1:100	Donkey anti-goat Alexa® 680 (ThermoFisher 1871998)	1:200
CD68 (BioRad MCA1957)	1:100	Goat anti-rat Alexa® 488 (ThermoFisher A-11006)	1:200
F4/80 (Abcam 111101)	1:50	Goat anti-rabbit Alexa® 594 (Abcam 150080)	1:100
CD163 (Abcam ab182422)	1:200	Goat anti-rabbit Alexa® 594 (Abcam 150080)	1:400

For the staining, the cross-sections were dewaxed via ethanol series and subjected to heat-mediated antigen retrieval in Tris-EDTA buffer for 25 min and cooled at room temperature for 15 min. Sections were then washed and blocked in 5% BSA in PBS-T (0.1% Tween-20) for 1 h at room temperature before being incubated in the appropriate primary antibody cocktails (Table 3.3) diluted in the blocking solution at 4°C overnight. Next, the sections were incubated with the corresponding secondary antibodies at room temperature for 1 h before being mounted in Fluoroshield Mounting Medium with DAPI. The stained sections were visualized with the EVOS® FL Cell Imaging System under 20X magnification. Quantification was performed within 10 randomly selected and non-overlapping, non-adjacent fields of view in each section using ImageJ analysis software.

3.3.10 Statistical analysis

All numerical values are represented as the mean ± standard deviation. Statistical analyses were performed using GraphPad Prism® version 6 by paired t-test or two-way ANOVA and followed with a Tukey's post-hoc test. Differences were considered statistically significant at $p<0.05$.

3.4 Results

3.4.1 Dynamic culturing did not affect the immunophenotype of the ASCs on the DAT

Multi-colour flow cytometry was performed to compare the immunophenotype of the ASCs that were cultured dynamically versus statically on the DAT scaffolds for 14 days. Representative flow plots for a single donor are shown in Appendix Figure A.7. Flow analysis of the cells that were enzymatically released from the scaffolds via collagenase digestion indicated that there was no significant difference in the percentage of $CD90^+CD29^+$ cells within the viable $CD31^-CD45^-$ population between the static and dynamic groups (Table 3.4). While donor-to-donor variability was observed, there were no significant differences in the average expression levels of CD26, CD34 or CD146 within the $CD90^+$ $CD29^+$ population between the groups (Table 3.4). In general, these findings suggest that dynamic culturing within the perfusion bioreactor did not significantly alter the immunophenotype of the ASCs on the DAT.

Table 3.4 The percentage of live $CD90^+CD29^+CD31^-CD45^-$ cells that were positive for $CD26^+$, $CD34^+$ and $CD146^+$ (n=6 scaffolds pooled, N=3 ASC donors).

	Static	Dynamic
$CD90^+CD29^+CD31^-CD45^-$ (of viable cells)	77.2 ± 8.0 %	84.0 ± 1.4 %
$CD90^+CD29^+CD31^-CD45^-$**$CD26^+$**	76.9 ± 12.4 %	86.9 ± 1.7 %
$CD90^+CD29^+$ $CD31^-CD45^-$ **$CD34^+$**	37.4 ± 4.7 %	39.6 ± 9.8 %
$CD90^+CD29^+$ $CD31^-CD45^-$**$CD146^+$**	27.8 ± 18.7 %	27.3 ± 13.9 %

3.4.2 Dynamic culturing of ASCs upregulated the expression of iNOS in the peripheral regions of the DAT scaffolds

Immunostaining was performed to assess the expression of iNOS and Arg-1 in the ASCs that were cultured statically or dynamically on the DAT scaffolds for 14 days. A high

density of $iNOS^+$ cells were visualized along the peripheral edges of the scaffolds in the dynamic group (Figure 3.1A), with a smaller number throughout the central regions of these scaffolds. In contrast, only low levels of $iNOS^+$ cells were visualized in both regions of the static culture group. Qualitative analysis of the Arg-1 staining patterns showed that $Arg\text{-}1^+$ cells were distributed throughout the central and peripheral regions of the scaffolds in both the static and dynamic groups. Co-staining results suggested that $iNOS^+Arg^+$ cells were present in both the static and dynamic groups (Figure 3.1A). While relatively few $iNOS^+Arg^+$ cells were observed in the statically cultured scaffolds, qualitatively more cells were visualized in the dynamic group, particularly along the scaffold border (Figure 3.1A).

Quantification of the $iNOS^+Arg\text{-}1^+DAPI^+$ cells in the central (> 200 μm from scaffold edge) and peripheral (< 200 μm from scaffold edge) regions of the scaffolds was performed. There was a significantly higher density of $iNOS^+Arg\text{-}1^+DAPI^+$ cells in the peripheral region of the dynamic scaffolds as compared to the central region in that group, as well as both regions of the static group (Figure 3.1B). Analysis of the number of $iNOS^+Arg\text{-}1^+DAPI^+$ cells relative to the total $DAPI^+$ cell population revealed that a significantly higher percentage of the ASCs co-expressed iNOS and Arg-1 within the peripheral region of the DAT scaffolds in the dynamic group (Figure 3.1C), suggesting that culturing within the perfusion bioreactor altered the phenotype of the ASCs within the scaffold periphery.

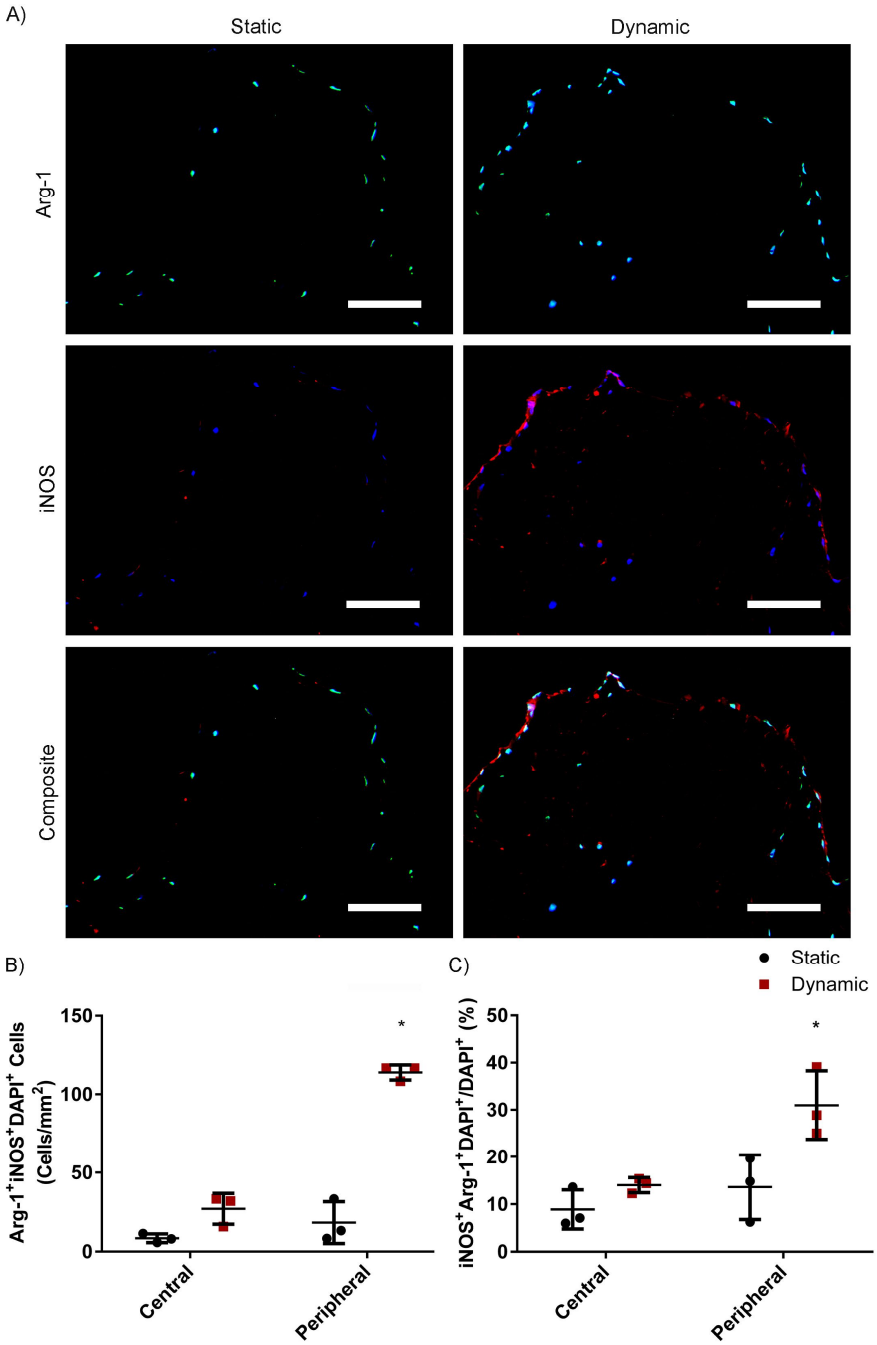

Figure 3.1 Dynamic culture on the DAT for 14 days increased the co-expression of iNOS and Arg-1 in the ASCs within the peripheral region of the scaffolds.
A) Representative immunostaining for Arg-1 (green) and iNOS (red) with DAPI (blue) for the static and dynamic groups at 14 days. Dashed lines indicate the edge of the DAT scaffolds. Scale bars represent 100 µm. B) The density of $iNOS^+Arg\text{-}1^+DAPI^+$ cells and C) the percentage of $iNOS^+Arg\text{-}1^+DAPI^+$ cells relative to the total $DAPI^+$ cell population in the central and peripheral regions of the scaffolds cultured statically or dynamically. Error bars represent standard deviation (n=3 cross-sections/scaffold, N=3 trials with different ASC donors). * = significant difference between the peripheral region of dynamic group and all other groups ($p<0.05$).

Further probing the expression levels of these functional markers, a significantly greater density of $iNOS^+DAPI^+$ cells was present in the peripheral regions of the dynamic scaffolds as compared to the central region in that group, as well as both the central and peripheral regions of the static cultured scaffolds (Appendix Figure A.8A). When assessed relative to the total $DAPI^+$ cell population, the percentage of $iNOS^+DAPI^+$ cells in the peripheral region of the dynamic group (33.2 ± 7.5%) was significantly different than the central region of the static group (14.7 ± 7.3%) (Appendix Figure A.8B). Similar to iNOS, a significantly greater density of $Arg\text{-}1^+DAPI^+$ cells was measured in the peripheral regions of the dynamic scaffolds (Appendix Figure A.8C). In general, a high percentage (>70%) of the ASCs within the DAT scaffolds expressed Arg-1 (Appendix Figure A.8D).

3.4.3 Dynamic culture of ASCs on the DAT scaffolds in the perfusion bioreactor altered angiogenic gene expression patterns

To probe whether culturing within the perfusion bioreactor modulated angiogenic gene expression in the ASCs cultured on the DAT scaffolds for 14 days, analysis with a Human Angiogenic Growth Factor RT^2 PCR Profiler Array was performed. Results compiled from 4 ASC donors indicated that 33 of the 84 genes analyzed were significantly different between the ASCs that were cultured dynamically versus statically on the DAT, including a variety of pro-angiogenic cytokines and growth factors, several ECM proteins, and a range of other signaling proteins implicated in angiogenesis (Figure 3.2). Of these genes, 24 were up-regulated and 9 were down-regulated in the dynamic group as compared to the static group.

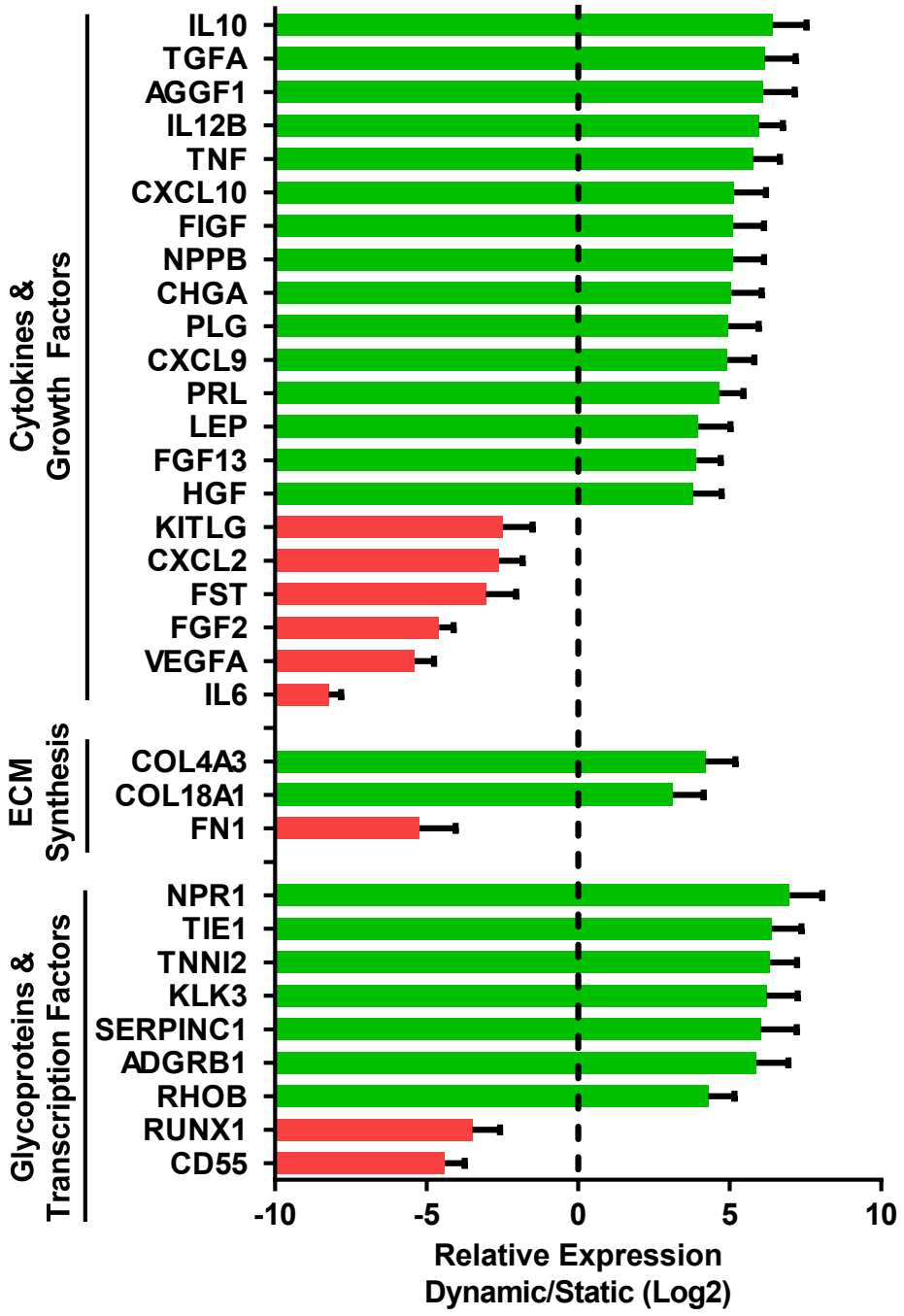

Figure 3.2 Dynamic culture alters the angiogenic gene expression profile of ASCs cultured on DAT scaffolds for 14 days. Fold regulation (Dynamic/Static) of the 33 genes on the PCR array that were significantly up- (green) or down- (red) regulated in the ASCs cultured dynamically versus statically. Statistical significance was determined via a multiple T-test (false discovery rate = 15%). Error bars represent standard deviation (N=4 trials with different ASC donors).

3.4.4 Dynamic culture alters the paracrine factor expression profile of the ASCs on the DAT scaffolds

To further probe whether dynamic culture altered the expression of a range of secreted pro-angiogenic and immunomodulatory factors in the ASCs on the DAT scaffolds, a custom Luminex® assay was performed to compare the protein expression levels of IL-10, TNF-α, HGF, CXCL-10, IL-6 and CXCL-2 in cell lysates from the static and dynamic groups after 14 days of culture. These factors were selected based on the PCR array results, as well as their known biological functions that may be important in the context of adipose tissue regeneration within the DAT. Consistent with the gene expression results, the protein expression levels of IL-10, CXCL-10, and HGF were significantly higher, and IL-6 expression was significantly lower, in the dynamic group as compared to the static group (Figure 3.3A, C, D, F). In contrast to the PCR results, no significant differences were observed in the protein expression levels of the pro-inflammatory cytokine TNF-α (Figure 3.3B) or the pro-inflammatory chemokine CXCL-2 (Figure 3.3E) between the groups.

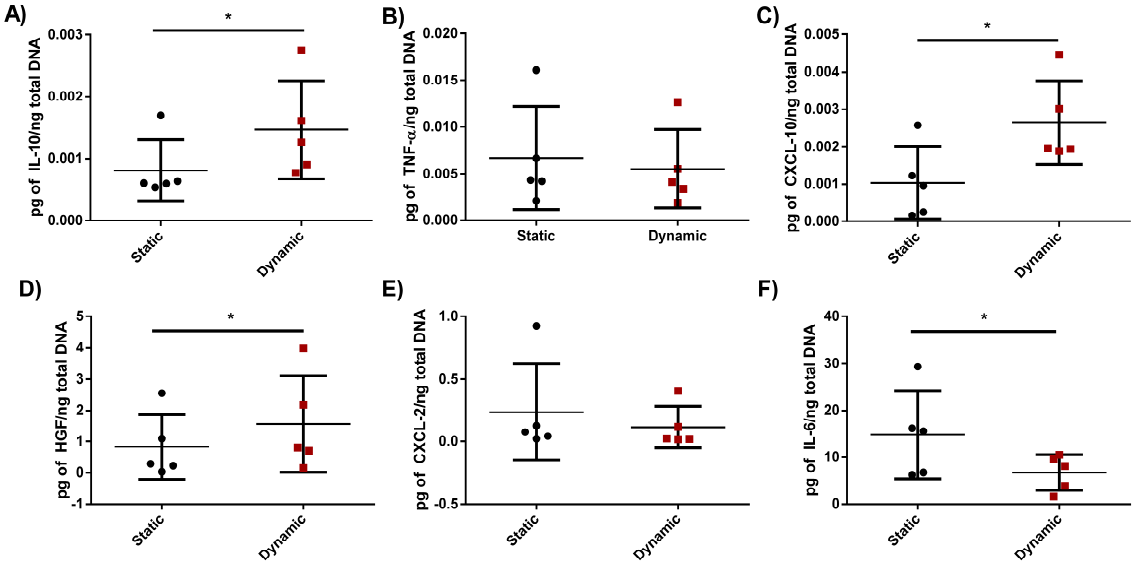

Figure 3.3 Dynamic culture within the perfusion bioreactor alters pro-angiogenic and immunomodulatory protein expression in the human ASCs cultured on the DAT scaffolds over 14 days. Expression of A) IL-10, B) TNF-α, C) CXCL-10, D) HGF, E) CXCL-2 and F) IL-6 as measured by Human Magnetic Luminex® Assay normalized to total dsDNA content. Error bars represent standard deviation (n=3 technical replicate scaffolds/trial, N=5 trials with different ASC donors). * = significant difference between static and dynamic groups ($p<0.05$; paired t-test).

3.4.5 Dynamic culture increased the number of ASCs expressing TNF-α and IL-10 in the DAT scaffolds at 14 days

Immunostaining was performed for Arg-1 in combination with TNF-α and IL-10 to assess whether dynamic culture modulated the presence and distribution of ASCs expressing these cytokines. A high density of Arg-1^+, TNF-α^+ and IL-10^+ cells were observed within the peripheral regions of the DAT scaffolds in the dynamic group (Figure 3.4A). A qualitatively smaller number of cells positive for each of these markers was observed in the central region of the dynamic group, as well as within both regions of the static group.

Quantification of the TNF-α^+DAPI$^+$ and IL-10^+DAPI$^+$ cell populations in the central (> 200 μm from scaffold edge) and peripheral (< 200 μm from scaffold edge) regions of the scaffolds was performed. Similar expression patterns were observed for both TNF-α (Figure 3.4B) and IL-10 (Figure 3.4C), with a significantly greater density of positive cells in the peripheral region of the scaffolds in the dynamic group as compared to all other regions. In addition, the TNF-α^+DAPI$^+$ and IL-10^+DAPI$^+$ cell densities were significantly greater in the central region of the dynamic group as compared to the central region of the static group. When expressed as a percentage of the total DAPI$^+$ cell population, a higher percentage of cells were TNF-α^+ in the peripheral region of the scaffolds in the dynamic group versus the static group (Appendix Figure A.9A). In contrast, no significant differences were observed in the percentage of IL-10^+ cells in either group (Appendix Figure A.9B).

Quantification also revealed that the Arg-1^+TNF-α^+IL-10^+DAPI$^+$ cell density was significantly higher in the peripheral region of the dynamic group as compared to all other regions (Figure 3.4D). Further, the percentage of TNF-α^+IL-10^+DAPI$^+$ cells (Appendix Figure A.9C) and Arg-1^+TNF-α^+IL-10^+DAPI$^+$ cells (Appendix Figure A.9D) relative to the total DAPI$^+$ cell population was significantly higher in the peripheral regions of the DAT scaffolds in the dynamic group as compared to the static group, suggesting that culturing in the perfusion bioreactor increased the relative number of ASCs that were expressing both TNF-α and IL-10, and the majority of these cells were also Arg-1^+.

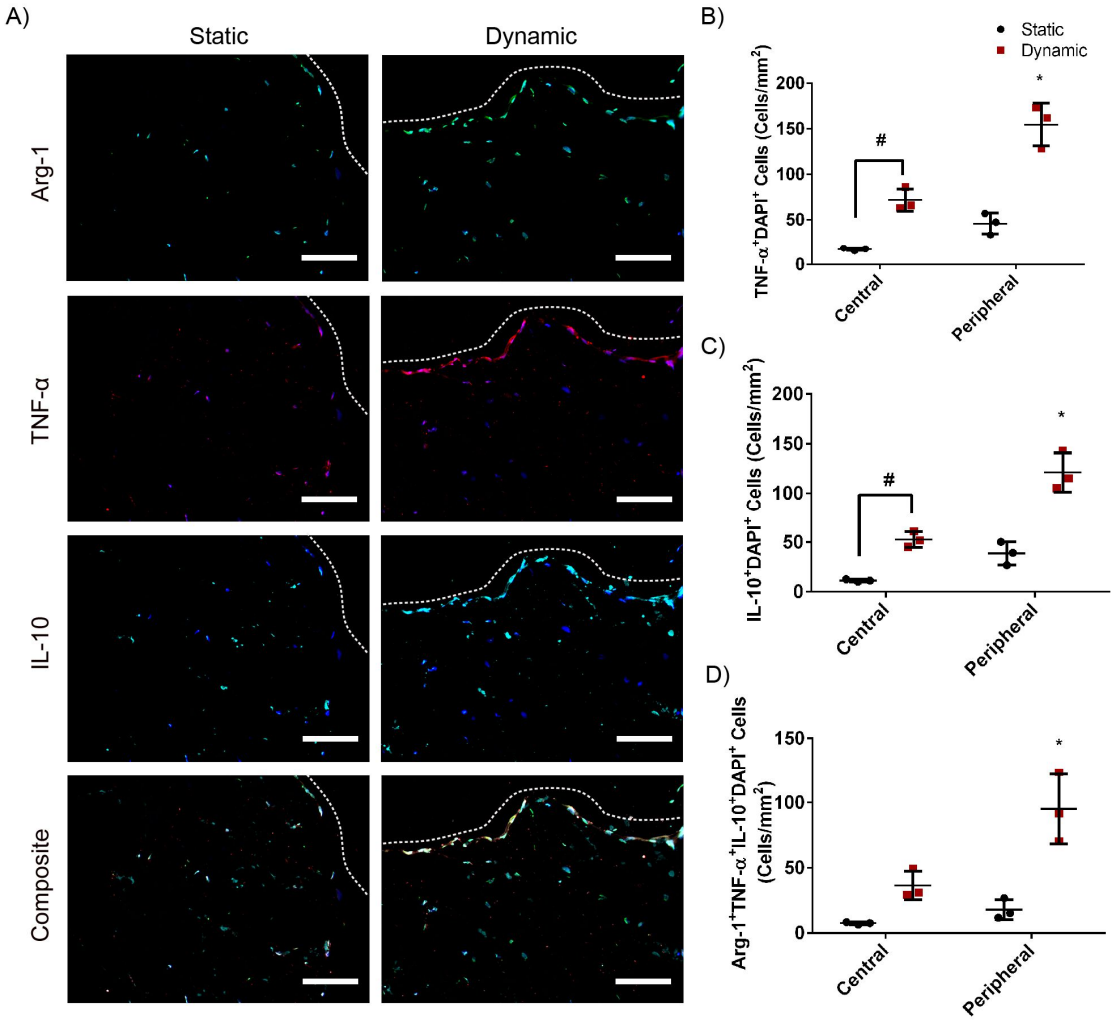

Figure 3.4 Dynamic culture increased the density of TNF-α$^+$ and IL-10$^+$ human ASCs in the peripheral region (< 200 µm from scaffold edge) of the DAT scaffolds that were cultured in the perfusion bioreactor for 14 days. A) Representative immunostaining showing Arg-1 (green), TNF-α (red) and IL-10 (cyan) expression with DAPI counterstaining (blue) for the static and dynamic groups. Dashed lines indicate the edge of the DAT scaffolds. Scale bars represent 100 µm. The B) TNF-α$^+$DAPI$^+$, C) IL-10$^+$DAPI$^+$ and D) Arg-1$^+$TNF-α$^+$IL-10$^+$DAPI$^+$ cell density in the central and peripheral regions of the DAT scaffolds in both the static and dynamic groups. Error bars represent standard deviation (n=3 cross-sections/scaffold, N=3 trials with different ASC donors). * = significant difference between the peripheral region of the dynamic group and all other regions, # = significant difference between the central region of the dynamic and static groups ($p<0.05$).

3.4.6 Dynamic culture of ASCs on the DAT enhanced CD31$^+$ endothelial cell recruitment into the scaffolds following implantation in the *nu/nu* mouse model

Following the *in vitro* characterization, *in vivo* studies were performed to probe how dynamic culture of the ASCs on the DAT modulated their capacity to stimulate the recruitment of a range of host cell populations into the DAT scaffolds at 1, 4 and 8 weeks post-implantation. Given the importance of angiogenesis in adipose tissue regeneration[328], the initial characterization focused on immunohistochemical staining to assess the presence and distribution of CD31$^+$ endothelial cells within the implants. CD31$^+$ vessels were observed within the implants at 1, 4 and 8 weeks in both the static and dynamic groups. At the 8-week timepoint, there were qualitatively more CD31$^+$ cells within the DAT implants in the dynamic group as compared to the static culture group, with some forming larger lumen structures (Figure 3.5A). Quantification of the staining confirmed that the CD31$^+$ cell density was significantly greater in the dynamic group as compared to the static group at all timepoints (Figure 3.5B).

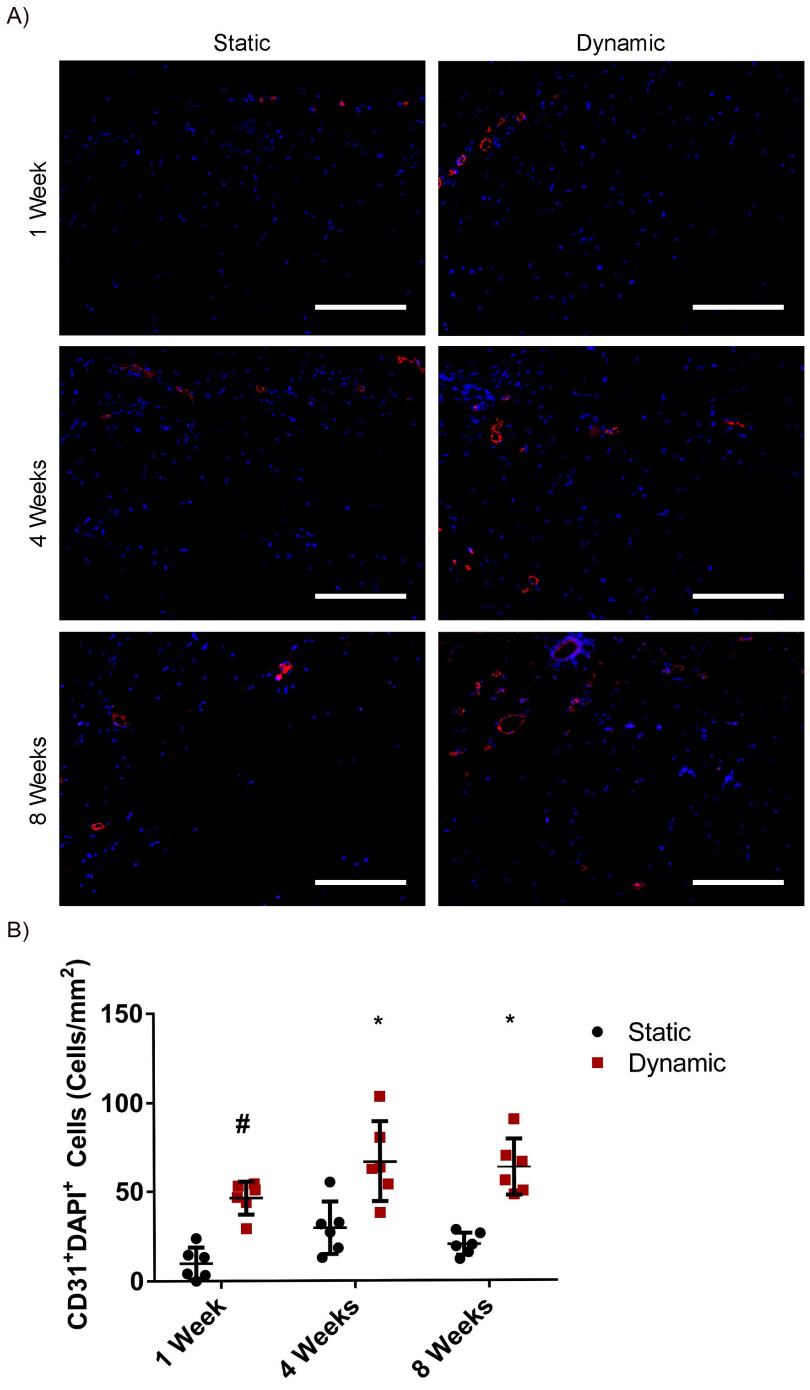

Figure 3.5 Dynamic culture of ASCs on the DAT scaffolds enhanced CD31$^+$ cell recruitment following implantation in the *nu/nu* mouse model. A) Representative immunostaining showing CD31 (red) with DAPI counterstaining within the DAT implants for both the static and dynamic groups at 1, 4 and 8 weeks. Scale bars represent 100 µm. B) CD31$^+$DAPI$^+$ endothelial cell density in the implants. Error bars represent the standard deviation (n=3 cross-sections/implant, N=6 implants/group). * = significant difference relative to the static group at 1, 4 and 8 weeks, # = significant difference relative to the static group at 1 and 8 weeks (*=$p<0.05$).

3.4.7 Dynamic culture of ASCs on the DAT scaffolds enhanced the recruitment of $CD26^+$ host cells at 1 week post-implantation in the *nu/nu* mouse model

Co-staining was performed for CD26 with human-specific Ku80 to probe host $CD26^+$ cell infiltration into the implants at 1, 4 and 8 weeks, as a potential marker of multipotent progenitor cells that can give rise to preadipocytes and adipocytes[416]. Qualitatively, the staining results showed a high density of $CD26^+$ cells in the dynamic group at 1 week (Figure 3.6A). The $Ku80^+$ human ASCs were distributed throughout the scaffolds in both the static and dynamic groups at all three timepoints, with $CD26^+Ku80^+$ cells observed (Figure 3.6A). Quantification of the $CD26^+Ku80^-DAPI^+$ cell population indicated that there was a significantly higher density of $CD26^+$ host cells in the DAT implants within the dynamic group as compared to the static group at 1 week (Figure 3.6B).

The $Ku80^+DAPI^+$ and $CD26^+Ku80^+DAPI^+$ human ASC populations were also quantified within the implants. Consistent with our previous work that demonstrated that dynamic culture under 2% O_2 within the perfusion bioreactor promoted human ASC expansion on the DAT[413], the $Ku80^+DAPI^+$ cell density was significantly higher in the dynamic group relative to the static group at 1 week (Appendix Figure A.10A). However, the number of human ASCs detected in the dynamic group was diminished at the later timepoints, with no significant differences observed in the $Ku80^+DAPI^+$ cell density between the static and dynamic groups at 4 or 8 weeks (Appendix Figure A.10A), similar to our previous findings[413]. The percentage of the human ASCs within the DAT implants that expressed CD26 also declined over time, with a significant decrease from 1 to 8 weeks, and no significant differences observed between the static and dynamic groups at any of the timepoints (Appendix Figure A.10B)

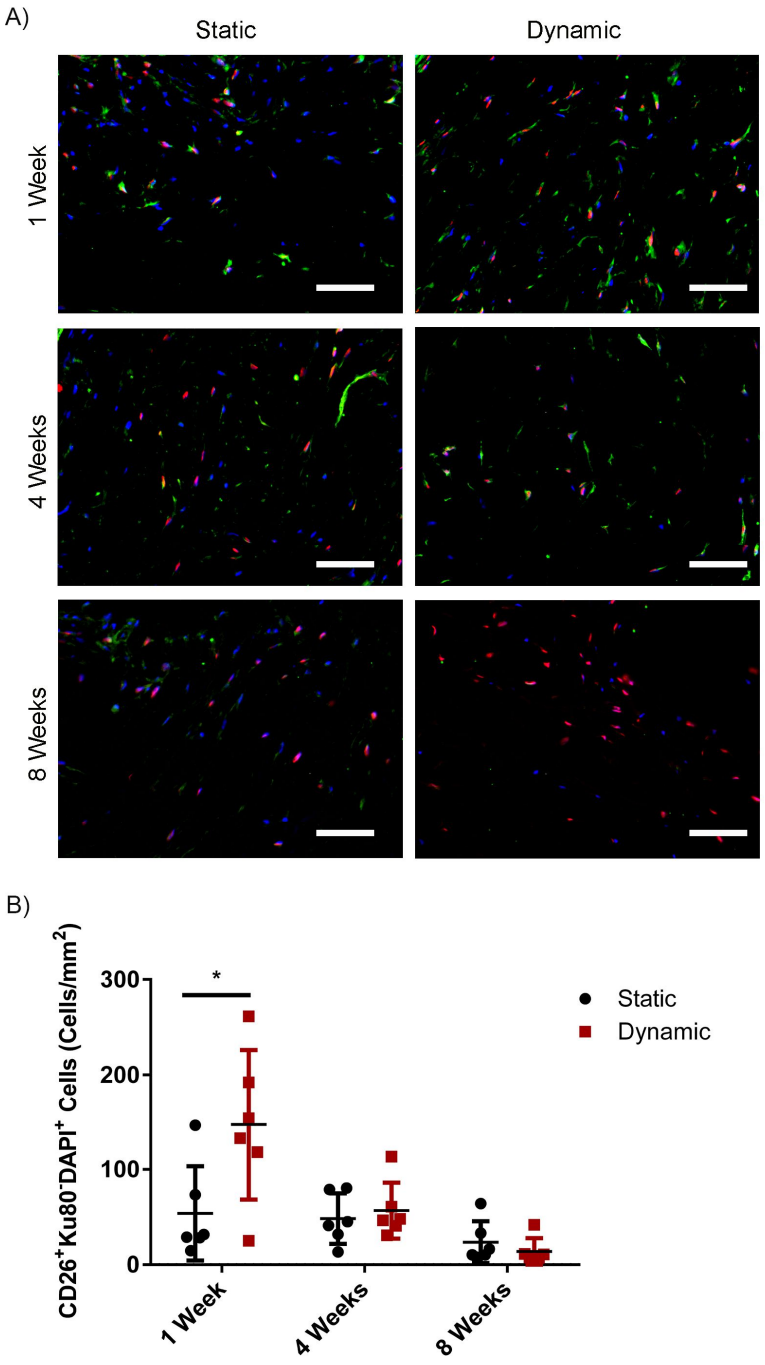

Figure 3.6 Dynamic culture of human ASCs on the DAT scaffolds enhanced the recruitment of CD26$^+$ host cells at 1 week post-implantation in the *nu/nu* mouse model. A) Representative immunostaining of CD26 (green) in combination with human-specific Ku80 (red), with DAPI counterstaining (blue) at 1, 4 and 8 weeks. Scale bars represent 50 µm. B) CD26$^+$ host cell (CD26$^+$Ku80$^-$DAPI$^+$) density within the DAT implants at 1, 4 and 8 weeks. Error bars represent standard deviation (n=3 cross-sections/implant, N=6 implants/group). * = significant difference between the static and dynamic groups at 1 week ($p<0.05$).

3.4.8 Dynamic culture of ASCs on the DAT scaffolds did not alter host macrophage recruitment following implantation in the *nu/nu* mouse model

To probe host macrophage infiltration into the DAT implants over time, immunostaining was performed for CD45 as a pan-leukocyte marker in combination with F4/80 as a marker of mature murine macrophages and CD68 as a marker of phagocytic macrophages (Figure 3.7A). Qualitatively, a high density of $CD45^+$, $F4/80^+$ and $CD68^+$ cells was observed within the DAT implants in both the static and dynamic groups at 1 week (Figure 3.7A), 4 weeks (Appendix Figure A.11) and 8 weeks (Appendix Figure A.12) post-implantation. Furthermore, $CD45^+$, $F4/80^+$ and $CD68^+$ cells were also observed in the fibrous capsules surrounding the implanted DAT at all three timepoints.

Quantification of the $CD45^+F4/80^+CD68^+DAPI^+$ cell density at 1, 4 and 8 weeks indicated that there were no significant differences between the static and dynamic groups at any of the timepoints (Figure 3.7B). However, a significant decline was observed in the dynamic group from 1 week to 8 weeks. Analysis of the percentage of $CD45^+$ cells that co-expressed both F4/80 and CD68 within the total $CD45^+DAPI^+$ cell population in the DAT implants indicated that the majority (>90%) of the $CD45^+$ cells were $F4/80^+CD68^+$ at 1 and 4 weeks, but a significant decline in this subpopulation was observed for both groups at 8 weeks (Figure 3.7C).

Individual analysis of the $CD45^+F4/80^+DAPI^+$ (Appendix Figure A.12A) and $CD45^+CD68^+DAPI^+$ (Appendix Figure A.12B) populations as a percentage of the total $CD45^+DAPI^+$ population within the implants confirmed that a high percentage (>90%) of the $CD45^+$ population expressed these macrophage markers at 1 and 4 weeks. However a significant decline in the relative expression of F4/80 was observed in the static group at 8 weeks as compared to both the dynamic and static groups at 1 and 4 weeks, and a significant decline in the relative expression of CD68 was observed in both groups at 8 weeks as compared to both groups at the earlier timepoints (Appendix Figure A.12).

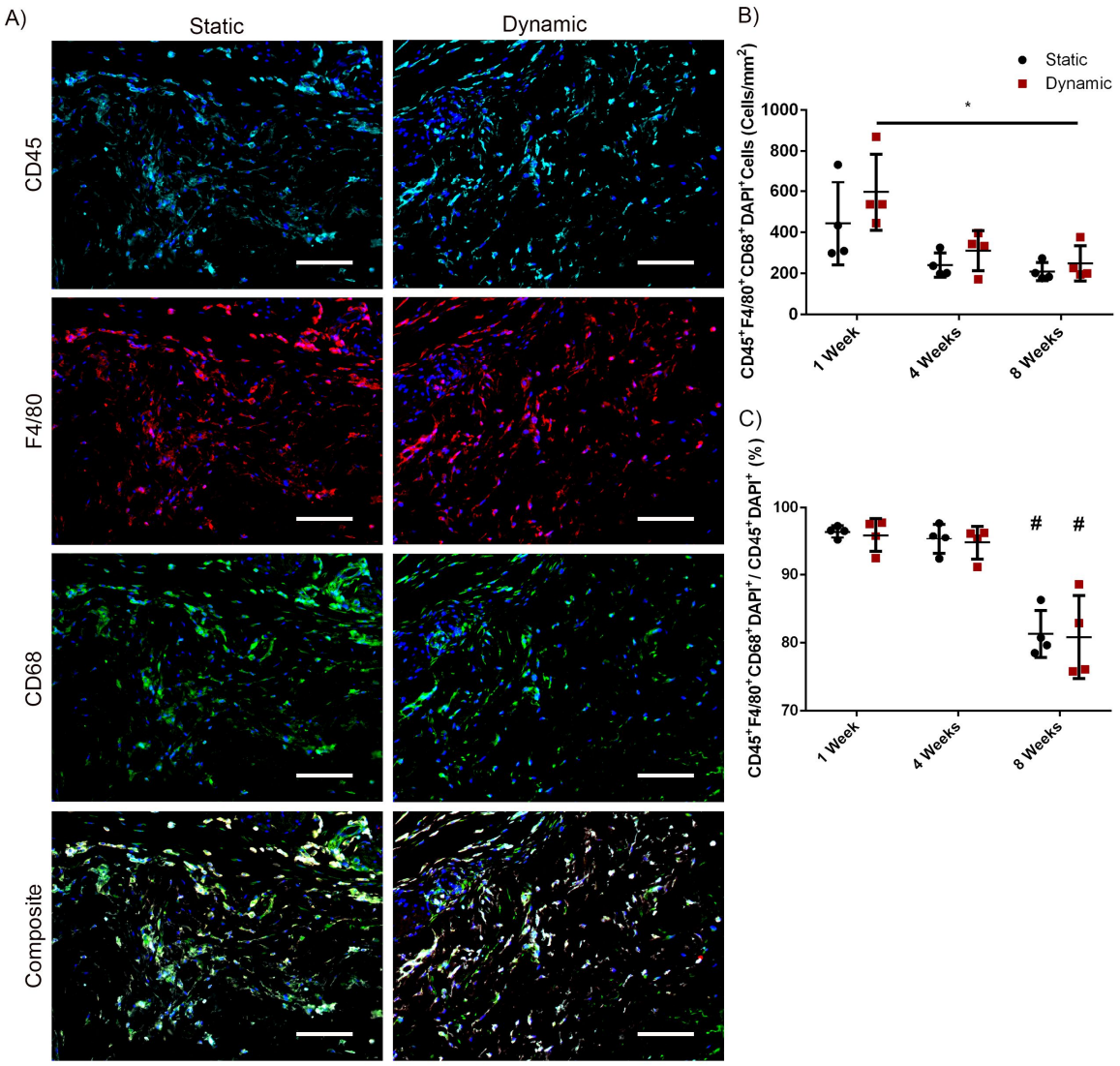

Figure 3.7 The recruitment of $CD45^+F4/80^+CD68^+$ macrophages was similar in both the dynamic and static cultured ASC-seeded DAT scaffolds in the *nu/nu* mouse model. A) Representative images showing CD45 (cyan), F4/80 (red) and CD68 (green) expression with DAPI counterstaining (blue) at 1 week. Scale bars represent 100 µm. B) $CD45^+F4/80^+CD68^+DAPI^+$ cell density in the static and dynamic groups. C) The percentage of $CD45^+F4/80^+CD68^+DAPI^+$ cells relative to the total $CD45^+DAPI^+$ cell population at 1, 4 and 8 weeks. Error bars represent the standard deviation (n=3 cross-sections/implant, N=4 implants/group). * = significant difference between the dynamic group at 1 and 8 weeks, # = significant difference between the indicated group and both the static and dynamic groups at 1 and 4 weeks ($p<0.05$).

3.4.9 Dynamic culture of ASCs on the DAT scaffolds modulated macrophage phenotype within the implants in the *nu/nu* mouse model

To probe the macrophage phenotype within the implants, co-staining was performed for the pan-leukocyte marker CD45 with the pro-regenerative macrophage marker CD163. $CD45^+CD163^+$ cells were observed in the fibrous capsules at the periphery of the implants at all three timepoints (Figure 3.8A). Interestingly, while $CD45^+$ cells were observed infiltrating the implants at 1, 4 and 8 weeks, very few $CD45^+CD163^+$ cells were visualized within the scaffolds, with the exception of the dynamic group at 8 weeks, which showed a relatively high density of infiltrating $CD45^+CD163^+$ cells (Figure 3.8A).

The density of $CD45^+CD163^+DAPI^+$ cells was quantified within the implanted scaffolds, excluding the fibrous capsule. The analysis confirmed that there were significantly more $CD45^+CD163^+DAPI^+$ cells within the DAT implants in the dynamic group at 8 weeks as compared to 1 and 4 weeks, as well as the static group at all three timepoints (Figure 3.8B). Additionally, the percentage of $CD45^+DAPI^+$ cells that were also $CD163^+$ was significantly greater in the dynamic group at 8 weeks (47.3 ± 6.5 %) as compared to all other conditions, supporting that there was a shift in macrophage phenotype in this group over time (Figure 3.8C).

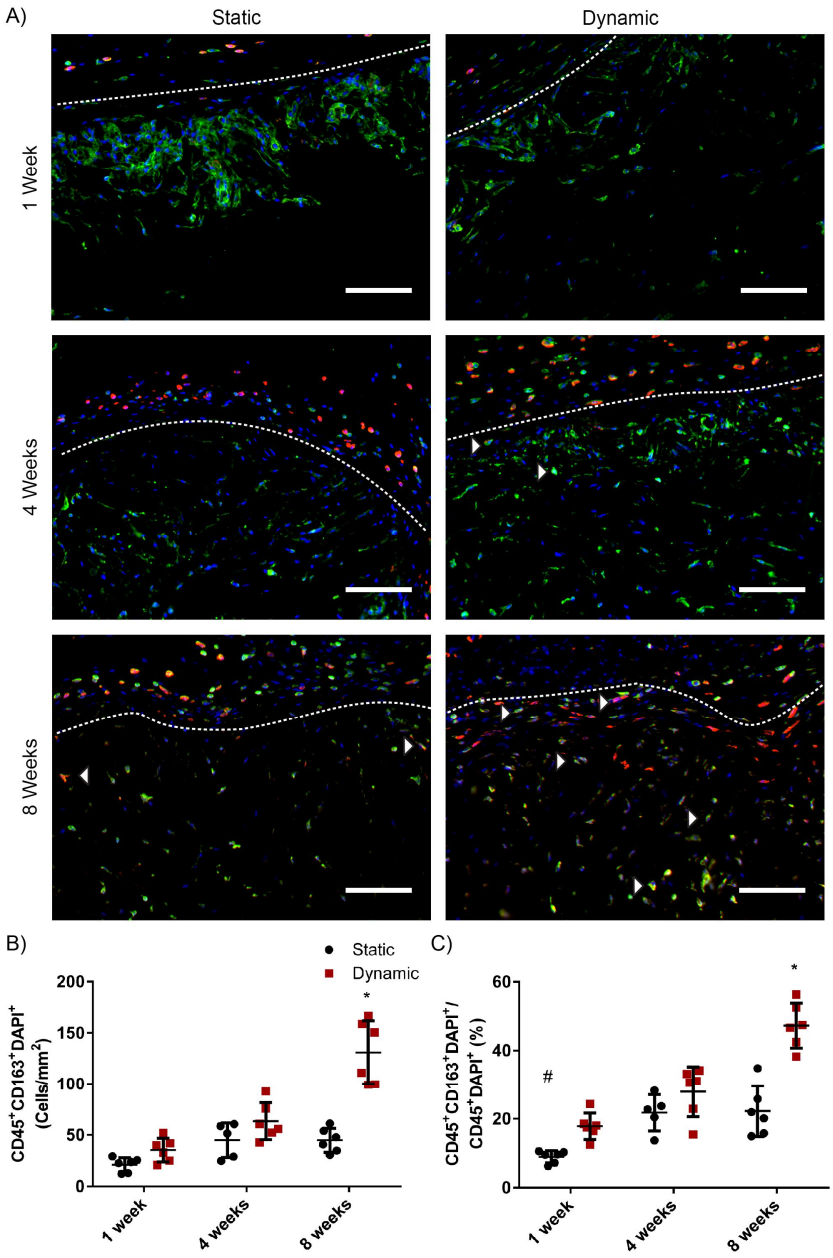

Figure 3.8 Dynamic culture of human ASCs on the DAT scaffolds enhanced the expression of the pro-regenerative macrophage marker CD163 in the CD45$^+$ host cell population at 8 weeks post-implantation in the *nu/nu* mouse model.
A) Representative images showing CD45 (green), CD163 (red) and DAPI (blue). Scale bars represent 100 µm. White arrowheads showing examples of CD45$^+$CD163$^+$ cells. Dashed lines indicate the border between the fibrous capsule (top) and the DAT implant (bottom). B) CD45$^+$CD163$^+$DAPI$^+$ cell density within the DAT implants. C) The percentage of CD45$^+$CD163$^+$DAPI$^+$ cells relative to the total CD45$^+$DAPI$^+$ population. Error bars represent standard deviation (n=3 cross-section/implant, N=6 implants/group). * = significant difference between the dynamic group at 8 weeks and all other conditions, # = significant difference between the static group at 1 week and the static and dynamic groups at both 4 and 8 weeks ($p<0.05$).

3.5 Discussion

Culturing human ASCs on the DAT scaffolds within the perfusion bioreactor system under 2% O_2 over 14 days was previously shown to markedly enhance *in vivo* angiogenesis and adipogenesis following subcutaneous implantation in the *nu/nu* mouse model[413]. The enhanced regeneration of host-derived adipose tissue was likely attributed in part to the fact that culturing within the bioreactor promoted the expansion of the human ASCs on the DAT, resulting in an estimated 2.2-fold increase in the number of ASCs delivered relative to the 2% O_2 static culture group that was included in the current study[413]. However, a growing body of evidence suggests that culturing under shear stress can also induce functional and phenotypic changes in MSC populations that may influence their capacity to stimulate regeneration[289–291]. As such, the focus of the current study was on assessing whether there were differences in the phenotype and paracrine function of the ASCs on the DAT following 14 days of culture under 2% O_2 within the bioreactor or under static conditions.

Flow cytometry analyses indicated that there were no significant differences in the immunophenotype of the ASCs cultured on the DAT in the static and dynamic groups. Interestingly, the expression levels of the markers analyzed were more similar to those reported for P0 or P1 ASCs as compared to P3 ASCs expanded on 2-D TCPS[417], suggesting that culturing on the DAT may have modulated ASC surface marker expression. In particular, while cell donor variability was observed, an average of ~40% of the $CD90^+CD29^+$ cell population was $CD34^+$, a marker that has been associated with pro-angiogenic functionality in MSC populations[418]. Previous studies have shown that CD34 is expressed on ~25% of the $CD45^-$ cells within the stromal vascular fraction (SVF) of adipose tissue[84], but that its expression rapidly diminishes following *in vitro* culture such that <5% of P3 ASCs are $CD34^+$[417]. Similarly, the CD146 expression levels were more similar to those reported for P0 ASCs than the ~5% reported at passage 3[417]. While CD146 is often regarded as a pericyte marker[419], its expression within ASC populations in humans has also been associated with enhanced pro-angiogenic function[420].

In addition, Arg-1 was found to be highly expressed in the ASCs cultured on the DAT scaffolds in both groups. Arg-1 is an enzyme that is commonly used as a marker of pro-regenerative macrophage polarization[421], which functions in breaking down L-arginine to generate urea[422]. iNOS also utilizes L-arginine as a substrate to generate nitric oxide (NO), and as such, Arg-1 can regulate iNOS activity[422]. In the present study, iNOS expression was enhanced in the ASCs within the peripheral region of the DAT scaffolds in the dynamic group. While the difference in the $iNOS^+$ cell density can be attributed in part to the overall higher density of ASCs in that region of the dynamic group[413], the fact that a significantly higher fraction of the total cell population was $iNOS^+Arg\text{-}1^+$ suggests that the shear stress stimulation may have altered the ASC phenotype in the dynamic group. Interestingly, previous studies have shown that iNOS expression is critical for the pro-regenerative immunomodulatory function of MSCs[124,133,149].

As a first step in probing the effects of dynamic culture on ASC function, the qPCR array identified 33 genes associated with angiogenesis that were differentially expressed between the dynamic and static groups. Mechanical stimulation through intermittent fluid flow has been previously reported to increase the production of pro-angiogenic factors including VEGFA, HGF, follistatin and leptin in cultured human ASCs[423]. Further, shear stress has been shown to enhance *FGF2* gene expression in human umbilical vein endothelial cells[424], as well as downregulate *VEGF* expression in cultured human umbilical veins[425]. In addition to activation of mechanotransduction pathways through dynamic culture, other factors that may have influenced the alterations in the gene expression patterns between the groups include the cell density, as well as a cascading effect of altered levels of other growth factors or cytokines. For example, elevated levels of TNF-α have been shown to induce the expression of chemokines including *CXCL10* in human endothelial and smooth muscle cells[426,427]. Likewise, the enhanced expression of HGF was found to decrease IL-6 and increase IL-10 expression in lipopolysaccaride (LPS)-induced macrophages *in vitro* and in interstitial macrophages in C57BL/6J mice[428].

To further assess whether culturing within the bioreactor modulated the paracrine profile of the ASCs on the DAT, a multiplex Luminex assay was performed to characterize the expression levels of a subset of factors selected from the PCR array that are known to

have the capacity to modulate various processes involved in soft tissue regeneration. IL-10 expression, which has been shown to promote a more pro-regenerative macrophage phenotype[135,429] and downregulate the expression of pro-inflammatory cytokines in immune cell populations[140,430], was significantly enhanced in the dynamic group, consistent with the gene expression results. In addition, the macrophage chemoattractant CXCL-10[431], as well as the pro-angiogenic factor HGF[115], were also detected at significantly higher levels in the lysates from the dynamic group. HGF can regulate endothelial cell survival, proliferation and migration[114], as well as endothelial tube formation[115]. As such, the enhanced expression of this factor may have played a role in the increased $CD31^+$ cell recruitment observed in the *in vivo* model. Further, HGF has also been shown to have immunomodulatory effects on monocytes and macrophages, promoting a more pro-regenerative response[432,433]. Also consistent with the gene expression results, the expression of IL-6, which is known to promote the pro-inflammatory polarization of monocytes[143,144], was significantly down-regulated in the dynamic group. In contrast to the gene array results, no significant differences were observed in the protein expression levels of the pro-inflammatory factors CXCL-2 or TNF-α within the lysates between the static and dynamic groups.

In contrast to the Luminex findings, the immunohistochemical analyses demonstrated that a significantly higher fraction of the ASCs in the peripheral region of the DAT scaffolds in the dynamic group expressed TNF-α relative to this same region in the static group, suggesting that the shear stress stimulation may have promoted the localized production of this factor. In addition, a significantly higher fraction of the ASCs in the peripheral region of the DAT in the dynamic group co-expressed both pro-inflammatory TNF-α and pro-regenerative IL-10, consistent with the mixed phenotype observed in the analysis of Arg-1 and iNOS expression. Although TNF-α and other pro-inflammatory factors are often regarded negatively for their association with chronic inflammation and disease[434,435], it is becoming increasingly recognized that inflammation plays an important role in stimulating angiogenesis and tissue regeneration[131,436]. As such, the locally enhanced expression of TNF-α may have been a mediating factor in the markedly increased host-derived adipose tissue regeneration in the dynamic group[413].

Building from the *in vitro* findings, *in vivo* studies were subsequently performed to further investigate whether dynamic culture on the DAT altered the capacity of the human ASCs to stimulate regeneration via paracrine-mediated mechanisms by assessing the effects on host cell recruitment. While there was a significantly higher density of human ASCs within the scaffolds in the dynamic group at 1 week post-implantation, there was no difference in human cell retention between the groups at either 4 or 8 weeks, consistent with our previous findings[413]. While the higher initial cell dose delivered in the dynamic group may have influenced the response, the *in vitro* characterization studies support that there were also differences in the phenotype and secretome of the ASCs within the DAT that could have impacted regeneration.

As a measure of angiogenesis within the implants, $CD31^+$ endothelial cell recruitment was significantly enhanced in the dynamic group at 1, 4, and 8 weeks. These findings are consistent with previous Masson's trichrome staining results that showed a significant increase in the density of erythrocyte-containing blood vessels in the DAT implants in the dynamic group at 4 and 8 weeks[413]. However, it is also possible that other non-endothelial $CD31^+$ cell populations, such as certain macrophage subsets[437], could also be present in the scaffolds and contributing to the higher density observed in the dynamic group.

The infiltration of host-derived $CD26^+$ cells was also probed. Recent studies have shown that CD26, also known as dipeptidylpeptidase IV (DPPIV), can be associated with an adipocyte precursor phenotype[375,416]. More specifically, a study by Merrick *et al.* demonstrated that a $CD26^+$ interstitial progenitor population within adipose tissue could give rise to an intermediate population that was committed to the adipogenic lineage and could differentiate into mature adipocytes *in vivo*[416]. Notably, CD26 expression was down-regulated as the progenitor cells began to differentiate[416]. In the present study, the higher density of host-derived $CD26^+$ cells observed at 1 week post-implantation may indicate that there was enhanced adipogenic progenitor cell recruitment in the dynamic group, contributing to the previously-characterized increased presence of host-derived adipocytes within this implant group at 8 weeks[413]. However, it is important to note that CD26 can also be expressed by other cell populations. For example, CD26 has been

associated with a more pro-fibrotic phenotype in fibroblast populations[438]. In addition, CD26 can be expressed on immune cells including dendritic cells[439,440], macrophages[440], and natural killer cells[441]. As such, further studies are required to more fully characterize the $CD26^+$ cells and determine more conclusively whether there is a link between this population and the enhanced adipogenesis observed in this group.

Macrophages have been indicated to play an important role in mediating both angiogenesis and adipose tissue regeneration within ECM-derived bioscaffolds[169,442,443]. As such, the effects of dynamic culture on host macrophage recruitment were probed through co-staining for CD45, F4/80 and CD68, which showed no significant differences in terms of cell densities between the groups at any of the timepoints. These findings are similar to previous studies showing that seeding the DAT with allogeneic ASCs did not significantly impact the $CD68^+$ macrophage density within the implants in an immunocompetent rat model over 12 weeks relative to unseeded controls[169]. Further, similar to the previous results[169], a high density of macrophages was observed within the DAT implants in both groups at all time points. Interestingly, within the $CD45^+$ cell population there was an increased percentage of cells that were $F4/80^-$ and $CD68^-$ within both implant groups at 8 weeks. These cells may be other macrophage subpopulations or dendritic cells that do not express these markers[444], or potentially natural killer cells[445]. However, further analyses using additional markers would be required to more fully characterize the $CD45^+F4/80^-CD68^-$ cell population and assess their potential effects within the implants.

While there was no difference in total macrophage recruitment, analysis of CD163 expression in the $CD45^+$ cell population suggested that there was a shift in macrophage phenotype at 8 weeks in the dynamic group. CD163 is a hemoglobin scavenger receptor found on macrophage subpopulations[446] that is upregulated by IL-10 and suppressed by pro-inflammatory mediators such as TNF-α[447,448]. The expression of CD163 in macrophages has been associated with a more pro-regenerative phenotype that is involved in both angiogenesis and ECM remodeling[351]. In the previous immunocompetent rat model, seeding the DAT with allogeneic ASCs was shown to enhance the fraction of $CD163^+$ cells within the implants relative to unseeded controls at

both 8 and 12 weeks, which also showed significantly greater remodeling into host-derived adipose tissue[169]. As such, the infiltrating $CD163^+$ macrophages may have contributed to the enhanced adipose tissue regeneration that was previously reported in the DAT implants that were cultured for 14 days under 2% O_2 prior to implantation[413].

3.6 Conclusions

The findings of the current study support that in addition to promoting cell expansion, dynamic culture of human ASCs on the DAT scaffolds within the perfusion bioreactor under 2% O_2 altered their phenotype and paracrine profile relative to controls cultured under static conditions. Interestingly, a fraction of the ASCs within the peripheral region of the DAT implants in the dynamic group were shown to exhibit both pro-inflammatory and anti-inflammatory characteristics, co-expressing iNOS and Arg-1, as well as both TNF-α and IL-10. Moreover, shear stress stimulation was shown to modulate the expression of a range of genes and proteins associated with the immunomodulatory and pro-angiogenic paracrine functionality of MSCs. These findings suggest that culturing within the perfusion bioreactor system may pre-condition the ASCs, altering their capacity to stimulate regeneration via paracrine-mediated mechanisms. Analysis in the *in vivo* model indicated that culturing within the bioreactor prior to implantation enhanced the recruitment of $CD31^+$ endothelial cells, as well as $CD26^+$ host cells, into the implants, which may have contributed to the enhanced angiogenesis and adipogenesis previously observed in this group. While there was no significant difference in total macrophage recruitment between the groups based on analysis of F4/80 and CD68 expression, greater infiltration of $CD163^+$ macrophages was observed in the dynamic group at 8 weeks, indicative of a shift towards a more pro-regenerative macrophage response. Future studies should focus on de-coupling the effects of increased initial cell density versus altered cell function in modulating the host response. Overall, the findings support the further investigation of shear stress stimulation as a means to pre-condition ASCs and enhance their capacity to stimulate angiogenesis and tissue regeneration through indirect mechanisms.

Chapter 4

4 Development of a rocking bioreactor system for the dynamic culture of adipose-derived stromal cells on decellularized adipose tissue coatings

4.1 Abstract

The development of bioreactor systems for promoting the expansion of pro-regenerative cell populations is of significant interest in the fields of tissue engineering and regenerative medicine. The mechanical stimulation that can be induced by dynamic culture can modulate cell phenotype and function, including paracrine factor secretion. The focus of this work was on the preliminary exploration of a novel rocking bioreactor system that incorporated coatings derived from tissue-specific extracellular matrix (ECM) as a dynamic preconditioning strategy for human adipose-derived stromal cells (ASCs). More specifically, the studies compared the response of ASCs seeded on fibrous coatings fabricated from human decellularized adipose tissue (DAT) or uncoated controls and cultured either dynamically on the rocking platform or statically for up to 7 days. Analysis of the ASC immunophenotype through multi-colour flow cytometry showed that dynamic culture on the DAT coatings significantly enhanced the expression of CD146 in the $CD90^{+}CD29^{+}$ ASC population compared to all other conditions. Further, pilot study results indicated that dynamic culture on the DAT coatings stimulated the expression of inducible nitric oxide synthase (iNOS) and promoted cell alignment at 7 days, suggesting that there was a change in cell phenotype in this group. Analysis of the expression of a range of pro-regenerative gene markers through a custom qPCR array identified no significant differences between the groups, suggesting that the dynamic culture conditions require further optimization. Collectively, these studies provide initial support for the further exploration of this new rocking bioreactor system incorporating the DAT coatings as a potential strategy to modulate the pro-regenerative capacity of human ASCs through cell expansion under dynamic conditions.

4.2 Introduction

The repair of damaged and deficient subcutaneous adipose tissue remains a significant clinical challenge in the fields of plastic and reconstructive surgery, and there is a clear need for new approaches that stimulate the regeneration of healthy host-derived adipose tissue and support long-term volume augmentation[18,377]. Recent advances in adipose tissue engineering have shown that combining tissue-specific bioscaffolds with regenerative cell populations may be a promising strategy for this clinical application[169,170,255,258,259,449].

Research in the Flynn lab has focused on the development of a broad range of bioscaffold formats derived from decellularized adipose tissue (DAT), including 3-D scaffolds[253], foams[227], microcarriers[257], coatings[385] and hydrogels[255]. These unique adipose-derived bioscaffolds have been shown to provide a highly supportive microenvironment for the adipogenic differentiation of human adipose-derived stromal cells (ASCs) in culture[253–255,257,260,385]. Moreover, DAT scaffolds seeded with allogeneic ASCs stimulated host-derived adipose tissue regeneration within the implants when delivered subcutaneously in immunocompetent Wistar rats[169,255].

Building from this work, a scaffold-based perfusion bioreactor system was developed with the goal of promoting human ASC expansion and infiltration on the DAT scaffolds[413]. Dynamic culture of the ASCs on the DAT scaffolds within the perfusion bioreactor under 2% O_2 for 14 days was shown to enhance ASC proliferation relative to bioreactor culture under 20% O_2 and static culture controls[413]. Further, when implanted subcutaneously in an athymic mouse (*nu/nu*) model, angiogenesis and adipogenesis were markedly enhanced in the ASC-seeded scaffolds that had been cultured within the bioreactor for 14 days under 2% O_2 prior to implantation[413]. Subsequent studies in Chapter 3 of this thesis supported that in addition to promoting ASC expansion, dynamic culture on the DAT scaffolds within the bioreactor modulated the ASC phenotype and paracrine factor secretion profile.

While the pro-regenerative effects were promising, scaling up the perfusion bioreactor system to be able to generate scaffolds of sizes suitable for clinical applications in

humans would be a significant challenge. In particular, ASCs cultured within this system were found in higher density along the periphery of the DAT scaffolds, suggesting that there was limited medium perfusion into the central regions of the DAT scaffolds[413]. In these previous studies, an integrated approach was applied in which the ASCs were expanded on the same DAT scaffolds on which they would be delivered. The findings suggest that a better strategy may be to develop separate platforms for ASC expansion and delivery that would be more readily scalable. Focusing on the ASC expansion platform, rocking bioreactor systems are an interesting alternative, as they have been successfully applied for the culture of embryonic stem cells (ESCs)[450], human bone marrow-derived mesenchymal stromal cells (MSCs)[451], dermal fibroblasts[452] and lymphocytes[453]. These systems leverage gravity to drive an oscillating fluid motion that ensures thorough mixing of the media and applies shear stress to the cells in culture[451]. This shear stress stimulation has the potential to promote cell expansion[454] and modulate cell phenotype including paracrine function[451].

The focus of this study was to perform a preliminary assessment of a novel rocking bioreactor system as a new approach for the dynamic preconditioning of human ASCs. Recognizing the innate cell-instructive capacity of the extracellular matrix (ECM)[256,260], the effects of incorporating fibrous DAT coatings (~150 μm thick) as a substrate within this system were explored. In contrast to conventional culture on tissue culture polystyrene (TCPS), the DAT coatings have a complex ECM ultrastructure and mechanical properties (Young's modulus ~40 kPa) more similar to native tissues[385]. Further, culturing human ASCs on the DAT coatings was shown to significantly enhance their expansion and adipogenic differentiation under static culture conditions relative to similar collagen-based coatings and uncoated TCPS controls[385]. In the current study, human ASCs were seeded onto the DAT coatings or uncoated controls and cultured for up to 7 days either dynamically on the rocking platform or statically under 2% O_2, selected based on the previous perfusion bioreactor studies[413]. Multi-colour flow cytometry was performed to characterize the ASC immunophenotype after 7 days of culture. Immunohistochemical analyses assessed the effects of dynamic culture on the ASC morphology and expression of inducible nitric oxide synthase (iNOS), a marker

associated with immunomodulatory function in MSCs[124,133,415]. Finally, gene expression analyses were conducted using a custom-made qPCR array to probe for changes in the expression levels of a range of markers associated with soft tissue regeneration between the groups.

4.3 Methods

4.3.1 Materials

Unless otherwise stated, all materials were purchased from Sigma Aldrich Canada Ltd. (Oakville, Canada), and all antibodies for immunostaining were purchased from Abcam (Cambridge, USA).

4.3.2 Human ASC isolation and DAT coating fabrication

Human adipose tissue was processed to either isolate ASCs[238] or decellularized[253] using published methods. In brief, surgically discarded adipose tissue was collected with informed consent from the University Hospital and St. Joseph's Hospital in London, Canada and transported to the laboratory in sterile phosphate buffered saline (PBS) with 2% bovine serum albumin (BSA) on ice. The protocols for this study were reviewed and approved by the Human Research Ethics Board at Western University (REB# 105426).

The ASCs were cultured (37°C, 5% CO_2) in proliferation medium comprised of DMEM:Ham's F12 (Wisent, St. Bruno, Canada) supplemented with 10% fetal bovine serum (FBS) (Wisent, St. Bruno, Canada) and 100 U/mL penicillin and 0.1 mg/mL streptomycin (1% pen-strep) (ThermoFisher, Waltham, USA). The cells were frozen at passage 1 (P1) until ready for use.

Decellularized tissues from multiple donors were pooled and fabricated into DAT coatings based on published work[385]. Briefly, the DAT was finely minced and cryo-milled prior to decontamination through rinsing in 70% ethanol overnight under constant agitation at room temperature. The milled DAT was then rinsed in PBS (3 x 15 min) and digested with α-amylase (3% w/v in 0.25 M NaH_2PO_4) at room temperature under constant agitation at 300 RPM for 3 days. The digested samples were then washed in 5% NaCl (w/v in deionized H_2O) for 10 min, resuspended at a concentration of 25 mg

DAT/mL in 0.2 M acetic acid, and homogenized (PowerGen Model 123 homogenizer, Fisher Scientific, Ottawa, Canada) to generate a DAT suspension. The DAT suspension was plated in 4-well rectangular plates (ThermoFisher) at a volume of 3 mL per well and air dried at room temperature within a biological safety cabinet overnight. For immunohistochemical characterization studies, rectangular glass coverslips were positioned within the wells prior to the coating application.

4.3.3 ASC seeding

The DAT coatings were washed twice in sterile PBS immediately prior to seeding. Passage 3 (P3) ASCs were seeded on the DAT coatings or uncoated control wells at a density of 5,000 cells/cm^2 in proliferation medium and incubated overnight (37°C, 5% CO_2, ~20% O_2) to promote cell attachment. Subsequently, the seeded well plates were transferred to the rocking platform (Thermo Scientific Compact Digital Rocker) (Appendix Figure A.14) and cultured dynamically at a frequency of 30 RPM and a rocking angle of 13° under 2% oxygen tension (2% O_2/93% N_2/5% CO_2, 37°C) controlled using a tri-gas incubator (ThermoFisher Forma Series II 3110) for up to 7 days. Static culture controls were also included in all assays, to generate a total of 4 experimental conditions: (i) static uncoated, (ii) static DAT-coated, (iii) dynamic uncoated, and (iv) dynamic DAT-coated.

4.3.4 Multi-colour flow cytometry

To explore the effects of dynamic culture on the DAT coatings on the ASC immunophenotype, multi-coloured flow cytometry analysis was performed to assess the expression levels of the positive ASC markers CD90 and CD29, along with the variable markers CD26, CD34 and CD146. Gating was performed to exclude any contaminating CD31$^+$ endothelial cells and CD45$^+$ hematopoietic cells. After 7 days of culture under static or dynamic conditions, the cells were trypsin-released through incubation in 0.25% Trypsin/EDTA (325-043-CL, Wisent, St. Bruno, Canada) for 10 min at 37°C. The suspended cells were filtered through a 100 µm nylon mesh and then stained with calcein violet-AM (BioLegend) for 25 min. The stained cells were then centrifuged at 500 xg for 7 min at 4°C prior to antibody staining and flow analysis following the methods

described in Section 3.3.4. For the analyses, duplicate wells were pooled per condition (n=2 wells pooled) to obtain sufficient cell numbers and the studies were repeated with a total of 3 different ASC donors (N=3).

4.3.5 Immunohistochemical analysis of ASC morphology and iNOS expression

A pilot study was performed to probe the effects of dynamic culture on the DAT coatings on the ASC morphology and expression of iNOS as a potential marker of phenotypic changes in the ASCs[133]. Samples prepared with ASCs from one donor (N=1) were collected after 1, 3 and 7 days of culture, fixed in 4% paraformaldehyde for 5 min, and washed 3 times in PBS. The samples were then stained overnight with a rabbit anti-iNOS antibody (ThermoFisher PA1-036, 1:200 dilution) diluted in PBS-T (0.1% Tween-20 supplemented with 1% BSA) at 4°C before being stained with a goat anti-rabbit antibody conjugated with Alexa Fluor® 594 (1:200 dilution) diluted in PBS-T for 1 h at room temperature. To visualize the cell morphology, staining with Alexa Fluor® 680 Phalloidin (Abcam AB176760) was performed in accordance with the manufacturer's protocols. Finally, the samples were counterstained with Hoechst 33258 (ThermoFisher) to visualize the cell nuclei and mounted in Fluoroshield Mounting Medium. The samples were visualized with an EVOS® FL Cell Imaging System under 20X magnification. The number of $iNOS^{+}Hochest^{+}$ cells was quantified using ImageJ software in 15 randomly selected non-adjacent fields of view per condition per timepoint.

4.3.6 PrimePCR™ array analysis of gene expression

To probe whether dynamic culture on the DAT coatings altered the gene expression profile of the human ASCs, analysis was performed using a custom-made PrimePCR™ Array (BioRad) that included genes associated with (i) angiogenesis, (ii) inflammation, (iii) ECM synthesis, and (iv) ECM remodeling. Appendix Table A.2 lists the specifics of the 26 genes of interest included in the array. The total cellular RNA from duplicate sample wells was extracted and pooled from all four conditions after 7 days of culture using PureZol® RNA Isolation Reagent (BioRad) and the Aurum® Total RNA Mini kit (BioRad). cDNA was synthesized from 2 μg of input RNA with an iScript® cDNA

synthesis kit (BioRad). The PrimePCR™ Array was performed in accordance with the manufacturer's protocols with duplicate samples (n=2) of 25 ng of cDNA per well, and repeated with ASCs from a total of three different donors (N=3). The expression of all genes of interest was normalized against the geometric mean of the reference genes UBC, *GAPDH* and *RSP18* using BioRad CFX Maestro® Software. Data was normalized against the static uncoated group for comparative purposes.

4.3.7 Statistical analysis

All numerical values are represented as the mean ± standard deviation. Statistical analyses were performed using GraphPad Prism® version 6 by one-way ANOVA and followed with a Tukey's post-hoc test. Differences were considered statistically significant at $p<0.05$.

4.4 Results

4.4.1 Dynamic culture of ASCs on the DAT coatings enhanced the expression of CD146 within the $CD90^+CD29^+$ human ASC population

Multi-colour flow cytometry analysis was performed to assess the effects of dynamic culture on the DAT coatings on the immunophenotype of the cultured human ASCs. For all groups, $CD31^+CD45^+$ cells accounted for <2.5% of all viable cells, and >90% of the viable $CD31^-CD45^-$ population was $CD90^+CD29^+$, confirming their stromal origin (Table 4.1). The $CD90^+CD29^+$ human ASCs were also highly positive for CD26 and showed donor-dependent variability in terms of CD34 expression, with no significant differences between the four culture conditions for either of these markers (Table 4.1). Interestingly, a significantly greater percentage of the $CD90^+CD29^+$ cell population was $CD146^+$ in the dynamic DAT-coated group as compared to all other conditions following 7 days of culture (Table 4.1). Representative scatter plots for the CD26 and CD34 analyses are shown in Appendix Figure A.15, and for CD146 are shown in Figure 4.1.

Table 4.1 The percentage of live $CD90^+$ $CD29^+CD31^-CD45^-$ cells that were positive for $CD26^+$, $CD34^+$ and $CD146^+$ (n=2 wells pooled, N=3 trials with different ASC donors).

	Static Uncoated	Static DAT-coated	Dynamic Uncoated	Dynamic DAT-coated
Viable Cells (calcein violet-AM^+)	94.7 ± 3.7 %	94.4 ± 1.5%	94.4 ± 4.8%	97.2 ± 1.0%
$CD90^+CD29^+CD31^-$ $CD45^-$ (of viable cells)	89.5 ± 6.7%	89.8 ± 1.6%	82.7 ± 4.8%	87.6 ± 6.8%
$CD90^+CD29^+CD31^-$ $CD45^-$**$CD26^+$**	94.3 ± 5.4%	94.7 ± 6.3%	92.8 ± 4.9%	91.5 ± 7.1%
$CD90^+CD29^+$ $CD31^-$ $CD45^-$ **$CD34^+$**	18.8 ± 25.0%	13.0 ± 18.3%	11.9 ± 15.4%	10.2 ± 12.7%
$CD90^+CD29^+$ $CD31^-$ $CD45^-$**$CD146^+$**	3.1 ± 1.1%	6.9 ± 4.4%	2.1 ± 0.8%	13.9 ± 3.2%

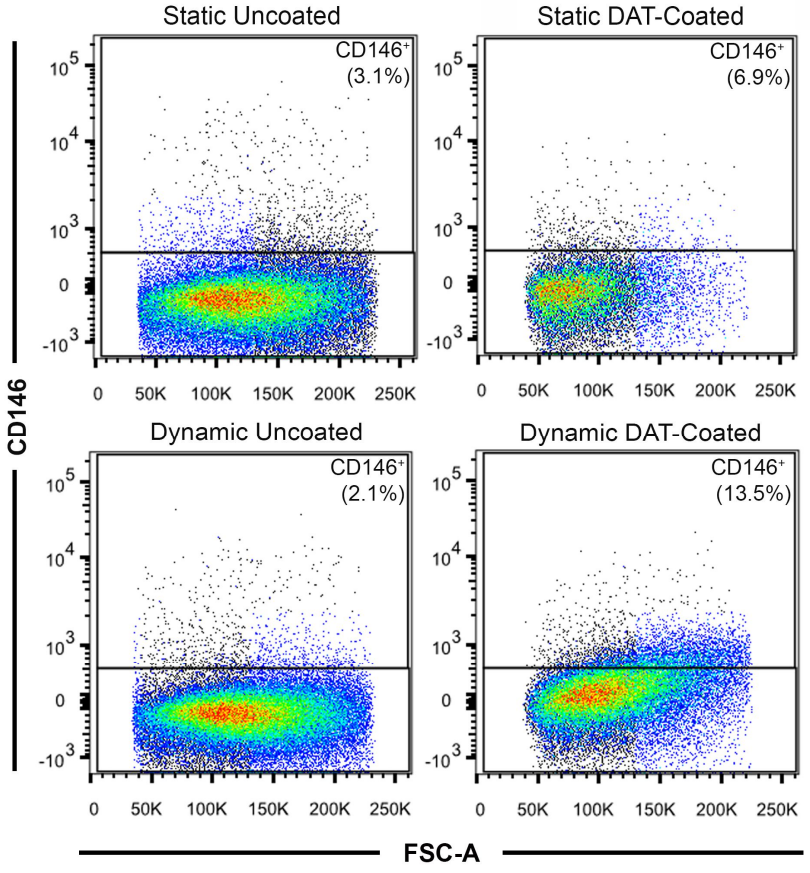

Figure 4.1 Dynamic culture of human ASCs on the DAT coatings for 7 days on the rocking platform enhanced the expression of CD146 in the $CD90^+CD29^+$ cell population. Representative scatter plots showing the fluorescence intensity of CD146 versus the forward scatter area (FSC-A).

4.4.2 Dynamic culture of ASCs on the DAT coatings promoted cell alignment and upregulated iNOS expression

Immunohistochemical analysis was performed to probe the morphology and iNOS expression patterns in the human ASCs that were cultured dynamically or statically on the DAT coatings or uncoated controls for 1, 3 and 7 days. Notably, there was a qualitative reduction in the number of cells visualized in the dynamic DAT-coated group from 1 to 3 days, suggesting that the shear stress stimulation may have caused initial cell detachment in this group, but higher densities were observed at day 7 (Figure 4.3A). At both 3 and 7 days, the ASCs were observed to have a more spindle-like morphology when cultured on the DAT coatings, with less cell spreading as compared to the uncoated controls. Interestingly, the ASCs in the dynamic DAT-coated group appeared to align perpendicular to the direction of the fluid flow at day 7 (Appendix Figure A.17). $iNOS^+$ cells were observed in the dynamic DAT-coated group at both 3 and 7 days. Quantification of the $iNOS^+Hoechst^+$ cell population indicated that there was a marked increase in the $iNOS^+$ cell density in the dynamic DAT-coated group as compared to all other groups at 7 days in this pilot study (Figure 4.3B).

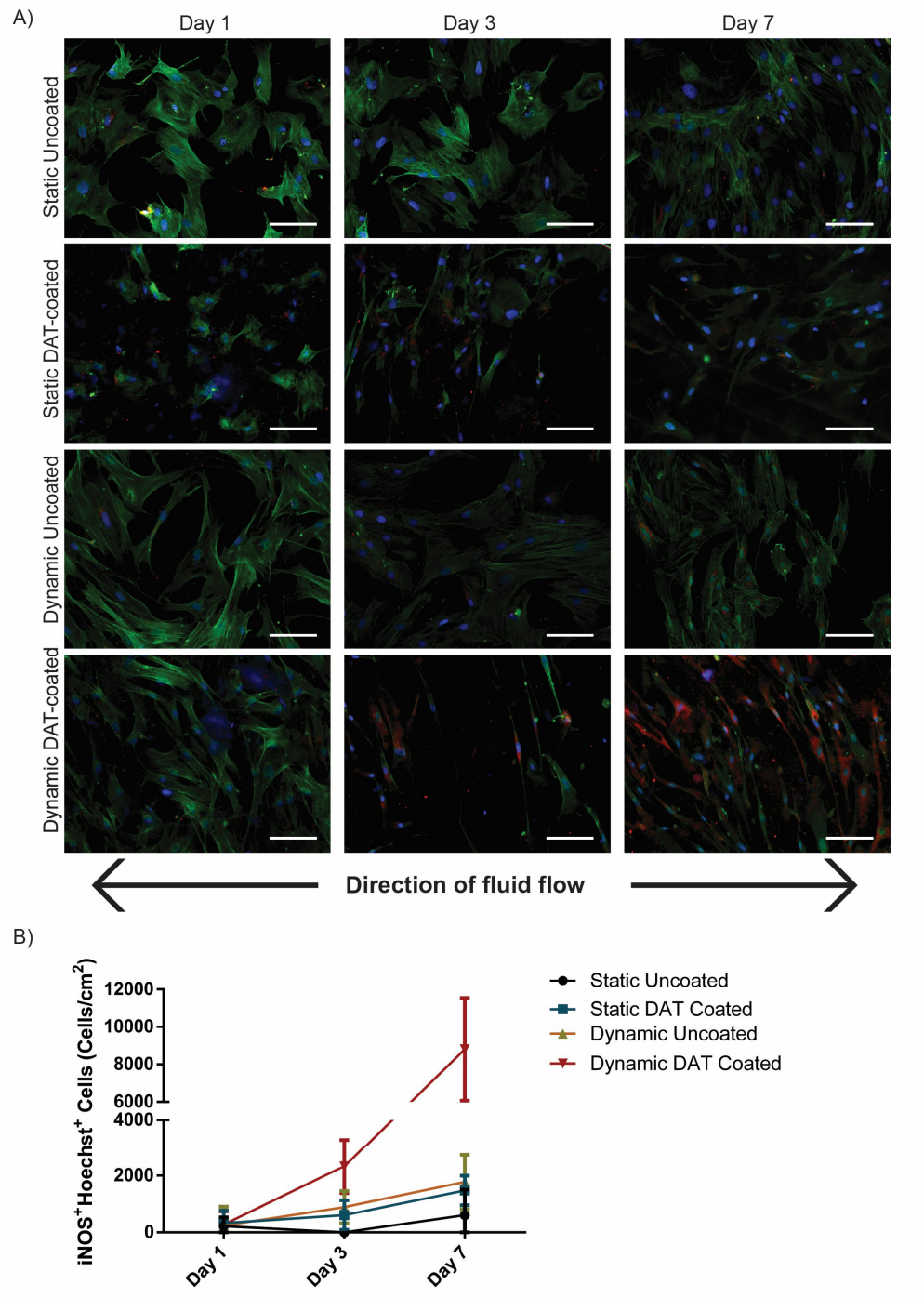

Figure 4.2 Dynamic culture of human ASCs on the DAT coatings promoted iNOS expression at 7 days *in vitro*. A) Representative images showing iNOS (red), F-actin (green) and nuclei (blue) at 1, 3 and 7 days of culture. ASCs cultured on the DAT coatings showed a more spindle-like morphology at 3 and 7 days, with alignment perpendicular to the direction of the fluid flow in the dynamic group at 7 days. Scale bars represent 100 µm. B) Quantification of $iNOS^{+}Hoechst^{+}$ cell density at 1, 3 and 7 days (N=1 trial with one ASC donor). A total of 15 non-overlapping images were analyzed in each sample. Values represent the mean ± standard deviation.

4.4.3 Dynamic culture of the human ASCs on the DAT coatings did not significantly alter the gene expression patterns of a range of pro-regenerative markers

The expression of 26 selected genes associated with (i) angiogenesis, (ii) inflammation, (iii) ECM synthesis and (iv) ECM remodeling was assessed through a custom-made PCR array to probe the effects of the rocking bioreactor strategy on the expression levels of a range of markers associated with soft tissue regeneration (Appendix Table A.2). Amplification was observed for all genes with the exception of *IL4*, which was excluded from the analysis. There was donor variability in the response, and no significant differences were observed between the various culture conditions for any of the genes (Figure 4.3). To aid in visualization of the trends, Appendix Figure A.16 shows the data alternatively plotted as a heat map. While not significant, many of the genes associated with angiogenesis and inflammation appeared to be down-regulated in the ASCs cultured statically or dynamically on the DAT coatings or dynamically on the uncoated controls relative to the static uncoated group. Notably while a number of the ECM synthesis markers (i.e. *COL3A1*, *COL4A1*, *CTGF*) were downregulated in the ASCs cultured dynamically on the DAT coatings relative to the static uncoated controls, the ECM remodeling markers *TGFB1*, *MMP1*, and *MMP2* were all upregulated, while *TIMP1* was downregulated (Figure 4.3D).

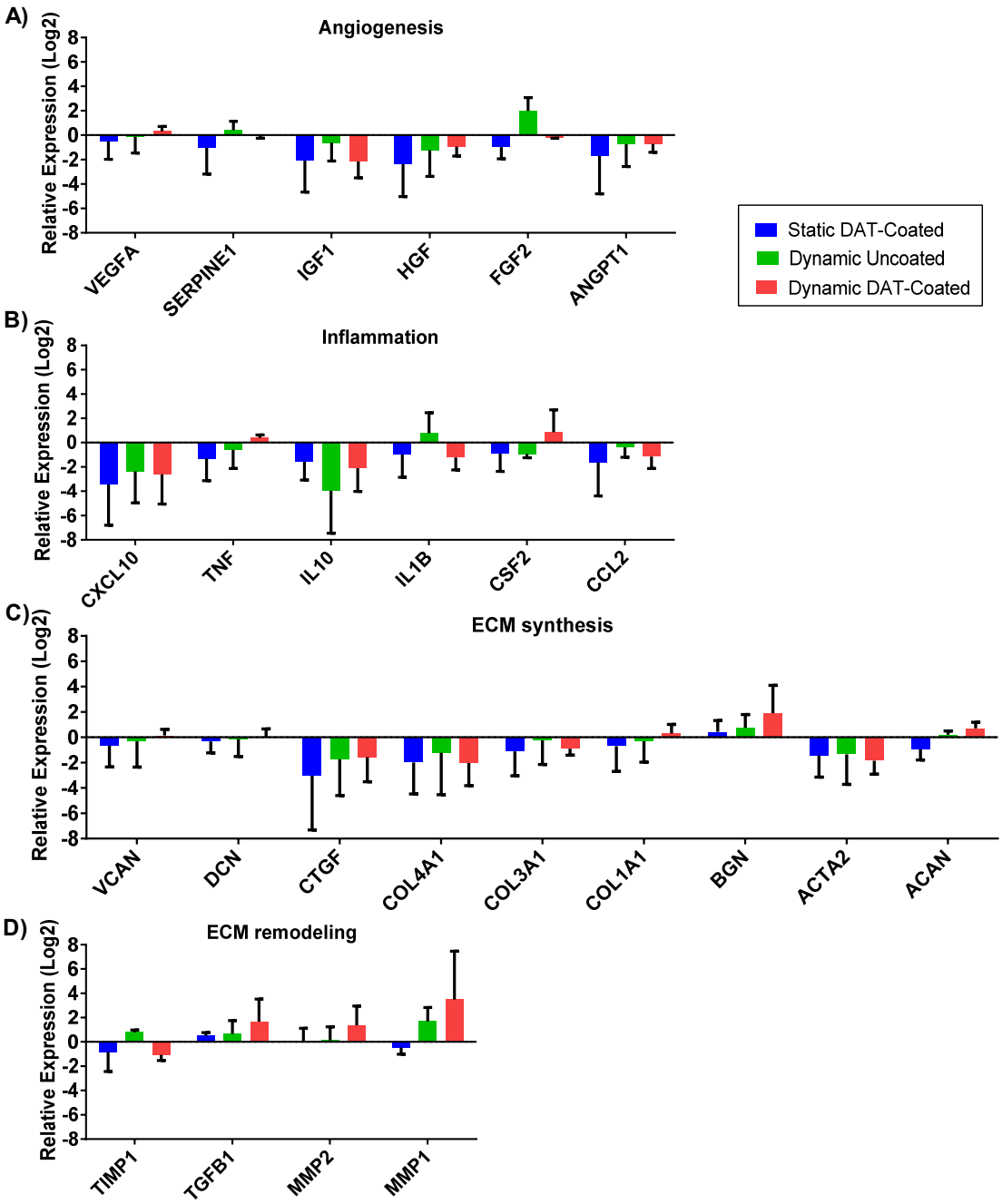

Figure 4.3 Analysis of the effects of the varying culture conditions on the expression levels of a range of gene markers associated with soft tissue regeneration in the ASCs after 7 days of culture. Relative expression levels normalized to the static uncoated group for gene markers associated with A) angiogenesis, B) inflammation, C) ECM synthesis and D) ECM remodeling. The data is plotted on a log2 scale and the error bars represent the standard deviation (n=2 technical replicate samples/trial, N=3 trials with different ASC donors).

4.5 Discussion

Many recent studies have emphasized that ASCs can be harnessed to stimulate regeneration within engineered bioscaffolds for a broad range of cell therapy applications, including adipose tissue engineering[40,449,455–459]. From a translational perspective, there is a need for improved cell expansion strategies that can be applied to obtain large populations of cells with predictable pro-regenerative functionality from relatively small tissue biopsies. While adipose tissue is regarded as a rich source of MSCs, typical yields of 1×10^5 - 4×10^5 ASCs can be extracted per gram of human adipose tissue[70,71], while it is estimated that cell doses in the range of 10^7 - 10^{10} cells/mL would be required for many clinical applications in humans[460].

Although conventional culture on 2-D TCPS remains the standard approach, prolonged culture on these rigid substrates is associated with a loss of regenerative potential in ASCs[257,393], including their capacity to proliferate and differentiate, which may impact the overall effectiveness of adipose tissue regeneration strategies applying these cell populations. To address this limitation, 3-D culture systems have been explored as an alternative expansion strategy[257,305,308,325,381,389–391,413]. In the context of adipose tissue engineering, a perfusion bioreactor system was previously applied to expand human ASCs on 3-D DAT scaffolds that could also be used as a cell delivery platform[413]. In addition to promoting ASC expansion, culturing the ASCs on the DAT scaffolds within the perfusion bioreactor under 2% O_2 for 14 days enhanced their capacity to stimulate *in vivo* adipose tissue regeneration[413]. However, scaling up this bioreactor system for clinical implementation in humans would be technically challenging. As such, an alternative, more scalable rocking bioreactor platform was explored in this pilot study.

Relative to 3-D perfusion bioreactor systems, the rocking bioreactor offers advantages in that it can both support cell expansion and act as a preconditioning platform, while remain highly scalable, as these systems can easily be stacked to enable mass culturing. Fundamentally, a rocking bioreactor platform leverages a back-and-forth rocking motion to drive an oscillating fluid flow, which can deliver fluid shear stress and promote the efficient distribution of nutrients to the cultured cell populations. Within the system

developed in the current study, all of the cells would be subjected to shear stress stimulation induced by the flow of the media. In contrast, previous evidence suggested that there was limited media perfusion into the central regions of the DAT scaffolds cultured within the perfusion bioreactor system, which resulted in heterogeneity in the cellular response in terms of both proliferation and phenotype[413].

Recognizing the importance of both the complex ECM composition and mechanical properties in directing cell function[461], DAT coatings were incorporated as a substrate within the new dynamic culture system[385]. Human DAT was selected as a tissue-specific substrate, as it has been shown to support ASC proliferation and adipogenesis[255,257,260,385]. For example, the favorable properties of DAT-based biomaterials in terms of ASC proliferation were demonstrated in a study where DAT-derived microcarriers were shown to better support the proliferation of human ASCs as compared to commercially-available Cultispher-S microcarriers, which are gelatin-based[257]. More recently, human ASC proliferation under static conditions was shown to be enhanced on DAT coatings similar to those used in the current study relative to both collagen-derived coatings and uncoated TCPS[385].

In addition to supporting cell expansion, there is evidence that culturing on DAT-derived biomaterials may be favorable for enhancing the secretion of pro-regenerative paracrine factors. More specifically, a recent comparison of human fibroblasts cultured on structurally and biomechanically similar DAT-derived and collagen-derived foams demonstrated that pro-angiogenic growth factor production was significantly increased in the cells cultured on the DAT foams, including hepatocyte growth factor (HGF) and vascular endothelial growth factor A (VEGFA)[462].

The findings in Chapter 3 of this thesis support that fluid shear stress stimulation can be applied to modulate the phenotype of the human ASCs and potentially enhance their pro-regenerative paracrine functionality. In the current study, the flow cytometry analyses support that fluid shearing can alter the ASC phenotype, with a significantly higher percentage of the $CD90^{+}CD29^{+}$ population expressing CD146 in the ASCs cultured on the DAT coatings on the rocking platform. Although CD146 is commonly regarded as a

surface marker for pericytes[419,420], its expression in ASCs has been associated with an increased capacity for proliferation, clonogenicity and trilineage differentiation[87]. Additionally, this surface marker is also strongly associated with an increased capacity to support endothelial tube formation, suggesting that this specific subpopulation is more pro-angiogenic[86,463]. While ASCs are known to express CD146, it is typically expressed in a small fraction of the overall population at early passages when cultured on TCPS (<10%)[464,465]. The marked enrichment of the $CD146^+$ population in the dynamic DAT coated group relative to the more conventional static uncoated group may be a positive indicator in terms of the pro-regenerative potential of the cells expanded on the new platform, which should be explored further in future work.

Preliminary evidence also suggests that the shearing forces from the rocking bioreactor system also induced iNOS expression in the ASCs that were cultured on the DAT coatings, consistent with the findings from the perfusion bioreactor study in Chapter 3. These observations are also similar to a study by Bassaneze *et al.* which demonstrated that subjecting ASCs to a shearing stress of 10 dyn/cm^2 for 96 h was sufficient to upregulate iNOS expression and promote nitric oxide (NO) production[289,466]. Since iNOS expression has been associated with an increase in the pro-regenerative capacity of MSCs[124,133,415], the pilot data from this study supports the further investigation and development of the new rocking bioreactor platform, including confirming the response in multiple ASC donors.

While the immunophenotype and IHC studies were a promising indication that culturing the ASCs on the DAT coatings under dynamic conditions on the rocking platform modulated the ASC response, the gene expression findings suggest that further optimization of the system is required. While no significant differences were observed between the groups, the trend towards the reduced levels of expression of a range of pro-angiogenic and immunomodulatory factors under dynamic conditions relative to the static uncoated controls is an indicator that the selected conditions were not favorable for stimulating paracrine factor expression in the cultured ASCs. Further, the qualitative reduction in the number of cells observed on the DAT coatings in the dynamic group from 1 to 3 days suggests that excessive shear forces may have been applied that were

disruptive to the cells and potentially the coatings. This interpretation may be supported by the qPCR array results that showed a shift towards higher expression of genes associated with matrix degradation, combined with reduced expression of a number of ECM components, suggestive of a more catabolic response that may be detrimental for regeneration[467]. Within the rocking bioreactor system, a broad range of parameters could be refined, including the rocking speed, rotation angle, media volume, and culture duration, with the goal of promoting a more desirable response. In addition, the gene expression results should be further validated at the protein level in a larger number of ASC donors.

4.6 Conclusions

The present study provided initial evidence to support the further investigation of this new scalable rocking bioreactor system integrating tissue-specific ECM-derived coatings to dynamically culture and precondition human ASCs, towards the long-term goal of promoting cell expansion and enhancing the pro-regenerative functionality of the cells through shear stress stimulation. The system is cost-effective and simple to use and appears to stimulate a more homogeneous response across the cultured ASC population relative to what was observed in the previous perfusion bioreactor strategy. Another advantage to this new approach is that the cells can easily be extracted from the DAT coatings through enzymatic digestion, for subsequent incorporation into a range of cell delivery platforms. The preliminary findings supported that dynamic culture on the DAT coatings modulated the ASC phenotype, enhancing the expression of CD146 and iNOS, which may be positive indicators in terms of their pro-angiogenic and immunomodulatory functionality. However, the gene expression results suggest that optimization is required to assess whether this dynamic culture strategy can be harnessed to stimulate ASC paracrine factor production. In addition, further studies are required to characterize ASC proliferation over time and the capacity of the expanded cells to support *in vivo* angiogenesis and adipose tissue regeneration.

Chapter 5

5 General discussion and future work

5.1 General discussion

To address the clinical need in plastic and reconstructive surgery for a therapeutic strategy with the capacity to promote the stable regeneration of subcutaneous soft tissues, the Flynn lab pioneered the development of decellularized adipose tissue (DAT) as an off-the-shelf adipose tissue substitute[253]. Over the past 10 years since its initial development, the DAT has been fabricated into an array of bioscaffolds that have been shown to have adipo-inductive properties[229,255,257,385,462]. Moreover, the DAT can be combined with adipose-derived stromal cells (ASCs), which was previously shown to significantly enhance angiogenesis and constructive remodeling of the scaffolds into host-derived adipose tissue in an immunocompetent rat model[169]. This work was crucial in highlighting the important role that ASCs can play in mediating key processes involved in adipose tissue regeneration. Recognizing both the capacity of the ASCs to stimulate regeneration and of the DAT to provide a supportive microenvironment for adipogenesis, a perfusion bioreactor strategy was developed with the goals of promoting (i) ASC expansion and infiltration on the DAT and (ii) enhancing the pro-regenerative function of the ASC-seeded DAT.

The capacity of the perfusion bioreactor system to support ASC expansion on the DAT addressed the limitations that were associated with the static seeding methods that had previously been applied, which can lead to low attachment and a heterogeneous distribution of ASCs primarily on the surface of the DAT. While it may be possible to expand a large number of ASCs on 2-D tissue culture polystyrene (TCPS) before seeding on the DAT, prolonged proliferation under these conditions is often associated with a decreased potential for the ASCs to promote regeneration[257,393]. As such, 3-D culture systems represent a promising approach to circumvent this challenge by enabling the cells to be directly expanded on a bioscaffold that more closely mimics the biochemical, biomechanical, and structural properties of the native cellular microenvironment, which play important roles in directing cell function[247,256,260]. In terms of 3-D culture systems, a

diverse range of bioreactors[257,305,308,325,381,389–391,413], including spinner flasks[254,308,388,392] and rotating wall vessels[88,306,307,309] have been explored. However, these bioreactor systems are typically designed such that the expanded cells are enzymatically released from their 3-D expansion platforms for downstream tissue engineering applications[303,394]. In contrast, the perfusion bioreactor system was designed with the goal of promoting cell expansion and *in vivo* delivery on the same scaffold system.

While perfusion bioreactor systems have primarily been explored for generating highly cellularized bone tissue grafts[310,312,314,316,317,319], the studies outlined in Chapter 2 provide a strong case for their use in adipose tissue engineering applications. In particular, the increased density of ASCs that was found along the periphery of the DAT scaffolds that were cultured in the perfusion bioreactor under hypoxic conditions (2% O_2) is consistent with previous studies[316,319]. For example, Xie *et al.* demonstrated that sheep bone marrow-derived mesenchymal stromal cells (MSCs) seeded on porous β-tricalcium phosphate ceramic bioscaffolds and cultured in a perfusion bioreactor were significantly more proliferative than controls cultured under static conditions over 28 days[317]. Furthermore, the perfused regions of the ceramic scaffolds contained a high density of MSCs with a homogeneous distribution[317]. While similar cell expansion effects were observed in the present study, the cell distribution patterns also suggest that the central regions of the DAT bioscaffolds may have been poorly perfused. The greater density of ASCs along the periphery of the scaffold may have been caused by an increased delivery of nutrients from the culture medium[397,398], which could have also driven the migration of cells from the central region to the periphery, in addition to promoting the proliferation of cells around the scaffold border. These observations provided a case for developing an alternative system where the cells could be in contact with the DAT but receive more uniform exposure to the media and shear stress stimulation, which served as the rationale for the development of the rocking bioreactor ASC expansion platform incorporating the DAT coatings outlined in Chapter 4.

Increasing the density of the ASCs on the DAT was likely a mechanism through which dynamic culturing in the perfusion bioreactor enhanced the capacity of the ASC-seeded DAT to promote blood vessel formation and constructive adipose tissue remodeling

following implantation in the subcutaneous thymic nude (*nu/nu*) mouse model in Chapter 2[413]. However, shear stress has also been shown to affect the function of MSC populations[290,291,313,326]. For example, Yuan *et al.* showed that subjecting human bone marrow-derived MSCs to 2 Pa of shear could increase vascular endothelial growth factor A (VEGFA) expression compared to static controls[290]. In a more recent study, Bravo *et al.* demonstrated that intermittent fluid flow upregulated the expression of VEGFA, hepatocyte growth factor (HGF) and follistatin in human ASCs *in vitro*[423]. These studies support that shear stress stimulation can be applied as a strategy to precondition MSCs to enhance their capacity to stimulate *in vivo* regeneration. Their findings contributed to the motivation to probe potential changes in the ASC phenotype and paracrine function following culture on the DAT within the perfusion bioreactor under 2% O_2 in Chapter 3.

Previous studies have shown that human ASCs that were subjected to 10 dyn/cm^2 of shear stress upregulated the expression of nitric oxide (NO) through inducible nitric oxide synthase (iNOS)[289]. As such, the increased iNOS expression in the ASCs within the peripheral regions of the DAT that were dynamically cultured in the perfusion system not only supports that those cells were experiencing fluid shear, but may be phenotypically altered. To further compare the ASCs that were cultured dynamically or statically on the DAT, the expression of key angiogenic factors and cytokines that were identified to be altered in the PCR array was analyzed with a multiplex Luminex Assay. An increase in interleukin 10 (IL-10) and C-X-C motif chemokine (CXCL-10) expression in the dynamically cultured ASCs suggests that there may be differences in the immunomodulatory function of the cells, as these factors have been associated with promoting an anti-inflammatory/pro-regenerative macrophage phenotype and macrophage recruitment, respectively[135,429]. Additionally, the increased expression of HGF in the dynamically cultured ASCs could correlate with an increased capacity to both promote angiogenesis[114,115,118] and a more anti-inflammatory/pro-regenerative macrophage response[433]. Further, the down-regulation of interleukin 6 (IL-6) in the dynamically cultured ASCs would suggest a decreased capacity to induce a pro-inflammatory macrophage response[143]. Together, the *in vitro* studies from Chapter 3 suggest that dynamic culturing may enhance the capacity of the ASCs to promote both a pro-angiogenic and a pro-regenerative macrophage response. These findings not only

align with the results of the *in vivo* studies, but also provide a strong rationale for applying the perfusion bioreactor strategy as a preconditioning system to increase the pro-regenerative paracrine capacity of human ASCs through shear stress stimulation.

ASCs are recognized for their capacity to promote angiogenesis via the secretion of pro-angiogenic paracrine factors[101,265,468,469], which has been leveraged for an array of tissue engineering and regenerative applications[101,170,470–472]. For example, a study by Matsuda *et al.* demonstrated that culturing human ASCs on decellularized cardiac tissue matrix (cardiogel) can lead to an increased expression of interleukin 8 (IL-8), basic fibroblast growth factor (bFGF) and stromal cell-derived factor 1 (SDF-1) than controls on plastic[170]. Furthermore, these ASCs were shown to better support blood vessel formation than cardiogel only control when delivered into the inguinal region of nude rats for 7 days[170]. Moreover, a study by Suga *et al.* demonstrated that the transplantation of allogeneic ASCs into the inguinal fat pad in mice promoted blood vessel formation in the target tissue at 14 days and this was achieved through the ASC-mediated secretion of HGF and VEGF[101]. In Chapter 3 of this thesis, the qPCR array identified a variety of pro-angiogenic factors that were up-regulated in the ASCs that were dynamically cultured on the DAT, including *HGF*, *TNF*, *FGF13*, *AGGF1*, and *PLG*. Follow-up studies to assess changes at the protein level confirmed upregulation of HGF using the Luminex® Assay, as well as the locally enhanced expression of tumour necrosis factor alpha (TNF-α) in the ASCs in the periphery of the DAT scaffolds within the dynamic culture group via immunostaining. The increased levels of these pro-angiogenic paracrine factors may have contributed to the increased $CD31^+$ endothelial cell recruitment observed starting at 1 week and the increased density of erythrocyte-containing blood vessels at both 4 and weeks in the DAT implants from the 2% O_2 dynamic culture group[413].

Previous studies have demonstrated that ASCs can also secrete a wide array of cytokines, which can modulate the immune response, including promoting a more pro-regenerative macrophage response[124,473,474]. For example, a study by Anderson *et al.* demonstrated that human ASCs could stimulate the anti-inflammatory polarization of mouse macrophages *in vitro* through the secretion of IL-10[475]. In a more recent study, human ASCs that were seeded on Integra Matrix, a commercially-available wound dressing, were shown to

promote macrophage infiltration and a decreased pro-inflammatory macrophage response, which led to increased wound closure at 21 days in C57BL/6 mice[476]. Consistent with these studies, the Flynn lab has previously shown that delivering allogeneic ASCs on the DAT subcutaneously into Wistar rats promoted a more pro-regenerative macrophage response associated with enhanced expression of CD163, as well as increased blood vessel formation and adipose tissue remodeling of the DAT bioscaffolds as compared to unseeded controls[169]. As previously discussed, the studies in the current thesis demonstrated that human ASCs that were dynamically cultured on the DAT expressed increased levels of IL-10 *in vitro*. When delivered *in vivo* into athymic nude mice, a more pro-regenerative macrophage response was observed, with enhanced infiltration of $CD163^+$ macrophages into the implants in the dynamic group, coupled with an increased angiogenic response and adipose tissue remodeling[413]. Collectively, the *in vivo* studies in Chapter 3 provided further support that ASCs could modulate the macrophage phenotype, which have been an important factor in mediating both angiogenesis[353] and extracellular matrix remodeling[351,447] within the implants.

In Chapter 2 of this thesis, significantly increased remodeling of the DAT into host-derived adipose tissue was observed at 8 weeks in the scaffolds that were cultured dynamically within the perfusion bioreactor under 2% O_2 for 14 days prior to implantation, as compared to all other groups. The timeframe in which adipose tissue formation was observed in this study was consistent with the previous rat study from the Flynn lab, where seeding the DAT with allogeneic ASCs was found to better promote adipose tissue remodeling as compared to the DAT scaffold alone at both 8 and 12 weeks[169]. Given the highly vascularized nature of mature adipose tissue, it is likely that a well-established vasculature and the infiltration of pro-regenerative macrophages with the capacity to remodel the DAT would be required before adipose tissue formation could occur[259,443,477]. This interpretation would be consistent with the timing of adipose tissue remodeling observed in the *in vivo* studies from Chapter 2, as well as the reduced adipogenic response in the other groups, where there were significantly fewer blood vessels infiltrating the implants.

Adipogenesis in the context of adipose tissue engineering is an understudied process, and little is known about the cell populations that can give rise to mature adipocytes within engineered bioscaffolds. However, a study by Rodeheffer *et al.* identified an adipocyte precursor population ($CD29^+CD34^+CD24$+stem cell antigen 1^+ (SCA-1)) in the stromal vascular fraction (SVF) of adipose tissue that could differentiate into adipocytes *in vivo*[374]. In a more recent study, a large percentage of this adipocyte precursor cell population was also identified as being $CD26^+$[375]. In Chapter 3 of this thesis, a greater host-derived $CD26^+$ cell population was found in the implants in the dynamic group at 1 week, which could suggest there was enhanced infiltration of adipogenic progenitor cells in this group. While CD26 is also expressed on non-adipocyte precursor cells including fibroblasts and immune cell populations[439–441], the $CD26^+$ cell population may have contributed to the increased perilipin$^+$ adipocytes observed at 8 weeks in the implants from the 2% O_2 dynamic culture group, as shown in Chapter 2.

5.2 Future directions

The studies highlighted in this thesis provided important insights into how dynamic culture systems could be applied to both expand and precondition ASCs to promote their capacity to stimulate adipose tissue regeneration within DAT scaffolds. Based on insights acquired from these studies, future work should focus on i) further exploring the effects of dynamic culture within the perfusion bioreactor system on modulating ASC function, ii) further investigating the mechanisms behind adipose tissue regeneration *in vivo* and iii) further development and optimization of the rocking bioreactor system.

The perfusion bioreactor was set at a flow rate of 0.5 mL/min in the studies in Chapter 2 and Chapter 3. While this parameter supported ASC expansion and promoted the expression of several key paracrine factors, it is possible that a different flow rate could impact the proliferative and secretory behaviour of these cells. For example, a previous study has shown that the proliferation capacity of bovine aortic endothelial cells was inversely correlated with shear force[478]. For the perfusion bioreactor used in this study, it is possible that the flow rate could be refined to further accelerate ASC expansion on the DAT. Moreover, shear stress could also affect the paracrine secretion of the ASCs, as shown in Chapter 3 and by Bassazene *et al.*[289]. While decreasing the flow rate could be

conducive for ASC expansion, it could also attenuate pro-regenerative paracrine factor secretion. Future studies should aim to test a range of flow rates that are both faster and slower than the current parameter (e.g. 0.25 mL/min to 1 mL/min). The *in vitro* studies in Chapter 2 could be used as a benchmark to assess proliferation, and the techniques developed in Chapter 3 could be adopted as a framework to guide the analysis of paracrine factor secretion. Upon *in vitro* refinement, additional *in vivo* studies using the subcutaneous implantation model in athymic nude mice could be performed for up to 12 weeks to determine the long-term effects of altering the dynamic culture parameters on angiogenesis and adipogenesis within the DAT.

The *in vivo* studies highlighted in Chapter 3 indicated that while dynamic culturing of ASCs on the DAT did not significantly impact the recruitment of macrophages in the *nu/nu* mouse model, it did result in a more pro-regenerative polarization within the DAT implants, with enhanced infiltration of $CD163^{+}$ macrophages. Given the dynamic nature of the immune system, it is possible that the bioreactor cultured implants could have also affected the phenotype of macrophages at earlier time points (e.g. 1, 2, 4 and 6 weeks). Additionally, dynamic culture was shown to up-regulate IL-10 expression in the human ASCs, which can promote a pro-regenerative macrophage phenotype and inhibit pro-inflammatory macrophage polarization. As such, it is possible that culturing the ASCs on the DAT scaffolds under dynamic conditions may have also inhibited the pro-inflammatory polarization of macrophages at earlier timepoints *in vivo*. Future studies could be performed to further examine the phenotype of macrophages at 1, 2, 4, 6 and 8 weeks. Potential markers of interest could include CD80, iNOS and Ly6c for pro-inflammatory macrophage polarization, as well as interleukin 4 (IL4), CD206, CD163 and Arg-1 for pro-regenerative macrophage polarization. In addition to the immunostaining analyses performed in Chapter 3, scaffolds could be digested to isolate the infiltrating cells for multi-colour flow cytometry analysis to identify specific macrophage populations with distinct functions that may be relevant for regeneration. An in-depth understanding of the immune response would provide important insights into the role of macrophages in mediating adipose tissue regeneration.

The selection of *in vivo* analyses in both Chapter 2 and Chapter 3 examined the effects of dynamic culturing of the ASCs on the DAT prior to implantation on the host response, with a particular focus on angiogenesis and the macrophage response. While increased angiogenesis and a more pro-regenerative macrophage phenotype are strongly correlated with constructive adipose tissue remodeling[169,259], how ASCs and/or the DAT promote the formation of new host-derived adipose tissue remains poorly understood. Chapter 3 of this thesis highlighted the increased infiltration of host-derived $CD26^+$ cells, which may have the potential to give rise to adipocytes, within the implants in the dynamic group at 1 week. However, it remains unclear whether this population contributed to adipogenesis. Therefore, further investigation of this cell population could provide greater insight into the potential mechanisms behind the observed adipose tissue regeneration within the DAT implants. More specifically, implanted DAT scaffolds could be extracted, and enzymatically digested to generate cell suspensions that could be analyzed using multi-colour flow cytometry for the adipocyte precursor markers CD26, CD24, CD34, CD29 and SCA-1[374]. Understanding if these cells are present and the role these cells may play in mediating adipogenesis would allow for the design of more targeted and efficient therapeutic strategies to support adipose tissue regeneration.

The preliminary development of the rocking bioreactor system described in Chapter 4 demonstrated initial promise as a dynamic culturing system that could harness the cell-instructive capacity of the DAT and shear stress stimulation to modulate the pro-regenerative potential of the ASCs. The PCR Array performed did not indicate significant differences in the gene expression levels of a range of pro-regenerative markers, which suggests that the parameters used for the rocking system require further refinement. More specifically, a combination of different rocking angles, frequencies and medium volumes should be tested to first identify the amount of shear (dyn/cm^2) the cells are experiencing before moving forward to determine parameters that could both promote ASC expansion as well as upregulate pro-angiogenic and immunomodulatory gene and protein expression. Given the initial cell attachment issues observed in the dynamic DAT-coated group, reducing the amount of shear by lowering the frequency from 30 RPM to 15 RPM, decreasing the rocking angle from 13° to 10° and increasing the media volume from 3 mL/well to 4 mL/well could be initially tested. In addition to immunophenotypic

analyses, further probing for angiogenic gene expression with qPCR and protein expression with Luminex® Assays would help to determine a range of parameters to move forward with *in vivo* assessments.

For *in vivo* analysis, the ASCs could be enzymatically released from the DAT coating and encapsulated within a previously-developed DAT-methacrylated chondroitin sulfate (MCS) composite hydrogel system[255]. The macrophage, angiogenic and adipogenic responses could subsequently be evaluated at 1, 4, 8, 12 and 24 weeks to evaluate both the short- and long-term potential of the system to promote angiogenesis and adipogenesis, following the methods described in Chapter 3. Overall, the *in vitro* optimization studies and subsequent *in vivo* validation would be an important next step to assess the feasibility of the approach and potential benefits of ASC pre-conditioning towards future clinical application.

5.3 Summary and significance

The body of work described in this thesis demonstrated that the perfusion bioreactor system can be used as both an expansion and preconditioning platform for the human ASCs on the DAT. Through dynamic culturing in the perfusion bioreactor system, the ASC-seeded DAT scaffolds promoted a more pro-regenerative *in vivo* response, resulting in an increased capacity to support angiogenesis, pro-regenerative macrophage polarization and adipogenesis. To the best of my knowledge, this is the first study to explore the application of a scaffold-based perfusion bioreactor system for adipose tissue engineering.

The perfusion bioreactor was initially developed as a dynamic culturing platform to support ASC expansion on the DAT. The *in vivo* study clearly demonstrated that the ASCs that were cultured on the DAT within this system under 2% O_2 exhibited an increased capacity to promote both angiogenesis and adipogenesis in immunocompromised animals *in vivo*. Beyond acting as a 3-D expansion platform, the perfusion bioreactor altered the ASC phenotype and increased the expression of key paracrine factors, which may have contributed to the enhanced infiltration of host-derived cell populations and the polarization of host macrophages towards a more

pro-regenerative phenotype within the implants. It is postulated that these cell populations played an important role in the substantial remodeling of the implants into host-derived adipose tissue that was observed in this group at 8 weeks.

Building on this work, pilot studies were performed to explore an alternative rocking bioreactor strategy as a more scalable system that allows for the 3-D culturing of ASCs. The preliminary studies performed demonstrated that the rocking bioreactor system incorporating the DAT coatings has the potential to alter the ASC phenotype. Overall, this work contributes to an emerging body of evidence that dynamic culture under shear stress can be applied to modulate the pro-regenerative capacity of MSCs during cell expansion.

References

1. McLafferty, E., Hendry, C. & Alistair, F. The integumentary system: anatomy, physiology and function of skin. *Nurs. Stand.* **27**, 35–42 (2012).

2. Kolarsick, P. A. J., Kolarsick, M. A. & Goodwin, C. Anatomy and Physiology of the Skin. *J. Dermatol. Nurses. Assoc.* **3**, 203–213 (2011).

3. Imanishi, N., Kishi, K., Chang, H., Nakajima, H. & Aiso, S. Three-dimensional venous anatomy of the dermis observed using stereography. *J. Anat.* **212**, 669–673 (2008).

4. McGrath, J. A. & Uitto, J. Anatomy and Organization of Human Skin. *Rook's Textb. Dermatology Eighth Ed.* **1**, 34–86 (2010).

5. Lancerotto, L. *et al.* Layers of the abdominal wall: anatomical investigation of subcutaneous tissue and superficial fascia. *Surg. Radiol. Anat.* **33**, 835–842 (2011).

6. Illouz, Y. G. Study of subcutaneous fat. *Aesthetic Plast. Surg.* **14**, 165–177 (1990).

7. Trayhurn, P. & Wood, I. S. Signalling role of adipose tissue: adipokines and inflammation in obesity. *Biochem. Soc. Trans.* **33**, 1078–1081 (2005).

8. Wajchenberg, B. L. Subcutaneous and Visceral Adipose Tissue: Their Relation to the Metabolic Syndrome. *Endocr. Rev.* **21**, 697–738 (2000).

9. Wajchenberg, B. L. Subcutaneous and Visceral Adipose Tissue : *Endocr. Rev.* **21**, 697–738 (2000).

10. Musi, N. & Guardado-Mendoza, R. Adipose Tissue as an Endocrine Organ. *Cell. Endocrinol. Heal. Dis.* **89**, 229–237 (2014).

11. Patrick, C. W. Tissue engineering strategies for adipose tissue repair. *Anat. Rec.* **263**, 361–366 (2001).

12. Statistics, P. American Society of Plastic Surgeons. 2018 Plastic Surgery Statistics

Report. Available at: https://www.plasticsurgery.org/documents/News/Statistics/2018/plastic-surgery-statistics-full-report-2018.pdf. Accessed Sept 27, 2019. *Plast. Surg.* 25 (2017).

13. Pearl, R. A., Leedham, S. J. & Pacifico, M. D. The safety of autologous fat transfer in breast cancer: Lessons from stem cell biology. *J. Plast. Reconstr. Aesthetic Surg.* **65**, 283–288 (2012).

14. Serletti, J. M., Man, L. X. & Selber, J. C. Abdominal wall following free TRAM or DIEP flap reconstruction: A meta-analysis and critical review. *Plast. Reconstr. Surg.* **124**, 752–764 (2009).

15. Parrett, B. M., Caterson, S. A., Tobias, A. M. & Lee, B. T. DIEP flaps in women with abdominal scars: Are complication rates affected? *Plast. Reconstr. Surg.* **121**, 1527–1531 (2008).

16. Futter, C. M., Webster, M. H. C., Hagen, S. & Mitchell, S. L. A retrospective comparison of abdominal muscle strength following breast reconstruction with a free TRAM or DIEP flap. *Br. J. Plast. Surg.* **53**, 578–583 (2000).

17. Choi, M. *et al.* The volumetric analysis of fat graft survival in breast reconstruction. *Plast. Reconstr. Surg.* **131**, 185–191 (2013).

18. Kaufman, M. R. *et al.* Autologous fat transfer for facial recontouring: Is there science behind the art? *Plast. Reconstr. Surg.* **119**, 2287–2296 (2007).

19. Kamakura, T. & Ito, K. Autologous cell-enriched fat grafting for breast augmentation. *Aesthetic Plast. Surg.* **35**, 1022–1030 (2011).

20. Pierre, S., Liew, S. & Bernardin, A. Basics of dermal filler rheology. *Dermatologic Surg.* **41**, S120–S126 (2015).

21. Kim, Z. H. *et al.* A composite dermal filler comprising cross-linked hyaluronic acid and human collagen for tissue reconstructions. *J. Microbiol. Biotechnol.* **25**, 399–406 (2014).

22. Mochizuki, M., Aoi, N., Gonda, K., Hirabayashi, S. & Komuro, Y. Evaluation of the in vivo kinetics and biostimulatory effects of subcutaneously injected hyaluronic acid filler. *Plast. Reconstr. Surg.* **142**, 112–121 (2018).

23. Cohen, J. L. Understanding, avoiding, and managing dermal filler complications. *Dermatologic Surg.* **34**, 92–99 (2008).

24. Hoeller, U. *et al.* Cosmesis from the patient's and the doctor's view. *Int. J. Radiat. Oncol.* **57**, 345–354 (2003).

25. Glynn, S. M. *et al.* Chronic Posttraumatic Stress Disorder After Facial Injury: A 1-year Prospective Cohort Study. *J. Trauma Inj. Infect. Crit. Care* **62**, 410–418 (2007).

26. Flynn, L., Prestwich, G. D., Semple, J. L. & Woodhouse, K. A. Adipose tissue engineering in vivo with adipose-derived stem cells on naturally derived scaffolds. *J. Biomed. Mater. Res. - Part A* **89**, 929–941 (2009).

27. Choi, J. H. *et al.* Adipose tissue engineering for soft tissue regeneration. *Tissue Eng. - Part B Rev.* **16**, 413–426 (2010).

28. McCarthy, M. E. *et al.* Therapeutic Applications for Adipose-Derived Stem Cells in Wound Healing and Tissue Engineering. *Curr. Stem Cell Reports* **4**, 127–137 (2018).

29. Saha, K. *et al.* Substrate modulus directs neural stem cell behavior. *Biophys. J.* **95**, 4426–38 (2008).

30. Xu, R., Boudreau, A. & Bissell, M. J. Tissue architecture and function: dynamic reciprocity via extra- and intra-cellular matrices. *Cancer Metastasis Rev.* **28**, 167–76 (2009).

31. Frantz, C., Stewart, K. M. & Weaver, V. M. The extracellular matrix at a glance. *J. Cell Sci.* **123**, 4195–4200 (2010).

32. Karamichos, D., Brown, R. A. & Mudera, V. Collagen stiffness regulates cellular contraction and matrix remodeling gene expression. *J. Biomed. Mater. Res. Part A* **83A**, 887–894 (2007).

33. Li, Q. *et al.* Photocrosslinkable polysaccharides based on chondroitin sulfate. *J. Biomed. Mater. Res. A* **68**, 28–33 (2004).

34. Ni, H.-C., Tseng, T.-C., Chen, J.-R., Hsu, S.-H. & Chiu, I.-M. Fabrication of bioactive conduits containing the fibroblast growth factor 1 and neural stem cells for peripheral nerve regeneration across a 15 mm critical gap. *Biofabrication* **5**, 035010 (2013).

35. Lutolf, M. P. *et al.* Synthetic matrix metalloproteinase-sensitive hydrogels for the conduction of tissue regeneration: engineering cell-invasion characteristics. *Proc Natl Acad Sci U S A* **100**, 5413–5418 (2003).

36. Hemmrich, K. *et al.* Autologous In Vivo Adipose Tissue Engineering in Hyaluronan-Based Gels-A Pilot Study. *J. Surg. Res.* **144**, 82–88 (2008).

37. Gilbert, T. W., Sellaro, T. L. & Badylak, S. F. Decellularization of tissues and organs. *Biomaterials* **27**, 3675–3683 (2006).

38. Huber, B., Borchers, K., Tovar, G. E. M. & Kluger, P. J. Methacrylated gelatin and mature adipocytes are promising components for adipose tissue engineering. *J. Biomater. Appl.* **30**, 699–710 (2016).

39. Zhou, Q., Li, L. & Li, J. Stem cells with decellularized liver scaffolds in liver regeneration and their potential clinical applications. *Liver Int.* **35**, 687–694 (2015).

40. Russo, V., Young, S., Hamilton, A., Amsden, B. G. & Flynn, L. E. Mesenchymal stem cell delivery strategies to promote cardiac regeneration following ischemic injury. *Biomaterials* **35**, 3956–3974 (2014).

41. Li, J. *et al. Iota* -carrageenan/chitosan/gelatin scaffold for the osteogenic

differentiation of adipose-derived MSCs *in vitro*. *J. Biomed. Mater. Res. Part B Appl. Biomater.* **103**, 1498–1510 (2015).

42. Heathman, T. R. *et al.* The translation of cell-based therapies: Clinical landscape and manufacturing challenges. *Regen. Med.* **10**, 49–64 (2015).

43. Hillel, A. T., Varghese, S., Petsche, J., Shamblott, M. J. & Elisseeff, J. H. Embryonic germ cells are capable of adipogenic differentiation in vitro and in vivo. *Tissue Eng. - Part A* **15**, 479–486 (2009).

44. Mauney, J. R. *et al.* Engineering adipose-like tissue in vitro and in vivo utilizing human bone marrow and adipose-derived mesenchymal stem cells with silk fibroin 3D scaffolds. *Biomaterials* **28**, 5280–5290 (2007).

45. Vashi, A. V. *et al.* Adipose differentiation of bone marrow-derived mesenchymal stem cells using Pluronic F-127 hydrogel in vitro. *Biomaterials* **29**, 573–579 (2008).

46. Stosich, M. S. *et al.* Vascularized adipose tissue grafts from human mesenchymal stem cells with bioactive cues and microchannel conduits. *Tissue Eng.* **13**, 2881–2890 (2007).

47. Fernyhough, M. E. *et al.* Mature adipocytes may be a source of stem cells for tissue engineering. *Biochem. Biophys. Res. Commun.* **368**, 455–457 (2008).

48. Eto, H. *et al.* The fate of adipocytes after nonvascularized fat grafting: Evidence of early death and replacement of adipocytes. *Plast. Reconstr. Surg.* **129**, 1081–1092 (2012).

49. Eto, H. *et al.* Characterization of structure and cellular components of aspirated and excised adipose tissue. *Plast. Reconstr. Surg.* **124**, 1087–1097 (2009).

50. Condé-Green, A., Gontijo De Amorim, N. F. & Pitanguy, I. Influence of decantation, washing and centrifugation on adipocyte and mesenchymal stem cell content of aspirated adipose tissue: A comparative study. *J. Plast. Reconstr.*

Aesthetic Surg. **63**, 1375–1381 (2010).

51. Cowan, C. A. *et al.* Derivation of Embryonic Stem-Cell Lines from Human Blastocysts. *N. Engl. J. Med.* **350**, 1353–1356 (2004).

52. Vats, A., Tolley, N. S., Bishop, A. E. & Polak, J. M. Embryonic stem cells and tissue engineering: Delivering stem cells to the clinic. *J. R. Soc. Med.* **98**, 346–350 (2005).

53. Kubo, A. *et al.* Development of definitive endoderm from embryonic stem cells in culture. *Development* **131**, 1651–1662 (2004).

54. D'Amour, K. A. *et al.* Efficient differentiation of human embryonic stem cells to definitive endoderm. *Nat. Biotechnol.* **23**, 1534–1541 (2005).

55. Tran, T. H. *et al.* Wnt3a-induced mesoderm formation and cardiomyogenesis in human embryonic stem cells. *Stem Cells* **27**, 1869–1878 (2009).

56. Zhang, P. *et al.* Short-term BMP-4 treatment initiates mesoderm induction in human embryonic stem cells. *Blood* **111**, 1933–1941 (2008).

57. Roche, E., Sepulcre, P., Reig, J. A., Santana, A. & Soria, B. Ectodermal commitment of insulin-producing cells derived from mouse embryonic stem cells. *FASEB J.* **19**, 1341–1343 (2005).

58. Rieske, P., Krynska, B. & Azizi, S. A. Human fibroblast-derived cell lines have characteristics of embryonic stem cells and cells of neuro-ectodermal origin. *Differentiation* **73**, 474–483 (2005).

59. Nussbaum, J. *et al.* Transplantation of undifferentiated murine embryonic stem cells in the heart: teratoma formation and immune response. *FASEB J.* **21**, 1345–1357 (2007).

60. Ilic, D. & Ogilvie, C. Concise Review: Human Embryonic Stem Cells-What Have We Done? What Are We Doing? Where Are We Going? *Stem Cells* **35**, 17–25

(2017).

61. Knoepfler, P. S. Deconstructing stem cell tumorigenicity: A roadmap to safe regenerative medicine. *Stem Cells* **27**, 1050–1056 (2009).

62. Pittenger, M. F. *et al.* Multilineage potential of adult human mesenchymal stem cells. *Science* **284**, 143–7 (1999).

63. Zuk, P. Adipose-Derived Stem Cells in Tissue Regeneration: A Review. *ISRN Stem Cells* **2013**, 1–35 (2013).

64. De Sousa, E. B., Casado, P. L., Neto, V. M., Duarte, M. E. L. & Aguiar, D. P. Synovial fluid and synovial membrane mesenchymal stem cells: Latest discoveries and therapeutic perspectives. *Stem Cell Res. Ther.* **5**, 1–6 (2014).

65. Romanov, Y. A. Searching for Alternative Sources of Postnatal Human Mesenchymal Stem Cells: Candidate MSC-Like Cells from Umbilical Cord. *Stem Cells* **21**, 105–110 (2003).

66. Hass, R., Kasper, C., Böhm, S. & Jacobs, R. Different populations and sources of human mesenchymal stem cells (MSC): A comparison of adult and neonatal tissue-derived MSC. *Cell Commun. Signal.* **9**, 12 (2011).

67. Dominici, M. *et al.* Minimal criteria for defining multipotent mesenchymal stromal cells. The International Society for Cellular Therapy position statement. *Cytotherapy* **8**, 315–317 (2006).

68. Pak, J. *et al.* Current use of autologous adipose tissue-derived stromal vascular fraction cells for orthopedic applications. *J. Biomed. Sci.* **24**, 1–12 (2017).

69. Locke, M., Windsor, J. & Dunbar, P. R. Human adipose-derived stem cells: Isolation, characterization and applications in surgery. *ANZ J. Surg.* **79**, 235–244 (2009).

70. Bourin, P. *et al.* Stromal cells from the adipose tissue-derived stromal vascular

fraction and culture expanded adipose tissue-derived stromal/stem cells: A joint statement of the International Federation for Adipose Therapeutics and Science (IFATS) and the International So. *Cytotherapy* **15**, 641–648 (2013).

71. Strem, B. M. *et al.* Multipotential differentiation of adipose tissue-derived stem cells. *Keio J. Med.* **54**, 132–41 (2005).

72. Zuk, P. A. *et al.* Multilineage cells from human adipose tissue: Implications for cell-based therapies. *Tissue Eng.* **7**, 211–228 (2001).

73. Haniffa, M. A. *et al.* Adult Human Fibroblasts Are Potent Immunoregulatory Cells and Functionally Equivalent to Mesenchymal Stem Cells. *J. Immunol.* **179**, 1595–1604 (2007).

74. Oliferenko, S., Kaverina, I., Small, J. V. & Huber, L. A. Hyaluronic acid (HA) binding to CD44 activates Rac1 and induces lamellipodia outgrowth. *J. Cell Biol.* **148**, 1159–1164 (2000).

75. Isacke, C. M. & Yarwood, H. The hyaluronan receptor, CD44. *Int. J. Biochem. Cell Biol.* **34**, 718–721 (2002).

76. Regateiro, F. S., Cobbold, S. P. & Waldmann, H. CD73 and adenosine generation in the creation of regulatory microenvironments. *Clin. Exp. Immunol.* **171**, 1–7 (2013).

77. Chung, M. T. *et al.* CD90 (Thy-1)-positive selection enhances osteogenic capacity of human adipose-derived stromal cells. *Tissue Eng. - Part A* **19**, 989–997 (2013).

78. Torsney, E., Charlton, R., Parums, D., Collis, M. & Arthur, H. M. Inducible expression of human endoglin during inflammation and wound healing in vivo. *Inflamm. Res.* **51**, 464–470 (2002).

79. Ilan, N., Mahooti, S., Rimm, D. L. & Madri, J. A. PECAM-1 (CD31) functions as a reservoir for and a modulator of tyrosine-phosphorylated β-catenin. *J. Cell Sci.* **112**, 3005–3014 (1999).

80. Nakano, A., Harada, T., Morikawa, S. & Kato, Y. Expression of Leukocyte Common Antigen (CD45) on Various Human Leukemia/Lymphoma Cell Lines. *Pathol. Int.* **40**, 107–115 (1990).

81. Christopherson, K. W., Hangoc, G. & Broxmeyer, H. E. Cell Surface Peptidase CD26/Dipeptidylpeptidase IV Regulates CXCL12/Stromal Cell-Derived Factor-1α-Mediated Chemotaxis of Human Cord Blood CD34 + Progenitor Cells . *J. Immunol.* **169**, 7000–7008 (2002).

82. Christopherson, K. W. Modulation of Hematopoietic Stem Cell Homing and Engraftment by CD26. *Science* **305**, 1000–1003 (2004).

83. Rinkevich, Y. *et al.* Identification and isolation of a dermal lineage with intrinsic fibrogenic potential. *Science* **348**, aaa2151–aaa2151 (2015).

84. Suga, H. *et al.* Functional implications of CD34 expression in human adipose-derived stem/progenitor cells. *Stem Cells Dev.* **18**, 1201–1209 (2009).

85. Traktuev, D. O. *et al.* A population of multipotent CD34-positive adipose stromal cells share pericyte and mesenchymal surface markers, reside in a periendothelial location, and stabilize endothelial networks. *Circ. Res.* **102**, 77–85 (2008).

86. Zheng, C. *et al.* Endothelial CD146 is required for in vitro tumor-induced angiogenesis: The role of a disulfide bond in signaling and dimerization. *Int. J. Biochem. Cell Biol.* **41**, 2163–2172 (2009).

87. Russell, K. C. *et al.* In vitro high-capacity assay to quantify the clonal heterogeneity in trilineage potential of mesenchymal stem cells reveals a complex hierarchy of lineage commitment. *Stem Cells* **28**, 788–798 (2010).

88. Fomby, P. *et al.* Stem cells and cell therapies in lung biology and diseases: Conference report. *Ann. Am. Thorac. Soc.* **12**, 181–204 (2010).

89. Gierloff, M. *et al.* Adipogenic differentiation potential of rat adipose tissue-derived subpopulations of stromal cells. *J. Plast. Reconstr. Aesthetic Surg.* **67**, 1427–1435

(2014).

90. Choy, L. & Derynck, R. Transforming Growth Factor-β Inhibits Adipocyte Differentiation by Smad3 Interacting with CCAAT/Enhancer-binding Protein (C/EBP) and Repressing C/EBP Transactivation Function. *J. Biol. Chem.* **278**, 9609–9619 (2003).

91. Brun, R. P. *et al.* Differential activation of adipogenesis by multiple PPAR isoforms. *Genes Dev.* **10**, 974–984 (1996).

92. Gregoire, F. M., Smas, C. M. & Sul, H. S. Understanding adipocyte differentiation. *Physiol. Rev.* **78**, 783–809 (1998).

93. Mehlhorn, A. T. *et al.* Differential effects of BMP-2 and TGF-β1 on chondrogenic differentiation of adipose derived stem cells. *Cell Prolif.* **40**, 809–823 (2007).

94. Langenbach, F. & Handschel, J. Effects of dexamethasone, ascorbic acid and β-glycerophosphate on the osteogenic differentiation of stem cells in vitro. *Stem Cell Res. Ther.* **4**, 117 (2013).

95. Rodbell, M. & Jones, A. Metabolism of isolated fat cells. *J. Biol. Chem.* **241**, 140–142 (1966).

96. Bunnell, B. A., Flaat, M., Gagliardi, C., Patel, B. & Ripoll, C. Adipose-derived stem cells: Isolation, expansion and differentiation. *Methods* **45**, 115–120 (2008).

97. Markarian, C. F. *et al.* Isolation of adipose-derived stem cells: A comparison among different methods. *Biotechnol. Lett.* **36**, 693–702 (2014).

98. Priya, N., Sarcar, S., Majumdar, A. Sen & SundarRaj, S. Explant culture: a simple, reproducible, efficient and economic technique for isolation of mesenchymal stromal cells from human adipose tissue and lipoaspirate. *J. Tissue Eng. Regen. Med.* **8**, 706–716 (2014).

99. Brunet, S. *et al.* Characterization of the TPX2 Domains Involved in Microtubule

Nucleation and Spindle Assembly in Xenopus nucleation around chromatin and functions in a network of other molecules , some of which also are regulated by. *Mol Biol Cell* **15**, 5318–5328 (2004).

100. Wosnitza, M., Hemmrich, K., Groger, A., Gräber, S. & Pallua, N. Plasticity of human adipose stem cells to perform adipogenic and endothelial differentiation. *Differentiation* **75**, 12–23 (2007).

101. Suga, H., Glotzbach, J. P., Sorkin, M., Longaker, M. T. & Gurtner, G. C. Paracrine Mechanism of Angiogenesis in Adipose-Derived Stem Cell Transplantation. *Ann. Plast. Surg.* **72**, 234–241 (2014).

102. Chazenbalk, G. *et al.* Novel pathway of adipogenesis through cross-talk between adipose tissue macrophages, adipose stem cells and adipocytes: evidence of cell plasticity. *PLoS One* **6**, e17834 (2011).

103. Kang, S., Kim, S.-M. & Sung, J.-H. Cellular and molecular stimulation of adipose-derived stem cells under hypoxia. *Cell Biol. Int.* **38**, 553–562 (2014).

104. Tsuji, W. Adipose-derived stem cells: Implications in tissue regeneration. *World J. Stem Cells* **6**, 312 (2014).

105. Frazier, T. P., Gimble, J. M., Kheterpal, I. & Rowan, B. G. Impact of low oxygen on the secretome of human adipose-derived stromal/stem cell primary cultures. *Biochimie* **95**, 2286–2296 (2013).

106. Thangarajah, H. *et al.* IFATS Collection: Adipose Stromal Cells Adopt a Proangiogenic Phenotype Under the Influence of Hypoxia. *Stem Cells* **27**, 266–274 (2009).

107. Kapur, S. K. & Katz, A. J. Biochimie Review of the adipose derived stem cell secretome. *Biochimie* **95**, 2222–2228 (2013).

108. Chung, A. S., Waldeck, H., Schmidt, D. R. & Kao, W. J. Monocyte inflammatory and matrix remodeling response modulated by grafted ECM-derived ligand

concentration. *J. Biomed. Mater. Res. - Part A* **91**, 741–752 (2009).

109. Khan, T. *et al.* Metabolic Dysregulation and Adipose Tissue Fibrosis: Role of Collagen VI. *Mol. Cell. Biol.* **29**, 1575–1591 (2009).

110. Sillat, T. *et al.* Basement membrane collagen type IV expression by human mesenchymal stem cells during adipogenic differentiation. *J. Cell. Mol. Med.* **16**, 1485–1495 (2012).

111. Hsiao, S. T. *et al.* Hypoxic conditioning enhances the angiogenic paracrine activity of human adipose-derived stem cells. *Stem Cells Dev.* **22**, 1614–1623 (2013).

112. Cross, M. J. & Claesson-Welsh, L. FGF and VEGF function in angiogenesis: Signalling pathways, biological responses and therapeutic inhibition. *Trends Pharmacol. Sci.* **22**, 201–207 (2001).

113. Christopher, M. J., Rao, M., Liu, F., Woloszynek, J. R. & Link, D. C. Expression of the G-CSF receptor in monocytic cells is sufficient to mediate hematopoietic progenitor mobilization by G-CSF in mice. *J. Exp. Med.* **208**, 251–260 (2011).

114. Kawaguchi, M. & Kataoka, H. Mechanisms of hepatocyte growth factor activation in cancer tissues. *Cancers (Basel).* **6**, 1890–1904 (2014).

115. Beilmann, M., Birk, G. & Lenter, M. C. Human primary co-culture angiogenesis assay reveals additive stimulation and different angiogenic properties of VEGF and HGF. *Cytokine* **26**, 178–185 (2004).

116. Kiec-Wilk, B. *et al.* The MAPK-dependent regulation of the Jagged/Notch gene expression by VEGF, bFGF or PPAR gamma mediated angiogenesis in HUVEC. *J. Physiol. Pharmacol.* **61**, 217–225 (2010).

117. Natori, T. *et al.* G-CSF stimulates angiogenesis and promotes tumor growth: Potential contribution of bone marrow-derived endothelial progenitor cells. *Biochem. Biophys. Res. Commun.* **297**, 1058–1061 (2002).

118. Shojaei, S., Tafazzoli-Shahdpour, M., Shokrgozar, M. A. & Haghighipour, N. Effects of mechanical and chemical stimuli on differentiation of human adipose-derived stem cells into endothelial cells. *Int. J. Artif. Organs* **36**, 663–673 (2013).

119. Chen, R. R., Silva, E. A., Yuen, W. W. & Mooney, D. J. Spatio-temporal VEGF and PDGF delivery patterns blood vessel formation and maturation. *Pharm. Res.* **24**, 258–264 (2007).

120. Lopatina, T. *et al.* Platelet-derived growth factor regulates the secretion of extracellular vesicles by adipose mesenchymal stem cells and enhances their angiogenic potential. *Cell Commun. Signal.* **12**, 1–12 (2014).

121. Rajkumar, V. S. *et al.* Platelet-derived growth factor-β receptor activation is essential for fibroblast and pericyte recruitment during cutaneous wound healing. *Am. J. Pathol.* **169**, 2254–2265 (2006).

122. Chislock, E. M., Ring, C. & Pendergast, A. M. Abl kinases are required for vascular function, Tie2 expression, and angiopoietin-1-mediated survival. *Proc. Natl. Acad. Sci. U. S. A.* **110**, 12432–12437 (2013).

123. Caplan, A. I. & Sorrell, J. M. The MSC curtain that stops the immune system. *Immunol. Lett.* **168**, 136–139 (2015).

124. Ren, G. *et al.* Mesenchymal Stem Cell-Mediated Immunosuppression Occurs via Concerted Action of Chemokines and Nitric Oxide. *Cell Stem Cell* **2**, 141–150 (2008).

125. Zhang, S. *et al.* Interleukin 6 Mediates the Therapeutic Effects of Adipose-Derived Stromal/Stem Cells in Lipopolysaccharide-Induced Acute Lung Injury. *Stem Cells* **32**, 1616–1628 (2014).

126. Huh, J. E. & Lee, S. Y. IL-6 is produced by adipose-derived stromal cells and promotes osteogenesis. *Biochim. Biophys. Acta - Mol. Cell Res.* **1833**, 2608–2616 (2013).

127. Hutton, D. L. *et al.* Tumor necrosis factor improves vascularization in osteogenic grafts engineered with human adipose-derived stem/stromal cells. *PLoS One* **9**, (2014).

128. Lee, M. J. *et al.* Proteomic analysis of tumor necrosis factor-α-induced secretome of human adipose tissue-derived mesenchymal stem cells. *J. Proteome Res.* **9**, 1754–1762 (2010).

129. Ogami, K. *et al.* Computational gene network analysis reveals TNF-induced angiogenesis. *BMC Syst. Biol.* **6**, 3–8 (2012).

130. Yuan, J., Fang, W., Lin, A., Ni, Z. & Qian, J. Angiopoietin-2/Tie2 Signaling Involved in TNF-α Induced Peritoneal Angiogenesis. *Int. J. Artif. Organs* **35**, 655–662 (2012).

131. Sainson, R. C. A. *et al.* TNF primes endothelial cells for angiogenic sprouting by inducing a tip cell phenotype. *Blood* **111**, 4997–5007 (2008).

132. English, K., Barry, F. P., Field-Corbett, C. P. & Mahon, B. P. IFN-γ and TNF-α differentially regulate immunomodulation by murine mesenchymal stem cells. *Immunol. Lett.* **110**, 91–100 (2007).

133. Maria, A. T. J. *et al.* iNOS Activity Is Required for the Therapeutic Effect of Mesenchymal Stem Cells in Experimental Systemic Sclerosis. *Front. Immunol.* **9**, 3056 (2018).

134. Manferdini, C. *et al.* Adipose stromal cells mediated switching of the pro-inflammatory profile of M1-like macrophages is facilitated by PGE2: in vitro evaluation. *Osteoarthr. Cartil.* **25**, 1161–1171 (2017).

135. Mocellin, S., Panelli, M. C., Wang, E., Nagorsen, D. & Marincola, F. M. The dual role of IL-10. *Trends Immunol.* **24**, 36–43 (2003).

136. Deng, B., Wehling-Henricks, M., Villalta, S. A., Wang, Y. & Tidball, J. G. IL-10 Triggers Changes in Macrophage Phenotype That Promote Muscle Growth and

Regeneration. *J. Immunol.* **189**, 3669–3680 (2012).

137. Liu, Z. G. Molecular mechanism of TNF signaling and beyond. *Cell Res.* **15**, 24–27 (2005).

138. Schwabe, R. F. & Brenner, D. A. Mechanisms of liver injury. I. TNF-α-induced liver injury: Role of IKK, JNK, and ROS pathways. *Am. J. Physiol. - Gastrointest. Liver Physiol.* **290**, 583–589 (2006).

139. Böcker, W. *et al.* IKK-2 is required for TNF-α-induced invasion and proliferation of human mesenchymal stem cells. *Journal of Molecular Medicine* vol. 86 1183–1192 (2008).

140. Martínez-Chaćon, G. *et al.* IL-10 suppresses TNF-A-induced expression of human aromatase gene in mammary adipose tissue. *FASEB J.* **32**, 3361–3370 (2018).

141. Akira, S., Hirano, T., Taga, T. & Kishimoto, T. Biology of multifunctional cytokines: IL 6 and related molecules (IL 1 and TNF). *FASEB J.* **4**, 2860–2867 (1990).

142. Díaz, L. *et al.* Calcitriol inhibits TNF-α-induced inflammatory cytokines in human trophoblasts. *J. Reprod. Immunol.* **81**, 17–24 (2009).

143. Mori, T. *et al.* IL-1β and TNFα-initiated IL-6-STAT3 pathway is critical in mediating inflammatory cytokines and RANKL expression in inflammatory arthritis. *Int. Immunol.* **23**, 701–712 (2011).

144. Wang, L. *et al.* IL-17 can promote tumor growth through an IL-6-Stat3 signaling pathway. *J. Exp. Med.* **206**, 1457–1464 (2009).

145. Baluk, P. *et al.* TNF-α drives remodeling of blood vessels and lymphatics in sustained airway inflammation in mice. *J. Clin. Invest.* **119**, (2009).

146. Rehman, J. *et al.* Secretion of angiogenic and antiapoptotic factors by human adipose stromal cells. *Circulation* **109**, 1292–8 (2004).

147. Kronsteiner, B. *et al.* Human mesenchymal stem cells and renal tubular epithelial cells differentially influence monocyte-derived dendritic cell differentiation and maturation. *Cell. Immunol.* **267**, 30–38 (2011).

148. Gordon, S. Alternative activation of macrophages. *Nat. Rev. Immunol.* **3**, 23–35 (2003).

149. Song, J. young *et al.* Umbilical cord-derived mesenchymal stem cell extracts ameliorate atopic dermatitis in mice by reducing the T cell responses. *Sci. Rep.* **9**, 1–9 (2019).

150. He, Y. & Lu, F. Development of Synthetic and Natural Materials for Tissue Engineering Applications Using Adipose Stem Cells. *Stem Cells Int.* **2016**, (2016).

151. Weiser, B. *et al.* In vivo development and long-term survival of engineered adipose tissue depend on in vitro precultivation strategy. *Tissue Eng. - Part A.* **14**, 275–284 (2008).

152. Kang, S. W., Seo, S. W., Choi, C. Y. & Kim, B. S. Porous poly(lactic-co-glycolic acid) microsphere as cell culture substrate and cell transplantation vehicle for adipose tissue engineering. *Tissue Eng. - Part C Methods* **14**, 25–34 (2008).

153. Salick, D. A., Kretsinger, J. K., Pochan, D. J. & Schneider, J. P. Inherent antibacterial activity of a peptide-based β-hairpin hydrogel. *J. Am. Chem. Soc.* **129**, 14793–14799 (2007).

154. Cronin, K. J. *et al.* New murine model of spontaneous autologous tissue engineering, combining an arteriovenous pedicle with matrix materials. *Plast. Reconstr. Surg.* **113**, 260–269 (2004).

155. Choi, Y. S. *et al.* Adipogenic differentiation of adipose tissue derived adult stem cells in nude mouse. *Biochem. Biophys. Res. Commun.* **345**, 631–637 (2006).

156. Marra, K. G. *et al.* FGF-2 enhances vascularization for adipose tissue engineering. *Plast. Reconstr. Surg.* **121**, 1153–1164 (2008).

157. Cho, S. W. *et al.* Engineered adipose tissue formation enhanced by basic fibroblast growth factor and a mechanically stable environment. *Cell Transplant.* **16**, 421–434 (2007).

158. Patrick, C. W. W., Chauvin, P. B. B., Hobley, J. & Reece, G. P. P. Preadipocyte Seeded PLGA Scaffolds for Adipose Tissue Engineering. *Tissue Eng.* **5**, 139–151 (1999).

159. Yu, S. C., Park, S. N. & Suh, H. Adipose tissue engineering using mesenchymal stem cells attached to injectable PLGA spheres. *Biomaterials* **26**, 5855–5863 (2005).

160. Kimura, Y., Ozeki, M., Inamoto, T. & Tabata, Y. Adipose tissue engineering based on human preadipocytes combined with gelatin microspheres containing basic fibroblast growth factor. *Biomaterials* **24**, 2513–2521 (2003).

161. Neuss, S. *et al.* Long-term survival and bipotent terminal differentiation of human mesenchymal stem cells (hMSC) in combination with a commercially available three-dimensional collagen scaffold. *Cell Transplant.* **17**, 977–986 (2008).

162. Von Heimburg, D. *et al.* Preadipocyte-loaded collagen scaffolds with enlarged pore size for improved soft-tissue engineering. *Int. J. Artif. Organs* **26**, 1064–1076 (2003).

163. Tan, H. *et al.* Thermosensitive injectable hyaluronic acid hydrogel for adipose tissue engineering. *Biomaterials* **30**, 6844–6853 (2009).

164. Borzacchiello, A. *et al.* Structural and rheological characterization of hyaluronic acid-based scaffolds for adipose tissue engineering. *Biomaterials* **28**, 4399–4408 (2007).

165. Chang, K. H., Liao, H. T. & Chen, J. P. Preparation and characterization of gelatin/hyaluronic acid cryogels for adipose tissue engineering: In vitro and in vivo studies. *Acta Biomater.* **9**, 9012–9026 (2013).

166. Choi, J. S. *et al.* Decellularized extracellular matrix derived from human adipose tissue as a potential scaffold for allograft tissue engineering. *J. Biomed. Mater. Res. - Part A* **97 A**, 292–299 (2011).

167. Choi, Y. C. *et al.* Decellularized Extracellular Matrix Derived from Porcine Adipose Tissue as a Xenogeneic Biomaterial for Tissue Engineering. *Tissue Eng. Part C Methods* **18**, 866–876 (2012).

168. Zhang, Q. *et al.* Decellularized skin/adipose tissue flap matrix for engineering vascularized composite soft tissue flaps. *Acta Biomater.* **35**, 166–184 (2016).

169. Han, T. T. Y., Toutounji, S., Amsden, B. G. & Flynn, L. E. Adipose-derived stromal cells mediate in vivo adipogenesis, angiogenesis and inflammation in decellularized adipose tissue bioscaffolds. *Biomaterials* **72**, 125–137 (2015).

170. Matsuda, K. *et al.* Adipose-derived stem cells promote angiogenesis and tissue formation for in vivo tissue engineering. *Tissue Eng. - Part A* **19**, 1327–1335 (2013).

171. Chircov, C., Grumezescu, A. M. & Bejenaru, L. E. Hyaluronic acid-based scaffolds for tissue engineering. *Rom. J. Morphol. Embryol.* **59**, 71–76 (2018).

172. Collins, M. N. & Birkinshaw, C. Hyaluronic acid based scaffolds for tissue engineering - A review. *Carbohydr. Polym.* **92**, 1262–1279 (2013).

173. Collins, M. N. & Birkinshaw, C. Hyaluronic acid based scaffolds for tissue engineering--a review. *Carbohydr. Polym.* **92**, 1262–1279 (2013).

174. Burdick, J. A. & Prestwich, G. D. Hyaluronic acid hydrogels for biomedical applications. *Adv. Mater.* **23**, H41–H56 (2011).

175. Halbleib, M., Skurk, T., de Luca, C., von Heimburg, D. & Hauner, H. Tissue engineering of white adipose tissue using hyaluronic acid-based scaffolds. I: in vitro differentiation of human adipocyte precursor cells on scaffolds. *Biomaterials* **24**, 3125–3132 (2003).

176. Hemmrich, K. *et al.* Implantation of preadipocyte-loaded hyaluronic acid-based scaffolds into nude mice to evaluate potential for soft tissue engineering. *Biomaterials* **26**, 7025–7037 (2005).

177. Tan, H., Chu, C. R., Payne, K. a. & Marra, K. G. Injectable in situ forming biodegradable chitosan-hyaluronic acid based hydrogels for cartilage tissue engineering. *Biomaterials* vol. 30 2499–2506 (2009).

178. Kirk, J. F. *et al.* Mechanical and biocompatible characterization of a cross-linked collagen-hyaluronic acid wound dressing. *Biomatter* **3**, e25633 (2013).

179. Lee, Y. *et al.* Thermo-sensitive, injectable, and tissue adhesive sol–gel transition hyaluronic acid/pluronic composite hydrogels prepared from bio-inspired catechol-thiol reaction. *Soft Matter* **6**, 977 (2010).

180. Chen, J.-P. & Cheng, T.-H. Preparation and evaluation of thermo-reversible copolymer hydrogels containing chitosan and hyaluronic acid as injectable cell carriers. *Polymer* **50**, 107–116 (2009).

181. Roth, C. C. *et al.* Bladder regeneration in a canine model using hyaluronic acid-poly(lactic-co-glycolic-acid) nanoparticle modified porcine small intestinal submucosa. *BJU Int.* **108**, 148–155 (2011).

182. Davidenko, N., Campbell, J. J., Thian, E. S., Watson, C. J. & Cameron, R. E. Collagen-hyaluronic acid scaffolds for adipose tissue engineering. *Acta Biomater.* **6**, 3957–3968 (2010).

183. Keck, M. *et al.* Adipose tissue engineering: Three different approaches to seed preadipocytes on a collagen-elastin matrix. *Ann. Plast. Surg.* **67**, 484–488 (2011).

184. Wu, X., Black, L., Santacana-Laffitte, G. & Patrick, C. W. Preparation and assessment of glutaraldehyde-crosslinked collagen–chitosan hydrogels for adipose tissue engineering. *J. Biomed. Mater. Res. Part A* **81A**, 59–65 (2007).

185. Yao, R., Zhang, R., Lin, F. & Luan, J. Biomimetic injectable HUVEC-

adipocytes/collagen/alginate microsphere co-cultures for adipose tissue engineering. *Biotechnol. Bioeng.* **110**, 1430–1443 (2013).

186. Heino, J. The collagen family members as cell adhesion proteins. *BioEssays* **29**, 1001–1010 (2007).

187. Kühn, K. Basement membrane (type IV) collagen. *Matrix Biol.* **14**, 439–45 (1995).

188. Dehsorkhi, A., Castelletto, V., Hamley, I. W., Adamcik, J. & Mezzenga, R. The effect of pH on the self-assembly of a collagen derived peptide amphiphile. *Soft Matter* **9**, 6033 (2013).

189. Choi, J. S. *et al.* Human extracellular matrix (ECM) powders for injectable cell delivery and adipose tissue engineering. *J. Control. Release* **139**, 2–7 (2009).

190. Vashi, A. V. *et al.* Adipose tissue engineering based on the controlled release of fibroblast growth factor-2 in a collagen matrix. *Tissue Eng.* **12**, 3035–3043 (2006).

191. Hiraoka, Y. *et al.* In situ regeneration of adipose tissue in rat fat pad by combining a collagen scaffold with gelatin microspheres containing basic fibroblast growth factor. *Tissue Eng.* **12**, 1475–1487 (2006).

192. Song, K. *et al.* Preparation, fabrication and biocompatibility of novel injectable temperature-sensitive chitosan/glycerophosphate/collagen hydrogels. *J. Mater. Sci. Mater. Med.* **21**, 2835–2842 (2010).

193. Zhang, Q. *et al.* Engineering vascularized soft tissue flaps in an animal model using human adipose-derived stem cells and VEGF+PLGA/PEG microspheres on a collagen-chitosan scaffold with a flow-through vascular pedicle. *Biomaterials* **73**, 198–213 (2015).

194. Hynes, R. O. The Extracellular Matrix: Not Just Pretty Fibrils. *Science* **326**, 1216–1219 (2009).

195. Badylak, S. F. The extracellular matrix as a biologic scaffold material.

Biomaterials **28**, 3587–3593 (2007).

196. Nagase, H., Visse, R. & Murphy, G. Structure and function of matrix metalloproteinases and TIMPs. *Cardiovasc. Res.* **69**, 562–573 (2006).

197. Mesenchymal, H. *et al.* Tailored Integrin – Extracellular Matrix Interactions to Direct. **21**, 2442–2456 (2012).

198. Page-McCaw, A., Ewald, A. J. & Werb, Z. Matrix metalloproteinases and the regulation of tissue remodelling. *Nat. Rev. Mol. Cell Biol.* **8**, 221–33 (2007).

199. Mariman, E. C. M. M. & Wang, P. Adipocyte extracellular matrix composition, dynamics and role in obesity. *Cell. Mol. Life Sci.* **67**, 1277–1292 (2010).

200. Knight, C. G. *et al.* The collagen-binding a-domains of integrins α1/β1 and α2/β1 recognize the same specific amino acid sequence, GFOGER, in native (triple-helical) collagens. *J. Biol. Chem.* **275**, 35–40 (2000).

201. Lahti, M., Heino, J. & Käpylä, J. Leukocyte integrins αlβ2, αmβ2 and αxβ2 as collagen receptors - Receptor activation and recognition of GFOGER motif. *Int. J. Biochem. Cell Biol.* **45**, 1204–1211 (2013).

202. Lee, S. H. *et al.* Fibronectin gene expression in human adipose tissue and its associations with obesity-related genes and metabolic parameters. *Obes. Surg.* **23**, 554–560 (2013).

203. Halliday, N. L. & Tomasek, J. J. Mechanical properties of the extracellular matrix influence fibronectin fibril assembly in vitro. *Experimental cell research* vol. 217 109–117 (1995).

204. Kapp, T. G. *et al.* A comprehensive evaluation of the activity and selectivity profile of ligands for RGD-binding integrins. *Sci. Rep.* **7**, 1–13 (2017).

205. Laterra, J., Silbert, J. E. & Culp, L. A. Cell surface heparan sulfate mediates some adhesive responses to glycosaminoglycan binding matrices, including fibronectin.

J. Cell Biol. **96**, 112–123 (1983).

206. Stamatoglou, S. C. & Keller, J. M. Correlation between cell substrate attachment in vitro and cell surface heparan sulfate affinity for fibronectin and collagen. *J. Cell Biol.* **96**, 1820–1823 (1983).

207. Wang, Y., Zhao, L., Smas, C. & Sul, H. S. Pref-1 interacts with fibronectin to inhibit adipocyte differentiation. *Mol. Cell. Biol.* **30**, 3480–92 (2010).

208. Smas, C. M., Chen, L. & Sul, H. S. Cleavage of membrane-associated pref-1 generates a soluble inhibitor of adipocyte differentiation. *Mol. Cell. Biol.* **17**, 977–88 (1997).

209. Durbeej, M. Laminins. *Cell Tissue Res.* **339**, 259–268 (2010).

210. Theocharis, A. D., Skandalis, S. S., Gialeli, C. & Karamanos, N. K. Extracellular matrix structure. *Adv. Drug Deliv. Rev.* **97**, 4–27 (2016).

211. van Dijk, a, Niessen, H. W. M., Zandieh Doulabi, B., Visser, F. C. & van Milligen, F. J. Differentiation of human adipose-derived stem cells towards cardiomyocytes is facilitated by laminin. *Cell Tissue Res.* **334**, 457–67 (2008).

212. Sur, S. *et al.* Synergistic regulation of cerebellar Purkinje neuron development by laminin epitopes and collagen on an artificial hybrid matrix construct . *Biomater. Sci.* **2**, 903–914 (2014).

213. Chen, S. *et al.* A laminin mimetic peptide SIKVAV-conjugated chitosan hydrogel promoting wound healing by enhancing angiogenesis, re-epithelialization and collagen deposition. *J. Mater. Chem. B* **3**, 6798–6804 (2015).

214. Ruoslahti, E. & Yamaguchi, Y. Proteoglycans as modulators of growth factor activities. *Cell* **64**, 867–869 (1991).

215. Dreyfuss, J. L. *et al.* Heparan sulfate proteoglycans: Structure, protein interactions and cell signaling. *An. Acad. Bras. Cienc.* **81**, 409–429 (2009).

216. Wang, Q. G., Hughes, N., Cartmell, S. H. & Kuiper, N. J. The composition of hydrogels for cartilage tissue engineering can influence glycosaminoglycan profiles. *Eur. Cells Mater.* **19**, 86–95 (2010).

217. Zhu, Y., Crewe, C. & Scherer, P. E. Hyaluronan in adipose tissue: Beyond dermal filler and therapeutic carrier. *Sci. Transl. Med.* **8**, (2016).

218. Liang, J., Jiang, D. & Noble, P. W. Hyaluronan as a therapeutic target in human diseases. *Adv. Drug Deliv. Rev.* **97**, 186–203 (2016).

219. Kang, L. *et al.* Hyaluronan accumulates with high-fat feeding and contributes to insulin resistance. *Diabetes* **62**, 1888–1896 (2013).

220. Ji, E. *et al.* Inhibition of adipogenesis in 3T3-L1 cells and suppression of abdominal fat accumulation in high-fat diet-feeding C57BL/6J mice after downregulation of hyaluronic acid. *Int. J. Obes.* **38**, 1035–1043 (2014).

221. Lu, P., Takai, K., Weaver, V. M. & Werb, Z. Extracellular matrix degradation and remodeling in development and disease. *Cold Spring Harb Perspect Biol* **3**, (2011).

222. Lin, D., Chun, T. & Kang, L. Adipose extracellular matrix remodelling in obesity and insulin. *Biochem. Pharmacol.* 1–9 (2016) doi:10.1016/j.bcp.2016.05.005.

223. Chavey, C. *et al.* Matrix metalloproteinases are differentially expressed in adipose tissue during obesity and modulate adipocyte differentiation. *J. Biol. Chem.* **278**, 11888–96 (2003).

224. Lin, D., Chun, T.-H. & Kang, L. Adipose extracellular matrix remodelling in obesity and insulin resistance. *Biochem. Pharmacol.* **119**, 8–16 (2016).

225. Kubota, S. & Takigawa, M. Cellular and molecular actions of CCN2/CTGF and its role under physiological and pathological conditions. *Clin Sci* **128**, 181–196 (2015).

226. Rosso, F. *et al.* Smart materials as scaffolds for tissue engineering. *J. Cell. Physiol.* **203**, 465–470 (2005).

227. Yu, C. *et al.* Porous decellularized adipose tissue foams for soft tissue regeneration. *Biomaterials* **34**, 3290–3302 (2013).

228. Hoshiba, T., Lu, H., Kawazoe, N. & Chen, G. Decellularized matrices for tissue engineering. *Expert Opin. Biol. Ther.* **10**, 1717–1728 (2010).

229. Turner, A. E. B., Yu, C., Bianco, J., Watkins, J. F. & Flynn, L. E. The performance of decellularized adipose tissue microcarriers as an inductive substrate for human adipose-derived stem cells. *Biomaterials* **33**, 4490–4499 (2012).

230. Voytik-Harbin, S. L. *et al.* Small intestinal submucosa: A tissue-derived extracellular matrix that promotes tissue-specific growth and differentiation of cells in vitro. *Tissue Eng.* **4**, 157–174 (1998).

231. Cheng, N.-C., Estes, B. T., Awad, H. A. & Guilak, F. Chondrogenic differentiation of adipose-derived adult stem cells by a porous scaffold derived from native articular cartilage extracellular matrix. *Tissue Eng. Part A* **15**, 231–241 (2009).

232. Wang, R. M. & Christman, K. L. Decellularized myocardial matrix hydrogels: In basic research and preclinical studies. *Adv. Drug Deliv. Rev.* **96**, 77–82 (2016).

233. Kleinman, H. K. *et al.* Basement Membrane Complexes with Biological Activity. *Biochemistry* **25**, 312–318 (1986).

234. Stillaert, F. *et al.* Host rather than graft origin of Matrigel-induced adipose tissue in the murine tissue-engineering chamber. *Tissue Eng.* **13**, 2291–2300 (2007).

235. Polykandriotis, E., Arkudas, A., Horch, R. E. & Kneser, U. To Matrigel or not to Matrigel. *Am. J. Pathol.* **172**, 1441–1442 (2008).

236. Badylak, S. F., Taylor, D. & Uygun, K. Whole-Organ Tissue Engineering: Decellularization and Recellularization of Three-Dimensional Matrix Scaffolds.

Annu. Rev. Biomed. Eng. **13**, 27–53 (2011).

237. Badylak, S. F., Weiss, D. J., Caplan, A. & MacChiarini, P. Engineered whole organs and complex tissues. *Lancet* **379**, 943–952 (2012).

238. Flynn, L., Semple, J. L. & Woodhouse, K. A. Decellularized placental matrices for adipose tissue engineering. *J. Biomed. Mater. Res. - Part A* **79**, 359–369 (2006).

239. Flynn, L., Prestwich, G. D., Semple, J. L. & Woodhouse, K. a. Adipose tissue engineering with naturally derived scaffolds and adipose-derived stem cells. *Biomaterials* **28**, 3834–42 (2007).

240. Gude, N. M., Roberts, C. T., Kalionis, B. & King, R. G. Growth and function of the normal human placenta. *Thromb. Res.* **114**, 397–407 (2004).

241. Altman, A. M. *et al.* Human adipose-derived stem cells adhere to acellular dermal matrix. *Aesthetic Plast. Surg.* **32**, 698–699 (2008).

242. Wolf, M. T. *et al.* A hydrogel derived from decellularized dermal extracellular matrix. *Biomaterials* **33**, 7028–7038 (2012).

243. Altman, A. M. *et al.* Dermal matrix as a carrier for in vivo delivery of human adipose-derived stem cells. *Biomaterials* **29**, 1431–1442 (2008).

244. Ting, A. C. H. *et al.* The adipogenic potential of various extracellular matrices under the influence of an angiogenic growth factor combination in a mouse tissue engineering chamber. *Acta Biomater.* **10**, 1907–1918 (2014).

245. Young, D. A., Choi, Y. S., Engler, A. J. & Christman, K. L. Stimulation of adipogenesis of adult adipose-derived stem cells using substrates that mimic the stiffness of adipose tissue. *Biomaterials* **34**, 8581–8588 (2013).

246. Haddad, S. M. H., Omidi, E., Flynn, L. E. & Samani, A. Comparative biomechanical study of using decellularized human adipose tissues for post-mastectomy and post-lumpectomy breast reconstruction. *J. Mech. Behav. Biomed.*

Mater. **57**, 235–245 (2016).

247. Omidi, E. *et al.* Characterization and assessment of hyperelastic and elastic properties of decellularized human adipose tissues. *J. Biomech.* **47**, 3657–3663 (2014).

248. Lago, F., Gómez, R., Gómez-Reino, J. J., Dieguez, C. & Gualillo, O. Adipokines as novel modulators of lipid metabolism. *Trends Biochem. Sci.* **34**, 500–510 (2009).

249. Pasarica, M. *et al.* Adipose tissue collagen VI in obesity. *J. Clin. Endocrinol. Metab.* **94**, 5155–5162 (2009).

250. Martinez-Santibañez, G. & Nien-Kai Lumeng, C. Macrophages and the Regulation of Adipose Tissue Remodeling. *Annu. Rev. Nutr.* **34**, 57–76 (2014).

251. Chun, T.-H. Peri-adipocyte ECM remodeling in obesity and adipose tissue fibrosis. *Adipocyte* **1**, 89–95 (2012).

252. Sun, K., Tordjman, J., Clément, K. & Scherer, P. E. Fibrosis and Adipose Tissue Dysfunction. *Cell Metab.* **18**, 470–477 (2013).

253. Flynn, L. E. The use of decellularized adipose tissue to provide an inductive microenvironment for the adipogenic differentiation of human adipose-derived stem cells. *Biomaterials* **31**, 4715–24 (2010).

254. Turner, A. E. B. & Flynn, L. E. Design and characterization of tissue-specific extracellular matrix-derived microcarriers. *Tissue Eng. - Part C Methods* **18**, 186–197 (2012).

255. Cheung, H. K. *et al.* Composite hydrogel scaffolds incorporating decellularized adipose tissue for soft tissue engineering with adipose-derived stem cells. *Biomaterials* **35**, 1914–1923 (2014).

256. Kuljanin, M., Brown, C. F. C., Raleigh, M. J., Lajoie, G. A. & Flynn, L. E.

Collagenase treatment enhances proteomic coverage of low-abundance proteins in decellularized matrix bioscaffolds. *Biomaterials* **144**, 130–143 (2017).

257. Yu, C., Kornmuller, A., Brown, C., Hoare, T. & Flynn, L. E. Decellularized adipose tissue microcarriers as a dynamic culture platform for human adipose-derived stem/stromal cell expansion. *Biomaterials* **120**, 66–80 (2017).

258. Wang, L., Johnson, J. A., Zhang, Q. & Beahm, E. K. Combining decellularized human adipose tissue extracellular matrix and adipose-derived stem cells for adipose tissue engineering. *Acta Biomater.* **9**, 8921–8931 (2013).

259. Young, D. ., Bajaj, V. & Christman, K. L. Award winner for outstanding research in the PhD category, 2014 society for biomaterials annual meeting and exposition, denver, colorado, april 16-19, 2014: Decellularized adipose matrix hydrogels stimulate in vivo neovascularization and adipose formation. *J. Biomed. Mater. Res. Part A* **102**, 1641–1651 (2014).

260. Brown, C. F. C. *et al.* Effect of decellularized adipose tissue particle size and cell density on adipose-derived stem cell proliferation and adipogenic differentiation in composite methacrylated chondroitin sulphate hydrogels. *Biomed. Mater.* **10**, 045010 (2015).

261. Baer, P. C. *et al.* Effect of different preconditioning regimens on the expression profile of murine adipose-derived stromal/stem cells. *Int. J. Mol. Sci.* **19**, (2018).

262. Herrmann, J. L. *et al.* Preconditioning mesenchymal stem cells with transforming growth factor-alpha improves mesenchymal stem cell-mediated cardioprotection. *Shock* **33**, 24–30 (2010).

263. Bader, A. M. *et al.* Hypoxic preconditioning increases survival and pro-Angiogenic capacity of human cord blood mesenchymal stromal cells in vitro. *PLoS One* **10**, (2015).

264. Shafiq, M., Jung, Y. & Kim, S. H. Insight on stem cell preconditioning and instructive biomaterials to enhance cell adhesion, retention, and engraftment for

tissue repair. *Biomaterials* **90**, 85–115 (2016).

265. Liu, L. *et al.* Hypoxia preconditioned human adipose derived mesenchymal stem cells enhance angiogenic potential via secretion of increased VEGF and bFGF. *Cell Biol. Int.* **37**, 551–560 (2013).

266. Zhang, W., Liu, L., Huo, Y., Yang, Y. & Wang, Y. Hypoxia-Pretreated Human MSCs Attenuate Acute Kidney Injury through Enhanced Angiogenic and Antioxidative Capacities. *Biomed Res. Int.* **2014**, (2014).

267. Ferreira, J. R. *et al.* Mesenchymal Stromal Cell Secretome: Influencing Therapeutic Potential by Cellular Pre-conditioning. *Front. Immunol.* **9**, 2837 (2018).

268. Lu, Z. *et al.* Activation and promotion of adipose stem cells by tumour necrosis factor-alpha preconditioning for bone regeneration. *J. Cell. Physiol.* **228**, 1737–1744 (2013).

269. Kong, P., Xie, X., Li, F., Liu, Y. & Lu, Y. Placenta mesenchymal stem cell accelerates wound healing by enhancing angiogenesis in diabetic Goto-Kakizaki (GK) rats. *Biochem. Biophys. Res. Commun.* **438**, 410–419 (2013).

270. Zimna, A. & Kurpisz, M. Hypoxia-Inducible Factor-1 in Physiological and Pathophysiological Angiogenesis: Applications and Therapies. *Biomed Res. Int.* **2015**, 1–13 (2015).

271. Abdollahi, H. *et al.* The role of hypoxia in stem cell differentiation and therapeutics. *J. Surg. Res.* **165**, 112–117 (2011).

272. J. A. Hudson and D. B. Cater. An analysis of factors affecting tissue oxygen tension. *Proc. R. Soc. London. Ser. B. Biol. Sci.* **161**, 247–274 (1964).

273. Hodson, L. Adipose tissue oxygenation. *Adipocyte* **3**, 75–80 (2014).

274. Pasarica, M. *et al.* Reduced adipose tissue oxygenation in human obesity. *Diabetes*

58, 718–725 (2009).

275. Ivan, M. *et al.* HIFα targeted for VHL-mediated destruction by proline hydroxylation: Implications for O2 sensing. *Science* **292**, 464–468 (2001).

276. Jaakkola, P. *et al.* Targeting of HIF-α to the von Hippel-Lindau ubiquitylation complex by O 2 -regulated prolyl hydroxylation. *Science* **292**, 468–472 (2001).

277. Ratcliffe, P. J., O'Rourke, J. F., Maxwell, P. H. & Pugh, C. W. Oxygen sensing, hypoxia-inducible factor-1 and the regulation of mammalian gene expression. *J. Exp. Biol.* **201**, 1153–1162 (1998).

278. Kanichai, M., Ferguson, D., Prendergast, P. J. & Campbell, V. A. Hypoxia promotes chondrogenesis in rat mesenchymal stem cells: A role for AKT and hypoxia-inducible factor (HIF)-1α. *J. Cell. Physiol.* **216**, 708–715 (2008).

279. Yun, S. P., Lee, M. Y., Ryu, J. M., Song, C. H. & Han, H. J. Role of HIF-1α and VEGF in human mesenchymal stem cell proliferation by 17β-estradiol: Involvement of PKC, PI3K/Akt, and MAPKs. *Am. J. Physiol. - Cell Physiol.* **296**, 317–326 (2009).

280. Berniakovich, I. & Giorgio, M. Low oxygen tension maintains multipotency, whereas normoxia increases differentiation of mouse bone marrow stromal cells. *Int. J. Mol. Sci.* **14**, 2119–2134 (2013).

281. Choi, J. R. *et al.* Impact of low oxygen tension on stemness, proliferation and differentiation potential of human adipose-derived stem cells. *Biochem. Biophys. Res. Commun.* **448**, 218–224 (2014).

282. Kakudo, N., Morimoto, N., Ogawa, T., Taketani, S. & Kusumoto, K. Hypoxia Enhances Proliferation of Human Adipose-Derived Stem Cells via HIF-1α Activation. *PLoS One* **10**, e0139890 (2015).

283. Chen, L. *et al.* Conditioned medium from hypoxic bone marrow-derived mesenchymal stem cells enhances wound healing in mice. *PLoS One* **9**, (2014).

284. Liu, J. *et al.* Hypoxia Pretreatment of Bone Marrow Mesenchymal Stem Cells Facilitates Angiogenesis by Improving the Function of Endothelial Cells in Diabetic Rats with Lower Ischemia. *PLoS One* **10**, e0126715 (2015).

285. Gnecchi, M. *et al.* Evidence supporting paracrine hypothesis for Akt-modified mesenchymal stem cell-mediated cardiac protection and functional improvement. *FASEB J.* **20**, 661–669 (2006).

286. Mojsilovic-Petrovic, J. *et al.* Hypoxia-inducible factor-1 (HIF-1) is involved in the regulation of hypoxia-stimulated expression of monocyte chemoattractant protein-1 (MCP-1/CCL2) and MCP-5 (Ccl12) in astrocytes. *J. Neuroinflammation* **4**, 1–15 (2007).

287. Stubbs, S. L. *et al.* Hypoxic Preconditioning Enhances Survival of Human Adipose-Derived Stem Cells and Conditions Endothelial Cells In Vitro. *Stem Cells Dev.* **21**, 1887–1896 (2012).

288. Hollenbeck, S. T. *et al.* Tissue engraftment of hypoxic-preconditioned adipose-derived stem cells improves flap viability. *Wound Repair Regen.* **20**, 872–878 (2012).

289. Bassaneze, V. *et al.* Shear stress induces nitric oxide-mediated vascular endothelial growth factor production in Human adipose tissue mesenchymal stem cells. *Stem Cells Dev.* **19**, 371–378 (2010).

290. Yuan, L., Sakamoto, N., Song, G. & Sato, M. High-level shear stress stimulates endothelial differentiation and VEGF secretion by human mesenchymal stem cells. *Cell. Mol. Bioeng.* **6**, 220–229 (2013).

291. Becquart, P. *et al.* Human mesenchymal stem cell responses to hydrostatic pressure and shear stress. *Eur. Cells Mater.* **31**, 160–173 (2016).

292. Stolberg, S. & McCloskey, K. E. Can shear stress direct stem cell fate? *Biotechnol. Prog.* **25**, 10–19 (2009).

293. Dalby, M. J. Topographically induced direct cell mechanotransduction. *Med. Eng. Phys.* **27**, 730–742 (2005).

294. Katsumi, A., Orr, A. W., Tzima, E. & Schwartz, M. A. Integrins in Mechanotransduction. *J. Biol. Chem.* **279**, 12001–12004 (2004).

295. Yeatts, A. B., Choquette, D. T. & Fisher, J. P. Bioreactors to influence stem cell fate: Augmentation of mesenchymal stem cell signaling pathways via dynamic culture systems. *Biochim. Biophys. Acta - Gen. Subj.* **1830**, 2470–2480 (2013).

296. Yuan, L., Sakamoto, N., Song, G. & Sato, M. Migration of human mesenchymal stem cells under low shear stress mediated by mitogen-activated protein kinase signaling. *Stem Cells Dev.* **21**, 2520–2530 (2012).

297. Scott, B. B. *et al.* TNF-α modulates angiopoietin-1 expression in rheumatoid synovial fibroblasts via the NF-κB signalling pathway. *Biochem. Biophys. Res. Commun.* **328**, 409–414 (2005).

298. Sunters, A. *et al.* Paclitaxel-induced nuclear translocation of FOXO3a in breast cancer cells is mediated by c-Jun NH2-terminal kinase and Akt. *Cancer Res.* **66**, 212–220 (2006).

299. McIlhenny, S. E. *et al.* Linear shear conditioning improves vascular graft retention of adipose-derived stem cells by upregulation of the α5β 1 integrin. *Tissue Eng. - Part A* **16**, 245–255 (2010).

300. Martin, I., Wendt, D. & Heberer, M. The role of bioreactors in tissue engineering. *Trends Biotechnol.* **22**, 80–86 (2004).

301. Lin, C. Y., Huang, C. H., Wu, Y. K., Cheng, N. C. & Yu, J. Maintenance of human adipose derived stem cell (hASC) differentiation capabilities using a 3D culture. *Biotechnol. Lett.* **36**, 1529–1537 (2014).

302. Kassem, M., Mygind, T., Bjerre, L. & Bu, C. E. Biomaterials Flow perfusion culture of human mesenchymal stem cells on silicate-substituted tricalcium

phosphate scaffolds. **29**, 2616–2627 (2008).

303. Nieponice, A. *et al.* In Vivo assessment of a tissue-engineered vascular graft combining a biodegradable elastomeric scaffold and muscle-derived stem cells in a rat model. *Tissue Eng. - Part A* **16**, 1215–1223 (2010).

304. Vunjak-Novakovic, G., Freed, L. E., Biron, R. J. & Langer, R. Effects of Mixing on the Composition and Morphology of Tissue-Engineered Cartilage. *AIChE J.* **42**, 850–860 (1996).

305. Dos Santos, F. *et al.* A xenogeneic-free bioreactor system for the clinical-scale expansion of human mesenchymal stem/stromal cells. *Biotechnol. Bioeng.* **111**, 1116–1127 (2014).

306. Bunpetch, V. *et al.* Strategies for MSC expansion and MSC-based microtissue for bone regeneration. *Biomaterials* **196**, 67–79 (2019).

307. Skardal, A., Sarker, S. F., Crabbé, A., Nickerson, C. A. & Prestwich, G. D. The generation of 3-D tissue models based on hyaluronan hydrogel-coated microcarriers within a rotating wall vessel bioreactor. *Biomaterials* **31**, 8426–8435 (2010).

308. Zhang, Z. Y. *et al.* A comparison of bioreactors for culture of fetal mesenchymal stem cells for bone tissue engineering. *Biomaterials* **31**, 8684–8695 (2010).

309. Nishi, M., Matsumoto, R., Dong, J. & Uemura, T. Engineered bone tissue associated with vascularization utilizing a rotating wall vessel bioreactor. *J. Biomed. Mater. Res. - Part A* **101 A**, 421–427 (2013).

310. Chen, X., Xu, H., Wan, C., McCaigue, M. & Li, G. Bioreactor Expansion of Human Adult Bone Marrow-Derived Mesenchymal Stem Cells. *Stem Cells* **24**, 2052–2059 (2006).

311. Grayson, W. L. *et al.* Optimizing the medium perfusion rate in bone tissue engineering bioreactors. *Biotechnol. Bioeng.* **108**, 1159–1170 (2011).

312. Papadimitropoulos, A. *et al.* Expansion of Human Mesenchymal Stromal Cells from Fresh Bone Marrow in a 3D Scaffold-Based System under Direct Perfusion. *PLoS One* **9**, e102359 (2014).

313. Alvarez-Barreto, J. F. *et al.* Enhanced osteoblastic differentiation of mesenchymal stem cells seeded in RGD-functionalized PLLA scaffolds and cultured in a flow perfusion bioreactor. *J. Tissue Eng. Regen. Med.* **5**, 464–475 (2011).

314. Ouyang, A. & Yang, S. T. A two-stage perfusion fibrous bed bioreactor system for mass production of embryonic stem cells. *Expert Opin. Biol. Ther.* **8**, 895–909 (2008).

315. Alvarez-Barreto, J. F., Linehan, S. M., Shambaugh, R. L. & Sikavitsas, V. I. Flow perfusion improves seeding of tissue engineering scaffolds with different architectures. *Ann. Biomed. Eng.* **35**, 429–442 (2007).

316. Sailon, A. M. *et al.* A Novel Flow-Perfusion Bioreactor Supports 3D Dynamic Cell Culture. *J. Biomed. Biotechnol.* **2009**, 1–7 (2009).

317. Xie, Y. *et al.* Three-dimensional flow perfusion culture system for stem cell proliferation inside the critical-size beta-tricalcium phosphate scaffold. *Tissue Eng.* **12**, 3535–3543 (2006).

318. Zhao, F. *et al.* Effects of Oxygen Transport on 3-D Human Mesenchymal Stem Cell Metabolic Activity in Perfusion and Static Cultures: Experiments and Mathematical Model. *Biotechnol. Prog.* **21**, 1269–1280 (2008).

319. Kim, J. & Ma, T. Perfusion regulation of hMSC microenvironment and osteogenic differentiation in 3D scaffold. *Biotechnol. Bioeng.* **109**, 252–261 (2012).

320. Gomes, M. E., Sikavitsas, V. I., Behravesh, E., Reis, R. L. & Mikos, A. G. Effect of flow perfusion on the osteogenic differentiation of bone marrow stromal cells cultured on starch-based three-dimensional scaffolds. *J. Biomed. Mater. Res. - Part A* **67**, 87–95 (2003).

321. Mitra, D., Whitehead, J., Yasui, O. W. & Leach, J. K. Bioreactor culture duration of engineered constructs influences bone formation by mesenchymal stem cells. *Biomaterials* **146**, 29–39 (2017).

322. Bjerre, L., Bünger, C. E., Kassem, M. & Mygind, T. Flow perfusion culture of human mesenchymal stem cells on silicate-substituted tricalcium phosphate scaffolds. *Biomaterials* **29**, 2616–2627 (2008).

323. Xie, L. *et al.* In vitro mesenchymal trilineage differentiation and extracellular matrix production by adipose and bone marrow derived adult equine multipotent stromal cells on a collagen scaffold. *Stem Cell Rev. Reports* **9**, 858–872 (2013).

324. Weyand, B. *et al.* A Differential Pressure Laminar Flow Reactor Supports Osteogenic Differentiation and Extracellular Matrix Formation from Adipose Mesenchymal Stem Cells in a Macroporous Ceramic Scaffold. *Biores. Open Access* **1**, 145–156 (2012).

325. Zhao, F. & Ma, T. Perfusion bioreactor system for human mesenchymal stem cell tissue engineering: Dynamic cell seeding and construct development. *Biotechnol. Bioeng.* **91**, 482–493 (2005).

326. Moser, C. *et al.* A Perfusion Culture System for Assessing Bone Marrow Stromal Cell Differentiation on PLGA Scaffolds for Bone Repair. *Front. Bioeng. Biotechnol.* **6**, (2018).

327. Gerlach, J. C. *et al.* Adipogenesis of human adipose-derived stem cells within three-dimensional hollow fiber-based bioreactors. *Tissue Eng. - Part C Methods* **18**, 54–61 (2012).

328. Laschke, M. W. *et al.* Angiogenesis in tissue engineering: Breathing life into constructed tissue substitutes. *Tissue Eng.* **12**, 2093–2104 (2006).

329. Madeddu, P. Therapeutic angiogenesis and vasculogenesis for tissue regeneration. *Exp. Physiol.* **90**, 315–326 (2005).

330. Li, W. W., Talcott, K. E., Zhai, A. W., Kruger, E. A. & Li, V. W. The role of therapeutic angiogenesis in tissue repair and regeneration. *Adv. Skin Wound Care* **18**, 491–500 (2005).

331. Betz, C., Lenard, A., Belting, H. G. & Affolter, M. Cell behaviors and dynamics during angiogenesis. *Dev.* **143**, 2249–2260 (2016).

332. Gerhardt, H. *et al.* VEGF guides angiogenic sprouting utilizing endothelial tip cell filopodia. *J. Cell Biol.* **161**, 1163–1177 (2003).

333. Logsdon, E. A., Finley, S. D., Popel, A. S. & MacGabhann, F. A systems biology view of blood vessel growth and remodelling. *J. Cell. Mol. Med.* **18**, 1491–1508 (2014).

334. Fantin, A. *et al.* Tissue macrophages act as cellular chaperones for vascular anastomosis downstream of VEGF-mediated endothelial tip cell induction. *Blood* **116**, 829–840 (2010).

335. Ausprunk, D. H. & Folkman, J. Migration and proliferation of endothelial cells in preformed and newly formed blood vessels during tumor angiogenesis. *Microvasc. Res.* **14**, 53–65 (1977).

336. Wacker, A. & Gerhardt, H. Endothelial development taking shape. *Curr. Opin. Cell Biol.* **23**, 676–685 (2011).

337. Ribatti, D. The discovery of the fundamental role of VEGF in the development of the vascular system. *Mech. Dev.* **160**, 103579 (2019).

338. Brudno, Y., Ennett-Shepard, A. B., Chen, R. R., Aizenberg, M. & Mooney, D. J. Enhancing microvascular formation and vessel maturation through temporal control over multiple pro-angiogenic and pro-maturation factors. *Biomaterials* **34**, 9201–9209 (2013).

339. Chen, W. *et al.* The endothelial tip-stalk cell selection and shuffling during angiogenesis. *J. Cell Commun. Signal.* **13**, 291–301 (2019).

340. Gebala, V., Collins, R., Geudens, I., Phng, L. K. & Gerhardt, H. Blood flow drives lumen formation by inverse membrane blebbing during angiogenesis in vivo. *Nat. Cell Biol.* **18**, 443–450 (2016).

341. Lenard, A. *et al.* In vivo analysis reveals a highly stereotypic morphogenetic pathway of vascular anastomosis. *Dev. Cell* **25**, 492–506 (2013).

342. Wakui, S. *et al.* Localization of Ang-1, -2, Tie-2, and VEGF expression at endothelial-pericyte interdigitation in rat angiogenesis. *Lab. Investig.* **86**, 1172–1184 (2006).

343. Vujasinovic, T., Buta, M., Markicevic, M. & Nikolic-Vukosavljevic, D. Angiogenesis: bFGF and VEGF in breast carcinoma. *Arch. Oncol.* **14**, 126–130 (2006).

344. Stratman, A. N., Schwindt, A. E., Malotte, K. M. & Davis, G. E. Endothelial-derived PDGF-BB and HB-EGF coordinately regulate pericyte recruitment during vasculogenic tube assembly and stabilization. *Blood* **116**, 4720–4730 (2010).

345. Guo, P. *et al.* Platelet-derived growth factor-B enhances glioma angiogenesis by stimulating vascular endothelial growth factor expression in tumor endothelia and by promoting pericyte recruitment. *Am. J. Pathol.* **162**, 1083–1093 (2003).

346. Raza, A., Franklin, M. J. & Dudek, A. Z. Pericytes and vessel maturation during tumor angiogenesis and metastasis. *Am. J. Hematol.* **85**, 593–598 (2010).

347. Erber, R. *et al.* Combined inhibition of VEGF and PDGF signaling enforces tumor vessel regression by interfering with pericyte-mediated endothelial cell survival mechanisms. *FASEB J.* **18**, 338–340 (2004).

348. Sounni, N. E., Paye, A., Host, L. & Noël, A. MT-MMPS as Regulators of Vessel Stability Associated with Angiogenesis. *Front. Pharmacol.* **2**, 1–11 (2011).

349. Saunders, W. B. *et al.* Coregulation of vascular tube stabilization by endothelial cell TIMP-2 and pericyte TIMP-3. *J. Cell Biol.* **175**, 179–191 (2006).

350. Peiser, L., Mukhopadhyay, S. & Gordon, S. Scavenger receptors in innate immunity. *Curr. Opin. Immunol.* **14**, 123–128 (2002).

351. Spiller, K. L. *et al.* The role of macrophage phenotype in vascularization of tissue engineering scaffolds. *Biomaterials* **35**, 4477–4488 (2014).

352. Badylak, S. F., Valentin, J. E., Ravindra, A. K., McCabe, G. P. & Stewart-Akers, A. M. Macrophage phenotype as a determinant of biologic scaffold remodeling. *Tissue Eng. Part A* **14**, 1835–1842 (2008).

353. Spiller, K. L., Freytes, D. O. & Vunjak-Novakovic, G. Macrophages Modulate Engineered Human Tissues for Enhanced Vascularization and Healing. *Ann. Biomed. Eng.* **43**, 616–627 (2015).

354. Martinez, F. O., Sica, A., Mantovani, A. & Locati, M. Macrophage activation and polarization. *Front. Biosci.* **13**, 453–61 (2008).

355. Murray, P. J. *et al.* Macrophage Activation and Polarization: Nomenclature and Experimental Guidelines. *Immunity* **41**, 14–20 (2014).

356. Hirano, R. *et al.* Human thymic stromal lymphopoietin enhances expression of CD80 in human CD14 + monocytes/macrophages. *Inflamm. Res.* **60**, 605–610 (2011).

357. Rutkowski, R. *et al.* CD80 and CD86 Expression on LPS-Stimulated Monocytes and the Effect of CD80 and CD86 Blockade on IL-4 and IFN-γ Production in Nonatopic Bronchial Asthma. *Arch. Immunol. Ther. Exp. (Warsz).* **51**, 421–428 (2003).

358. Buechler, C. *et al.* Regulation of scavenger receptor CD163 expression in human monocytes and macrophages by pro- and antiinflammatory stimuli. *J. Leukoc. Biol.* **67**, 97–103 (2000).

359. Das, A. *et al.* Monocyte and Macrophage Plasticity in Tissue Repair and Regeneration. *Am. J. Pathol.* **185**, 2596–2606 (2015).

360. Zhang, M. Z. *et al.* CSF-1 signaling mediates recovery from acute kidney injury. *J. Clin. Invest.* **122**, 4519–4532 (2012).

361. Reefman, E. *et al.* Cytokine Secretion Is Distinct from Secretion of Cytotoxic Granules in NK Cells. *J. Immunol.* **184**, 4852–4862 (2010).

362. Wynn, T. A. & Vannella, K. M. Macrophages in Tissue Repair, Regeneration, and Fibrosis. *Immunity* **44**, 450–462 (2016).

363. Lukacs, N. W., Strieter, R. M., Chensue, S. W., Widmer, M. & Kunkel, S. L. TNF-alpha mediates recruitment of neutrophils and eosinophils during airway inflammation. *J. Immunol.* **154**, 5411–7 (1995).

364. Novak, M. L. & Koh, T. J. Phenotypic transitions of macrophages orchestrate tissue repair. *Am. J. Pathol.* **183**, 1352–1363 (2013).

365. Arras, M. *et al.* Monocyte activation in angiogenesis and collateral growth in the rabbit hindlimb. *J. Clin. Invest.* **101**, 40–50 (1998).

366. Dal-Secco, D. *et al.* A dynamic spectrum of monocytes arising from the in situ reprogramming of CCR2+ monocytes at a site of sterile injury. *J. Exp. Med.* **212**, 447–456 (2015).

367. Pradere, J. P. *et al.* Hepatic macrophages but not dendritic cells contribute to liver fibrosis by promoting the survival of activated hepatic stellate cells in mice. *Hepatology* **58**, 1461–1473 (2013).

368. Pellicoro, A. *et al.* Elastin accumulation is regulated at the level of degradation by macrophage metalloelastase (MMP-12) during experimental liver fibrosis. *Hepatology* **55**, 1965–1975 (2012).

369. Sica, A. & Mantovani, A. Macrophage plasticity and polarization: in vivo veritas. *J. Clin. Invest.* **122**, 787–795 (2012).

370. Salans, L. B., Cushman, S. W. & Weismann, R. E. Studies of human adipose

tissue. Adipose cell size and number in nonobese and obese patients. *J. Clin. Invest.* **52**, 929–941 (1973).

371. Spiegelman, B. M. & Flier, J. S. Obesity and the regulation of energy balance. *Cell* **104**, 531–543 (2001).

372. Arner, E. *et al.* Adipocyte Turnover : Relevance to Human Adipose Tissue. *Diabetes* **59**, 105–109 (2010).

373. Jeffery, E. *et al.* The Adipose Tissue Microenvironment Regulates Depot-Specific Adipogenesis in Obesity. *Cell Metab.* **24**, 142–150 (2016).

374. Rodeheffer, M. S., Birsoy, K. & Friedman, J. M. Identification of White Adipocyte Progenitor Cells In Vivo. *Cell* **135**, 240–249 (2008).

375. Shook, B. A. *et al.* Myofibroblast proliferation and heterogeneity are supported by macrophages during skin repair. *Science* **362**, (2018).

376. Shenaq, S. M. & Yuksel, E. New research in breast reconstruction: Adipose tissue engineering. *Clin. Plast. Surg.* **29**, 111–125 (2002).

377. Šmahel, J. Experimental implantation of adipose tissue fragments. *Br. J. Plast. Surg.* **42**, 207–211 (1989).

378. Gomillion, C. T. & Burg, K. J. L. Stem cells and adipose tissue engineering. *Biomaterials* **27**, 6052–6063 (2006).

379. Zhao, J., Hu, L., Liu, J., Gong, N. & Chen, L. The effects of cytokines in adipose stem cell-conditioned medium on the migration and proliferation of skin fibroblasts in vitro. *Biomed Res. Int.* **2013**, (2013).

380. Pathi, P., Ma, T. & Locke, B. R. Role of nutrient supply on cell growth in bioreactor design for tissue engineering of hematopoietic cells. *Biotechnol. Bioeng.* **89**, 743–758 (2005).

381. Gomes, M. E., Bossano, C. M., Johnston, C. M., Reis, R. L. & Mikos, A. G. In

vitro localization of bone growth factors in constructs of biodegradable scaffolds seeded with marrow stromal cells and cultured in a flow perfusion bioreactor. *Tissue Eng.* **12**, 177–188 (2006).

382. Oswald, J. *et al.* Mesenchymal Stem Cells Can Be Differentiated Into Endothelial Cells In Vitro. *Stem Cells* **22**, 377–384 (2004).

383. Lee, E. Y. *et al.* Hypoxia-enhanced wound-healing function of adipose-derived stem cells: Increase in stem cell proliferation and up-regulation of VEGF and bFGF. *Wound Repair Regen.* **17**, 540–547 (2009).

384. Allard, J. *et al.* Immunohistochemical toolkit for tracking and quantifying xenotransplanted human stem cells. *Regen. Med.* **9**, 437–452 (2014).

385. Shridhar, A. *et al.* Culture on Tissue-Specific Coatings Derived from α-Amylase-Digested Decellularized Adipose Tissue Enhances the Proliferation and Adipogenic Differentiation of Human Adipose-Derived Stromal Cells. *Biotechnol. J.* **15**, 1900118 (2020).

386. Wendt, D., Marsano, A., Jakob, M., Heberer, M. & Martin, I. Oscillating perfusion of cell suspensions through three-dimensional scaffolds enhances cell seeding efficiency and uniformity. *Biotechnol. Bioeng.* **84**, 205–214 (2003).

387. Grayson, W. L. *et al.* Effects of initial seeding density and fluid perfusion rate on formation of tissue-engineered bone. *Tissue Eng. - Part A.* **14**, 1809–1820 (2008).

388. Hewitt, C. J. *et al.* Expansion of human mesenchymal stem cells on microcarriers. *Biotechnol. Lett.* **33**, 2325–2335 (2011).

389. Teixeira, G. Q., Barrias, C. C., Lourenço, A. H. & Gonçalves, R. M. A multicompartment holder for spinner flasks improves expansion and osteogenic differentiation of mesenchymal stem cells in three-dimensional scaffolds. *Tissue Eng. - Part C Methods* **20**, 984–993 (2014).

390. Zhu, Y. *et al.* Ex vivo expansion of adipose tissue-derived stem cells in spinner

flasks. *Biotechnol. J.* **4**, 1198–1209 (2009).

391. Gadelorge, M. *et al.* Clinical-scale expansion of adipose-derived stromal cells starting from stromal vascular fraction in a single-use bioreactor: proof of concept for autologous applications. *J. Tissue Eng. Regen. Med.* **12**, 129–141 (2018).

392. Carmelo, J. G., Fernandes-Platzgummer, A., Diogo, M. M., da Silva, C. L. & Cabral, J. M. S. A xeno-free microcarrier-based stirred culture system for the scalable expansion of human mesenchymal stem/stromal cells isolated from bone marrow and adipose tissue. *Biotechnol. J.* **10**, 1235–1247 (2015).

393. Banfi, A. *et al.* Proliferation kinetics and differentiation potential of ex vivo expanded human bone marrow stromal cells. *Exp. Hematol.* **28**, 707–715 (2000).

394. Haskett, D. G. *et al.* An exploratory study on the preparation and evaluation of a "same-day" adipose stem cell–based tissue-engineered vascular graft. *J. Thorac. Cardiovasc. Surg.* **156**, 1814-1822.e3 (2018).

395. Haykal, S. *et al.* Double-chamber rotating bioreactor for dynamic perfusion cell seeding of large-segment tracheal allografts: Comparison to conventional static methods. *Tissue Eng. - Part C Methods* **20**, 681–692 (2014).

396. Frohlich, M., Cells, S., Culture, B., Gimble, J. M. & Ph, D. Bone Grafts Engineered from Human Adipose-Derived. *Tissue Eng. Part A* **16**, 179–189 (2010).

397. Bieback, K. *et al.* Altered gene expression in human adipose stem cells cultured with fetal bovine serum compared to human supplements. *Tissue Eng. - Part A* **16**, 3467–3484 (2010).

398. Lindroos, B. *et al.* Differential gene expression in adipose stem cells cultured in allogeneic human serum versus fetal bovine serum. *Tissue Eng. - Part A* **16**, 2281–2294 (2010).

399. Ciria, M. *et al.* Mesenchymal Stem Cell Migration and Proliferation Are Mediated

by Hypoxia-Inducible Factor-1α Upstream of Notch and SUMO Pathways. *Stem Cells Dev.* **26**, 973–985 (2017).

400. Pugh, C. W. & Ratcliffe, P. J. Regulation of angiogenesis by hypoxia: role of the HIF system. *Nat. Med.* **9**, 677–684 (2003).

401. Dong, Z., Peng, Z., Chang, Q. & Lu, F. The survival condition and immunoregulatory function of adipose stromal vascular fraction (SVF) in the early stage of nonvascularized adipose transplantation. *PLoS One* **8**, 1–11 (2013).

402. Noguchi, M. *et al.* In vitro characterization and engraftment of adipocytes derived from human induced pluripotent stem cells and embryonic stem cells. *Stem Cells Dev.* **22**, 2895–2905 (2013).

403. Torio-Padron, N., Baerlecken, N., Momeni, A., Stark, G. B. & Borges, J. Engineering of adipose tissue by injection of human preadipocytes in fibrin. *Aesthetic Plast. Surg.* **31**, 285–293 (2007).

404. Al-Khaldi, A. *et al.* Postnatal bone marrow stromal cells elicit a potent VEGF-dependent neoangiogenic response in vivo. *Gene Ther.* **10**, 621–629 (2003).

405. Nishimura, S. *et al.* Adipogenesis in Obesity Requires Close Interplay Between Differentiating Adipocytes, Stromal Cells, and Blood Vessels. *Diabetes* **56**, 1517–1526 (2007).

406. Fukumura, D. *et al.* Paracrine Regulation of Angiogenesis and Adipocyte Differentiation During In Vivo Adipogenesis. *Circ. Res.* **93**, e88–e97 (2003).

407. Parisi-Amon, A., Mulyasasmita, W., Chung, C. & Heilshorn, S. C. Protein-Engineered Injectable Hydrogel to Improve Retention of Transplanted Adipose-Derived Stem Cells. *Adv. Healthc. Mater.* **2**, 428–432 (2013).

408. Cai, L., Dewi, R. E. & Heilshorn, S. C. Injectable hydrogels with in situ double network formation enhance retention of transplanted stem cells. *Adv. Funct. Mater.* **25**, 1344–1351 (2015).

409. Brett, E. *et al.* A review of cell-based strategies for soft tissue reconstruction. *Tissue Eng. - Part B Rev.* **23**, 336–346 (2017).

410. Choi, J. S. *et al.* Fabrication of porous extracellular matrix scaffolds from human adipose tissue. *Tissue Eng. Part C. Methods* **16**, 387–396 (2010).

411. Suga, H. *et al.* Adipose tissue remodeling under ischemia: Death of adipocytes and activation of stem/ progenitor cells. *Plast. Reconstr. Surg.* **126**, 1911–1923 (2010).

412. Pizzute, T., Lynch, K. & Pei, M. Impact of Tissue-Specific Stem Cells on Lineage-Specific Differentiation: A Focus on the Musculoskeletal System. *Stem Cell Rev. Reports* **11**, 119–132 (2015).

413. Han, T. T. Y. & Flynn, L. E. Perfusion bioreactor culture of adipose-derived stromal cells on decellularized adipose tissue scaffolds enhances in vivo regeneration. *bioRxiv* 2020.04.10.036194 (2020) doi:10.1101/2020.04.10.036194.

414. Prichard, H. L., Reichert, W. & Klitzman, B. IFATS Collection: Adipose-Derived Stromal Cells Improve the Foreign Body Response. *Stem Cells* **26**, 2691–2695 (2008).

415. Li, W. *et al.* Mesenchymal stem cells: A double-edged sword in regulating immune responses. *Cell Death Differ.* **19**, 1505–1513 (2012).

416. Merrick, D. *et al.* Identification of a mesenchymal progenitor cell hierarchy in adipose tissue. *Science* **364**, eaav2501 (2019).

417. Mitchell, J. B. *et al.* Immunophenotype of human adipose-derived cells: temporal changes in stromal-associated and stem cell-associated markers. *Stem Cells* **24**, 376–385 (2006).

418. Scheubel, R. J. *et al.* Paracrine effects of CD34 progenitor cells on angiogenic endothelial sprouting. *Int. J. Cardiol.* **139**, 134–141 (2010).

419. Li, H. *et al.* Adipogenic potential of adipose stem cell subpopulations. *Plast.*

Reconstr. Surg. **128**, 663–672 (2011).

420. Wang, Y. *et al.* Relative contributions of adipose-resident CD146+ pericytes and CD34+ adventitial progenitor cells in bone tissue engineering. *npj Regen. Med.* **4**, (2019).

421. Yang, Z. & Ming, X. F. Functions of arginase isoforms in macrophage inflammatory responses: Impact on cardiovascular diseases and metabolic disorders. *Front. Immunol.* **5**, 1–10 (2014).

422. Santhanam, L. *et al.* Inducible NO synthase-dependent S-nitrosylation and activation of arginase1 contribute to age-related endothelial dysfunction. *Circ. Res.* **101**, 692–702 (2007).

423. Bravo, B. *et al.* Opposite Effects of Mechanical Action of Fluid Flow on Proangiogenic Factor Secretion From Human Adipose-Derived Stem Cells With and Without Oxidative Stress. *J. Cell. Physiol.* **232**, 2158–2167 (2017).

424. Passerini, A. G., Milsted, A. & Rittgers, S. E. Shear stress magnitude and directionality modulate growth factor gene expression in preconditioned vascular endothelial cells. *J. Vasc. Surg.* **37**, 182–190 (2003).

425. Gan, L. M., Miocic, M., Doroudi, R., Selin-Sjoögren, L. & Jern, S. Distinct regulation of vascular endothelial growth factor in intact human conduit vessels exposed to laminar fluid shear stress and pressure. *Biochem. Biophys. Res. Commun.* **272**, 490–496 (2000).

426. Harris, D. P., Bandyopadhyay, S., Maxwell, T. J., Willard, B. & DiCorleto, P. E. Tumor necrosis factor (TNF)-α induction of CXCL10 in endothelial cells requires protein arginine methyltransferase 5 (PRMT5)-mediated nuclear factor (NF)-κB p65 Methylation. *J. Biol. Chem.* **289**, 15328–15339 (2014).

427. Hardaker, E. L. *et al.* Regulation of TNF-α and IFN-γ induced CXCL10 expression: participation of the airway smooth muscle in the pulmonary inflammatory response in chronic obstructive pulmonary disease. *FASEB J.* **18**,

191–193 (2004).

428. Kamimoto, M., Mizuno, S. & Nakamura, T. Reciprocal regulation of IL-6 and IL-10 balance by HGF via recruitment of heme oxygenase-1 in macrophages for attenuation of liver injury in a mouse model of endotoxemia. *Int. J. Mol. Med.* **24**, 837–43 (2009).

429. Boehler, R. M. *et al.* Lentivirus delivery of IL-10 to promote and sustain macrophage polarization towards an anti-inflammatory phenotype. *Biotechnol. Bioeng.* **111**, 1210–1221 (2014).

430. Peranteau, W. H. *et al.* IL-10 overexpression decreases inflammatory mediators and promotes regenerative healing in an adult model of scar formation. *J. Invest. Dermatol.* **128**, 1852–1860 (2008).

431. Petrovic-Djergovic, D. *et al.* CXCL10 induces the recruitment of monocyte-derived macrophages into kidney, which aggravate puromycin aminonucleoside nephrosis. *Clin. Exp. Immunol.* **180**, 305–315 (2015).

432. Chen, P.-M. *et al.* Induction of immunomodulatory monocytes by human mesenchymal stem cell-derived hepatocyte growth factor through ERK1/2. *J. Leukoc. Biol.* **96**, 295–303 (2014).

433. Choi, W., Lee, J., Lee, J., Lee, S. H. & Kim, S. Hepatocyte growth factor regulates macrophage transition to the M2 phenotype and promotes murine skeletal muscle regeneration. *Front. Physiol.* **10**, (2019).

434. Maachi, M. *et al.* Systemic low-grade inflammation is related to both circulating and adipose tissue TNFα, leptin and IL-6 levels in obese women. *Int. J. Obes.* **28**, 993–997 (2004).

435. Bulló, M., García-Lorda, P., Megias, I. & Salas-Salvadó, J. Systemic inflammation, adipose tissue tumor necrosis factor, and leptin expression. *Obes. Res.* **11**, 525–531 (2003).

436. Kwon, Y. W. *et al.* Tumor necrosis factor-α-activated mesenchymal stem cells promote endothelial progenitor cell homing and angiogenesis. *Biochim. Biophys. Acta - Mol. Basis Dis.* **1832**, 2136–2144 (2013).

437. McKenney, J. K., Weiss, S. W. & Folpe, A. L. CD31 expression in intratumoral macrophages: A potential diagnostic pitfall. *Am. J. Surg. Pathol.* **25**, 1167–1173 (2001).

438. Mah, W. *et al.* Elevated CD26 Expression by Skin Fibroblasts Distinguishes a Profibrotic Phenotype Involved in Scar Formation Compared to Gingival Fibroblasts. *Am. J. Pathol.* **187**, 1717–1735 (2017).

439. Gliddon, D. R. & Howard, C. J. CD26 is expressed on a restricted subpopulation of dendritic cells in vivo. *Eur. J. Immunol.* **32**, 1472–1481 (2002).

440. Zhong, J. *et al.* A potential role for dendritic cell/macrophage-expressing DPP4 in obesity-induced visceral inflammation. *Diabetes* **62**, 149–157 (2013).

441. Mantovani, A., Gray, P. A., Van Damme, J. & Sozzani, S. Macrophage-derived chemokine (MDC). *J. Leukoc. Biol.* **68**, 400–4 (2000).

442. Lilja, H. E. *et al.* An adipoinductive role of inflammation in adipose tissue engineering: key factors in the early development of engineered soft tissues. *Stem Cells Dev.* **22**, 1602–13 (2013).

443. Debels, H. *et al.* Macrophages play a key role in angiogenesis and adipogenesis in a mouse tissue engineering model. *Tissue Eng.* **19**, 2615–2625 (2013).

444. Sun, X., Jones, H. P., Dobbs, N., Bodhankar, S. & Simecka, J. W. Dendritic Cells Are the Major Antigen Presenting Cells in Inflammatory Lesions of Murine Mycoplasma Respiratory Disease. *PLoS One* **8**, e55984 (2013).

445. Krzywinska, E. *et al.* CD45 Isoform Profile Identifies Natural Killer (NK) Subsets with Differential Activity. *PLoS One* **11**, e0150434 (2016).

446. Fabriek, B. O., Dijkstra, C. D. & van den Berg, T. K. The macrophage scavenger receptor CD163. *Immunobiology* **210**, 153–160 (2005).

447. Lurier, E. B. *et al.* Transcriptome analysis of IL-10-stimulated (M2c) macrophages by next-generation sequencing. *Immunobiology* **222**, 847–856 (2017).

448. Buechler, C. *et al.* Regulation of scavenger receptor CD163 expression in human monocytes and macrophages by pro- and antiinflammatory stimuli. *J. Leukoc. Biol.* **67**, 97–103 (2000).

449. Storck, K., Fischer, R., Buchberger, M., Haller, B. & Regn, S. Delivered adipose-derived stromal cells improve host-derived adipose tissue formation in composite constructs in vivo. *Laryngoscope* **127**, E428–E436 (2017).

450. Davis, B. M., Loghin, E. R., Conway, K. R. & Zhang, X. Automated Closed-System Expansion of Pluripotent Stem Cell Aggregates in a Rocking-Motion Bioreactor. *SLAS Technol.* **23**, 364–373 (2018).

451. Tsai, A. C., Liu, Y., Yuan, X., Chella, R. & Ma, T. Aggregation kinetics of human mesenchymal stem cells under wave motion. *Biotechnol. J.* **12**, 1–13 (2017).

452. Fortier, G. M., Gauvin, R., Proulx, M., Vallée, M. & Fradette, J. Dynamic culture induces a cell type-dependent response impacting on the thickness of engineered connective tissues. *J. Tissue Eng. Regen. Med.* **7**, 292–301 (2013).

453. Sadeghi, A. *et al.* Large-scale bioreactor expansion of tumor-infiltrating lymphocytes. *J. Immunol. Methods* **364**, 94–100 (2011).

454. Clincke, M. F. *et al.* Very high density of Chinese hamster ovary cells in perfusion by alternating tangential flow or tangential flow filtration in WAVE bioreactor™-part II: Applications for antibody production and cryopreservation. *Biotechnol. Prog.* **29**, 768–777 (2013).

455. Amos, P. J. *et al.* Human Adipose-Derived Stromal Cells Accelerate Diabetic Wound Healing: Impact of Cell Formulation and Delivery. *Tissue Eng. Part A* **16**,

1595–606 (2010).

456. Agrawal, H. *et al.* Human adipose-derived stromal/stem cells demonstrate short-lived persistence after implantation in both an immunocompetent and an immunocompromised murine model. *Stem Cell Res. Ther.* **5**, 142 (2014).

457. Song, Y. H., Shon, S. H., Shan, M., Stroock, A. D. & Fischbach, C. Adipose-derived stem cells increase angiogenesis through matrix metalloproteinase-dependent collagen remodeling. *Integr. Biol. (United Kingdom)* **8**, 205–215 (2016).

458. Pers, Y.-M. *et al.* Adipose Mesenchymal Stromal Cell-Based Therapy for Severe Osteoarthritis of the Knee: A Phase I Dose-Escalation Trial. *Stem Cells Transl. Med.* **5**, 847–856 (2016).

459. Young, S. A., Flynn, L. E. & Amsden, B. G. Adipose-derived stem cells in a resilient in situ forming hydrogel modulate macrophage phenotype. *Tissue Eng. - Part A* **24**, 1784–1797 (2018).

460. Kirouac, D. C. & Zandstra, P. W. The Systematic Production of Cells for Cell Therapies. *Cell Stem Cell* **3**, 369–381 (2008).

461. Robb, K. P., Shridhar, A. & Flynn, L. E. Decellularized Matrices As Cell-Instructive Scaffolds to Guide Tissue-Specific Regeneration. *ACS Biomater. Sci. Eng.* **4**, 3627–3643 (2018).

462. Morissette Martin, P., Grant, A., Hamilton, D. W. & Flynn, L. E. Matrix composition in 3-D collagenous bioscaffolds modulates the survival and angiogenic phenotype of human chronic wound dermal fibroblasts. *Acta Biomater.* **83**, 199–210 (2019).

463. Lin, Y. *et al.* A novel antibody AA98 VH/L directed against CD146 efficiently inhibits angiogenesis. *Anticancer Res.* **27**, 4219–4224 (2007).

464. Baer, P. C. Adipose-derived mesenchymal stromal/stem cells: An update on their

phenotype in vivo and in vitro. *World J. Stem Cells* **6**, 256 (2014).

465. Varma, M. J. O. *et al.* Phenotypical and functional characterization of freshly isolated adipose tissue-derived stem cells. *Stem Cells Dev.* **16**, 91–104 (2007).

466. Malek, A. & Izumo, S. Physiological fluid shear stress causes downregulation of endothelin-1 mRNA in bovine aortic endothelium. *Am. J. Physiol. Physiol.* **263**, C389–C396 (1992).

467. Kim, U. J., Park, J., Joo Kim, H., Wada, M. & Kaplan, D. L. Three-dimensional aqueous-derived biomaterial scaffolds from silk fibroin. *Biomaterials* **26**, 2775–2785 (2005).

468. Rehman, J. *et al.* Secretion of Angiogenic and Antiapoptotic Factors by Human Adipose Stromal Cells. *Circulation* **109**, 1292–1298 (2004).

469. Rehman, J. *et al.* Secretion of Angiogenic and Antiapoptotic Factors by Human Adipose Stromal Cells. *Circulation* **109**, 1292–1298 (2004).

470. Park, I. S., Chung, P. S. & Ahn, J. C. Adipose-derived stem cell spheroid treated with low-level light irradiation accelerates spontaneous angiogenesis in mouse model of hindlimb ischemia. *Cytotherapy* **19**, 1070–1078 (2017).

471. Lopatina, T. *et al.* PDGF enhances the protective effect of adipose stem cell-derived extracellular vesicles in a model of acute hindlimb ischemia. *Sci. Rep.* **8**, 1–12 (2018).

472. Huang, H. *et al.* Preferred M2 Polarization by ASC-Based Hydrogel Accelerated Angiogenesis and Myogenesis in Volumetric Muscle Loss Rats. *Stem Cells Int.* **2017**, 1–13 (2017).

473. Melief, S. M., Geutskens, S. B., Fibbe, W. E. & Roelofs, H. Multipotent stromal cells skew monocytes towards an anti-inflammatory interleukin-10-producing phenotype by production of interleukin-6. *Haematologica* **98**, 888–895 (2013).

474. Razmkhah, M. *et al.* Adipose derived stem cells (ASCs) isolated from breast cancer tissue express IL-4, IL-10 and TGF-β1 and upregulate expression of regulatory molecules on T cells: Do they protect breast cancer cells from the immune response? *Cell. Immunol.* **266**, 116–122 (2011).

475. Anderson, P. *et al.* Adipose-derived mesenchymal stromal cells induce immunomodulatory macrophages which protect from experimental colitis and sepsis. *Gut* **62**, 1131–1141 (2013).

476. Zomer, H. D., Jeremias, T. da S., Ratner, B. & Trentin, A. G. Mesenchymal stromal cells from dermal and adipose tissues induce macrophage polarization to a pro-repair phenotype and improve skin wound healing. *Cytotherapy* **000**, 1–14 (2020).

477. Brown, B. N. *et al.* Macrophage phenotype as a predictor of constructive remodeling following the implantation of biologically derived surgical mesh materials. *Acta Biomater.* **8**, 978–987 (2012).

478. Levesque, M. J., Nerem, R. M. & Sprague, E. A. Vascular endottielial cell proliferation in culture and the influence of flow. *Biomaterials* **11**, 702–707 (1990).

Appendix A: Supplemental Figures and Tables

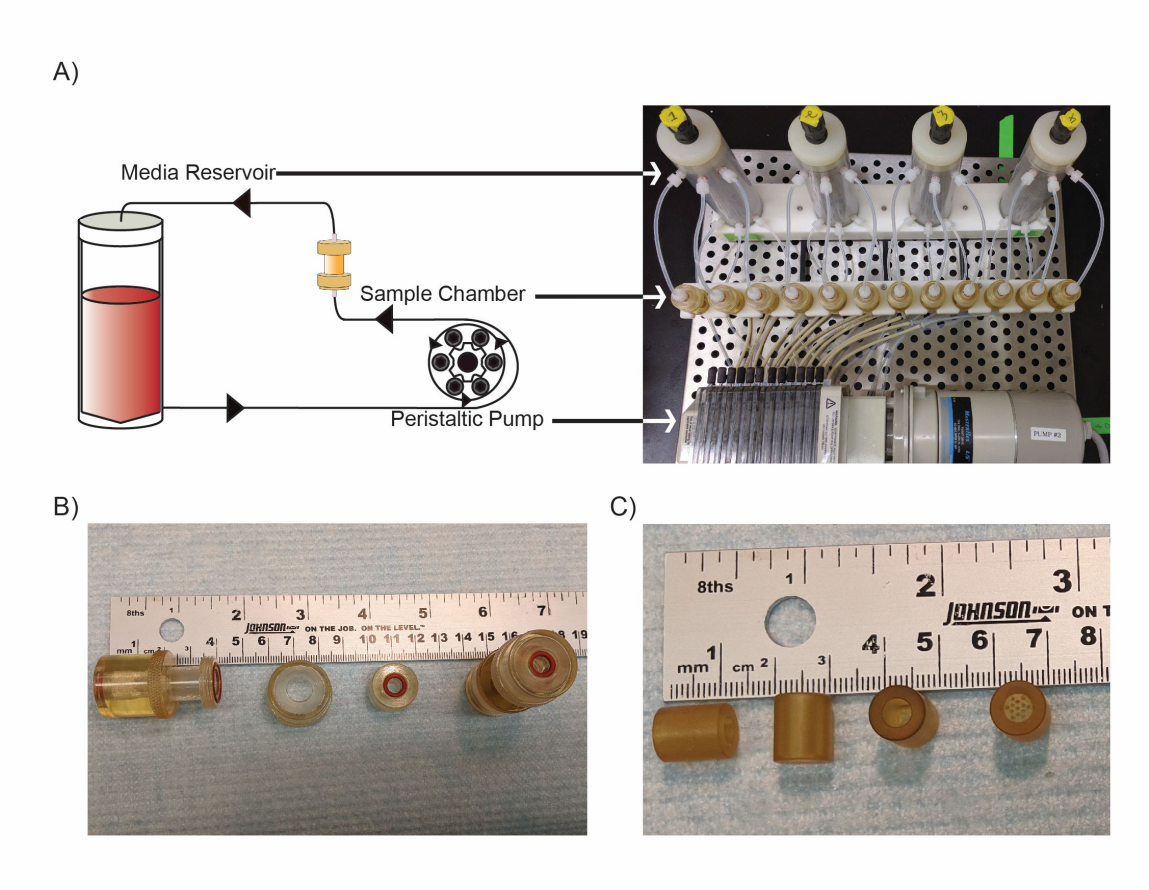

Figure A.1 Schematic of the perfusion bioreactor system. A) Culture media is pumped unidirectionally via the peristaltic pump through the sample chamber before being recycled back into the media reservoir. B-C) The components of the sample chamber (B) and culture inserts (C).

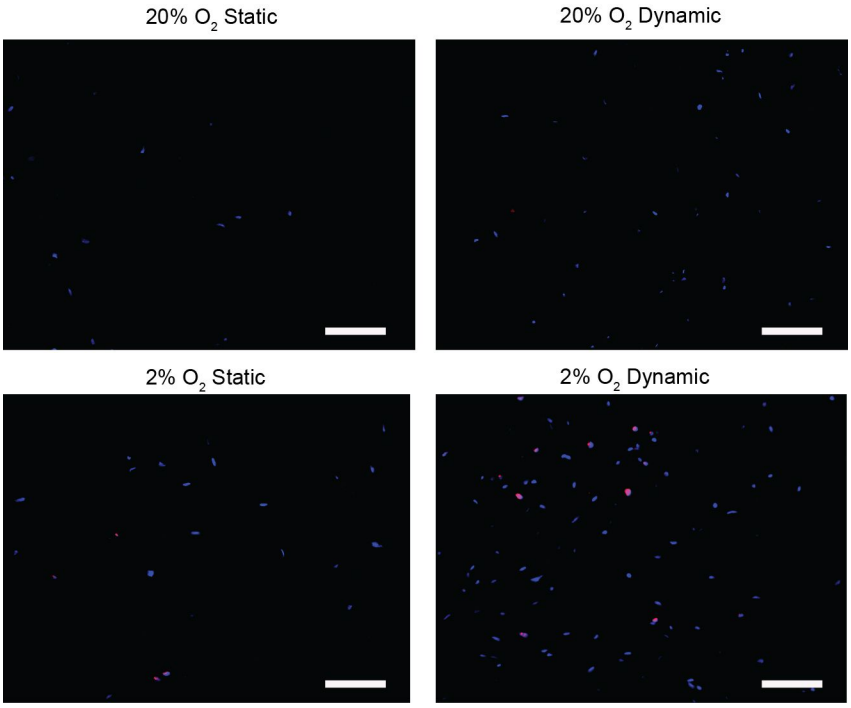

Figure A.2 Representative Ki-67 staining in the central regions of the ASC-seeded DAT scaffolds cultured under static or dynamic conditions within the bioreactor for 14 days. Ki-67 expression is shown in red and DAPI counterstaining in blue. Scale bars represent 100 μm.

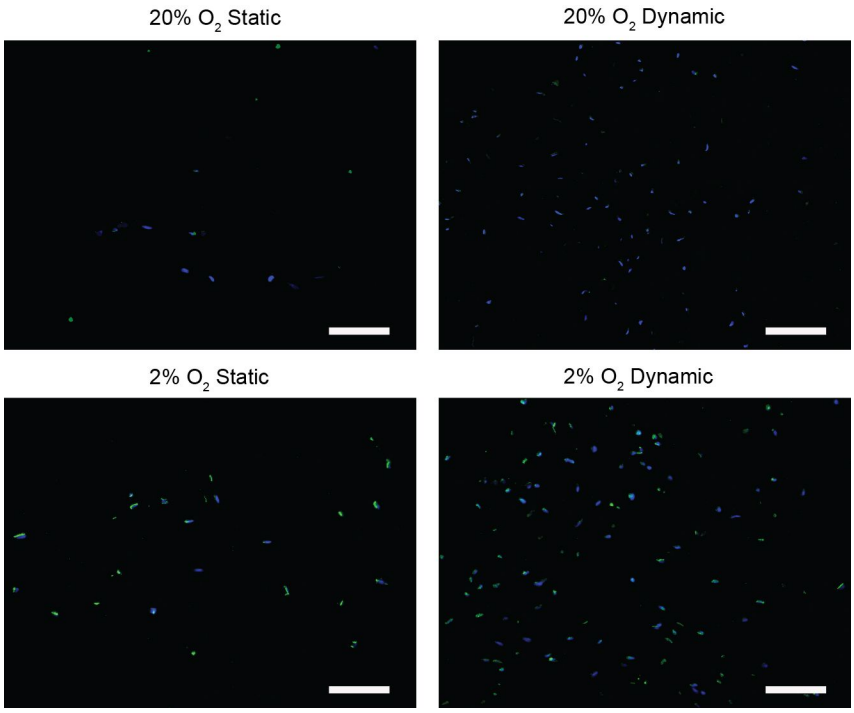

Figure A.3 Representative HIF-1α staining in the central regions of the ASC-seeded DAT scaffolds cultured under static or dynamic conditions within the bioreactor for 14 days. HIF-1α^{+} cells are shown in green and DAPI counterstaining in blue. Scale bars represent 100 μm.

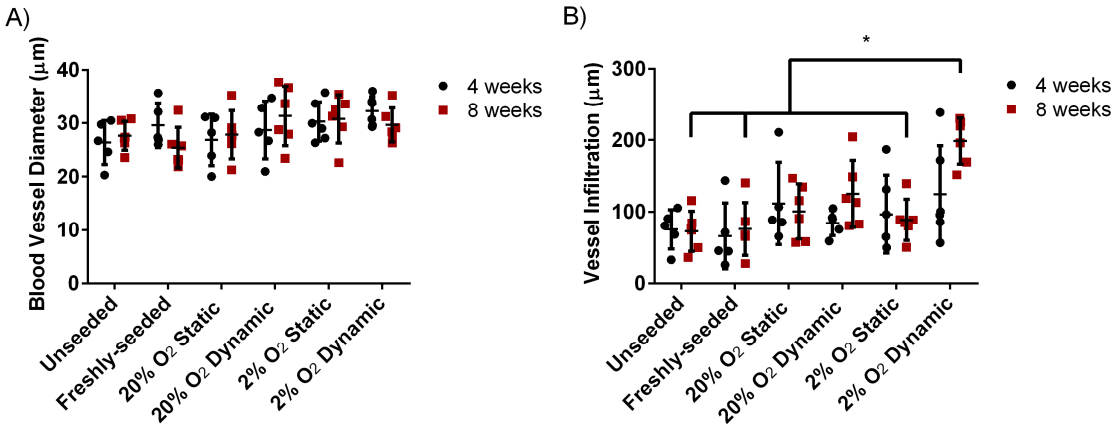

Figure A.4 The average erythrocyte-containing blood vessel A) diameter and B) depth of infiltration in the DAT scaffolds following subcutaneous implantation in the *nu/nu* mouse model for 4 and 8 weeks. Error bars represent standard deviation (n=3 cross-sections/implant, N=6 implants/group). *=significant difference in the 2% O_2 dynamic group as compared to the unseeded, freshly-seeded and 2% O_2 static groups at 8 weeks ($p<0.05$).

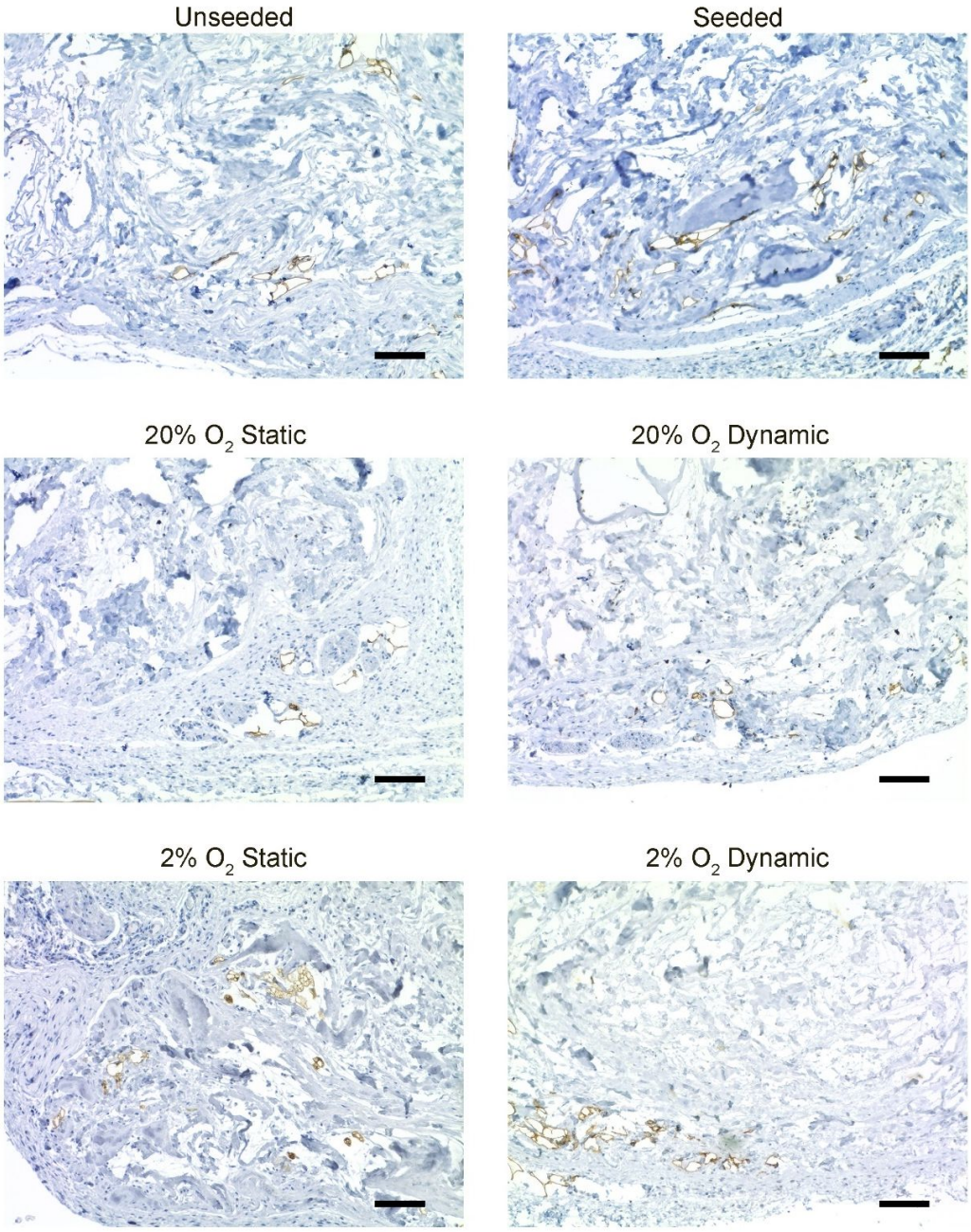

Figure A.5 Representative images showing perilipin staining (brown) in the DAT scaffolds implanted subcutaneously in the *nu/nu* mouse model for 4 weeks. Scale bars represent 100 μm.

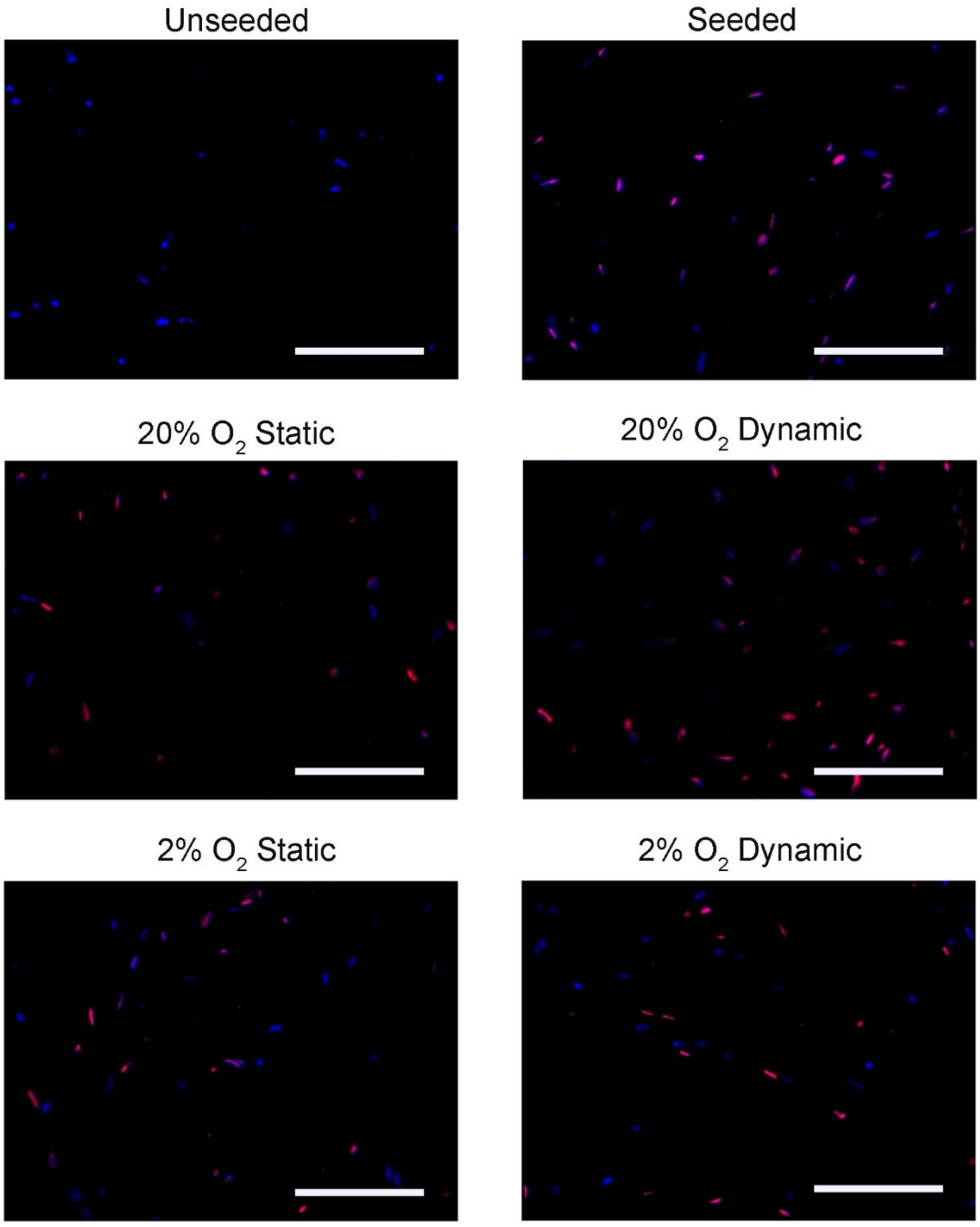

Figure A.6 Representative immunostaining showing Ku80$^+$ (red) human ASCs counterstained with DAPI (blue) in the DAT scaffolds that implanted subcutaneously in the *nu/nu* mouse model for 4 weeks. Scale bars represent 100 μm.

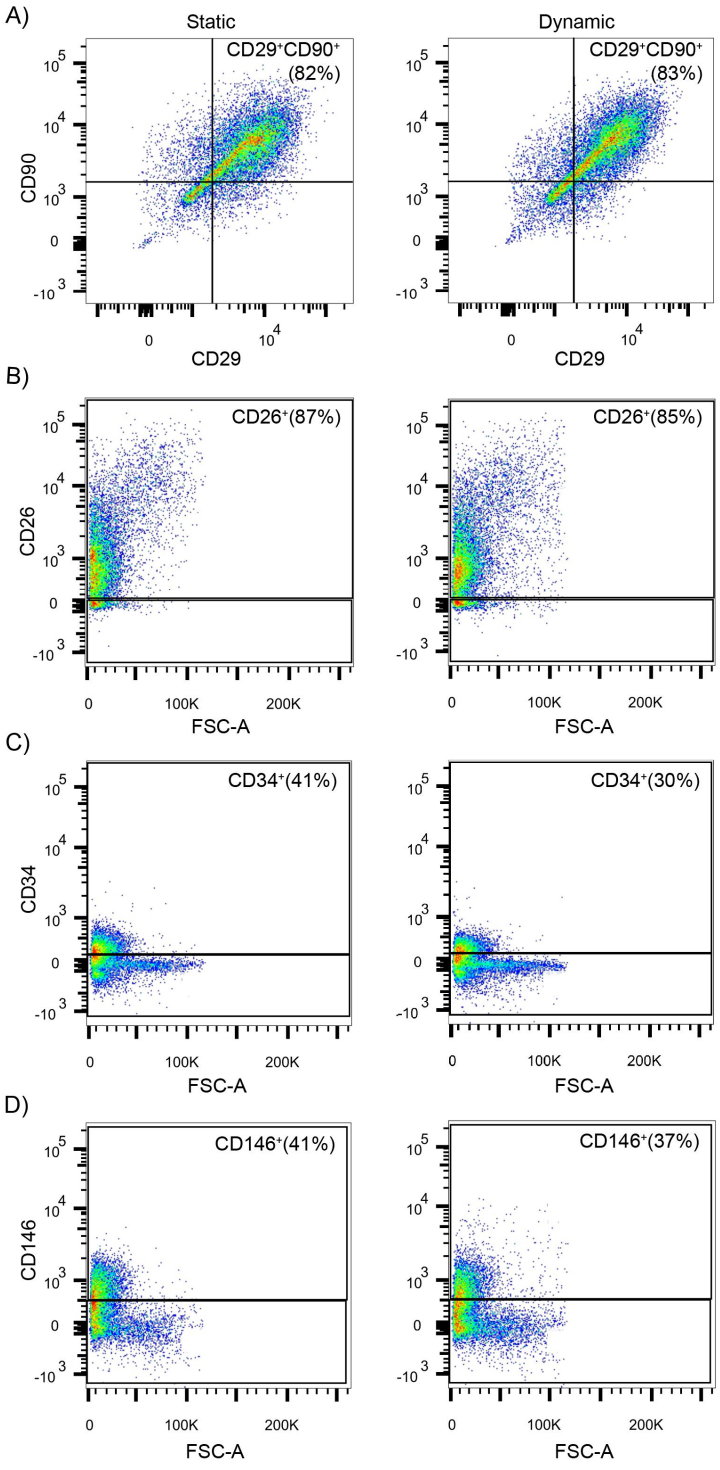

Figure A.7 Representative scatter plots showing that dynamic culture did not significantly alter the immunophenotype of the ASCs on the DAT scaffolds. The ASCs were enzymatically-released from the DAT for flow analysis. A) Representative scatter plots for one ASC donor showing the percentage of $CD90^{+}CD29^{+}$ cells in the calcein violet-$AM^{+}CD31^{-}CD45^{-}$ subset. Representative scatter plots showing the percentage of this population that also expressed B) CD26, C) CD34 or D) CD146.

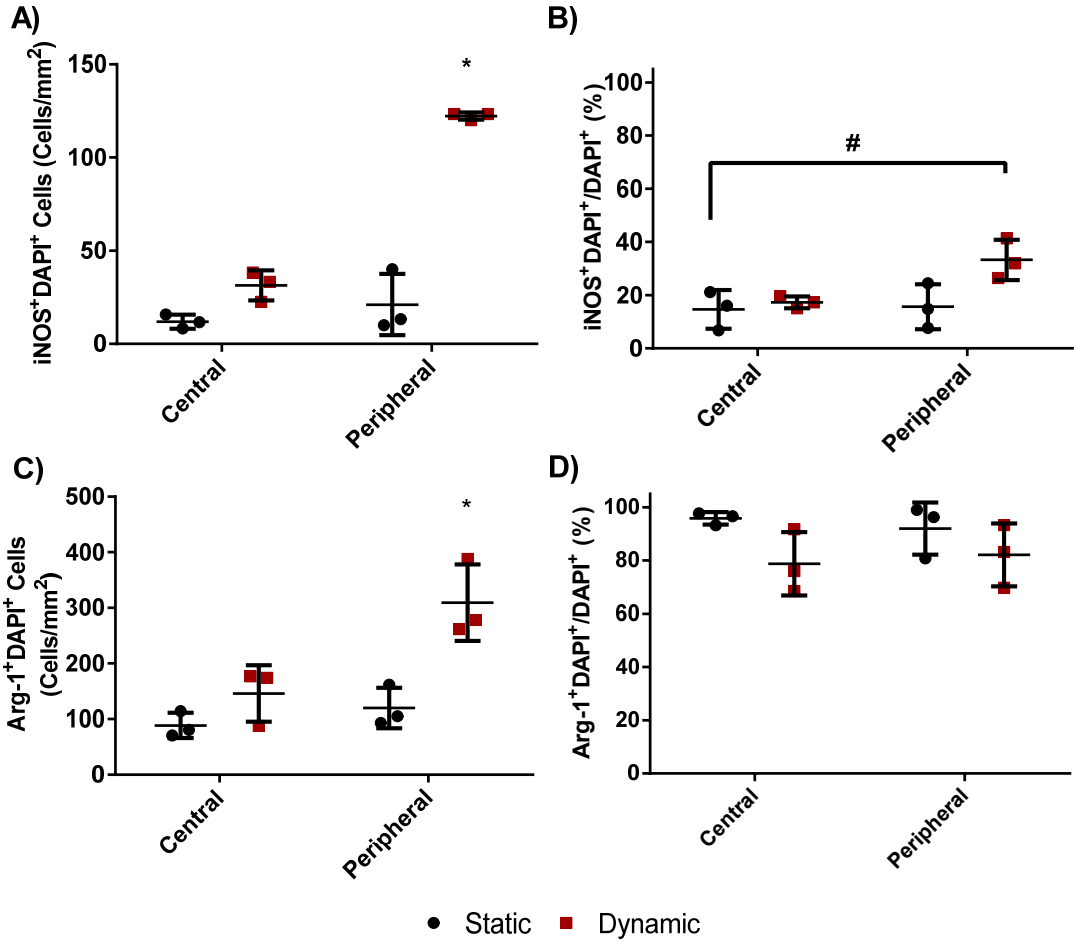

Figure A.8 Analysis of iNOS and Arg-1 expression in the ASC-seeded DAT scaffolds cultured *in vitro* statically or dynamically for 14 days. A) The density of $iNOS^+DAPI^+$ cells and B) $iNOS^+DAPI^+$ cells as a percentage of the total $DAPI^+$ cell population, and C) the density of $Arg\text{-}1^+DAPI^+$ cells and D) $Arg\text{-}1^+DAPI^+$ cells as a percentage of the total $DAPI^+$ cell population in both the central (> 200 µm from scaffold border) and peripheral (< 200 µm from scaffold border) regions of the DAT scaffolds. Error bars represent standard deviation (n=3 cross-sections/scaffold, N=3 trials with different ASC donors). * = significant difference between the peripheral region of the dynamic group and all other groups, # = significant difference between the peripheral region of the dynamic group and the central region of the static group ($p<0.05$).

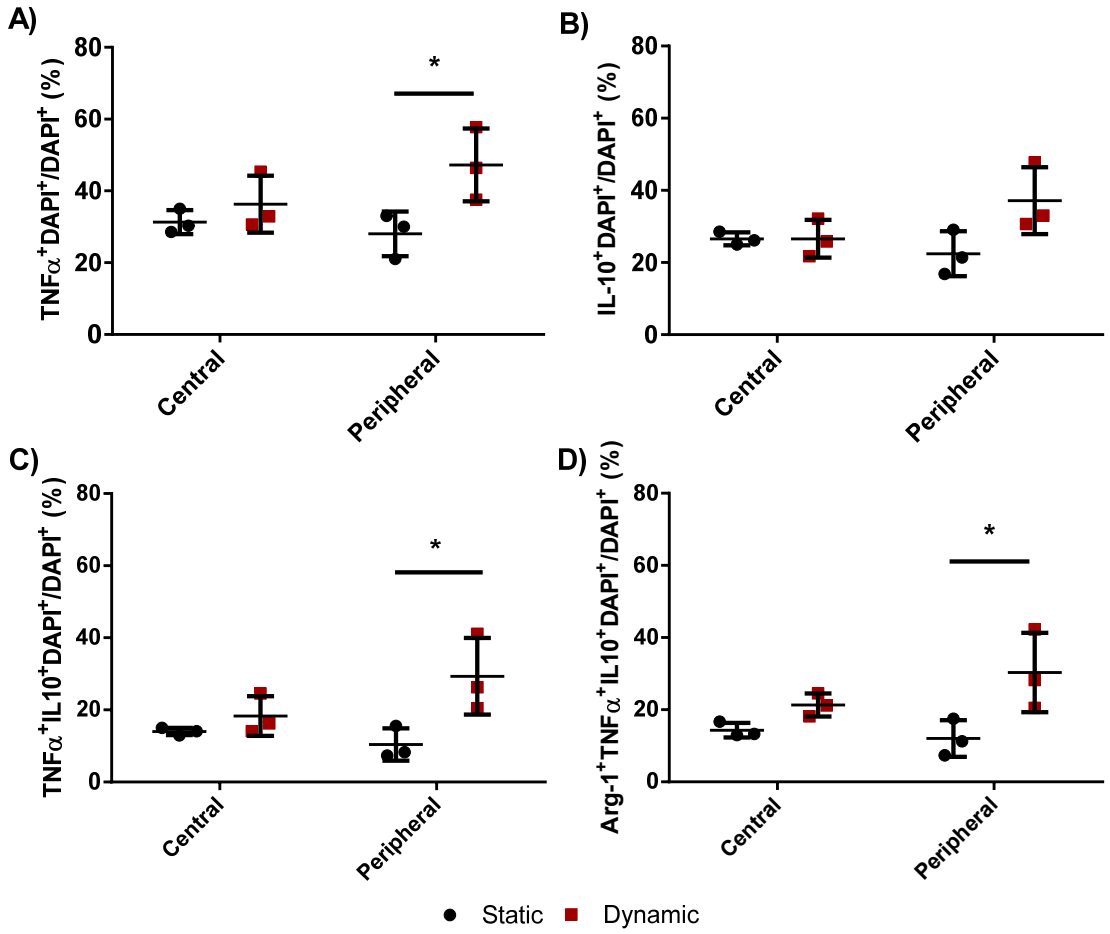

Figure A.9 Analysis of TNF-α and IL-10 expression in the ASCs cultured statically or dynamically on the DAT for 14 days. The percentage of the total $DAPI^+$ human ASC population that was A) TNF-α^+DAPI^+, B) IL-10^+DAPI^+, C) TNF-α^+IL-10^+DAPI^+ and D) Arg-1^+TNF-α^+IL-10^+ $DAPI^+$ in both the central (> 200 µm from scaffold border) and peripheral (< 200 µm from scaffold border) regions of the DAT scaffolds. Error bars represent standard deviation (n=3 cross-sections/scaffold, N=3 trials with different ASC donors). * = significant difference between indicated groups ($p<0.05$).

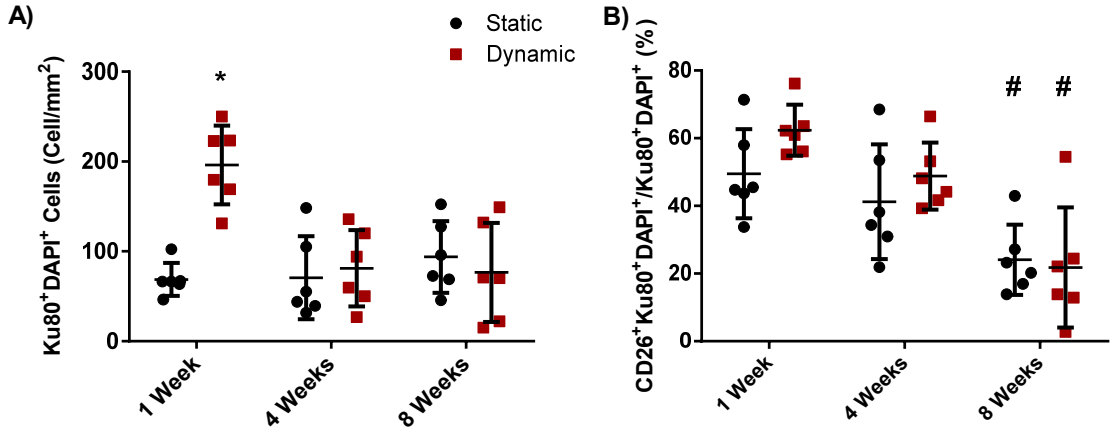

Figure A.10 The A) density of Ku80$^+$DAPI$^+$ human ASCs within the DAT implants and B) the CD26$^+$ human ASCs as a percentage of the total Ku80$^+$DAPI$^+$ human ASC population in the DAT implants at 1, 4 and 8 weeks. Error bars represent standard deviation (n=3 cross-sections/implant, N=6 implants/group). * = significant difference between the dynamic group at 1 week and all other groups, # = significant difference between the indicated group and both the static and dynamic groups at 1 week, as well as the dynamic group at 4 weeks ($p<0.05$).

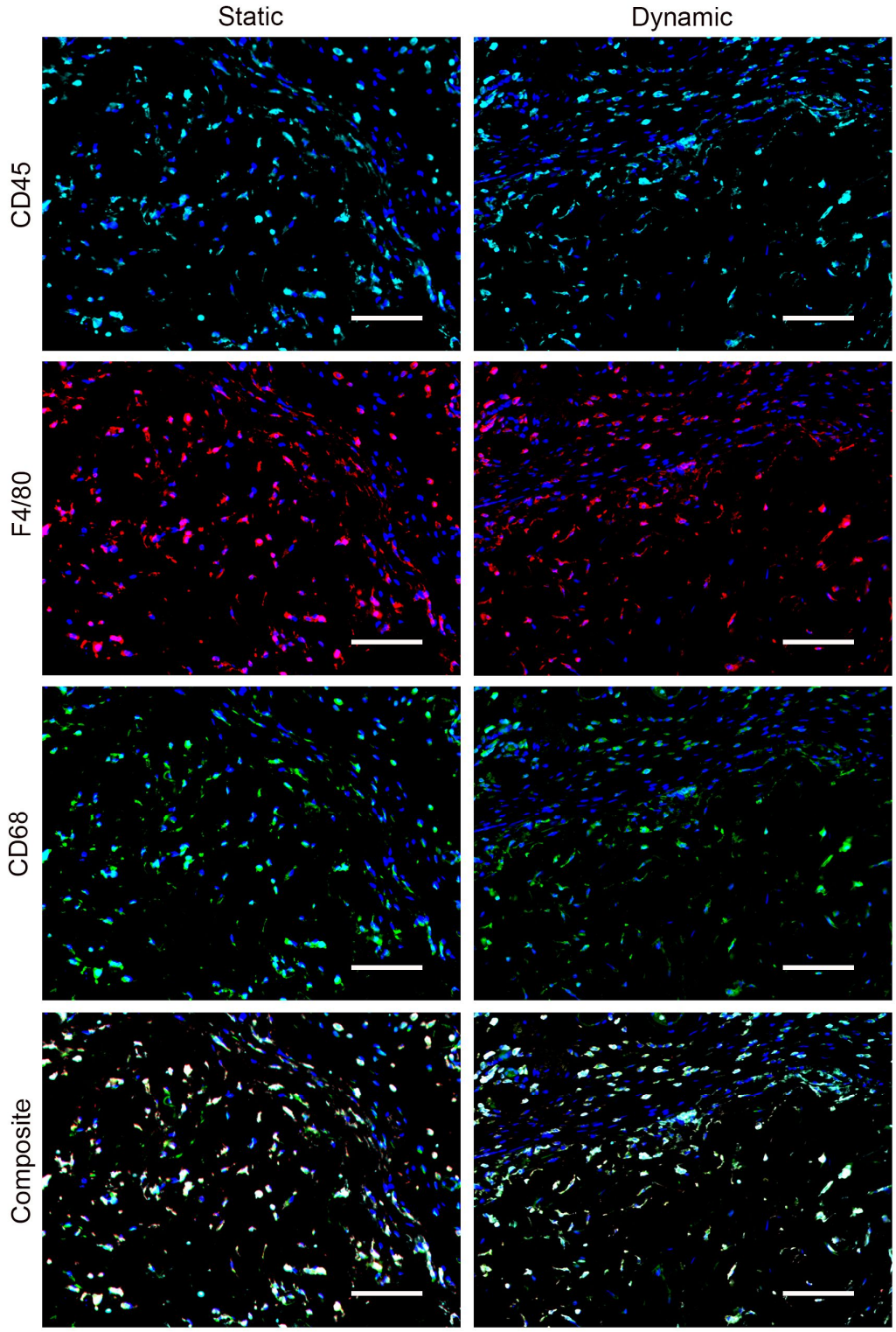

Figure A.11 Representative immunostaining for CD45 (cyan), F4/80 (red) and CD68 (green) with DAPI counterstaining (blue) in the static and dynamic implants at 4 weeks. Scale bars represent 100 μm.

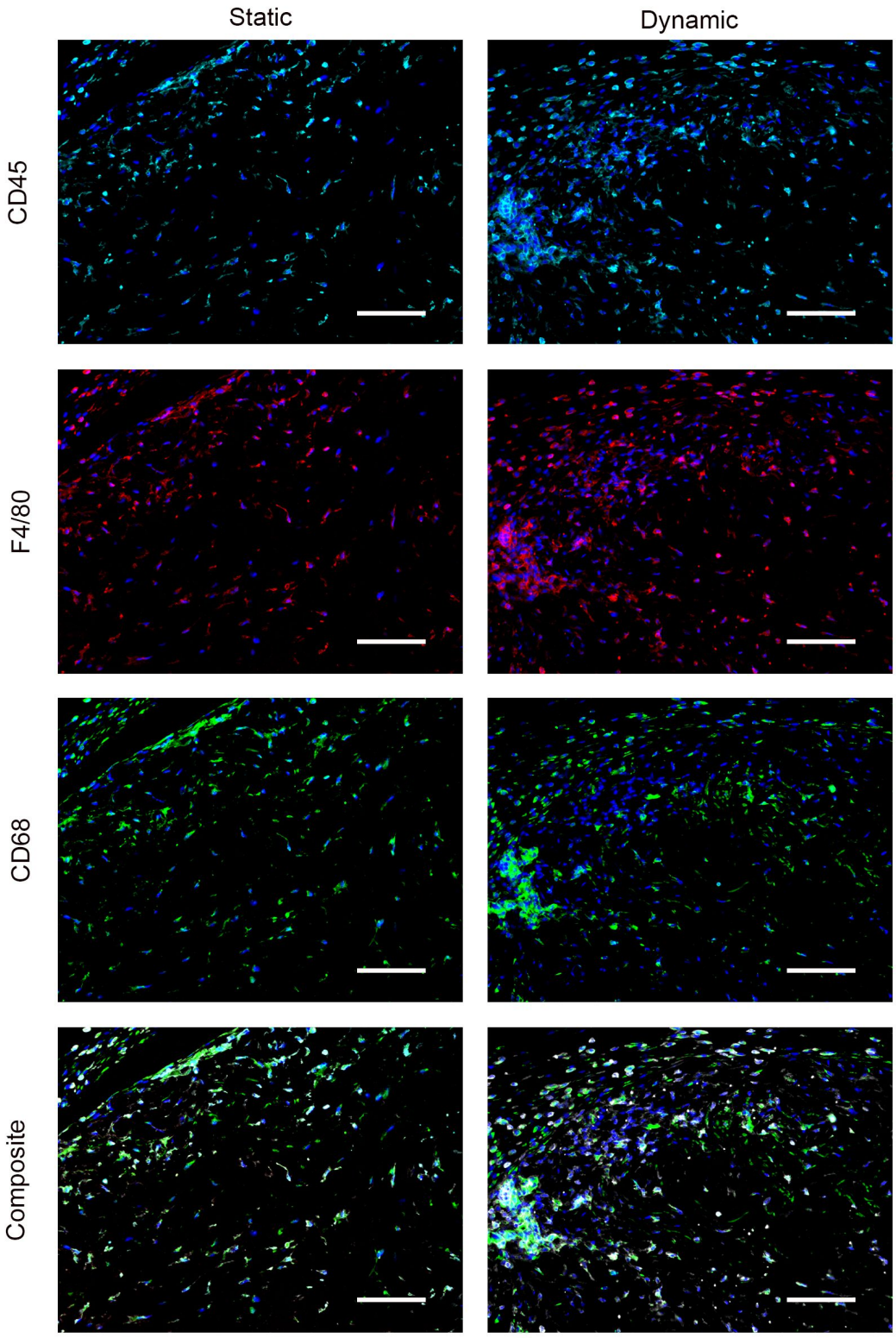

Figure A.12 Representative immunostaining for CD45 (cyan), F4/80 (red) and CD68 (green) with DAPI counterstaining (blue) in the static and dynamic implants at 8 weeks. Scale bars represent 100 μm.

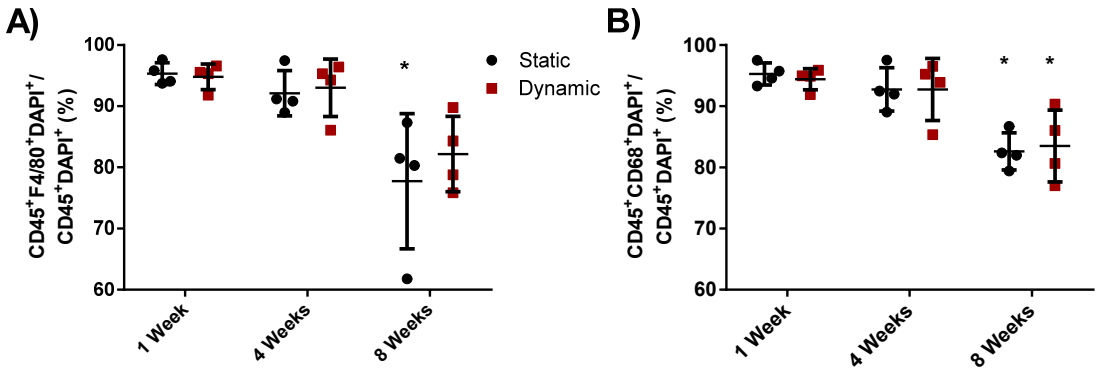

Figure A.13 The percentage of A) $CD45^+F4/80^+DAPI^+$ cells and B) $CD45^+CD68^+DAPI^+$ relative to the total $CD45^+DAPI^+$ cell population in the DAT implants at 1, 4 and 8 weeks. Error bars represent standard deviation (n=3 cross-sections/implant, N=4 implants/group). * = significant difference between the indicated group and both the static and dynamic groups at 1 and 4 weeks ($p<0.05$).

Figure A.14. Images of the rocking bioreactor platform.

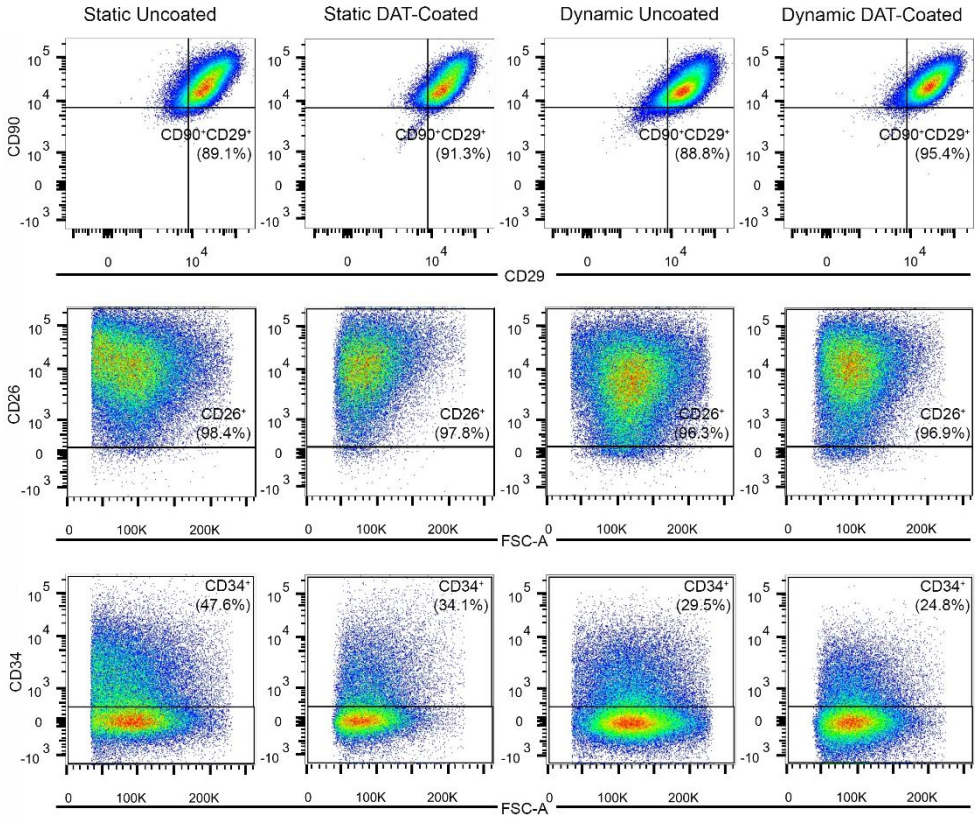

Figure A.15 Representative scatter plots showing the fluorescence intensity of CD90 versus CD29 in the calcein violet^{+}CD31^{-}CD45^{-} cell population, and the fluorescence intensity of CD26 or CD34 versus FSC-A in the viable CD90^{+}CD29^{+} subpopulation following 7 days of culture.

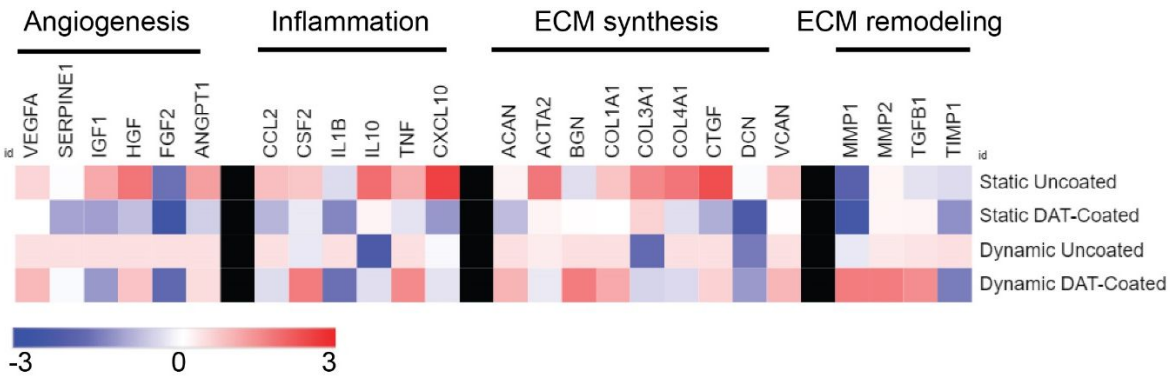

Figure A.16. Heatmap showing the relative expression levels for each gene of interest in the various culture conditions after 7 days of culture. Data shown was normalized against the geometric mean of the housekeeping genes in each respective sample. Genes with low average expression are indicated in blue and high expression in red on a log2 scale.

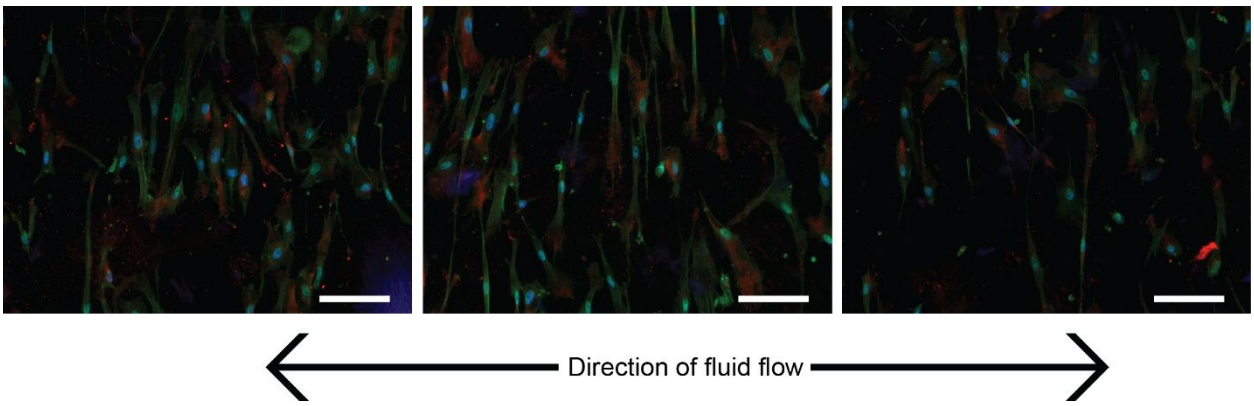

Figure A.17 ASCs appeared to align perpendicular to the direction of the fluid flow in the dynamic DAT-coated group at 7 days. Representative images taken from various regions on the DAT coating showing iNOS (red), F-actin (green) and nuclei (blue). Scale bars represent 100 μm.

Table A.1 A list of genes assessed in the Human Angiogenic Growth Factor PCR Array

Gene Symbol	Gene Name
AGGF1	Angiogenic factor with G patch and FHA domains 1
AMOT	Angiomotin
ANG	Angiogenin, ribonuclease, RNase A family, 5
ANGPT1	Angiopoietin 1
ANGPT2	Angiopoietin 2
ANGPTL1	Angiopoietin-like 1
ADGRB1	Brain-specific angiogenesis inhibitor 1
BMP2	Bone morphogenetic protein 2
BTG1	B-cell translocation gene 1, anti-proliferative
CCL15	Chemokine (C-C motif) ligand 15
CCL2	Chemokine (C-C motif) ligand 2
CD55	CD55 molecule, decay accelerating factor for complement (Cromer blood group)
CD59	CD59 molecule, complement regulatory protein
CHGA	Chromogranin A (parathyroid secretory protein 1)
COL18A1	Collagen, type XVIII, alpha 1
COL4A3	Collagen, type IV, alpha 3 (Goodpasture antigen)
CSF3	Colony stimulating factor 3 (granulocyte)
CXCL10	Chemokine (C-X-C motif) ligand 10
CXCL11	Chemokine (C-X-C motif) ligand 11
CXCL12	Chemokine (C-X-C motif) ligand 12
CXCL13	Chemokine (C-X-C motif) ligand 13
CXCL14	Chemokine (C-X-C motif) ligand 14
CXCL2	Chemokine (C-X-C motif) ligand 2
CXCL3	Chemokine (C-X-C motif) ligand 3
CXCL5	Chemokine (C-X-C motif) ligand 5
CXCL6	Chemokine (C-X-C motif) ligand 6 (granulocyte chemotactic protein 2)
CXCL9	Chemokine (C-X-C motif) ligand 9
EDIL3	EGF-like repeats and discoidin I-like domains 3
EREG	Epiregulin
FGF1	Fibroblast growth factor 1 (acidic)
FGF13	Fibroblast growth factor 13
FGF2	Fibroblast growth factor 2 (basic)
FGFBP1	Fibroblast growth factor binding protein 1
FIGF	C-fos induced growth factor (vascular endothelial growth factor D)
FN1	Fibronectin 1
FOXO4	Forkhead box O4
FST	Follistatin

GRN	Granulin
GRP	Gastrin-releasing peptide
HGF	Hepatocyte growth factor (hepapoietin A; scatter factor)
IFNA1	Interferon, alpha 1
IFNB1	Interferon, beta 1, fibroblast
IFNG	Interferon, gamma
IL10	Interleukin 10
IL12A	Interleukin 12A (natural killer cell stimulatory factor 1, cytotoxic lymphocyte maturation factor 1, p35)
IL12B	Interleukin 12B (natural killer cell stimulatory factor 2, cytotoxic lymphocyte maturation factor 2, p40)
IL17F	Interleukin 17F
IL6	Interleukin 6 (interferon, beta 2)
CXCL8	Interleukin 8
KITLG	KIT ligand
KLK3	Kallikrein-related peptidase 3
LEP	Leptin
MDK	Midkine (neurite growth-promoting factor 2)
NPPB	Natriuretic peptide B
NPR1	Natriuretic peptide receptor A/guanylate cyclase A (atrionatriuretic peptide receptor A)
PDGFB	Platelet-derived growth factor beta polypeptide
PDGFD	Platelet derived growth factor D
PF4	Platelet factor 4
PGF	Placental growth factor
PLG	Plasminogen
PPBP	Pro-platelet basic protein (chemokine (C-X-C motif) ligand 7)
PRL	Prolactin
PROK1	Prokineticin 1
PTN	Pleiotrophin
RHOB	Ras homolog gene family, member B
RNH1	Ribonuclease/angiogenin inhibitor 1
RUNX1	Runt-related transcription factor 1
SERPINC1	Serpin peptidase inhibitor, clade C (antithrombin), member 1
SERPINE1	Serpin peptidase inhibitor, clade E (nexin, plasminogen activator inhibitor type 1), member 1
SERPINF1	Serpin peptidase inhibitor, clade F (alpha-2 antiplasmin, pigment epithelium derived factor), member 1
SPINK5	Serine peptidase inhibitor, Kazal type 5
STAB1	Stabilin 1
TGFA	Transforming growth factor, alpha
TGFB1	Transforming growth factor, beta 1

THBS1	Thrombospondin 1
TIE1	Tyrosine kinase with immunoglobulin-like and EGF-like domains 1
TIMP1	TIMP metallopeptidase inhibitor 1
TIMP2	TIMP metallopeptidase inhibitor 2
TIMP3	TIMP metallopeptidase inhibitor 3
TNF	Tumor necrosis factor
TNNI2	Troponin I type 2 (skeletal, fast)
TNNI3	Troponin I type 3 (cardiac)
TYMP	Thymidine phosphorylase
VEGFA	Vascular endothelial growth factor A

Table A.2 List of genes included in the PrimePCR™ array analysis.

Angiogenesis	
Gene Symbol	**Gene Name**
ANGPT1	Angiopoietin-1
FGF2	Basic fibroblast growth factor
HGF	Hepatocyte growth factor
IGF1	Insulin like growth factor-1
SERPINE1	Serpin family E member-1
VEGFA	Vascular endothelial growth factor A
Inflammation	
Gene Symbol	**Gene Name**
CCL2	C-C motif chemokine ligand 2
CSF2	Colony stimulating factor 2
IL1B	Interleukin-1 beta
IL4	Interleukin-4
IL10	Interleukin-10
TNF	Tumor necrosis factor
CXCL10	C-X-C motif chemokine ligand-10
ECM synthesis	
Gene Symbol	**Gene Name**
ACAN	Aggrecan
ACTA2	Smooth muscle actin alpha 2
BGN	Biglycan
COL1A1	Collagen type 1 alpha 1 chain
COL3A1	Collagen type III alpha 1 chain
COL4A1	Collagen type IV alpha 1 chain
CTGF	Connective tissue growth factor
DCN	Decorin
VCAN	Versican
ECM remodeling	
Gene Symbol	**Gene Name**
MMP1	Matrix metalloproteinase-1
MMP2	Matrix metalloproteinase-2
TGFB1	Transforming growth factor-beta 1
TIMP1	Tissue inhibitor of metalloproteinases-1
Housekeeping	
Gene Symbol	**Gene Name**
GAPDH	Glyceraldehyde 3-phosphate dehydrogenase
RPS18	Ribosomal protein S18
UBC	Ubiquitin C

Appendix B: Human Ethics Approval

Western Research

Research Ethics

Western University Health Science Research Ethics Board
HSREB Delegated Initial Approval Notice

Principal Investigator: Dr. Lauren Flynn
Department & Institution: Schulich School of Medicine and Dentistry\Anatomy & Cell Biology,Western University

HSREB File Number: 105426
Study Title: Tissue Engineering with Adipose-derived Stem Cells
Sponsor: Canadian Institutes of Health Research

HSREB Initial Approval Date: August 13, 2014
HSREB Expiry Date: August 31, 2019

Documents Approved and/or Received for Information:

Document Name	Comments	Version Date
Other	Letter for OR and Clinic Staff to Introduce the Study (received June 2/14)	
Western University Protocol		2014/07/23
Letter of Information & Consent		2014/07/23

The Western University Health Science Research Ethics Board (HSREB) has reviewed and approved the above named study, as of the HSREB Initial Approval Datenoted above.

HSREB approval for this study remains valid until the HSREB Expiry Date noted above, conditional to timely submission and acceptance of HSREB ContinuingEthics Review. If an Updated Approval Notice is required prior to the HSREB Expiry Date, the Principal Investigator is responsible for completing andsubmitting an HSREB Updated Approval Form in a timely fashion.

The Western University HSREB operates in compliance with the Tri-Council Policy Statement Ethical Conduct for Research Involving Humans (TCPS2), theInternational Conference on Harmonization of Technical Requirements for Registration of Pharmaceuticals for Human Use Guideline for Good Clinical PracticePractices (ICH E6 R1), the Ontario Personal Health Information Protection Act (PHIPA, 2004), Part 4 of the Natural Health Product Regulations, Health CanadaMedical Device Regulations and Part C, Division 5, of the Food and Drug Regulations of Health Canada.

Members of the HSREB who are named as Investigators in research studies do not participate in discussions related to, nor vote on such studies when theyare presented to the REB.

The HSREB is registered with the U.S. Department of Health & Human Services under the IRB registration number IRB 00000940.

Ethics Officer, on behalf of Dr. Joseph Gilbert, HSREB Chair

Ethics Officer to Contact for Further Information

Erika Basile	Grace Kelly	Mina Mekhail	Vikki Tran vikki.tran@uwo.ca

This is an official document. Please retain the original in your files.

Western Research

Date: 24 July 2019

To: Dr. Lauren Flynn

Project ID: 105426

Study Title: Tissue Engineering with Adipose-derived Stem Cells

Application Type: Continuing Ethics Review (CER) Form

Review Type: Delegated

REB Meeting Date: 06/Aug/2019

Date Approval Issued: 24/Jul/2019

REB Approval Expiry Date: 13/Aug/2020

Dear Dr. Lauren Flynn,

The Western University Research Ethics Board has reviewed the application. This study, including all currently approved documents, has been re-approved until the expiry date noted above.

REB members involved in the research project do not participate in the review, discussion or decision.

Western University REB operates in compliance with, and is constituted in accordance with, the requirements of the TriCouncil Policy Statement: Ethical Conduct for Research Involving Humans (TCPS 2); the International Conference on Harmonisation Good Clinical Practice Consolidated Guideline (ICH GCP); Part C, Division 5 of the Food and Drug Regulations; Part 4 of the Natural Health Products Regulations; Part 3 of the Medical Devices Regulations and the provisions of the Ontario Personal Health Information Protection Act (PHIPA 2004) and its applicable regulations. The REB is registered with the U.S. Department of Health & Human Services under the IRB registration number IRB 00000940.

Please do not hesitate to contact us if you have any questions.

Sincerely,

Daniel Wyzynski, Research Ethics Coordinator, on behalf of Dr. Joseph Gilbert, HSREB Chair

Note: This correspondence includes an electronic signature (validation and approval via an online system that is compliant with all regulations).

Appendix C: Animal Ethics Approval

Western

2015-049:5:

AUP Number: 2015-049
AUP Title: Characterization of Soft Tissue Regeneration with Bioscaffolds and Adipose-derived Stem/Stromal Cells (ASCs)
Yearly Renewal Date: 11/01/2019

The YEARLY RENEWAL to Animal Use Protocol (AUP) 2015-049 has been approved by the Animal Care Committee (ACC),
and will be approved through to the above review date.

Please at this time review your AUP with your research team to ensure full understanding by everyone listed within this AUP.

As per your declaration within this approved AUP, you are obligated to ensure that:

1) Animals used in this research project will be cared for in alignment with:
   a) Western's Senate MAPPs 7.12, 7.10, and 7.15
   http://www.uwo.ca/univsec/policies_procedures/research.html
   b) University Council on Animal Care Policies and related Animal Care Committee procedures
   http://uwo.ca/research/services/animalethics/animal_care_and_use_policies.html
2) As per UCAC's Animal Use Protocols Policy,
   a) this AUP accurately represents intended animal use;
   b) external approvals associated with this AUP, including permits and scientific/departmental peer approvals, are complete and accurate;
   c) any divergence from this AUP will not be undertaken until the related Protocol Modification is approved by the ACC; and
   d) AUP form submissions - Annual Protocol Renewals and Full AUP Renewals - will be submitted
   and attended to within timeframes outlined by the ACC. http://uwo.ca/research/services/animalethics/animal_use_protocols.html
3) As per MAPP 7.10 all individuals listed within this AUP as having any hands-on animal contact will
   a) be made familiar with and have direct access to this AUP;
   b) complete all required CCAC mandatory training (training@uwo.ca); and
   c) be overseen by me to ensure appropriate care and use of animals.
4) As per MAPP 7.15,
   a) Practice will align with approved AUP elements;
   b) Unrestricted access to all animal areas will be given to ACVS Veterinarians and ACC Leaders;
   c) UCAC policies and related ACC procedures will be followed, including but not limited to:

i) Research Animal Procurement
ii) Animal Care and Use Records
iii) Sick Animal Response
iv) Continuing Care Visits

5) As per institutional OH&S policies, all individuals listed within this AUP who will be using or potentially exposed to hazardous materials will have completed in advance the appropriate institutional OH&S training, facility-level training, and reviewed related (M)SDS Sheets, http://www.uwo.ca/hr/learning/required/index.html

Submitted by: Copeman, Laura
on behalf of the Animal Care Committee
University Council on Animal Care

The University of Western Ontario
Animal Care Committee / University Council on Animal Care
London, Ontario Canada N6A 5C1
519-661-2111 x 88792 Fax 519-661-2028
auspc@uwo.caï¿½ http://www.uwo.ca/research/services/animalethics/index.html

Appendix D: Permission to Use Copyrighted Materials

Nursing Standard. 2012. 27(3): 35-42 Figure 1

Order Date	09-Apr-2020	**Type of Use**	Republish in a thesis/dissertation
Order license ID	1027612-1	**Publisher**	R C N PUBLISHING CO.
ISSN	0029-6570	**Portion**	Image/photo/illustration

LICENSED CONTENT

Publication Title	Nursing standard	**Country**	United Kingdom of Great Britain and Northern Ireland
Author/Editor	ROYAL COLLEGE OF NURSING (GREAT BRITAIN)	**Rightsholder**	RCNi
Date	01/01/1987	**Publication Type**	Journal
Language	English		

REQUEST DETAILS

Portion Type	Image/photo/illustration	**Distribution**	Worldwide
Number of images / photos / illustrations	1	**Translation**	Original language of publication
Format (select all that apply)	Electronic	**Copies for the disabled?**	No
Who will republish the content?	Academic institution	**Minor editing privileges?**	Yes
Duration of Use	Life of current edition	**Incidental promotional use?**	No
Lifetime Unit Quantity	Up to 499	**Currency**	CAD
Rights Requested	Main product		

NEW WORK DETAILS

Title	3-D Culture Strategies for the Dynamic Preconditioning of Adipose-derived Stromal Cells on Decellularized Adipose Tissue Bioscaffolds	**Institution name**	University of Western Ontario
		Expected presentation date	2020-05-29
Instructor name	Tim Tian Han		

ADDITIONAL DETAILS

Order reference number	N/A	**The requesting person / organization to appear on the license**	Tim Tian Han

REUSE CONTENT DETAILS

Title, description or numeric reference of the portion(s)	Figure 1, The skin showing the layers of the epidermis and main structures of the dermis	**Title of the article/chapter the portion is from**	The integumentary system: anatomy, physiology and function of skin
		Author of portion(s)	ROYAL COLLEGE OF NURSING (GREAT BRITAIN)
Editor of portion(s)	Ella McLafferty		
Volume of serial or monograph	27	**Issue, if republishing an article from a serial**	3
Page or page range of portion	36	**Publication date of portion**	2012-01-01

Trends in Biotechnology. 2004. 22(2): 80-86. Figure 1

This Agreement between Tim Tian Han ("You") and Elsevier ("Elsevier") consists of your license details and the terms and conditions provided by Elsevier and Copyright Clearance Center.

License Number	4804940206034
License date	Apr 09, 2020
Licensed Content Publisher	Elsevier
Licensed Content Publication	Trends in Biotechnology
Licensed Content Title	The role of bioreactors in tissue engineering
Licensed Content Author	Ivan Martin,David Wendt,Michael Heberer
Licensed Content Date	Feb 1, 2004
Licensed Content Volume	22
Licensed Content Issue	2
Licensed Content Pages	7
Start Page	80
End Page	86
Type of Use	reuse in a thesis/dissertation
Portion	figures/tables/illustrations
Number of figures/tables/illustrations	1
Format	electronic
Are you the author of this Elsevier article?	No
Will you be translating?	No
Title	3-D Culture Strategies for the Dynamic Preconditioning of Adipose-derived Stromal Cells on Decellularized Adipose Tissue Bioscaffolds
Institution name	The University of Western Ontario
Expected presentation date	May 2020
Portions	Figure 1
Requestor Location	Tim Tian Han
	Attn:
Publisher Tax ID	GB 494 6272 12
Total	**0.00 USD**
Terms and Conditions	

Immunity. 2016. 44(3): 450-462. Figure 1

This Agreement between Tim Tian Han ("You") and Elsevier ("Elsevier") consists of your license details and the terms and conditions provided by Elsevier and Copyright Clearance Center.

License Number	4804940416963
License date	Apr 09, 2020
Licensed Content Publisher	Elsevier
Licensed Content Publication	Immunity
Licensed Content Title	Macrophages in Tissue Repair, Regeneration, and Fibrosis
Licensed Content Author	Thomas A. Wynn,Kevin M. Vannella
Licensed Content Date	Mar 15, 2016
Licensed Content Volume	44
Licensed Content Issue	3
Licensed Content Pages	13
Start Page	450
End Page	462
Type of Use	reuse in a thesis/dissertation
Portion	figures/tables/illustrations
Number of figures/tables/illustrations	1
Format	electronic
Are you the author of this Elsevier article?	No
Will you be translating?	No
Title	3-D Culture Strategies for the Dynamic Preconditioning of Adipose-derived Stromal Cells on Decellularized Adipose Tissue Bioscaffolds
Institution name	The University of Western Ontario
Expected presentation date	May 2020
Portions	Figure 1
Requestor Location	Tim Tian Han
	Attn:
Publisher Tax ID	GB 494 6272 12
Total	**0.00 CAD**
Terms and Conditions	

Curriculum Vitae

Name: Tim Tian Yu Han

Post-secondary Education and Degrees:

Queen's University
Kingston, Ontario, Canada
2005 – 2009, B.Sc. (Honors, Life Sciences)

Queen's University
Kingston, Ontario, Canada
2010-2012, M.Sc. (Neuroscience)

The University of Western Ontario
London, Ontario, Canada
2015-Present Ph.D. (Anatomy & Cell Biology)

Awards:

Frederick Banting and Charles Best Award (CGS-M)
Canadian Institutes of Health Research
2011-2012

Ontario Graduate Scholarship
2015-2017

Alexander Graham Bell Canada Graduate Scholarship (CGS-D)
Natural Sciences and Engineering Research Council
2017-2019

Related Work Experience

Teaching Assistant
Queen's University
2011-2012

Research Assistant
Queen's University
2012-2014

Teaching Assistant
The University of Western Ontario
2016-2017

Publications:

1. Nair DG, Han T, Lourenssen S, Blennerhassett MG. (2011). Proliferation modulates intestinal smooth muscle phenotype *in vitro* and in colitis *in vivo*. *American Journal of Physiology Gastrointestinal and liver physiology*, *300*(5), G903-13

2. Gougeon PY, Lourenssen S, Han T, Nair D, Ropoleski M, Blennerhassett MG (2012). The pro-inflammatory cytokine IL-1β and TNF-α are neurotrophic for enteric neurons. *Journal of Neuroscience*, 33(8), 3339-51

3. Cheung HK, Han T, Marecak D, Watkins JF, Amsden BG, and Flynn LE. (2014). Composite photocrosslinkable hydrogel scaffolds incorporating decellularized adipose tissue for soft tissue engineering with adipose-derived stem cell. *Biomaterials*, 35(6), 1914-23

4. Brown C, Yan J, Han T, Amsden BG, Flynn LE. Effects of decellularized adipose tissue particle size on adipose-derived stem cell proliferation and adipogenic differentiation in composite methacrylated chondroitin sulphate hydrogels. (2015). *Biomedical Materials*, 10(4), 045010

5. Han T, Lourenssen S, Miller KG, Blennerhassett MG. Intestinal smooth muscle phenotype determines enteric neuronal survival via GDNF expression. (2015). *Neuroscience*, 290, 357-68

6. Han T, Toutounji S, Amsden BG, Flynn LE. Adipose-derived stromal cells mediate *in vivo* adipogenesis, angiogenesis and inflammation in decellularized adipose tissue bioscaffolds. (2015). *Biomaterials*, 72, 125-37.

7. (Book Chapter) Han T, Shridhar A, Robb K, Brown C, Flynn L. *Fundamental Principles of Smart Materials for Tissue Engineering*: Natural materials as smart scaffolds for tissue engineering. (2016) Cambridge, UK: Royal Society of Chemistry, 124-62.

8. Han T, Flynn LE. Perfusion bioreactor culture of adipose-derived stromal cells on decellularized adipose tissue scaffolds enhances *in vivo* regeneration. 2020.04.10.036194

Presentations:

1. Han T, Lourenssen S and Blennerhassett M. Intestinal smooth muscle proliferation decreases GDNF production. Canadian Digestive Disease Week 2012, Canadian Association of Gastroenterology. Montreal, Quebec, Canada. February 2011

2. Han T, Lourenssen S and Blennerhassett M. GDNF expression in ISMC determines enteric neuron survival *in vitro*. Research in Progress, Gastrointestinal Disease Research Unit - Kingston General Hospital. Kingston, Ontario, Canada. April 2012

3. Han T, Amsden B, Flynn L. Adipose-derived stem cells enhance the angiogenic and adipogenic potential of decellularized adipose tissue *in vivo*. The 31st Annual Meeting of The Canadian Biomaterial Society. Halifax, Nova Scotia, Canada. June 2014

4. Han T, Amsden B, Flynn L. Adipose-derived stem cells mediate *in vivo* soft tissue regeneration in decellularized adipose tissue bioscaffolds. TERMIS-AM Annual Conference and Exposition 2014. Washington, DC, USA. December 2014.

5. Han T, Flynn L. Development of a dynamic culture pre-conditioning strategy for adipose-derived stem/stromal cells on decellularized adipose tissue bioscaffolds. The 33rd Annual Meeting of The Canadian Biomaterial Society. Winnipeg, Manitoba, Canada. May 2017

6. Han T, Flynn L. Dynamic preconditioning of adipose-derived stromal cells on engineered bioscaffolds for the regeneration of subcutaneous adipose tissue. London Health Research Day 2018. London, Ontario, Canada. May 2018